Advanced Lectures 1988

The climate of the world
Part 1

LONDON, METEOROLOGICAL OFFICE.
Advanced Lectures 1988

The climate of the world. Part 1.

00241088 551.58 FG2
551.513.1

ORGS UKMO A

National Meteorological Library
FitzRoy Road, Exeter, Devon. EX1 3PB

arters, Bracknell

METEOROLOGICAL OFFICE
152895
23 SEP 1988
LIBRARY
C

These Lecture Notes have also been produced as Long-Range Forecasting and Climate Research Memoranda Nos 22 to 24.

Advanced Lectures 1988

The climate of the world
Part I

C.K. Folland

D.E. Parker

Permission to quote from this document must be obtained from the Principal, Meteorological Office College, Shinfield Park, Reading RG2 9AU

The climate of the world

Part I

1. **Introduction to world climate**
   C.K. Folland and D.E. Parker
2. **Description of world climate**
   C.K. Folland and D.E. Parker
3. **Climatic forcing and feedback processes**
   I - Forcing from above
   C.K. Folland and D.E. Parker
4. **Climatic forcing and feedback processes**
   II - Interactions with the land surface
   C.K. Folland and D.E. Parker
5. **Ocean-atmosphere interaction**
   D.E. Parker and C.K. Folland

INTRODUCTION TO WORLD CLIMATE

C K FOLLAND AND D E PARKER

MET O 13

SUMMARY

This lecture introduces some approaches to the study of climate and provides a set of general definitions of a subject. Some major statistical techniques are discussed. A review of the World Climate Programme emphasises its constituent World Climate Research Programme and sub-programmes such as the Tropical Ocean-Global Atmosphere programme, the World Ocean Circulation Experiment, and the planned Global Energy and Water Cycle Experiment. The Sahel region, introduced in this lecture to illustrate recent observed climatic change, is a recurrent theme throughout the series, and we are now able to include under "research into climate" some recent rudimentary but physically-based attempts to predict climate in the Sahel and other regions one or more seasons ahead.

1.1 INTRODUCTION

There are several complementary approaches to the study of climate. A traditional image of climate is the one often presented at school. In the preface to his book 'Climatology' (9th Edition 1961) the famous Reading University geographer Professor Austin Miller wrote 'The nature of the relief, the vegetation, the habits of the people, their architecture and their occupations will be attuned to the prevailing rainfall and temperature conditions and it is the response rather than the cause which the geographer wishes to know'. This is still the main approach of the many 'human' geographers who wish to use climatic data to explain the development of society and industry in the context of the physical environment. It is nevertheless a legitimate use of climatic data, paralleled by the wide-spread use of climatic data by industry and agriculture for planning. Here, an understanding of how climate operates

is much less important than the goal of collecting and validating climatic data to provide reliable analyses of those data tuned to user's needs. However, a qualitative understanding of climate is still very desirable when deciding on the choice of appropriate statistics and of suitable data; nowadays many of the analyses needed are far removed from the calculation of simple climatic averages. This 'applied' climatological activity is important in several branches of the Meteorological Office.

Over the last few decades, research into the physical basis of climate and more recently its variability has become increasingly feasible and productive as a result of developments in meteorological theory, computers and thus in meteorological models. In addition, our ability to collect and validate reliable worldwide data has considerably increased. Research into the mechanisms and behaviour of climate is essential if useful predictions of climate are to become possible, especially the prediction or simulation of the consequences of increased concentrations of carbon dioxide and other trace gases in the atmosphere, and the persistent and socially disruptive droughts in parts of the tropics. In the following lectures most emphasis will therefore be placed on the physical approach to climate.

We shall frequently refer to the Met O 20 advanced lectures on the physics and dynamics of the climate system. There is no hard and fast rule for the difference between the two sets of lectures; however Met O 20's lectures emphasise the physical causes and principles underlying the atmospheric and oceanic circulation. Our lectures will have a similar background but are more concerned with the observed behaviour of statistical ensembles of weather events (climate) and the reasons for that behaviour. We will also have an eye on the question: how could we predict these variations? So our lectures will emphasise the near surface environment that affects man, animals and plants. Of course the atmosphere is 3-dimensional and discussion of 'higher' climatic matters will be brought in as necessary.

1.2 WHAT IS CLIMATE?

The Scientific Plan for the World Climate Research Programme (World Meteorological Organization (WMO) (1984a)) provides several useful definitions:-

- Weather is the manifestation of a state of the atmosphere at a particular instant in time and the evolution of this state through the generation, growth and decay of individual transient (synoptic scale) disturbances.

- Climate is the synthesis of weather over the whole of a period long enough to establish its statistical ensemble properties (mean values, variances, probabilities of extreme events ...) and is largely independent of any (particular) instantaneous atmospheric state. A climatic state is described by these statistical properties.

- Climatic change (or climatic signal) is measured by the difference between mean values of a climatic parameter or statistic, i.e. the difference between climatic states.

- Climatic variability is measured by the deviations of monthly, seasonal and annual values from the mean value of the climatic state established over an ensemble of such periods. The differences from the mean associated with an individual event are called anomalies.

A given' climate' is commonly estimated by means of measurements made over a period of 30 years. Climatic variability is in principle a manifestation of the variations of time-averaged weather that contribute to a given climate: eg the fact that last January was markedly different from the previous January would usually reflect 'climatic variability', but if the average temperature for the last 30 Januarys had been markedly different from the average temperture of the preceeding 30 Januarys, we

could legitimately talk about "climatic change". Climatic 'variability' of course includes a stochastic component due to transient variations associated with weather.

1.3 METHODS OF STUDYING CLIMATE

1.3.1 Empirical methods

Most (but not all) scientific knowledge is based on observations. We usually need to make observations in order to develop theories or choose between competing alternatives. Much empirical work on climate is basically 'detective' work which attempts to find out how the atmosphere and oceans behave on time scales longer than a few days, as few theories yet exist for such behaviour. An outstanding example of an important climatic fluctuation which has been studied empirically is the remarkable 20 year drought in the Sahel region of Africa (1968-date) whose continued persistence since the well known initial drought sequence of 1968-1974 was only verified in 1982 (Lamb (1982)) but whose consequences are now painfully obvious (Figure 1.1). On a shorter time scale there is a tendency for the extratropical north Pacific/north American/subtropical west Atlantic atmosphere to adopt a special 'PNA' pattern of geographical variation on time scales of weeks in the winter half year. This variation has an equivalent-barotropic structure in the vertical and seems to be distinct from synoptic scale variability as it exhibits the characteristics of a stationary wave with a non-zonal orientation (Figure 1.2). This atmospheric 'regime' was discovered about 50 years ago by Walker and Bliss (1932), confirmed quite recently by Wallace and Gutzler (1981) and is now found to exist in several atmospheric general circulation models (AGCMs) eg Qiu and Esbensen (1984). The PNA pattern seems to be one of several internal atmospheric modes that can be self stimulated within the atmosphere or in AGCM's but might also be preferentially stimulated (or suppressed?) by external forcing eg due to sea surface temperature anomalies etc (Fig 1.2). These wave-like patterns are sometimes called teleconnections, as the fluctuations of a given variable, eg 500 mb

geopotential, at a selected location tend to be persistently positively or negatively correlated with those at selected distant locations. Teleconnections have long been used in long range forecasting.

Synoptic climatology is a branch of climatology which up to recently has been the province of the empiricist. There are many definitions of the subject but in essence it tries to provide explanations or predictions of regional or local climates in terms of large scale fluctuations of the atmosphere. Only one book purely devoted to synoptic climatology has been published so far (Barry and Perry (1973)), written before the use of AGCM's started to make an impact on the subject. The 'synoptic method' involves the study of changes in circulation patterns measured at fixed times or averaged over fixed intervals. It can be quite a powerful technique when used in a discriminating way; thus it provided the foundations of practical short-range weather forecasting prior to the extensive use of mathematical forecasting models. One prominent technique of synoptic climatology is to classify time-averaged circulation patterns into 'types' which have markedly different consequences for regional surface weather or which appear to reflect different physical generating mechanisms. The PNA pattern mentioned above would be a good example of a 'circulation type'. Other examples of circulation types include the 4 basic 'elementary circulation mechanisms' of Dzerdzeevski (with 41 sub-units) (see p164 of Barry and Perry (1973)) that attempt to summarise different patterns of extratropical Northern Hemisphere circulation. These patterns were developed to help long-range forecasting in Russia (Figure 1.3), and have been used by Kalnicky (1987) both to define natural seasons and to analyse climatic changes. A local example is the catalogue of the so called 'Lamb' types of daily surface circulation patterns over UK whose aggregate over long periods has often been found useful in climate studies and in long-range forecasting for the UK (Lamb (1972)). Figure 1.4 gives examples of Lamb types. Both Lamb"s and Dzerdzeevski's patterns were subjectively determined, but recent advances in computing technology and statistical theory have encouraged the development of objective methods of classification of patterns of atmospheric circulation (and of other fields such as rainfall or sea surface temperature). Barnston and Livezey (1987) used orthogonally rotated principal component analysis of time-series of

monthly fields of 700 mb geopotential height to classify atmospheric circulation patterns over the Northern Hemisphere. The PNA pattern was prominent in their results, as was the North Atlantic Oscillation which is a "see-saw" of geopotential (and sea-level pressure) between the Azores region and the Greenland-Iceland region (Figure 1.5). There are, however, a number of pitfalls in principal component analysis: it is necessary to ensure that the patterns generated faithfully represent the original data and are physically meaningful. To this end, a choice between different matrix rotations may be needed (Richman (1986)), and statistical tests must be applied to estimate sampling errors in the estimation of the principal components or empirical orthogonal functions (North et al (1982)), and to determine which patterns account for sufficient variance in the original data to be classified as "signal" rather than "noise" (Overland and Preisendorfer (1982)).

Empirical analysis of climatic data also includes the determination of the regularity and magnitude of changes in time. This may be done by filtering (Bath (1974)), by direct Fourier transformation of the data, by Fourier transform of the lag-autocorrelation function of the data (Blackman and Tukey (1959)), or by the maximum entropy power spectral method (Ulrych and Bishop (1975)). The structure of time-series is often investigated also by the autoregressive and moving-average techniques pioneered by Box and Jenkins (1976). Figure 1.6 shows a maximum-entropy power-spectrum of a 5-year time-series of daily Central England Temperature. The data were derived from observations for several stations using the principles laid down for monthly Central England Temperature by Manley (1974). Nearly 50% of the variance in the series is seen to be on time-scales of 10 days to 2 months, and there is a peak of variability on an 8-month time-scale. However, different 5 year periods provide spectra which, although often similar in form, are different in detail, indicating that apparent regularities either are short-lived or are manifestations of physical forcings active on a band of time-scales. Over longer periods, spectra may change radically (Fig 1.7). It is therefore essential to assess the statistical significance of apparent periodiaties or peaks in power-spectra or Fourier transforms. This may be done by an extension of analysis-of-variance techniques or by Monte Carlo sampling, in which are

computed power spectra of many randomly-generated samples having the same autoregressive structure (ie degree of "persistence" or "red noise") as the series under analysis.

Another useful technique is the stratification and averaging together of fields (or local values) according to their temporal relationship with particular events, such as major volcanic eruptions, or El nino warmings in the East Tropical Pacific Ocean. In this way it is possible to compare, for example, average global fields of mean-sea-level pressure at the time of "key events" such as El Nino warmings with corresponding fields one year earlier. The technique is sometimes called "superposed epoch analysis". In a similar vein, fields for a particular time of year may be averaged over successive periods (of eg 30 years) in order to seek indications of climatic change. As in other techniques, statistical significance must be assessed carefully. At a given point, a t-test may be used to measure the statistical significance of the difference between the average of one set of values and that of the other, but allowance must be made for any reduction in the number of degrees of freedom or enhancement of the standard error, resulting from time-lagged autocorrelation (Brooks and Carruthers (1953), p326). For an entire field, a proportion p of points will have statistically significant differences at the 100(1-p)% level of confidence if the original data are random numbers, and the field can only be reckoned as statistically significant at the 100(1-p)% level of confidence if the number of significant points exceeds that expected to occur on 100(1-p)% of occasions according to binomial probability theory (Livezey and Chen (1983)). Furthermore, the interdependence of the data at differing points in the field must be taken into account when estimating the effective number of independent data or degrees of freedom in the field, which needs to be known when applying the binomial theory. Livezey and Chen therefore recommend Monte Carlo sampling as a means of assessment of statistical significance of fields. The selection and averaging together of fields, and computation of local significance tests, is repeated many times with the same sample size as in the original comparison, but with randomly selected periods, or with randomly selected dates instead of the dates of actual "key events". It is assumed that, because the fields are from the same set as those originally compared, the

spatial structure of the composites is the same. The number of significant points in the original comparison is compared with the frequency distribution of the number of significant points in the set of random comparisons.

1.3.2 Numerical Modelling

This subject is extensively discussed in the Met O 20 advanced lectures on the physics and dynamics of the climate system. A recent development has been the interactive use of synoptic climatological methods and AGCM's to study short time scale climatic fluctuations. The best example so far is the ongoing, extensive, international study of the El Nino/Southern Oscillation (eg Nihoul (Ed) (1985)) where AGCM and OGCM (ocean GCM) experiments have been firmly guided by a series of climatological investigations (eg Rasmusson and Carpenter (1982)). Our own works on simulation and prediction of seasonal rainfall variations in subsaharan Africa is a further example. Some of the results of the GCM experiments already go beyond what would soundly be deduced from available observations alone (see Lectures 5 and 6 in this series). In this way the modelling results stimulate new ways of looking at the observations allowing interactive studies to flourish.

Numerical modelling has also become a useful adjunct to observational studies in palaeoclimatology, especially for the period from the late Glacial until the present (Lectures 7 and 8). For studies of the effects of changes of land surface albedo and moisture availability, and of the effects of increasing concentrations of carbon dioxide and other trace gases in the atmosphere, numerical modelling has long been to the fore, and results are discussed both in Lectures 4, 5 and 10 and in the Met O 20 lectures.

The increase in computing power in the last decade or so has begun to allow the completion of sets or "ensembles" of numerical model integrations, each integration having slightly different initial conditions. Alternatively, very long integrations are completed and individual sections of the integrations are regarded as separate samples of

the simulated climate. The experiments are repeated with different forcing, eg doubled atmospheric carbon dioxide. The sets of samples of the two simulated climates are then compared and the statistical significance of, say, atmospheric circulation changes is estimated. In such cases the aforementioned methods advocated by Livezey and Chen (1983) for estimating field significance should be applied.

1.4 THE WORLD CLIMATE PROGRAMME

In 1974 the Executive Committee of WMO decided that it was important for WMO to take a lead in promoting studies of climatic changes and their impact on the natural environment and on food production. So, jointly with ICSU, the International Council of Scientific Unions, they arranged a high level scientific and technical World Climate Conference in 1979 which represented the climate-sensitive branches of national economies including agriculture, energy, water resources, fisheries and health (WMO (1979)). They reviewed knowledge of climatic change and variability and their implications for human activities. There followed an outline plan and basis for the World Climate Programme (WCP) 1980-1983 (WMO 540) (1980).

WMO's role is to support and help co-ordinate national activities, not to run them. They have set up a World Climate Programme Office within the Office of the WMO/ICSU Joint Planning Staff at Geneva and have established a Joint Scientific Committee (JSC) with ICSU to provide, amongst other things, scientific guidance for the international aspects of the World Climate Research Programme which is a sub-unit of WCP. The JSC determines the main research objectives and facilitates the exchange of information between scientists.

The World Climate Programme is divided into 4 main sections:-

1.4.1. World Climate Data Programme (WCDP)

It might be thought that the voluminous data being collected to support weather forecasting should also be sufficient for climate studies. Indeed the data collected for weather forecasting, including those archived

in the form of initialised meteorological fields, are increasingly valuable for studies of climate. Nevertheless elucidation of many of the processes essential to climatic fluctuations or climatic change, as well as monitoring how the climate is currently behaving, requires many more atmospheric data from above the oceans and remote land areas than are at present available. Even more importantly, reliable worldwide data from the ocean surface and from the depths of the ocean are badly needed. The study of climatic change also demands long, homogeneous, records. If we are to make more progress with observational studies of climatic change not only must the future coverage of atmospheric, land surface and ocean data be more complete, but we must be able to make use of existing historic data. Many of these are not at present easily accessible nor have they been properly validated.

So major goals of WCDP are improvement of future observational coverage of the atmosphere and the boundary surfaces and here satellite data will be vitally important. Working groups have begun to organise the identification and assembly of data for reliable "reference stations", of lengthy climatic data sets covering the last 100 years, and of as complete a set as possible of atmospheric, ocean and land-surface data for about the last 30 years.The WCDP includes the "CLICOM" project (WMO 1986c)) in which small computers and appropriate software and training are supplied to developing nations to enable them to archive and process their climatic data, with a view to local applications as well as the improvement of the global data base. There are also projects for rescue of manuscript data in danger of irretrievable loss: for example, a mobile unit recently toured several countries and microfilmed their records.

1.4.2 World Climate Applications Programme (WCAP)

Specific goals of WCAP are to enlighten people and policy-makers concerning the value of applying climatic data to socio-economic problems and to ensure that relevant knowledge is available to them. Examples include agriculture, water, energy and health. In fact such applications are already quite highly developed in some countries eg in the UK. In the UK climatic data are extensively used to aid agriculture eg to advise on

irrigation and on preventive measures for disease control, to design oil rigs guarded against extremes of wind and waves, and to design and simulate the behaviour of storm water sewers and culverts in a cost-effective way etc. Clearly these activities are appropriate in many parts of the world. Figure 1.8 provides an example of a practical application of climatic data to agriculture; Fig 1.8 can be used, with additional information, to decide where in England and Wales it may be cost effective to grow maize to make a form of silage to feed animals in the winter.

1.4.3 World Climate Impact Studies Programme (WCIP)

This is a more open-ended program that seems to come nearest to the 'geographers' approach to climate. The main objectives are to study the impact of climatic variability and climatic changes on the main economic activities in society (eg agriculture, transport, land use and water resources) and the way that society reacts to these fluctuations with emphasis on the range of impacts in different human societies throughout the world. These societies might be chosen for their different levels of development and different natural environments. The WCIP includes the International Satellite Land-Surface Climatology Project (ISLSCP) for monitoring changes in land-use and vegetation cover, for generating input parameters for climate models, and for providing data on which to base improvements of parametrizations of land-surface/atmosphere interactions.

1.4.4 World Climate Research Programme (WCRP)

This is the most important unit of the World Climate Programme from the point of view of these lectures. This programme developed from the Global Atmospheric Research Programme of the 1970's. Its main objectives (see WMO (1984a)) are bold: to determine to what extent climate can be predicted and the extent of man's influence on climate. The primary approach for meeting these objectives is based on the use of physical-mathematical models (eg general circulation models) capable of simulating and eventually (perhaps) predicting climatic fluctuations and changes. The programme is divided into three streams:-

(a) Stream 1

This stream is meant to establish the basis for long-range weather forecasting, i.e. the prediction of weather anomalies on time scales of 1-2 months (perhaps a little more). Thus the development of long-range weather forecasting is now elevated in an international context to a primary concern of meteorology and climatology. WMO (1984 (b)) gives a detailed picture of developments, and further references. The crucial importance of ocean-atmosphere interaction for long-range weather forecasting is illustrated by WMO (1986 (a)).

(b) Stream 2

This stream aims at predicting variations of global climate over periods of several years. This is an even bolder aim and a special sub-programme of the World Climate Research Programme called TOGA (Tropical Ocean Global Atmosphere Research Programme) was set up in 1985. This programme recognises the crucial role that anomalies in the circulation and heat content of the tropical ocean have in interannual climatic variability. It also recognises the fact that variations in the temperature of the upper layers of the tropical oceans, for example, can to some extent be understood without attempting to model the remainder of the global ocean in full detail. This strategy is a consequence of current ideas about the dynamics of the tropical oceans. Here the Coriolis force is weak giving rise to several dynamical processes which differ from those in mid latitudes and whose purely marine effects tend to be confined to the tropics.

The overall objectives of TOGA are:

(i) To gain a description of the tropical oceans and the global atmosphere as a time-dependent system, in order to determine the extent to which this system is predictable on time-scales of months to years, and to understand the mechanisms and processes underlying its variability.

(ii) To study the feasibility of modelling the coupled ocean-atmosphere system for the purpose of predicting its variations on time-scales of months to years.

(iii) To provide the scientific background for designing an observing and data transmission system for operational prediction if this capability is demonstrated by coupled atmosphere-ocean models.

A description of the progress made in TOGA may be found in WMO (1987d).

(c) Stream 3

This stream aims at studying the patterns of climatic fluctuation and variation over several decades or more and assessing the potential response of climate to man-made or natural influences. For example, these influences might be the increase of carbon dioxide and other trace gases in the atmosphere or slow changes in the large scale global oceanic circulation. Thus a key sub-programme will be the World Ocean Circulation Experiment (WOCE) planned for the 1990's (WMO (1986b)).

The first goal of WOCE is to develop models useful for predicting climatic change and to collect the data necessary to test them. Specific objectives within this goal are to determine and understand on a global basis the following aspects of the world oceanic circulation and their relation to climate:

(i) The large-scale fluxes of heat and fresh water, their divergences over 5 years, and their annual and interannual variability.

(ii) The dynamical balance of the world oceanic circulation and its response to changing surface fluxes.

(iii) Components of oceanic variability on months to years, megameters to global scale, and the statistics on smaller scales.

(iv) The rates and nature of formation, ventilation and circulation of water masses that influence the climate system on time scales from ten to one hundred years.

The second goal of WOCE is to determine the representativeness of the specific WOCE data sets for the long-term behaviour of the ocean, and to find methods for determining long-term changes in the oceanic circulation. Specific objectives with this goal are:

(i) To determine the representativeness of the specific WOCE data sets.

(ii) To identify those oceanographic parameters, indices and fields that are essential for continuing measurements in a climate observing system on decadal time scales.

(iii) To develop cost effective techniques suitable for deployment in an ongoing climate observing system.

Within WOCE are three core projects designed to achieve these goals. The "global description" project will involve worldwide hydrographic sections (e.g. Figure 1.9) and fixed-location time-series as well as satellite-based altimetry and routine data from merchant shipping. The second project will concentrate on the Southern Ocean, in particular meridional transfers and interactions with the atmosphere. The third project, the Gyre Dynamics Experiment, will survey the large-scale features of gyres in the Gulf Stream in sufficient detail to further the interpretation of other oceanic observations and to support model development.

1.5 ADDITIONAL WCRP EXPERIMENTS

An experiment planned for the mid-1990's under the aegis of WCRP is the Global Energy and Water Cycle Experiment (GEWEX). Its scientific objectives (WMO (1987b, 1988b)) are:

(i) To describe and understand the transport of water (vapour, liquid and solid) and energy fluxes in the global atmosphere and at the underlying surface.

(ii) To develop methods of predicting changes in the distribution of water within the global atmosphere and on the underlying surface, which may occur naturally or through the influence of man's activity.

These objectives span all three streams of WCRP.

A further objective of GEWEX is to promote scientific advances and technical developments in observing systems, especially for remote sensing, which could find operational applications in the prediction of weather and climate. The timing of GEWEX has been chosen to take advantage of plans for space stations around the mid 1990's.

The WCRP also includes the International Satellite Cloud Climatology Project (WMO (1987a)) which has the aims of obtaining, validating and assessing satellite-based cloud parameters, improving algorithms for retrieving cloud properties from satellite-observed radiances, furthering the description of the life cycle and radiative properties of clouds so as to improve parameterization schemes, and deepening our understanding of the effects of cloud-radiation feedbacks on climate. Related to this and to GEWEX is the Global Precipitation Climatology Project, which is summarized in WMO (1987c) and involves the synthesis of geostationary satellite infrared data and polar-orbiting satellite microwave data with conventional rain-gauge data and radar data, to produce an improved precipitation climatology for the globe: details of progress in the project are recorded in WMO (1988a).

1.6 THE CHALLENGE OF WCRP

Figures 1.6, 1.10 and 1.11 give examples of why research activities in all three streams of the WCRP are challenging and interesting. Figure 1.6 shows that nearly 50% of the detrended variance of temperatures in Central England (when the annual cycle is removed) in a recent 5 year period occurred on time scales of 10 days to 2 months. Can we predict some of this 'Stream 1' variance? There are many commercial and industrial concerns who would find it useful if we could do this. Figure 1.10 shows that fluctuations in many meteorological parameters occur in the Pacific region which are coherent from season to season and year to year and which fluctuate on time scales of a few years. Can we predict these 'Stream 2' time-scale fluctuations? These may be linked (Lecture 5) to many

irregularly recurring tropical anomalies, including drought in east Australia and floods in coastal Equador and north Peru. Figure 1.11 shows that average global and hemispheric near surface land temperatures have almost certainly fluctuated appreciably over the last century (Stream 3). There have also been roughly parallel quite large variations in atmospheric circulation patterns and in ice cover in some regions. Is this a real effect? These fluctuations need to be understood if we are to predict the consequences of say, a large increase in atmospheric carbon dioxide over the next century with any accuracy. A stimulating introduction to the three streams of the WCRP is given in chapter 1 of 'The Global Climate' edited by J T Houghton (1984).

1.7 CONCLUSION

We have tried to introduce the vast range of climatic studies and why they are important. In the next lecture we shall explore in outline present-day climates of the major regions of the world including some features of their interannual variability.

REFERENCES TO LECTURE 1

BARNSTON, A.G. and LIVEZEY, R.E (1987) Classification, seasonality and persistence of low-frequency atmospheric circulation patterns Mon. Weath. Rev., 115, 1083-1126.

BARRY, R.G. and PERRY, A.H. (1973) Synoptic Climatology. Methuen.

BATH, M. (1974) Spectral analysis in geophysics. Developments in Solid Earth Geophysics, 7, Elsevier, Amsterdam, 563pp.

BLACKMAN, R.B and TUKEY, J.W (1959) The measurement of power spectra from the point of view of communications engineering. Dover Publs., New York, 2nd Ed., 190pp

BOX, G.E.P and JENKINS, G.M. (1976) Time series analysis: forecasting and control. Holden-Day, San Francisco. Revised Ed., 575pp.

BROOKS, C.E.P and CARRUTHERS, N. (1953) Handbook of statistical methods in meteorology. M.O.538. HMSO, London 412pp.

HANSEN, J and LEBEDEFF, S (1987) Global trends of measured surface air temperature. J. Geophys. Res., 92, 13345-13372.

HOUGH, M.N. (1978) Mapping areas of Britain suitable for maize on the basis of Ontario Units. ADAS Q. Rev., 31, Winter 1978, 217-227.

HOUGHTON, J.T.(Ed) (1984) The Global Climate. Cambridge University Press. 233 pp.

KALNICKY, R.A (1987) Seasons, singularities and climatic changes over the midlatitudes of the Northern Hemisphere during 1899-1969. J. Clim. Appl. Met., 26, 1496-1510.

LAMB, H.H. (1972) British Isles Weather types and a register of the daily sequence of circulation patterns 1861-1971. Met. Off. Geophys. Mem. Vol. XVI, No. 116. HMSO. 85 pp.

LAMB, P.J. (1982) Persistence of Sub-Saharan drought. Nature, 299, 46-48.

LIVEZEY, R.E. and CHEN, W.Y (1983) Statistical field significance and its determination by Monte Carlo techniques. Mon. Weath. Rev., 111, 46-59.

MANLEY, G. (1974) Central England temperatures: monthly means 1659 to 1973. Quart. J. Roy. Met. Soc., 100, 389-405.

MILLER, A.A. (1961) Climatology. Methuen.

NICHOLSON, S.E. (1985) Sub-Saharan rainfall 1981-84. J. Clim. Appl. Met., 24. 1388-1391.

NIHOUL, J. (Ed) (1985) Coupled Ocean-Atmosphere Models. Proceedings of 16th Liege Conference on ocean Hydrodynamics (1985). Elsevier.

NORTH, G.R., BELL, T.L., CAHALAN, R.F. and MOENG, F.J. (1982) Sampling errors in the estimation of empirical othogonal functions. Mon. Wea. Rev., 110, 699-706.

OVERLAND, J.E and PREISENDORFER, R.W (1982) A significance test for principal components applied to a cyclone climatology. Mon. Weath. Rev., 110, 1-4.

QIU, G-Q and ESBENSEN, S.K (1984) Teleconnection patterns simulated by the OSU AGCM. Climatic Res. Inst. Report No. 51. Oregon State University, Corvallis, Oregon.

RASMUSSON, E.M. and CARPENTER, T.H. (1982) Variations in tropical sea surface temperature and surface wind fields associated with the Southern Oscillation/El Nino. Mon. Weath Rev., 110, 354-384.

RICHMAN, M.B. (1986) Rotation of principal components. J.Climatology, 6, 293-335.

SCHONWIESE, C-D (1987) Moving spectral variance and coherence analysis and some applications on long air temperature series. J. Clim. Appl. Met., 26, 1723-1730.

ULRYCH, T.J and BISHOP, T.N. (1975) Maximum entropy spectral analysis and autoregressive decomposition. Rev. Geophys. Space Phys., 13, 183-200.

WALKER, G.T. and BLISS, E.W. (1932) World Weather V. Mem. Roy. Met. Soc., 4, 53-84.

WALLACE, J.M. and GUTZLER, D.S. (1981) Teleconnections in the geopotential height field during the Northern Hemisphere Winter. Mon. Weath Rev., 109, 784-812.

WMO (1979) Proceedings of the World Climate Conference, Geneva, 12-23 February 1979. WMO No. 537.

WMO (1980) Outline plan and basis for the World Climate Programme 1980-83. WMO No. 540.

WMO (1983) Plan for the World Climate Data Programme. WCP-59.

WMO (1984a) Scientific Plan for the World Climate Research Programme. WCRP Pub. Series No. 2. WMO/TD No. 6.

WMO (1984b) Report of the Session of the Commission for Atmospheric Sciences Working Group on Long-Range Weather Forecasting Research. WMO Long-Range Forecasting Research Report Series No 4.

WMO (1986a) Meeting of experts on ocean-atmosphere interaction relevant to long-range weather forecasting. WMO Long-Range Forecasting Research Report Series, No. 5. WMO/TD - No.85.

WMO (1986b) Scientific plan for the World Ocean Circulation Experiment. WCRP Publ. Ser., No. 6. WMO/TD-No. 122.

WMO (1986c) CLICOM Project (Climate data management system). WCP-119. WMO/TD-NO. 131.

WMO (1987a) Report of the fifth session of the international working group on data management for the International Satellite Cloud Climatology Project (ISCCP). WCP-123. WMO/JTD-No. 161.

WMO (1987b) Report of the workshop on space systems possibilities for a Global Energy and Water Cycle Experiment. WCP-137. WMO/TD-No. 180.

WMO (1987c) Report of the sixth session of the JSC/CCCO TOGA Scientific Steering Group. WCP-141. WMO/TD-No. 199.

WMO (1987d) WMO/IOC Inter-Governmental TOGA Board Report of the first session. WMO/TD-No 216.

WMO (1988a) Validation of satellite precipitation measurements for the Global Precipitation Climatology Project. WCRP-1. WMO/TD-No 203.

WMO (1988b) Concept of the Global Energy and Water Cycle Experiment. WCRP-5. WMO/TD-No 215.

WRIGHT, P.B. (1977) The Southern Oscillation - patterns and mechanisms of the teleconnections and the persistence. Hawaii Inst. Geoph., Univ. of Hawaii HIG-77-13.

WYRTKI, K. (1975) El Nino - The dynamic response of the Equatorial Pacific Ocean to atmospheric forcing. J. Phys. Oceanogr. 5, 572-584.

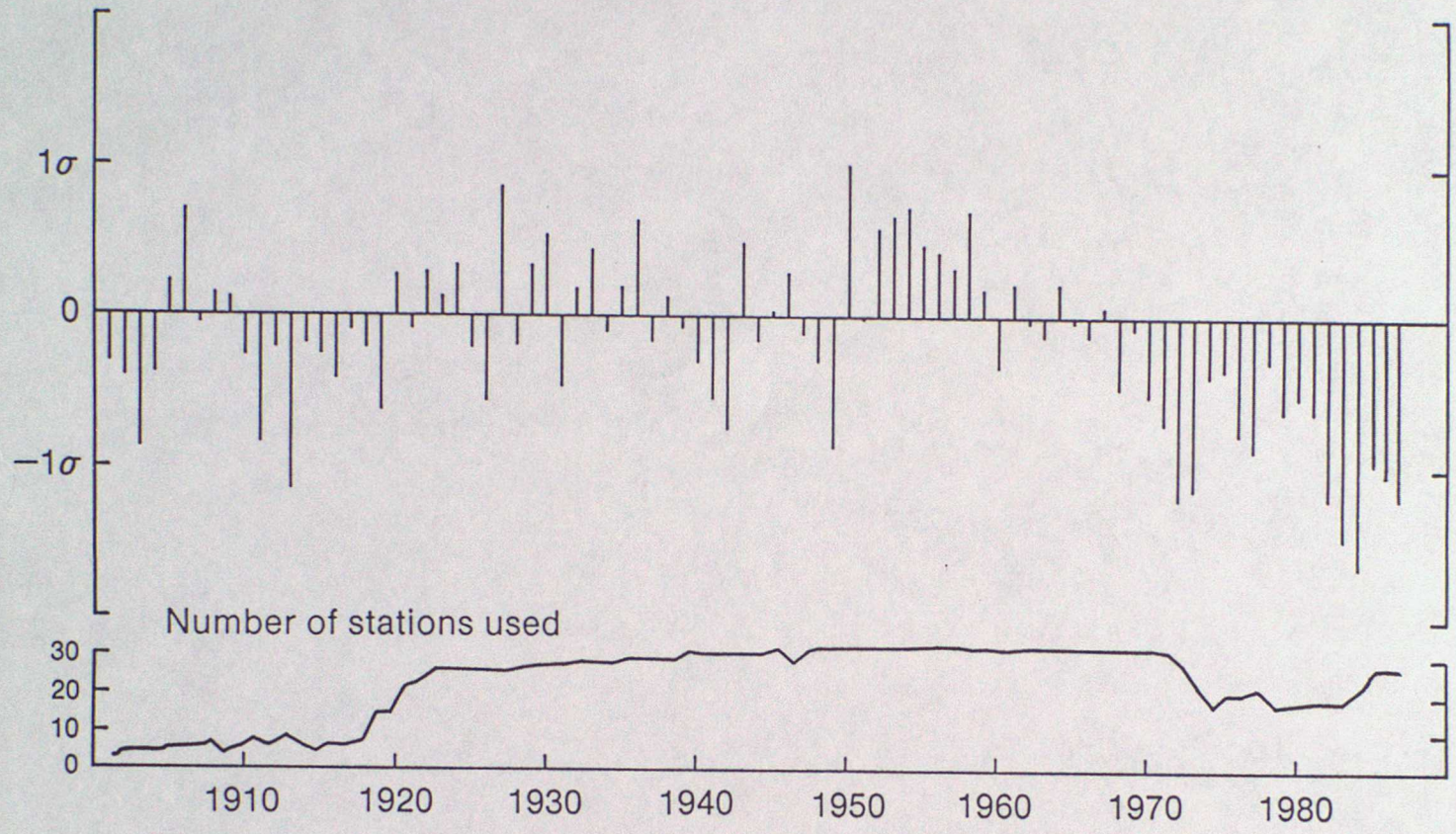

Figure 1.1 Standardised annual rainfall anomalies for the Sahel, 1901-87. Values to 1984 after Nicholson (1985): 1985-87 estimated from CLIMAT reports.

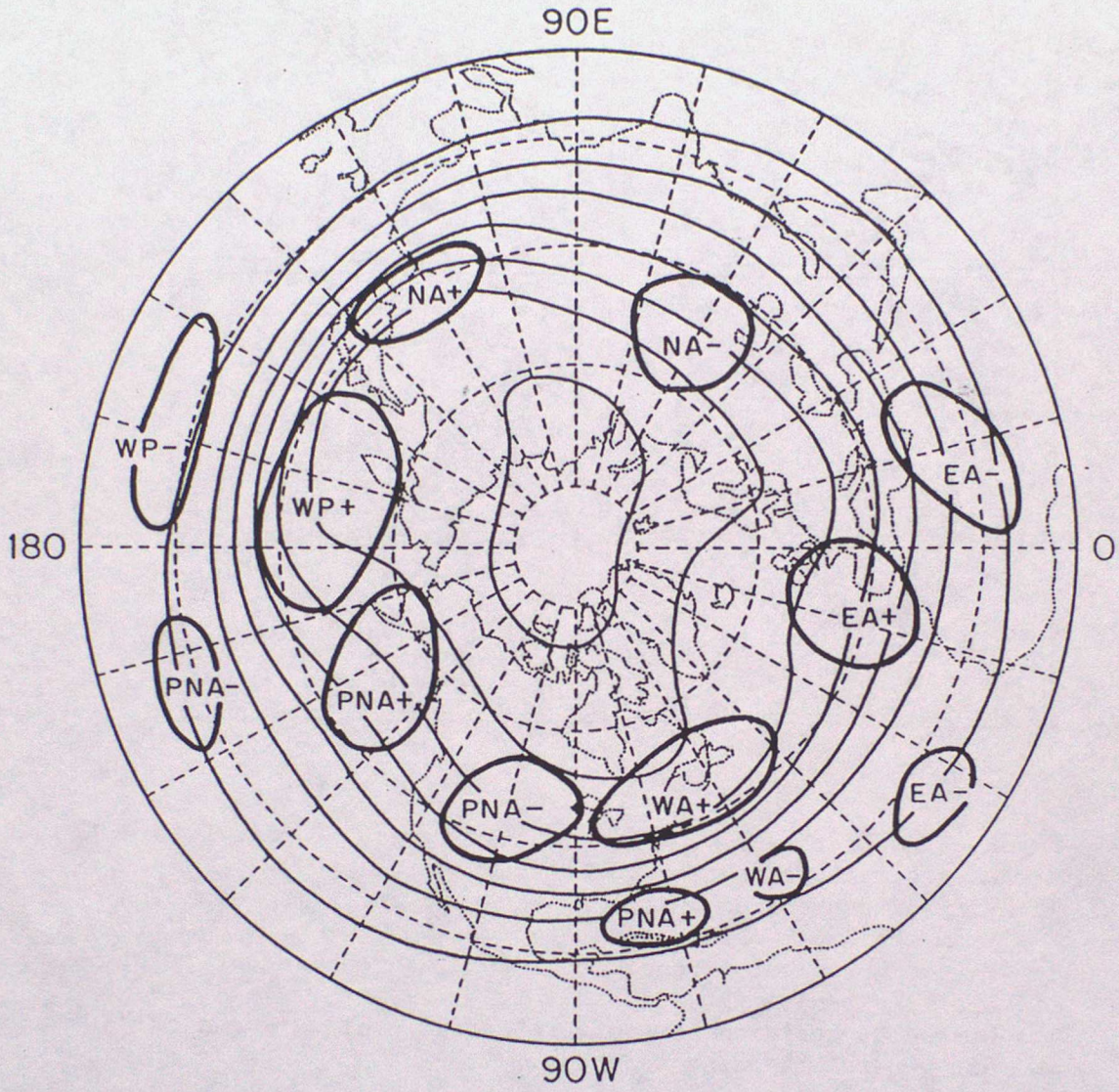

Figure 1.2. Teleconnections in Oregon State University AGCM also seen in a similar way in the atmosphere in northern winter. After Qiu and Esbensen (1984).
"PNA" : Pacific-North American pattern. "WP" : West Pacific pattern.
"EA" : East Atlantic pattern. "WA" : West Atlantic pattern.
"NA" : North Asian pattern.
The map shows the "centres of action" of the teleconnections in the simulated 400mb height field. The isopleths of the ± 0.6 correlation coefficient between indices of each of the five patterns and the 400mb height anomaly field are shown as heavy lines.

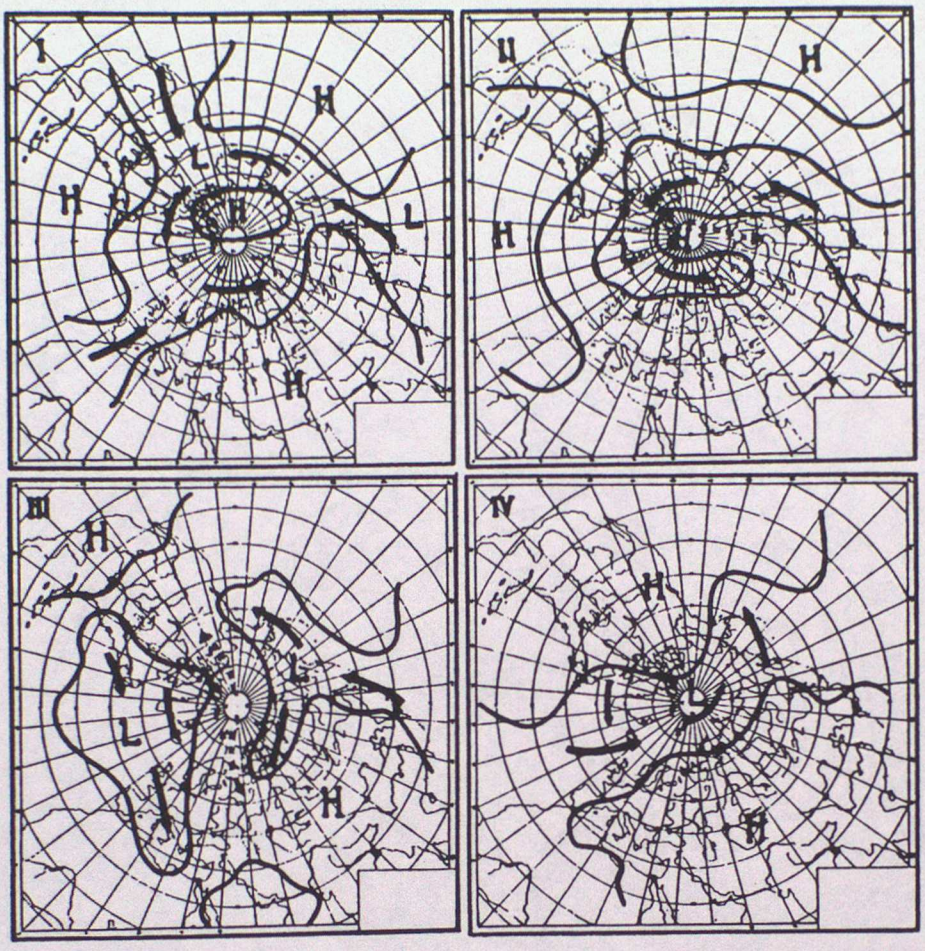

Figure 1.3 Dzerdzeevski's circulation types. (Solid (broken) arrows are cyclone (anticyclone) tracks)

I. Ring of depression tracks around pole and some advection from the South-mainly zonal type.

II. Mainly zonal but strongly meridional in one sector (i.e. blocking tendency)

III. Generally meridional-strong interchange of warm and cold air-general blocking tendency.

IV. Strog flux. of warm air toward pole in one sector with depressions moving near central Arctic (Atlantic sector favoured in Winter).

After Barry and Perry (1973)

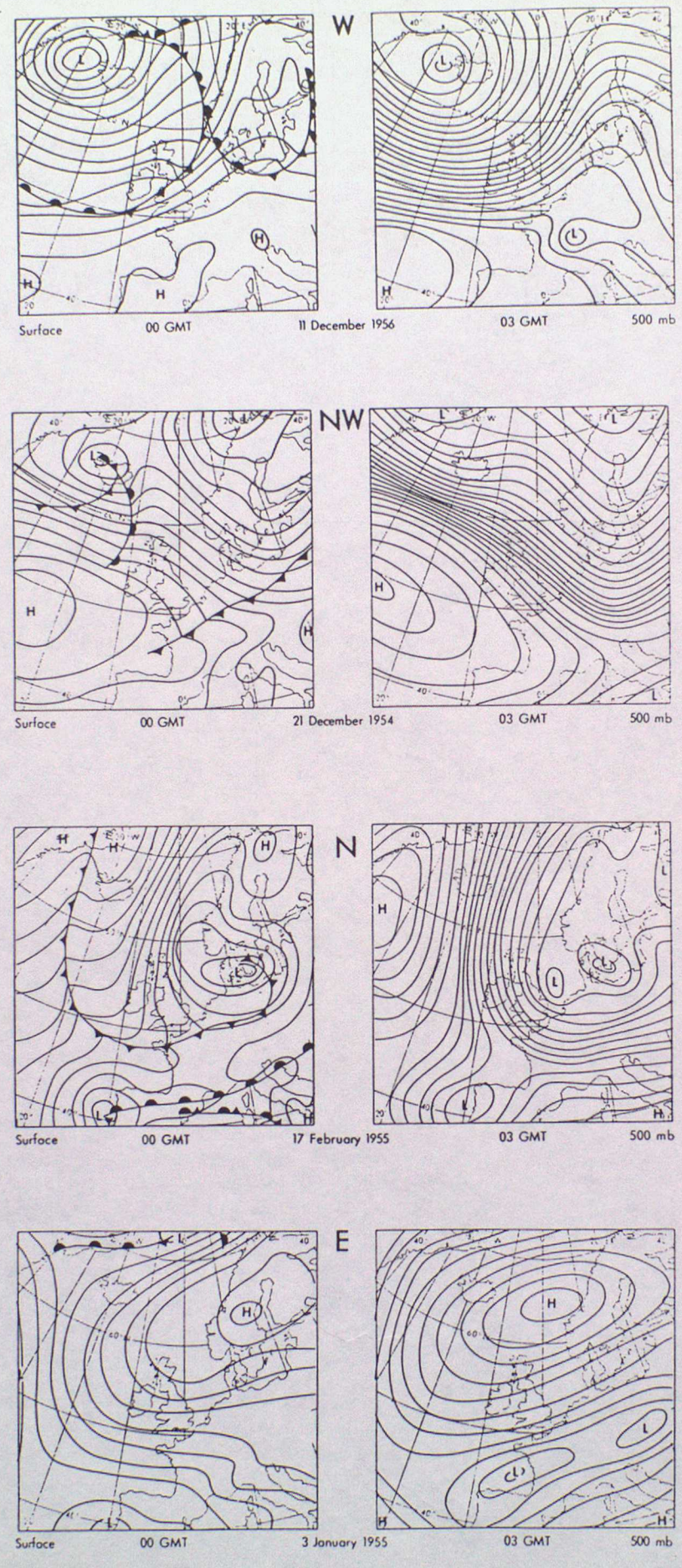

Figure 1.4. Examples of Lamb Westerly (W); Northwesterly (NW); Northerly (N); and Easterly (E) circulation types.

After Lamb (1972).

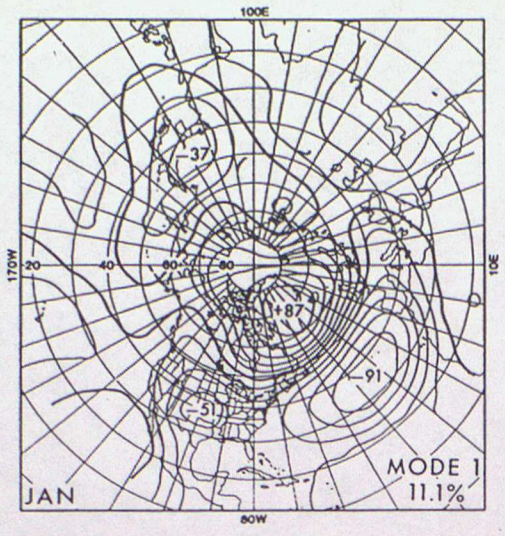

(A)

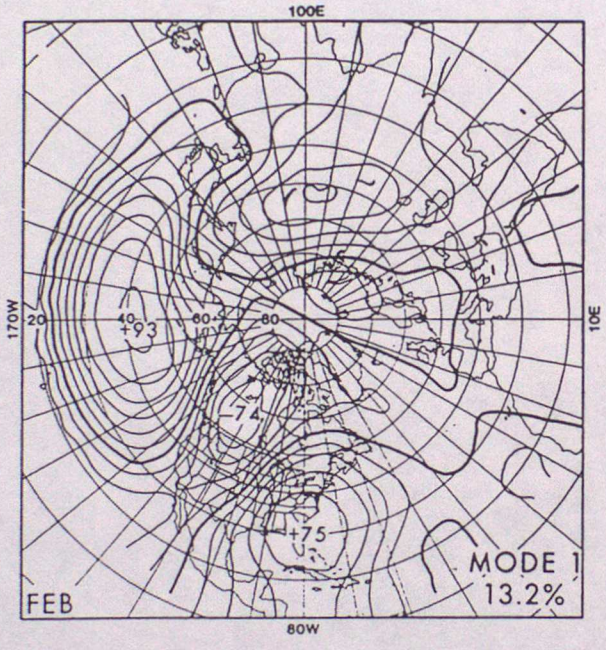

(B)

Figure 1.5. (A). The North Atlantic Oscillation at 700mb in January. This is the first principal component and accounts for 11.1% of the interannual variance.

(B). The Pacific-North American pattern at 700mb in February. This is the first principal component and accounts for 13.2% of the interannual variance.

After Barnston and Livezey (1987).

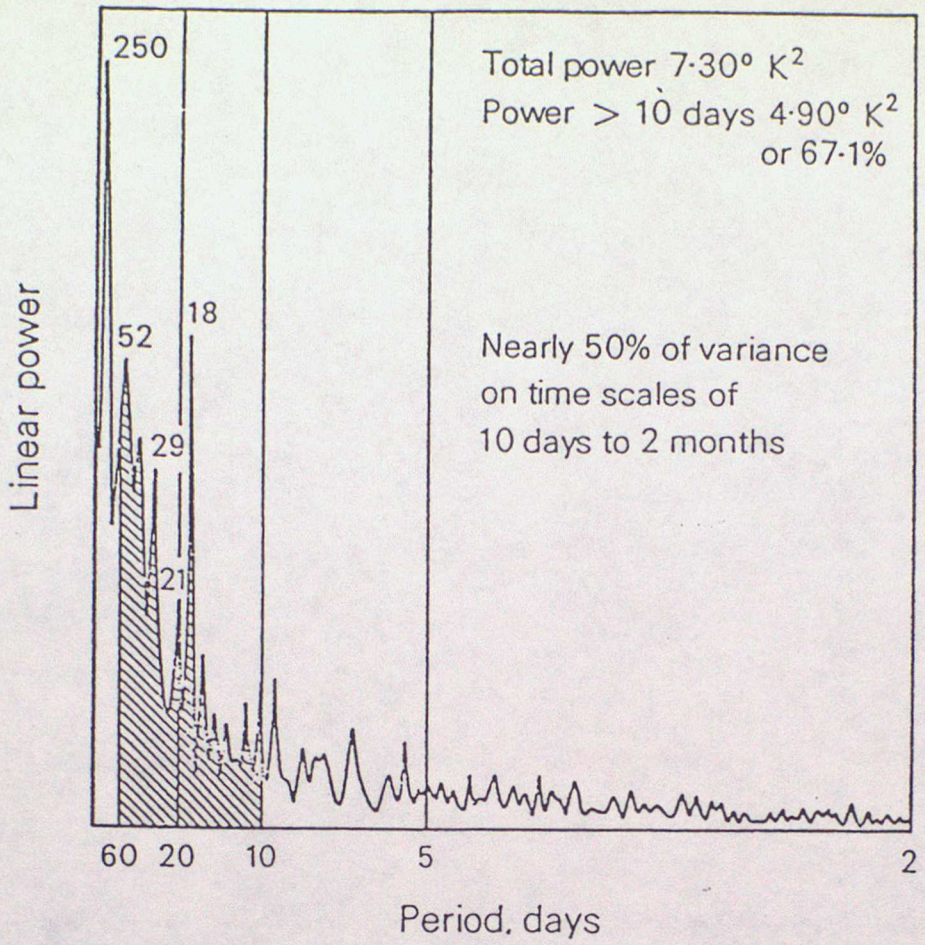

Figure 1.6 Power spectrum of daily central England temperature (1976-1980) with annual cycle removed

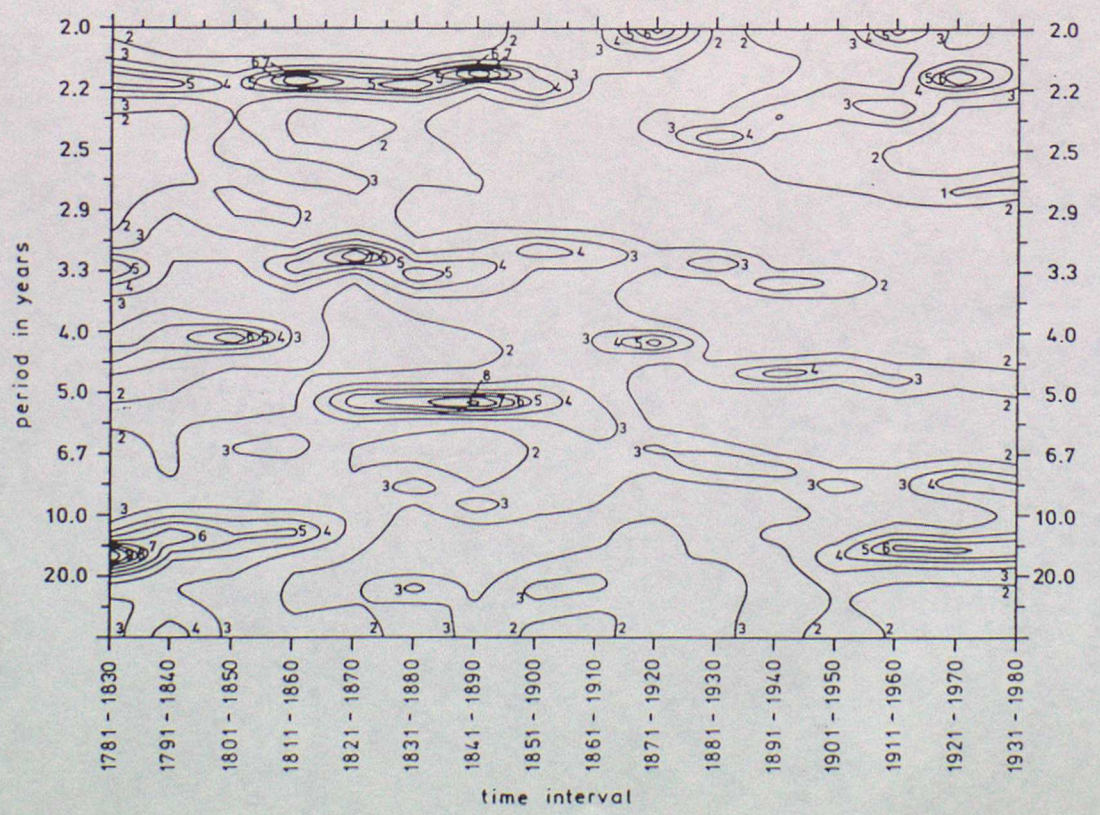

Figure 1.7 Moving maximum entropy spectrum (MESA) of the Hohenpeissenberg annual mean temperatures, 1781–1980, in 50-yr subintervals and overlapping 10-yr steps (each subinterval spectrum 15 coefficients). The numbers denote "contour lines" of the relative variance in tenths. From Schonwiese(1987).

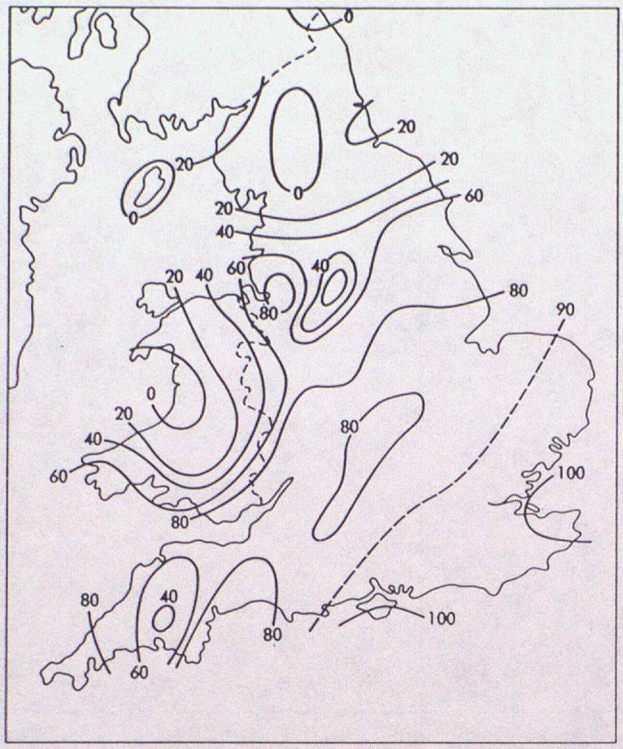

Figure 1.8 Percentage of years suitable for making Tower Silage from maize in England, Wales and the Isle of Man.(From Hough 1978.)

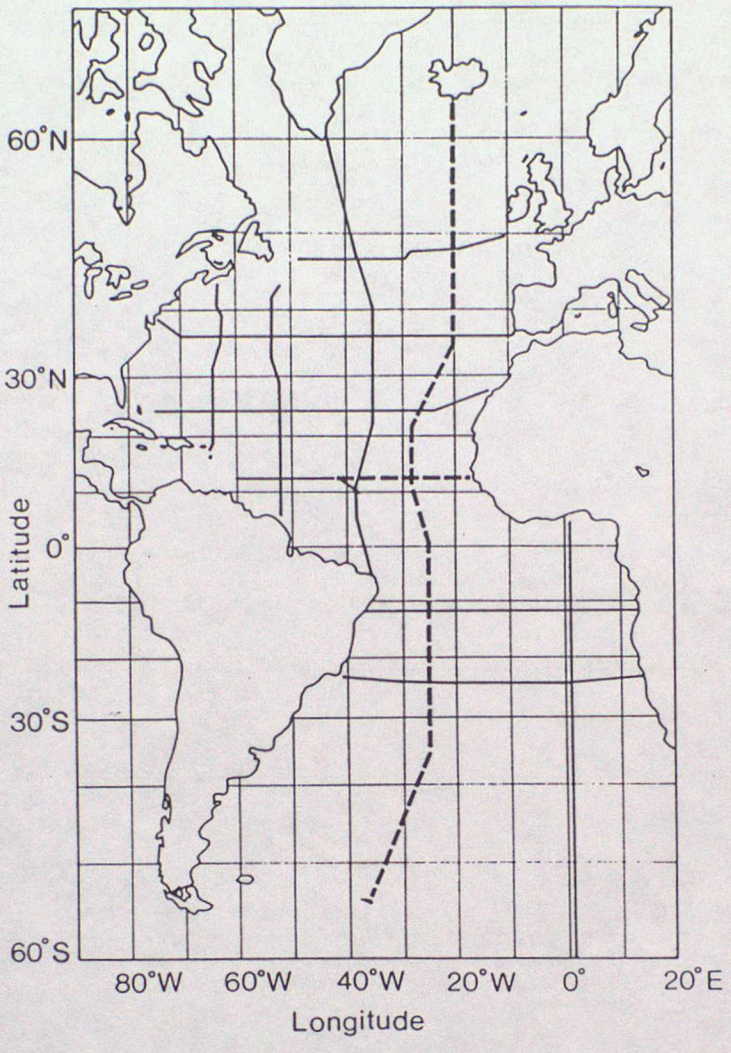

Sections planned (dotted lines) and recently occupied (solid lines) in the Atlantic through the efforts of several laboratories. The North Atlantic coverage is indicative of that required globally.

Figure 1.9

From the Scientific plan for the World Ocean Circulation Experiment (WMO (1986b)).

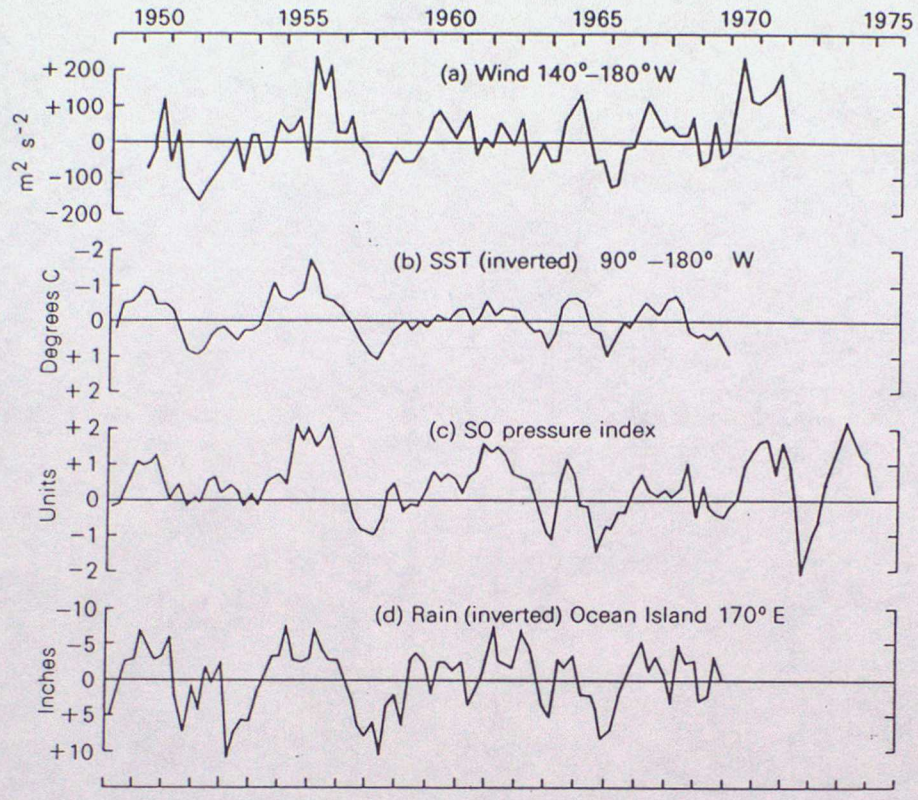

Parameters of the Southern Oscillation (after Wright 1977).

(a) Zonal component of wind stress, 4°N–4°S, 140°W–180°W, seasonal anomalies relative to 1950–69 mean (after Wyrtki 1975).

(b) Sea surface temperatures, 10°N–10°S, 90°W–180°W, seasonal anomalies relative to 1949–69 means.

(c) Southern Oscillation seasonal pressure index (southeast Pacific minus N.Australia/Indonesia).

(d) Rainfall at Ocean Island, 0°52'S, 169°35'E, mean monthly anomalies for each season relative to 1950–69 mean.

Ticks along the top and bottom margins denote northern autumn of the year immediately preceding.

Figure 1.10.

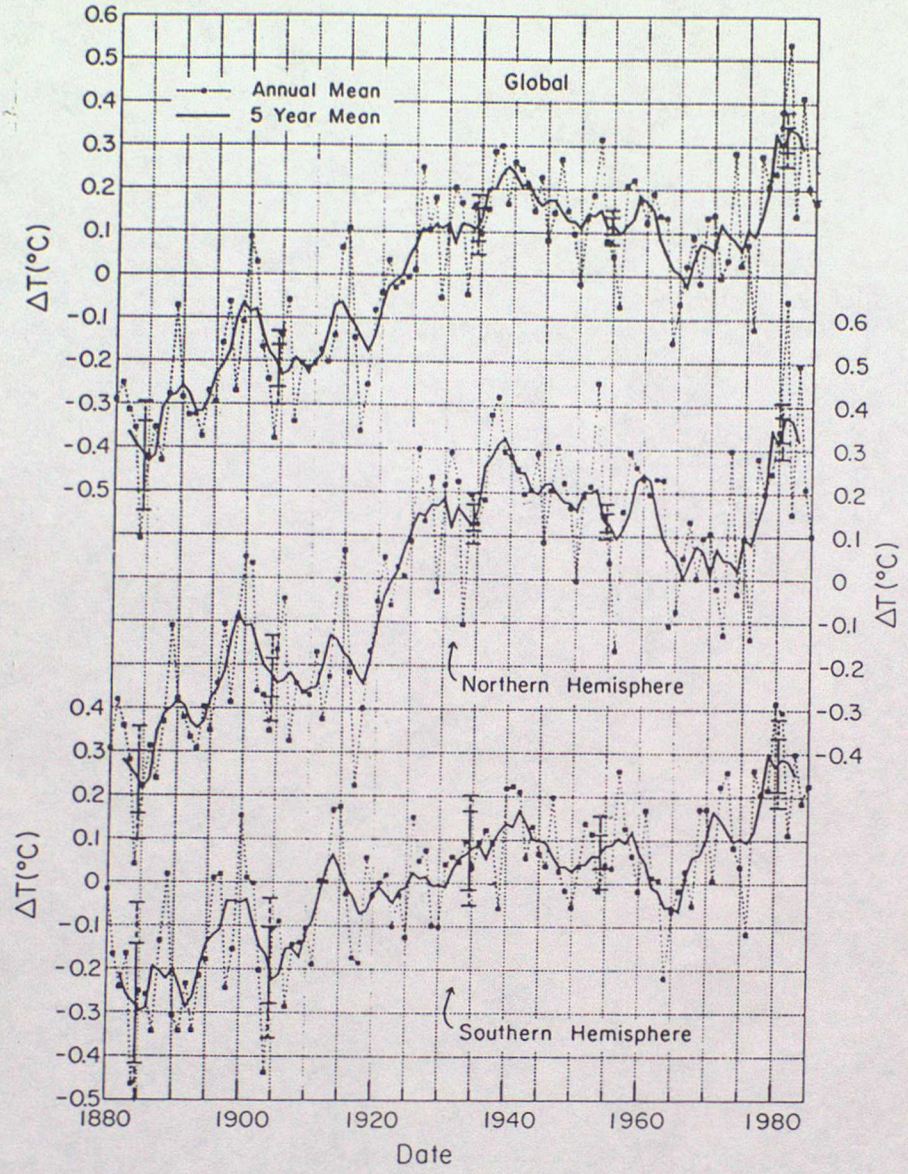

Global and hemispheric surface air temperature change estimated from meteorological station records. The northern hemisphere scale is on the right. The 5-year running mean is the linear average for the 5 years centered on the plotted year. The uncertainty bars (95% confidence limits) are based on the error analysis in section 5 of HANSEN AND LEBEDEFF; the inner bars refer to the 5-year mean and the outer bars to the annual mean.

Figure 1.11. After Hansen and Lebedeff (1987).

DESCRIPTION OF WORLD CLIMATE

C.K, FOLLAND AND D.E, PARKER

MET O 13

SUMMARY

Major features of the general circulation of the atmosphere, both at the surface and aloft, are introduced and related to thermal and topographic forcings. After a brief review of schemes for classifying regional and local climates, selected climates are described and interpreted in the light of the seasonal progression of the atmospheric general circulation and its variability. Some of the more unusual local climatic features are mentioned.

2.1 INTRODUCTION

The Met O 20 lectures have shown that ideas of a simple symmetric atmospheric circulation are far from correct but nevertheless useful. Fig 2.1A shows an idealised wind circulation for the globe, while Fig 2.1B gives a more realistic picture where the central role of the mid-latitude transient eddies is shown. Fig 2.2 is a representation of the mean meridional circulation in the Northern Hemisphere: The strong upward motion at the Inter-Tropical Convergence Zone (ITCZ), which varies in position, helps to give rise to a Hadley cell to the north, with descending motion generally around 30°N but further north in summer. A "Ferrel" cell is shown further north still: it is the net result of eddy activity in mid-latitudes on several time-scales. Finally there is a more intermittent Polar cell.

Even in the Tropics, a simple picture of dominant mean motion resulting from a Hadley cell is rather misleading: besides eddy motions, there is a substantial set of more or less east-west circulations whose east-west components are called "Walker" cells (Fig 2.3). These cells are

thought to be driven by the strong longitudinal variations of thermal forcing near the equator. The most prominent cell has a rising branch over and near the Tropical W Pacific in northern winter extending over SE Asia in the northern summer. The descending branch occurs over the relatively cool tropical east Pacific just to the west of S America. Fig 2.4 shows, from Newell et al (1974), estimates of the mean mass flux in the Walker circulation cells: the strongest mass fluxes are only a little less than those in the Hadley cells in Spring and Autumn, (Newell et al (1969)).

A partial explanation of these cells, which affect precipitation in equatorial regions very strongly, lies in the geography of tropical continents and oceans. Fig 2.5 shows the January and July climatological mean sea surface temperature (SST) (for 1951-80), largely derived from the Meteorological Office Historical Sea Surface Temperature data set (MOHSST) (Bottomley et al (1988)). In the tropical Pacific and the tropical Atlantic there is a west-east surface temperature gradient. In the Pacific, the difference in SST at 10°S between 150°E and the S American coast is about 6-7°C in January (southern summer) and almost 10°C in July. In the Pacific, these longitudinal SST differences are comparable to those between the Equator and about 30°S in the same seasons, which of course help to drive the regional Hadley circulation. Not surprisingly, convective activity is usually very weak or non-existent in the tropical east Pacific south of the Equator but this situation is apparently rather unstable and a dramatic warming of the east tropical Pacific can sometimes occur (the El Nino-Southern Oscillation (ENSO) events, Lecture 6). The result of these mean motions is that air-flow trajectories in the tropics are far different from those that could be derived from the simple picture of a meridional Hadley cell superimposed on an otherwise rather zonal circulation.

Fig 2.6 shows a map of global ocean currents which partially explain the SST variations. The currents are of course driven mainly by the pattern of surface winds (Fig 2.7). The tropical anticyclonic ocean gyres are driven by the trade-wind circulations to the equatorward and the westerlies to the poleward. These gyres are associated with strong, warm western ocean boundary currents: the Gulf Stream (GS) and Kuro Shio (KS) in the Northern Hemisphere, and in the Southern Hemisphere the Brazil (BC) and

Agulhas (AG) currents (the latter off S Africa). Eastern boundary currents are cold: the Canary (west of N Africa) and Californian (CC) currents in the Northern Hemisphere and the very cold Humboldt (HC) and Benguela (BC) currents in the Southern Hemisphere. So it is not surprising that SST is very low, for example, off Peru, though upwelling of water from below is an additional factor in all cold currents in tropical regions. Upwelling results from an off-shore Ekman drift which is driven by the prevailing off-shore winds. In the Indian Ocean, currents tend to reverse in direction with the seasons and are driven by the SW (Summer) and NE (Winter) monsoons.

2.2 SEASONAL VARIATIONS OF ATMOSPHERIC CIRCULATION

The climate of the world can only be understood by including the seasonal variations in atmospheric circulation, SST, snow and ice etc.

2.2.1 January and July pressure and wind fields

Important features in Figs 2.7-2.8 are as follows.

January - Note the subtropical highs; the low pressure trough of the ITCZ near to or south of the Equator; the intense Siberian high with surface air streaming away from it. Being a cold high, the Siberian high decreases in intensity with height and is overlain by the midlatitude westerlies. In the N Pacific and N Atlantic there are deep lows (the Aleutian and Icelandic lows).

In the S Hemisphere (Summer) the subtropical highs form an almost continuous belt, with centres over the cool oceans; heat lows dominate the three main continental land masses.

July - The northern subtropical highs are further north with considerable mean-sea level pressure (PMSL) differences between land and sea in the same latitudes; heat lows exist over the southern United States, the Sahara, and, most prominently, southern Asia. The Icelandic low is still present but rather weak, but there is now very little sign of the

Aleutian low, the east Pacific high being placed surprisingly far to the north. Fig 2.7 shows that the ITCZ moves further away from the Equator over land than over the oceans. Being largely the result of vertical convective processes, the tropical lows shown in Fig 2.8 decrease in intensity with height, unlike the Iceland low, which merely slopes to the west with height.

Note that the ITCZ lies where the trade winds meet. When this is far from the Equator, the air that crosses the Equator turns southwesterly in direction because of the change in direction of the Coriolis force though a westerly component sometimes develops before the Equator is crossed, eg over the Indian Ocean in July. Fig 2.9 shows that the picture of a single ITCZ moving North over the Indian Ocean in summer is far from correct. The apparent double ITCZ structure, if that is what it is, is poorly understood but is the subject of current research. The double structure is visible in the vertical velocity field for northern summer presented by Savijarvi (1988). A possible explanation is that individual zones of tropical convergence tend to occur above individual absolute SST maxima if those maxima exceed about 27-28°C (Gadgil et al (1984)). On Fig 2.5 for mean July SST, there is a suggestion of a SST maximum near the southern of the two convergence zones as well as a further SST maximum adjacent to the coast of the Indian sub-continent.

2.2.2 Upper level flow

2.2.2.1 Tropics and Sub-tropics

Figs 2.10 and 2.11 show the 850 mb and 200 mb streamlines during Dec-Feb and June-Aug. At 850 mb, the anticyclonic centres over the oceans are clearly seen in both seasons, overlain by a strong westerly flow at 200 mb. In June-Aug a strong warm anticyclonic centre is seen at 200 mb over N India/Tibet, with cyclonic motion at 850 mb. This vertical structure is the result of convective heating over N India and heating of the very elevated Tibetan plateau (height 4000-5000 m) resulting in a high-level warm anticyclone over this region; this gives rise to a strong 200 mb easterly flow to its south which extends all the way from the tropical W

Pacific to the tropical Atlantic. At the surface, the flow is mainly westerly. Over coastal W Africa from the equator to Senegal Fig 2.7B indicates a south westerly flow at the surface though at 850 mb Fig 2.10 suggests a generally south-easterly or anticyclonic flow. A problem in this region (see section 2.5.1 and Lecture 5) is that interannual and longer time scale variability has been very large in recent decades so different, rather short, data periods may give different results. In the Southern Hemisphere in Dec-Feb, a monsoon-like heat low over S Africa at the surface (cyclonic centre marked C in Fig 2.10) is overlain by a warm 200 mb anticyclonic centre; there is a similar feature over the Bolivian Plateau. To the north and north east of the latter feature, there exists strong mean 850 mb north westerly flow over W Brazil and Bolivia which is evident there and further southeast in June-Aug. This north-westerly tropical circulation is thought to depend on the fact that the Andes form a sharp physical western barrier to flow over these regions (Schwerdtfeger (1976)). This is the only tropical region in the S Hemisphere where low level tropical north westerlies are common, except perhaps near Papua-New Guinea in northern winter.

2.2.2.2 Mid-latitudes (500 mb)

Figs 2.12A,B from Palmen and Newton (1969) show the 500 mb flow in the Northern Hemisphere with its attendant ridges and troughs. Here it is worth mentioning that the Southern Hemisphere 500 mb flow is more symmetrical but there is a marked tendency to a broad trough over the Southern Ocean between about 30°W and 40°E. This feature is associated with long-term SST and air temperature averages up to 5°C below the average for their latitude between 50°-60°S (Hoflich, (1984)). Fig 2.13 shows the mean Southern Hemisphere 500 mb flow in January (summer). Between about 40°S and the South Pole, mean 500 mb flow is of similar strength to that in the Northern Hemisphere winter in a similar latitude band (which of course includes the same month, January). In the Southern Hemisphere the strength of the flow in local winter hardly changes from that in summer because the surface temperature gradient between equator and pole scarcely alters through the seasons.

2.3 MEAN SEASONAL SNOW AND ICE VARIATIONS

Ice and snow are an important feature of the mean seasonal variation of climate (Fig 2.14A). Taken together, the regions of permanent sea and land ice in the Northern Hemisphere are currently slightly smaller than those in the Southern Hemisphere, but the maximum seasonal extent of ice and snow in winter is much larger in the Northern Hemisphere. Sea ice around Antarctica fluctuates from a typical minimum extent of 2.5×10^6 km^2 (Feb/March) to a typical maximum of 15×10^6 km^2 (September) (note that the area of Antarctica itself is 14×10^6 km^2). Over the Northern Hemisphere the typical minimum extent of sea ice is about 8×10^6 km^2 (September) with an additional 1.8×10^6 km^2 of land ice contributed by Greenland. However the maximum extent of ice and snow together is apparently about 55×10^6 km^2 in the Northern Hemisphere (February) (Untersteiner (1984)). There are pronounced interannual fluctuations of Northern Hemisphere snow and ice extent (see Fig 2.14B from Hahn (1981)). Reliable measurements of fluctuations in Antarctic sea ice on time scales of several years are just beginning to emerge (Chiu (1983)). Reliable satellite plus conventional assessments of global seasonal cryospheric extent only began about 1973, and there are systematic differences between climatologies based on different observing techniques (Dewey (1987)).

2.4 CLIMATE CLASSIFICATION AND WORLD CLIMATE

In one lecture we cannot attempt to cover the climate of the whole world in detail. We shall briefly discuss climate classification and then select a few main regions for discussion. We shall also mention some lesser known but perhaps thought-provoking characteristics of regional climates.

2.4.1 Climate classification

The climate of even a small area is composed of a large number of locally-varying climatic elements and it is nearly impossible for two places to have identical climates. So condensation and ordering is needed

to facilitate analysis and explanation. Classification consists of recognising important characteristics which individuals have in common and grouping the individuals into a few classes or types in order to establish generalisations.

Classifications can be based on the way climates are generated, or on their effects eg on surface vegetation or on specialised practical problems like the reliability with which maize can be grown in UK (discussed in Lecture 1). In fact applied classifications are now numerous but are usually of main interest to specific users, though as a result many useful climatic maps of extremes or the frequencies of given thresholds of rainfall amount, temperature, wind speed etc have been produced.

The generic type of classification appeals to meteorologists but it must be simple and there is a danger that the facts of climate may be forced into a preconceived and not wholly appropriate explanatory structure. Empirical classification starts from the observed facts but the basis of division can be arbitrary and its validity depends of course on the use to which it is put.

The best known empirical classification is that due to W Koppen (1931). A considerable number of Koppen's climatic types and subtypes do in fact coincide with broadscale features of the general circulation which allow the numerous and important deviations from a "standard" world pattern to be realistically highlighted. Koppen's system is known throughout the world and was the result of half a century's study and refinement. His classification is quantitative and is based upon annual and monthly means of temperature and precipitation; it accepts native vegetation as the best expression of climate so that many of the climatic boundaries are selected with vegetation limits in mind. It recognises that plant development depends on available water as well as on temperature so that precipitation and evaporation are included in the classification scheme. Because evaporation measurements are not usually available, evaporation is estimated from temperature and precipitation. Many authors have proposed modified schemes based on Koppen's scheme; they mostly differ in the method of expressing the available water for plant growth. Annex 1 to this

lecture describes Koppen's scheme in detail and has been taken from Lamb (1972). It is interesting that Koppen's scheme has already been used to help interpret the results of an AGCM experiment (Manabe and Holloway (1975)).

Fig 2.15 shows a climate classification scheme due to Critchfield (1983) which is rather like a simplified version of Koppen's or Trewartha's system, and we shall use Critchfield's scheme as a background for our description of world climate. Three main climatic classes are defined (subjectively, not rigorously) in terms of monthly mean temperatures, basically according to freedom from frost and the length of the growing season, with an extra highland climate class which includes all temperature classes and can occur anywhere in the world. Arid climates are a subgroup of the three main types where precipitation is less than potential evaporation. Like most schemes, Critchfield's scheme subdivides classes according to whether or not there is a dry season and when in the year it occurs (except for highland climates). Fig 2.16 shows a map of mean annual world precipitation which provides a useful background to the following description.

2.5 DESCRIPTION OF SELECTED WORLD CLIMATES

2.5.1 Tropical climates

Consider first the air flowing around the oceanic cells of the sub-tropical high pressure belt centred about 25-35°N and S. The air flowing toward the equator on the eastern side of the cells and not far from the latitude of the centre of the cells is stable and dry, and subsides strongly because of the large-scale divergence caused by the Hadley cell. This gives rise to a low level temperature inversion (Riehl (1979)) (Fig 2.17). As a result, the eastern half of the sub-tropical oceans has fairly dry and sometimes sunny climate so that islands such as the Canaries tend to be arid, though orographic precipitation on high mountains can be considerable. The subsidence also gives rise to extremely

arid coastal regions on the western sides of the continents in latitudes 20-30°N and S such as the Kalahari and Chile-Peruvian deserts and the western margin of the Sahara.

The dry Equator-ward moving air picks up heat and moisture from the sea, so that the trade-wind inversion steadily weakens and rises as the air turns more and more to the west. The air beneath the Trade-wind inversion becomes deeper and more unstable and increasingly subject to convection. Riehl shows theoretically and from observations that the trade wind inversion is not a physical barrier: sinking and diverging air from above descends through the inversion as shown in Fig 2.17, the descending motion being forced by the large scale divergence around the high pressure cell. The descending air is heated and moistened from below as it sinks; thus the inversion rises as more air is incorporated beneath it. The air becomes quite rapidly warmer and moister because sea temperatures also tend to rise towards the western halves of the tropical oceans.

As the air approaches the Equatorial trough of low pressure, it meets the corresponding flow from the other hemisphere and is subjected to strong convergence and lifting, and so creates the great deep convective cloud systems of the ITCZ. Although the Trade Winds are mostly dry, fair-weather winds on the eastward sides of the high pressure cells, their Equatorward and western sectors are subject to synoptic-scale disturbances including tropical storms in the western sectors if SST is high enough and the latitude exceeds about 8°. So the amounts of cloud and precipitation in the west are considerably greater though most rain falls near the ITCZ itself. Much of the latent heat energy released in the upward branch of the Hadley cell re-enters the lower atmosphere well away from the Equator and a considerable amount of this energy is conveyed back towards the Equator by the trade winds (thus the trade winds tend to "heat the equator"). Upward motion in the region of the ITCZ is confined at any one time to small areas concentrated in mesoscale convective systems which have a bewildering range of sizes which are poorly understood. The ITCZ follows the annual path of the vertical midday sun but moves much further in some longitudes than in others, tending to move most over continents. So a fundamental division of tropical humid climates is between those regions

near the Equator which have considerable rainfall all the year round (tropical wet climates or equatorial rain climates) and those regions which have a pronounced dry season in the local winter when the ITCZ has moved well away or even into the other hemisphere so that the region is subject to subsidence from the sub-tropical anticyclone (tropical wet and dry climates).

This difference of climate has a great influence on vegetation and differentiates the jungles, the hardwood forests and swamps of the Congo, the Amazon basin, south east Asia and parts of Central America from the lighter more deciduous forests and tree studded grasslands often called savannah which are typically located to the north and south of the equatorial region. Good examples of savannah exist in South Central Brazil, northernmost South America and in tropical Africa. It is not certain whether the existence of savannah is always caused by drought conditions in winter or whether it is caused by the frequent fires that sweep the grasslands and from which trees do not recover. It is interesting that man himself in recent centuries may have inadvertently created apparently natural savannah. New savannahs are now being deliberately created, especially around the edges of the Amazon jungle.

Much work on the General Circulation and climate concentrates on the tropical and equatorial zone: this is the major source of energy for the atmosphere and it covers about 40% of the world. It is also one of the zones about which least is understood. It was once thought that tropical climates were simple and followed regular patterns but this is now known to be far from correct. Most importantly, the physical details of the climates are not easily explained, especially their tendency to pronounced inter-annual variability.

Africa probably provides the best examples of the expected arrangement of the climatic zones of the tropics, and we shall look at the structure of the atmosphere over West Africa where the arrangement of the climatic zones is simplest. Please refer to Figs 2.7, 2.8, 2.10, 2.11 and 2.18 and note the following:-

a. The Southern Hemisphere south east Trade Winds cross the Equator to become moist south westerlies (sometimes called "monsoon" air). (Fig 2.7B).

b. The north east Trade Winds over the Sahara originate from near the Mediterranean (and their specific humidity is fairly low). (Fig 2.7B).

c. The ITCZ does not normally move south of the Equator in the longitude of W Africa even in winter because the tropical S Atlantic Ocean is relatively cool. This means that the Gulf of Guinea coastal region is wet in the northern winter.

d. Further east in tropical Africa, the behaviour of the ITCZ becomes more complex especially in Ethiopia, Kenya and Uganda. It is much affected by the high mountains and plateaux of this region and in summer by the Indian monsoon circulation. So this is a poorly understood region - one of the earth's "problem climates".

The vertical structure of the atmospheric flow in the tropical W African region in August and some of its interannual variability is shown as a function of latitude in Fig 2.18A and B (Newell and Kidson (1984)). These diagrams show the zonal and meridional components of the wind through the depth of the atmosphere for two sets of recent years. In one set the Sahel region (Region 5 south of the Sahara desert in Fig 2.15) was wetter than normal and in the other set it was drier than normal. Referring to Fig 2.11, we would expect to see, north of about 5°S, fairly strong upper level easterlies extending from the Asian monsoon circulation. These easterlies are clearly present in both sets. In the years marked wet, the upper easterlies are slightly stronger than in the years marked dry but the sample is too small to be sure of the significance of this. Lower down, there is a pronounced easterly jet near 700-800 mb near 15-20°N which is more pronounced in the dry years. This result is probably due to an enhanced low-level thermal gradient between the relatively cool wet regions near the coast and the more than usually dry region of the North Sahel.

This anomlous dryness should give rise to more sensible heating of the ground and thus the lower layers of the overlying atmosphere should be warmer. A low-level south westerly flow is evident in both wet and dry years between 10°S and 20°N but is markedly less deep and certainly is less strong in the dry years. In fact the ITCZ annually reaches 20-22°N where practically no rain falls; the boundary between the northerly and southerly components of the flow near the ground in August does not seem to vary greatly between wet and dry years. However Fig 2.18B suggests that the flux of warm, moist air from the S Atlantic is weaker in the dry years. In Lecture 5 we present recent research into climatic variability in sub-Saharan Africa in fuller detail.

The detailed mechanisms of rainfall release near the ITCZ are complex and ill-understood but certainly are not solely accomplished by the random occurrence of isolated thunderstorms. Fig 2.19 and 2.20, taken from Hastenrath (1985) quoting Reed et al (1977), show a composite of organised synoptic disturbances, known as "easterly waves", observed during GATE (The GARP Atlantic Tropical Experiment of 1974). When viewed from a satellite, easterly waves can look like a very large mesoscale "cloud cluster" (Fig 2.20C and D) though there are other types of cloud cluster. In Fig 2.19 the surface winds are southerly to the south of the trough line and north easterly to the north, and there is a cyclonic circulation at 850 mb and a trough at 700 mb. The low-level convergence indicated by Fig 2.20A is accompanied by ascent, and by divergence in the upper troposphere (Fig 2.20B). Diagrams of seasonal mean conditions like Fig 2.18A and B are the net result of many individual synoptic features.

Referring back to Fig 2.15, we can see several nearly parallel climatic zones in W Africa. Zone "4" is the western Sahara desert where rainfall is always rare; zone "5" is the Sahel which is placed north of about 10°N in the west of W Africa but which tends to be located a few degrees to the south further east. The Sahel depends, as discussed above, for its rainfall on the northward movement of moist air south of the ITCZ into the region in July-Sep. See also the analysis of water vapour transport presented by Cadet and Nnoli (1987), but note that this was based on a single year, 1979, when the First GARP Global Experiment (FGGE) was

conducted and observing networks were enhanced. Area "3" is fairly wet for most of the year as it is affected by the ITCZ, or the moist unstable air just to its south, for much of the time. The small area "5" in south Togo is sufficiently far enough south in summer to escape much influence from the ITCZ so has a summer dry season. The very wet region "2" around Liberia and Sierra Leone is an anomaly probably partly caused by local convergence due to mountains just inland from the coast, otherwise it would be like area "3". A detailed classification of West African climates is presented by Anyadike (1987).

Atypical of these latitudes is the dry zone of tropical East Africa near the Indian Ocean coast that stretches from about 4°S to at least 10°N. This region has been the subject of much study. The Indian (northern summer) monsoon flow strongly affects this region and the moist easterlies experienced by other continental eastern margins near the equator are replaced by a south-south westerly flow that seems to be relatively dry but does not extend very far inland. This "Somali low-level jet" is described and discussed by Hastenrath (1985). The lack of rain in northern Somalia in the northern summer may result from the influence of the strong seasonal upwelling of cold water offshore near 10°N during the Indian south westerly monsoon season (Bottomley et al (1988)), in addition to the influence of the dry southerly airflow and (Flohn (1987)) topographically-induced divergence. The lack of rain in the south Somalia/Kenya desert region in southern summer seems to be related to an airstream which is derived from an anticyclone over Arabia rather than from the warm ocean.

We shall not discuss the Indian or other monsoon in more detail: please see Hastenrath (1985). In passing one might note that much of India is classed by Critchfield (1983) (Fig 2.15) as a tropical wet and dry climate though the dry season on much of the mountainous west coast is short and there is enough soil moisture during the dry months to support tropical rain forests. The true tropical wet climate starts further east in Burma and Malaysia. A typical example of this climate is also enjoyed by Belem at the mouth of the Amazon. The mean temperature of every month is close to 26°C while average monthly rainfall varies between about 100 and 450 mm. Sunshine averages 5.5-6 hrs a day. So even here a short dry

season exists and in fact only restricted areas of the equatorial regions have a uniformly wet climate eg in the western Amazon basin and in western Colombia on the other side of the Andes north of the Equator. This remarkable climate, which is hardly understood, is uniformly extremely wet; Fig 2.21 shows daily rainfall for a station in western Colombia for the year 1928 which totalled 7089 mm and was remarkably uniformly distributed through the year. By contrast there is a small, heavily populated, dry area in NE Brazil (the "Nordeste") (Fig 2.22) whose climate is again ill-understood but which is being intensively studied (Lecture 5: see also Hastenrath et al (1984); Kousky (1985); Sikdar and Elsner (1987)). Much hardship is quite regularly caused here by drought.

Turning to an ocean climate, the "desert islands" just south of the Equator in the central and eastern Pacific, stretching from near the dateline to the Galapagos Islands, represent one of the most extraordinary of world climates. These islands stretch a quarter of the way round the world and owe their unusual dryness to the fact that a cool sea is normally maintained by the wind circulation so that the ITCZ is almost always north of the Equator. The cool sea near the Equator seems to be maintained by Ekman divergence. However, every few years the sea becomes very warm and the ITCZ moves over the area for much of the high-sun season, giving intense convective activity. Indeed the tropical sea surface temperature maximum, viewed in the north-south direction, tends to move over the islands. Average yearly rainfall totals of 500-700 mm are quoted for many of the islands but this hides the fact that in dry years perhaps only 50-150 mm of rain falls and in the few wet years there may be as much as 2500 mm. These fluctuations are now known to be intimately related to the El Nino-Southern Oscillation (ENSO) phenomenon which happens sufficiently often that these islands could be truly said to have a bi-modal "almost intransitive" (Lorenz (1968, 1970, 1975) non-seasonal climate (see Fig 1.10 in Lecture 1, and Lecture 6).

Before leaving the tropics, we might note some interesting features of highland tropical climates. Tropical glaciers are surprisingly numerous eg there are many in the tropical Andes, several in Africa in the Ruwenzori Mountains of Uganda and on Mounts Kenya and Kilimanjaro above about 4500 m.

Surprisingly there is even a 7 km^2 ice cap in the Star Mountains of W Irian, Indonesia, known as the Caarstenz Glacier (McAlpine et al (1983)). This glacier exists at a height of about 4500-5000 m despite being surrounded by the warmest SST in the world. However at about 15°-25°S in the Andes no glaciers are found at these or even much higher levels. The determining factor here is lack of precipitation and lack of cloudiness so only very small glaciers are found above 6000 m. By contrast in the cloudy Andes of Ecuador near 0° one glacier extends down to almost 4300 m. Many tropical glaciers are slowly receding and may not be in equilibrium with the current tropical climate.

2.5.2 Subtropical climates

2.5.2.1 Mediterranean climates

On the western margins of the continents in both hemispheres there are regions where summer is dominated by the anticyclones of the desert zone (ie the descending branch of the Hadley circulation); these anticyclones are particularly stable being on the eastern cool sides of the subtropical oceanic circulation. However in winter these areas come under the influence of mid-latitude travelling cyclones and are consequently much wetter with changeable weather. These are the areas of Mediterranean climate, characterised by (1) a concentration of the year's rainfall in winter and sometimes in autumn, while the summers are mainly dry, (2) they have warm to hot summers and mild winters, (3) there is abundant sunshine especially in summer. The five regions where the Mediterranean climate occurs are fairly similar in latitude: the border lands of the Mediterranean Sea stretching for 2500 km into Eurasia, the coastal strip of central and southern California, central Chile, the south western tip of Africa and parts of southernmost W Australia, S Australia and Victoria.

In California and Chile the Mediterranean climate ends abruptly at high mountains 100-300 km inland with mountain-induced desert on the eastern side. The remaining continents of the S Hemisphere only just reach the appropriate latitudes while the Mediterranean Sea itself acts as a

cool-season convergence zone and route for winter depressions. In this respect the Mediterranean is different from the other areas and some of these winter depressions penetrate well into Asia.

It might be thought that Mediterranean summer climates would always be hot but in coastal S California and Central Chile cold offshore currents (see Figs 2.5 and 2.6) keep coasts 10°C or more cooler than inland and more than this by day. The coasts have frequent fogs and low stratus and strong sea breezes set in because of the contrast in afternoon temperature with the hot interior. In the poleward parts of these regions occasional winter frosts occur and as the winter of 1984-5 showed on the French Riviera, snow may on rare occasions reach down to the coast. (Eastern Spanish beaches in January 1963).

2.5.2.2 Subtropical Eastern sides of continents

The subtropical eastern sides of continents receive, in summer, unstable or neutral tropical maritime air because subsidence in the subtropical anticyclone on the western side of the oceans is weak and the atmospheric boundary layer is moist. This favours convective activity and abundant summer rain aided by the development of tropical storms, some of which gain the structure of mid-latitude depressions as they pass over or near these regions. There is also a tendency for monsoon circulations to develop, especially in south east China and to some extent in the south east United States. This climate is also represented in all 3 southern continents, ie S Brazil, East Australia and SE South Africa. It differs from the Mediterranean type by having tropical humid climates on its equatorial flank, instead of tropical hot dry climates. These tropical humid regions provide a source of sultry heat in summer rather than the dry heat that exists adjacent to the Mediterranean climates.

In the N Hemisphere, a severe continental climate exists on the poleward flank of the subtropical eastern continental climates which can bring intense cold in winter for brief spells. For example, Nanking in eastern China at 31°N has occasional severe snow storms and frequent frosts in winter. Even further south, in N America, occasional very low night

minima are a feature of the climate of central and northern Florida. Summers are hot, the monthly mean temperature averaging 24-27°C or slightly higher, with high accompanying humidity from the dominating tropical maritime air, giving rather oppressive nights. Annual rainfall is relatively high (1000-1500 mm is typical) and tends to be concentrated towards the summer and autumn seasons, when tropical cyclones are most frequent and when cold fronts moving from the north-west can give very heavy precipitation, especially in USA.

The subtropical area of south east Asia has a complicated, ill-understood, climate. In winter the subtropical branch of the jetstream flows around the southern slopes of the Himalayas, while the polar-front jet flows to the north of the Tibetan plateau; both meet in an upper convergence zone over China (Fig 2.10). This upper convergence zone leads to subsidence over inner China and therefore to generally fine weather in winter. The two jet streams tend to reinforce each other over Japan, forming part of the very strong E Asian trough and giving extremely high wind speeds which can regularly reach 100 m/sec at the 200 mb level. In summer the subtropical jet stream moves to the north of Tibet and the polar front jet recedes further north so that the upper convergence zone over China disappears. In Japan an early summer rainfall maximum occurs, the "Bai-U" rains, followed by a later summer maximum. A similar double rainy season occurs in southeastern China (Lau et al (1988)). Fig 2.23 gives a schematic picture of the surface wind fields over SE Asia in summer (SW monsoon) and in winter (NE monsoon).

2.5.3 Mid-latitude climates

2.5.3.1 General Discussion

These are dominated by the influence of the upper westerlies and their attendant troughs and ridges, and on the western sides of the continents the surface westerlies are also very prominent. So the natural subdivision is into maritime and continental climates. The maritime climates are found on the extreme western sides of N America, over much of Europe, and in the S Hemisphere in Southern Chile, in Tasmania and over most of New Zealand.

Truly continental climates are found (in the N Hemisphere) either well inland or on the eastern sides of the continents where extreme seasonal variations of temperature result from their leeward location and the influence of summer monsoonal wind systems. Patagonia in Southern Argentina has some of the characteristics of an eastern mid-latitude climate but the continent is too narrow for the temperatures to be extreme while the influence of the Andes renders the climate extremely dry.

The mid-latitude oceanic climates mostly lie poleward of 40° and stretch well towards the poles because of the influence of ocean currents which are warm or relatively warm for their latitude. In N and S America, the Rockies and Andes cause the climates to occupy very narrow belts only 200-300 km wide with an extraordinarily rapid transition zone to dry climates to the east. For example in parts of Northern Oregon and S Washington states the transition from the mid-latitude oceanic to the inland dry climate can be accomplished in a day's walk. The major characteristics of this oceanic climate are cool summers, mild winters, changeable weather, considerable cloudiness, and mostly adequate rainfall at all seasons. The seasonal emphasis in rainfall tends to be towards late autumn and winter on the extreme western margins, and late summer and early autumn further inland. Over north west Europe, there is a tendency for late spring to be driest, due to a peak frequency of blocking anticyclones at that season. Nevertheless seasonal rainfall deficiency does not cause a dormant period for plant growth.

Unusual aspects of the mid-latitude oceanic climate include the rather dry summers in the north west United States, probably caused by the northerly extension of the N Pacific high over the Gulf of Alaska, and the exceptionally mild winters over large areas of W Europe and the coastal fringe of Norway beyond the Arctic Circle, caused by the openness of these regions to the warmth of the eastern N Atlantic. The oceanic margins also exhibit a strong decrease of temperature with altitude and therefore in the length of the summer growing season. The tree line in NW Scotland is at only about 1000 ft, though man has removed some of the remaining trees and it sometimes appears to be almost at sea level. This very low tree line is also partly a result of the exceptional windiness of the climate.

The Chilean mid-latitude climate is one of the cloudiest in the world as frequent depressions in the stormy sub-Antarctic summers and winters (see Fig 2.13) meet the formidable, steep, highland barrier of the southern Andes. The combination of extreme cloudiness, heavy precipitation and steep mountains has created one of the most remarkable climatically-caused phenomena in the world. Fig 2.24 and Charles Darwin's words (1979 reprint) speak eloquently:- "In Eyre's Sound, in the latitude of Paris, there are immense glaciers, and yet the loftiest neighbouring mountain is only 6200 feet high. In this Sound, about fifty icebergs were seen at one time floating outwards, and one of them must have been at least 168 feet in total height. Some of the icebergs were loaded with blocks of no inconsiderable size, of granite and other rocks, different from the clay-slate of the surrounding mountains. The glacier furthest from the Pole, surveyed during the voyages of the Adventure and Beagle, is in lat 46° 50', in the Gulf of Penas. It is 15 miles long, and in one part 7 broad, and descends to the sea-coast. But even a few miles northward of this glacier, in the Laguna de San Rafael, some Spanish missionaries encountered "many icebergs, some great, some small, and others middle-sized," in a narrow arm of the sea, on the 22nd of the month corresponding with our June, and in a latitude corresponding with that of the Lake of Geneva!"

These glaciers, descending from the mid-latitude Patagonian ice-sheet, set Darwin thinking about the causes of the ice ages in subsequent pages of "Voyage of the Beagle".

The mid-latitude temperate continental climates (here defined as having a cold month under 0°C) exhibit a cold winter, with a durable snow cover, and a warm summer season, so that the annual range of temperature is large. In the maritime climate the temperature of one winter is much like that of another, but wide deviations from the normal seasonal temperature are characteristic of continental mid-latitude winters. These deviations may be as much as 10°C in extreme climates. Summer is the season of maximum rain, which is mostly convective.

A feature of some northern hemisphere mid-latitude climates is "blocking" which is a strong influence on UK weather variations. The characteristics of blocking are interruption of the prevailing westerlies, both near the surface, where easterlies usually replace them; and in the middle and upper troposphere, where the westerlies split into two branches skirting the northern and southern flanks of the blocking region. The transient eddies in these branches appear to play a major role in at least the maintenance of the block (Shutts (1986)). Fig 2.25 from Lejenas and Okland (1983) shows the longitudinal variation of blocking in the N Hemisphere. In the S Hemisphere blocking is rarer but not uncommon near New Zealand for instance. The effect of blocking on weather over a month or a season can be surprisingly large. Fig 2.26 show two contrasting "blocked" and "westerly" Januaries over NW Europe (Folland (1983)). The reasons for blocking are currently an area of much research.

2.5.3.2 Continental anticyclones

Blocking is, superficially, a result of stationary large amplitude ridges in the westerlies: anticyclones associated with the block have a warm core. In winter, however, the Eurasian and N American continents have cold anticyclones as a prominent feature of the climate: they are situated to the west of the regional climatological mean upper troughs. These cold anticyclones do not extend very far upwards into the troposphere but bring intensely cold weather to the eastern half of the continents. The Siberian anticyclone is firmly sited well away from the western seaboard and is thus relatively undisturbed by mid-latitude depressions. However the N American winter anticyclone tends to be sited over or to the east of the Rocky Mountains and it is not as stable a feature as the Siberian high, often being disrupted by depressions moving in from the west so that the winter weather of Central and Northern USA is decidedly changeable. Surges in the Siberian anticyclone can bring intense cold to Japan and even to south China (a subtropical climate) so that even maritime Hong Kong (22°N) has suffered air frost in winter.

2.5.4 Dry Climates

The essential feature of a dry climate is that the potential annual water loss through evapotranspiration at the earth's land surface exceeds the annual gain from precipitation. Thus dry climates do not have a constantly replenished ground water. Fig 2.15 shows that arid climates cover a broad latitude band and occupy a considerable part of the earth's land surface. The deserts are usually surrounded by semi-arid lands (called steppes in Asia) where rainfall is very unreliable.

2.5.4.1 Typical types of desert climate are:-

The tropical dry climates lying at about 20 or 25°N and S with their northern and southern margin at about 15° and near 35°. These climates coincide fairly closely with the subsiding branch of the Hadley cell. The deserts do not usually reach the eastern coasts of continents because in these regions the subtropical anticyclones are much less stable. There are two types of semi-arid regions around these deserts: those that lie on their equatorial side and experience rainfall at the time of high sun due to the northward progression of the ITCZ, and those that lie on the poleward side of the deserts and receive rain from the mid-latitude westerly circulation in winter. In N Africa, parts of the Atlas Mountains and Tunisia can receive 500-800 mm of rain. Typical desert rainfalls are much less (Cairo 30 mm in a year; Yuma, Arizona 80 mm; Calama, northern Chile usually no rainfall in the year). Average summer temperatures are about 30-35°C so maxima are as a rule near 40-45°C, and in the winter months a mean of 10-15°C is typical. On poleward highland margins snow may fall and lie and mean winter temperatures may be similar to those of UK but with a much larger daily range. In the Central Asian deserts, in northern Tibet, China, and parts of Mongolia winter temperatures are much lower.

2.5.4.2 West coast margins of dry climates

Here cool ocean currents strongly affect air temperature which can be as much as 10°C lower than normal for the latitude, with a small annual range. There are surprising features of these dry oceanic climates, particularly their exceptional dryness, eg in northern Chile. Lettau and Lettau (1978) have shown that along the western margin of the Chilean desert the juxtaposition of very cold sea and intensely heated land gives rise to a low level jet stream (500 m above the ground) which flows from south to north (Fig 2.27). This is considered to arise from a sea breeze type of circulation which is so strong that it persists by night as well as by day. This persistence results in a strong influence by the Coriolis force, so that the wind tends to blow northwards parallel to the coast in geostrophic equilibrium with high pressure to the west and low pressure to the east but with a sea breeze circulation cell superimposed. The subsiding component of this sea breeze component occurs over a narrow band of ocean immediately adjacent to the coast and is thought to give rise to the long thin, cloudless strip of ocean off the Chilean coast often seen on satellite photographs. So air moving in this jet undergoes a corkscrewing, helical type of motion. The additional effects, if any, of the low level jet on rainfall are not clear.

2.5.5 Climate of the South Pacific and Southern Ocean 150E-70W

This is the region least well observed but it is large in extent, covering 120° of longitude, and has some unexpected features. Figs 2.28 and 2.29 show that, in addition to the expected features which can be deduced from Figs 2.8-2.11 and 2.13, there is a zone of cloudiness and cyclogenesis stretching southeastwards from near the Equator across the whole width of the Pacific to mid-latitudes. Thus the ITCZ in the tropical W Pacific appears to be directly connected with the westerlies near Cape Horn. This "South Pacific Convergence Zone (SPCZ)" represents convergence of air between the almost permanent anticyclone near Easter Island in the eastern Pacific and the more mobile anticyclones to the east of Australia and New Zealand. Detailed studies (Fig 2.29) show that there is a high

frequency of cyclogenesis along this cloud band at least as far south as 40°S with a maximum near 150°W between about 25°S and 35°S. Of course the data are poor and details are uncertain. Some atmospheric general circulation models reproduce this feature quite well, though it has not yet been much studied even in the models. Hurrell and Vincent (1987) have, however, demonstrated the importance of the SPCZ in the energetics of the Southern Hemisphere. James and Anderson (1984) discuss a similar but less permanent feature that may exist in the S Atlantic and does exist in the ECMWF model. Streten and Zillman (1984) give an extensive description of the climate of the S Pacific Ocean.

Another peculiar feature of the southern oceans, including the S Pacific region, is that the mean latitude of the depression belt around Antarctica varies semi-annually (Fig 2.30). This fluctuation is related to a more general semi-annual variation of circulation in the S Hemisphere (Hsu and Wallace (1976)).

2.6 CONCLUSION

This long lecture has tried to show that the climate of the world and its variability is very interesting, complex and nowhere completely understood. It is a fitting subject for the World Climate Research Programme. We recommend the 15 volumes of the "World Survey of Climatology" (which include Schwerdtfeger (1976)) for those who require factual detail on specific regions.

REFERENCES TO LECTURE 2

ANYADIKE, R N C (1987) A multivariate classification and regionalization of West African climates. J Climatology, 7, 157-164.

BERKOFSKY, L and BERTONI, E A (1955) Mean topographic charts for the entire earth. Bull Amer Met Soc, 36, 350-354.

BOTTOMLEY, M, FOLLAND, C K, HSIUNG, J, NEWELL, R E and PARKER, D E (1988) Global Ocean Surface Temperature Atlas (GOSTA). A joint project of the Meteorological Office and Massachusetts Institute of Technology. In Press.

CADET, D L and NNOLI, N O (1987) Water vapour transport over Africa and the Atlantic Ocean during summer 1979. QUART J Roy Met Soc, 113, 581-602.

CHIU, L S (1983) Variation of Antarctic Sea Ice: an update. Mon Weath Rev, 111, 578-580.

CRITCHFIELD, H J (1983) General Climatology. 4th Edition. Prentice-Hall.

DARWIN, C (1979) Reprint of "Voyage of the Beagle" (p. 235). J M Dent.

DEWEY, K F (1987) Satellite-derived maps of snow cover frequency for the Northern Hemisphere. J Clim Appl Met, 26, 1210-1229.

FLOHN, H (1987) Rainfall teleconnections in northern and northeastern Africa. Theor Appl Clim, 38, 191-197.

FOLLAND, C K (1983) Regional-scale interannual variability of climate - a north west European perspective. Met Mag, 112, 163-183.

GADGIL S, JOSEPH, P V, and JOSHI, N V (1984) Ocean-atmosphere coupling over monsoon regions. Nature, 312, 141-143.

HAHN, D G (1981) Summary requirements of GCM's for observed snow and ice cover data. In Snow Watch 1980 Ed: G Kukla et al. World Data Centre A for Glaciology.

HASTENRATH, S (1985) Climate and circulation of the tropics. Atmospheric Sciences Library ASL 8, Dordrect (D Reidel Publ Co), 455 pp.

HASTENRATH, S, WU, M-C, and CHU, P-S (1984) Toward the monitoring and prediction of N E Brazil droughts. Quart J Roy Met Soc, 110, 411-425.

HOFLICH, O (1984) Climate of the S Atlantic Ocean. In World Survey of Climatology; Climate of the Oceans. Ed: H VAN LOON, Vol 15, 1-192.

HSU, C P F and WALLACE, J M (1976) The global distribution of the annual and semiannual cycles in sea level pressure. Mon Weath Rev, 104, 1597-1601.

HURRELL, J W and VINCENT, D G (1987) Significance of the South Pacific Convergence Zone (SPCZ) in the energy budget of the Southern Hemisphere tropics. Mon Weath Rev, 115, 1797-1801.

JACOBS, I (1958) Met Abh, Inst Met Geoph, Freien Univ, Berlin, 4, No. 2, 47 pp (Part I); 121 pp (Part II).

JAMES, I N and ANDERSON, D L T (1984) The seasonal mean flow distribution of large-scale weather systems in the southern hemisphere: the effects of moisture transports. Quart J Roy Met Soc, 110, 943-966.

KOPPEN, W (1931) Grundriss der Klimakunde, Berlin.

KORNFIELD, J and HASLER, A F (1969) A photographic summary of the earth's cloud cover for the year 1967. J Appl Met, 8, 687-699.

KOUSKY, V E (1985) Atmospheric circulation changes associated with rainfall anomalies over tropical Brazil. Mon Weath Rev, 113, 1951-1957.

LAMB, H H (1972) Climate Present, Past and Future. Volume 1. Methuen.

LAU, K-M, YANG, G J and SHEN, S H, Seasonal and intraseasonal climatology of summer monsoon rainfall over East Asia. Mon Weath Rev, 116, 18-37.

LEJENAS, H and OKLAND, H (1983) Characteristics of northern hemisphere blocking as determined from a long time-series of observational data. Tellus, 35A, 350-362.

LETTAU, H H and LETTAU, K (Eds) (1978) Exploring the World's driest climate. Inst for Env Studies Rep 101, Univ of Wisconsin, pp 182-248.

LORENZ, E N (1968) Climatic determinism, Meteorological Monographs, 5, 1-3.

LORENZ, E N (1970) Climatic change as a mathematical problem, J Appl Met, 9, 325-329.

LORENZ, E N (1975) Climate predictability Report of the Intl Study Conf on the Physical Basis of Climate and Climate Modelling, App 2.1, pp 132-136, GARP Publications Series No 16, WMO-ICSU.

MANABE, S and HOLLOWAY, J L (1975) The seasonal variation of the hydrological cycle as measured by a global model of the atmosphere. J Geophys Res, 80, 1617-1649.

McALPINE, J R, KEIG, G, and FALLS, R (1983) Climate of Papua New Guinea. CSIRO. Aust Nat Univ Press.

MEIER, M F (1983) Snow and ice in a changing hydrological world. Hydrol. Sci. Journ. 28, 3-22.

NEWELL, R E and KIDSON, J W (1984) African mean wind changes between Sahelian wet and dry periods. J Climatology, 4, 27-33.

NEWELL, R E, KIDSON, J W, VINCENT, D G and BOER, G J (1974) The General Circulation of the Tropical Atmosphere. Vol 2, 151 pp, MIT Press.

NEWELL, R E, VINCENT, D G, DOPPLICK, T G, FERRUZA, D and KIDSON, J W (1969) The energy balance of the global atmosphere. In "The Global Circulation of the Atmosphere", Roy Met Soc, pp 42-90.

PALMEN, E AND NEWTON, C W (1969) Atmospheric circulation systems. Their structure and physical interpretation. International Geophysics series, Vol 13, Academic Press, New York and London.

PERRY, A H AND WALKER, J M (1977) The ocean-atmosphere system. Longman, London and New York.

REED, R J, NORQUIST, D C and RECKER, E E (1977) The structure and properties of African wave disturbances as observed during phase III of GATE. Mon Weath Rev, 105, 317-333.

RIEHL, H (1979) Climate and weather in the tropics. Academic Press.

SAVIJARVI, H I (1988) Global energy and moisture budgets from rawinsonde data. Mon. Weath Rev 116, 417-430.

SCHWERDTFEGER, W (1976) Introduction to the Climate of Central and South America. In World Survey of Climatology; Climate of C and S America. Ed: W SCHWERDTFEGER, Vol 12.

SHUTTS, G J (1986) A case study of eddy forcing during an Atlantic blocking episode. Advances in Geophysics, 29, 135-162.

SIKDAR, D N and ELSNER, J B (1987) Large-scale circulation departures related to wet episodes in north-east Brazil. Quart J Roy Met Soc, 113, 567-580.

STRETEN, N A (1973) Some characteristics of satellite-observed bands of persistent cloudiness over the southern hemisphere. Mon. Weath. Rev., 101, 486-495.

STRETEN, N A (1980) Some synoptic indices of the southern hemisphere mean sea level circulation 1972-1977. Mon Weath Rev, 108, 18-36.

STRETEN, N A and TROUP, A J (1973) A synoptic climatology of satellite observed cloud vortices over the southern hemisphere. Quart J Roy Met Soc, 99, 56-72.

STRETEN, N A and ZILLMAN, J W (1984) Climate of the South Pacific Ocean. In World Survey of Climatology; Climate of the Oceans. Ed: H VAN LOON, Vol 15, pp 263-429.

TALJAARD, J J, VAN LOON, H, CRUTCHER, H L and JENNE, R L (1969) Climate of the Upper Air: Southern Hemisphere, Vol I. Temperatures, Dew Points and Heights at Selected Pressure Levels. NAVAIR 50-1C-55, Washington, DC, 135 pp.

TREWARTHA, G T and HORN, L H (1980) An introduction to climate. 5th Edition. McGraw-Hill.

UNTERSTEINER, N (1984) The cryosphere. In The Global Climate. Ed: J T HOUGHTON, Cambridge University Press, pp. 121-140

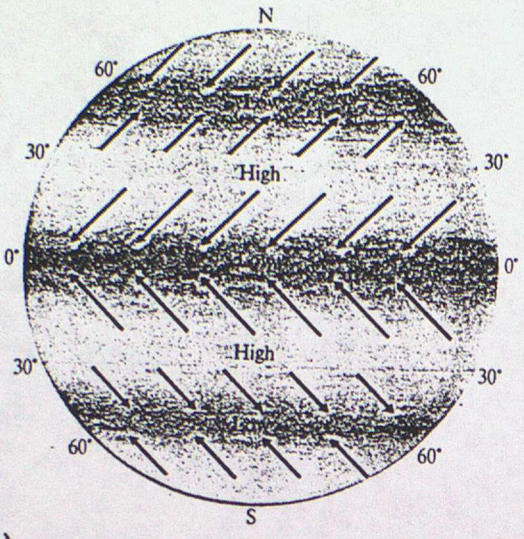

a) Idealized pattern of pressure and winds over the surface of the globe.

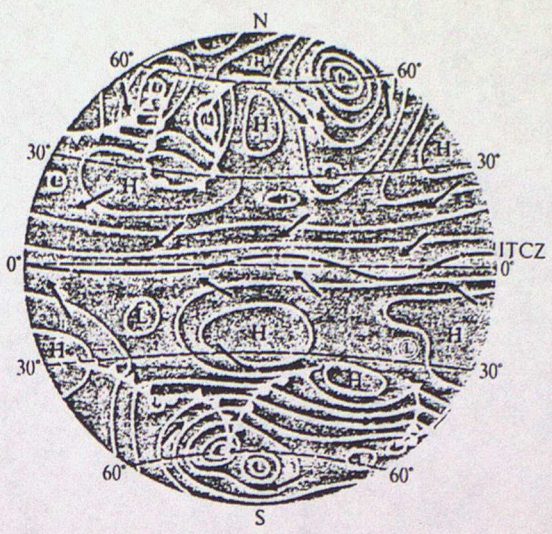

b) Typical distribution of pressure systems, winds and fronts near an equinox.

Figure 2.1 After Perry and Walker (1977)

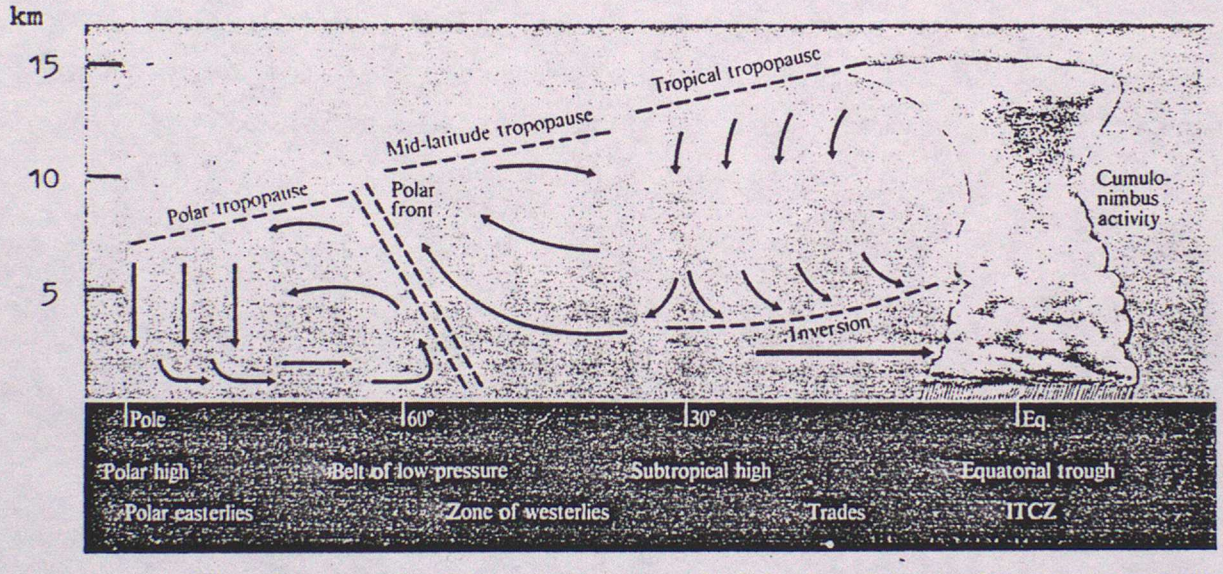

Schematic representation of the atmospheric general circulation, in vertical section from polar regions to the equator.

Figure 2.2 After Perry and Walker (1977)

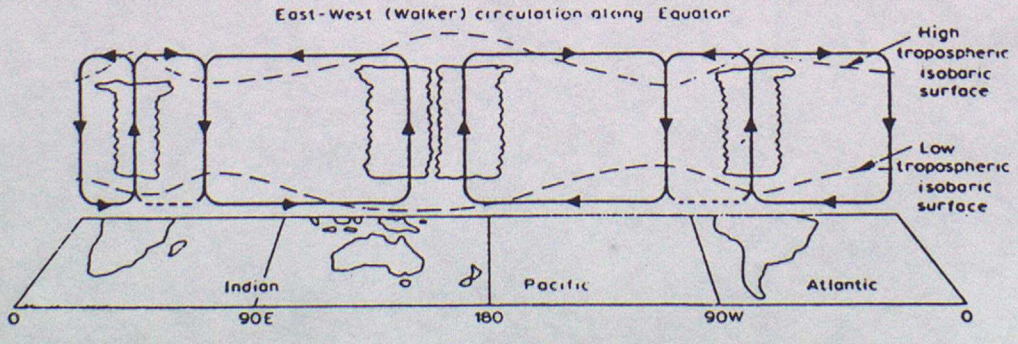

Figure 2.3 From Streten and Zillman (1984)

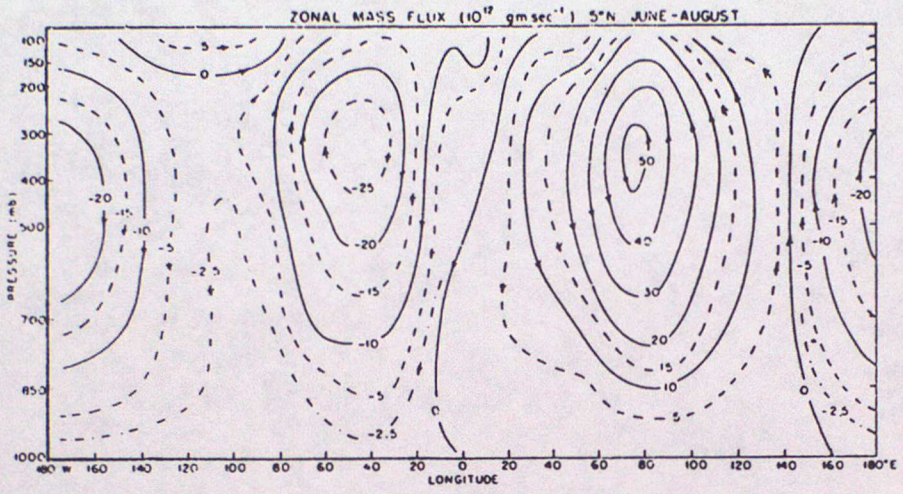

Figure 2.4 A representation of the zonal mass flux averaged over the region 0-10°N for June to August. Contours do not correspond to streamlines, but give a fairly good representation of the velocity field associated with the Walker circulation.
From Newell et al (1974)

AVERAGE SEA SURFACE TEMPERATURES (1951-80)
UNITS ARE DEGREES CELSIUS
MONTH JANUARY

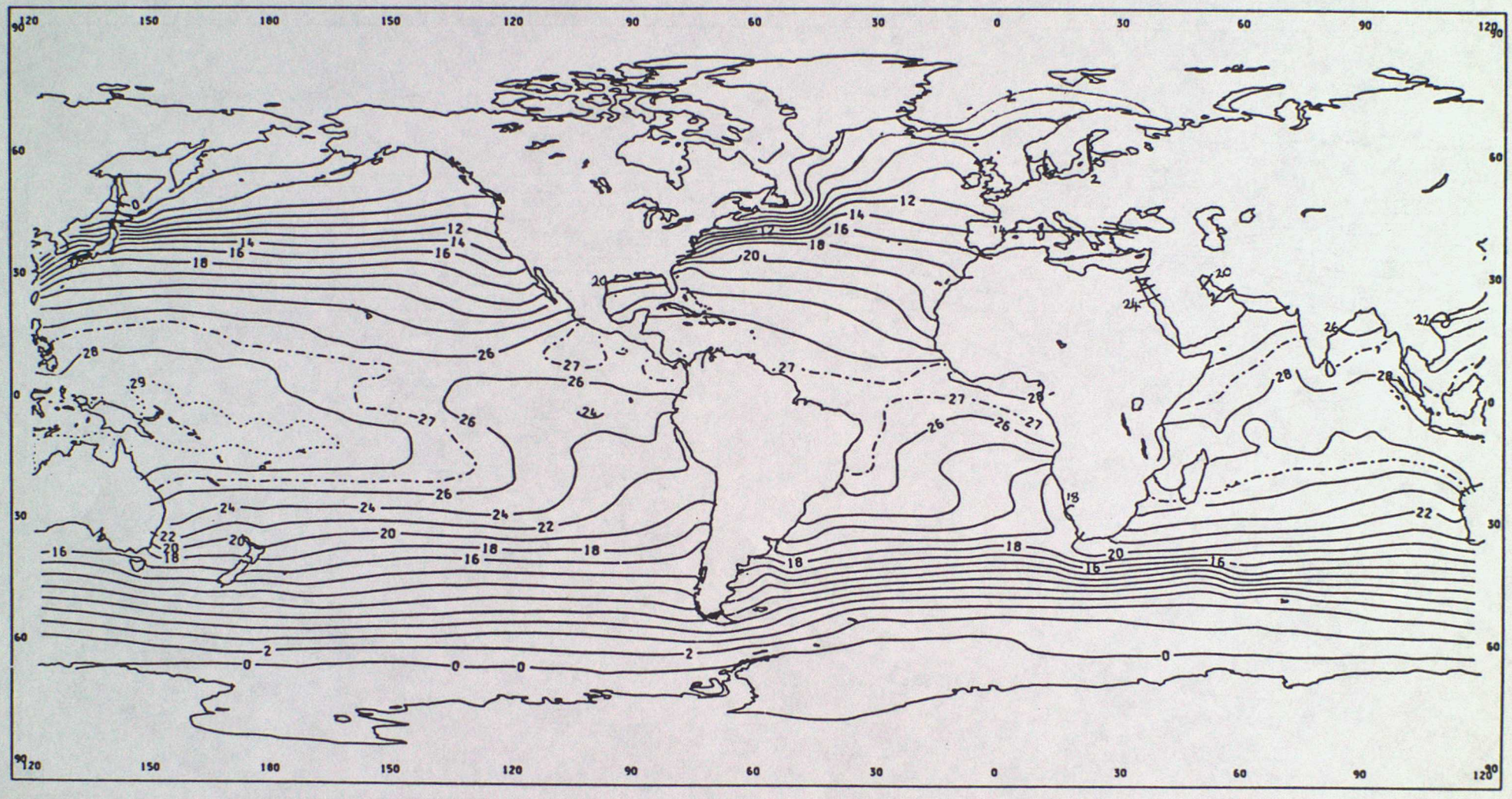

Figure 2.5A.

AVERAGE SEA SURFACE TEMPERATURES (1951-80)
UNITS ARE DEGREES CELSIUS
MONTH JULY

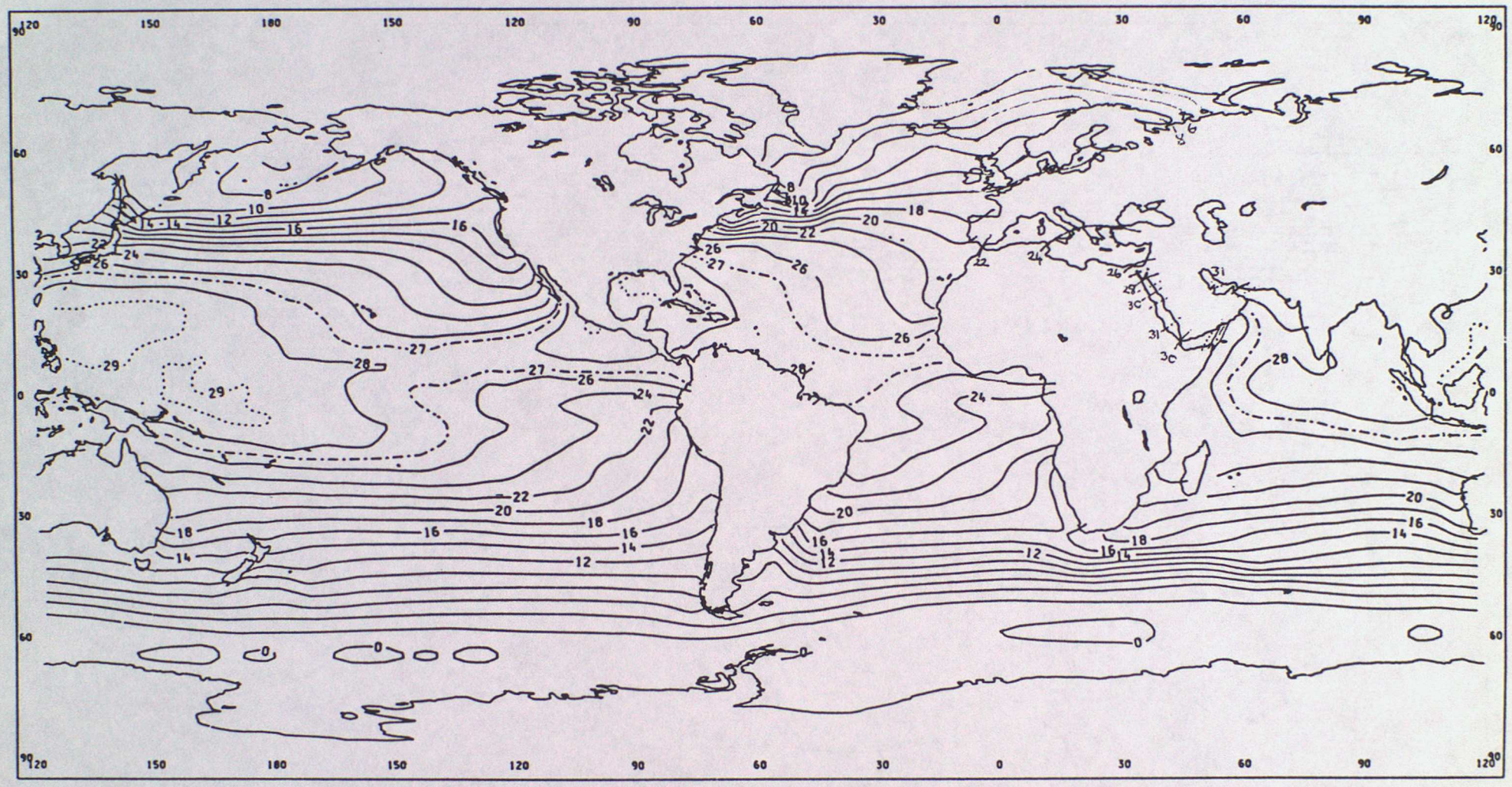

Figure 2.5B.

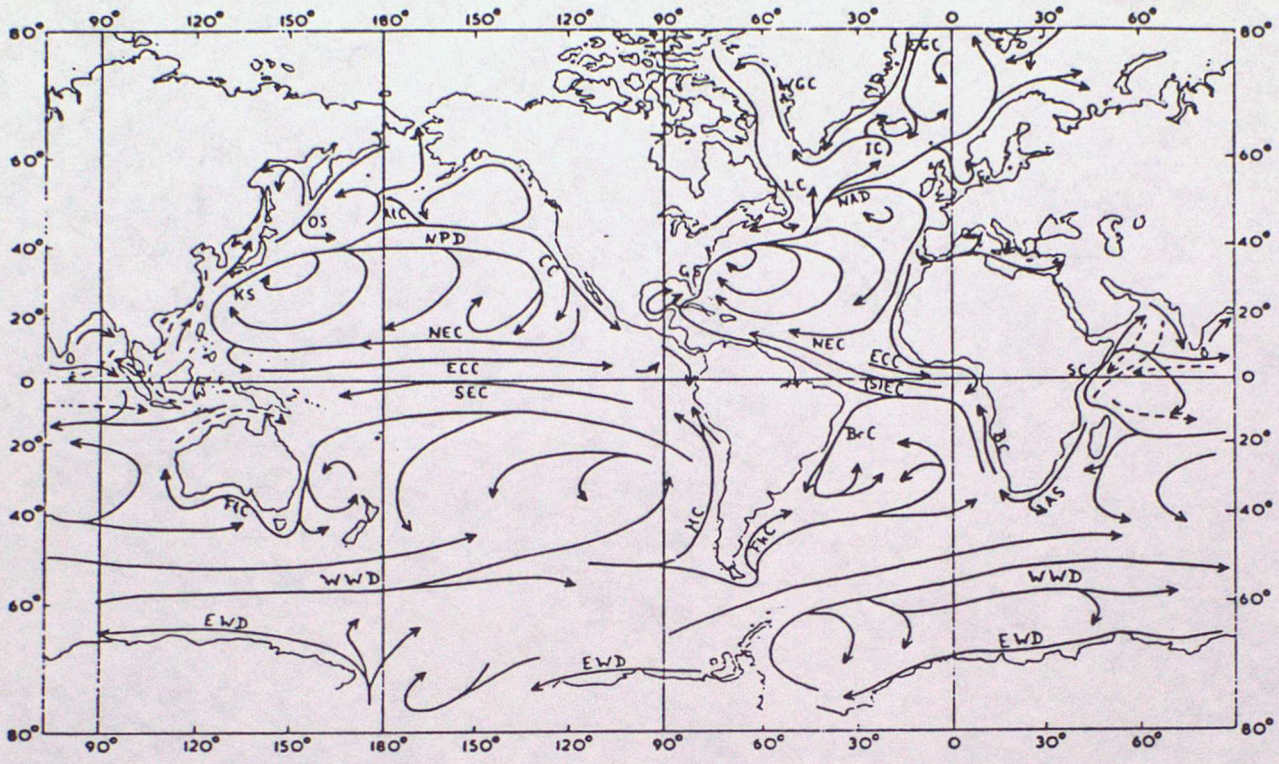

Figure 2.6 Main surface currents of the oceans. From Lamb(1972). The abbreviations for the names of the currents are expanded in table 8.2 of Lamb(1972)

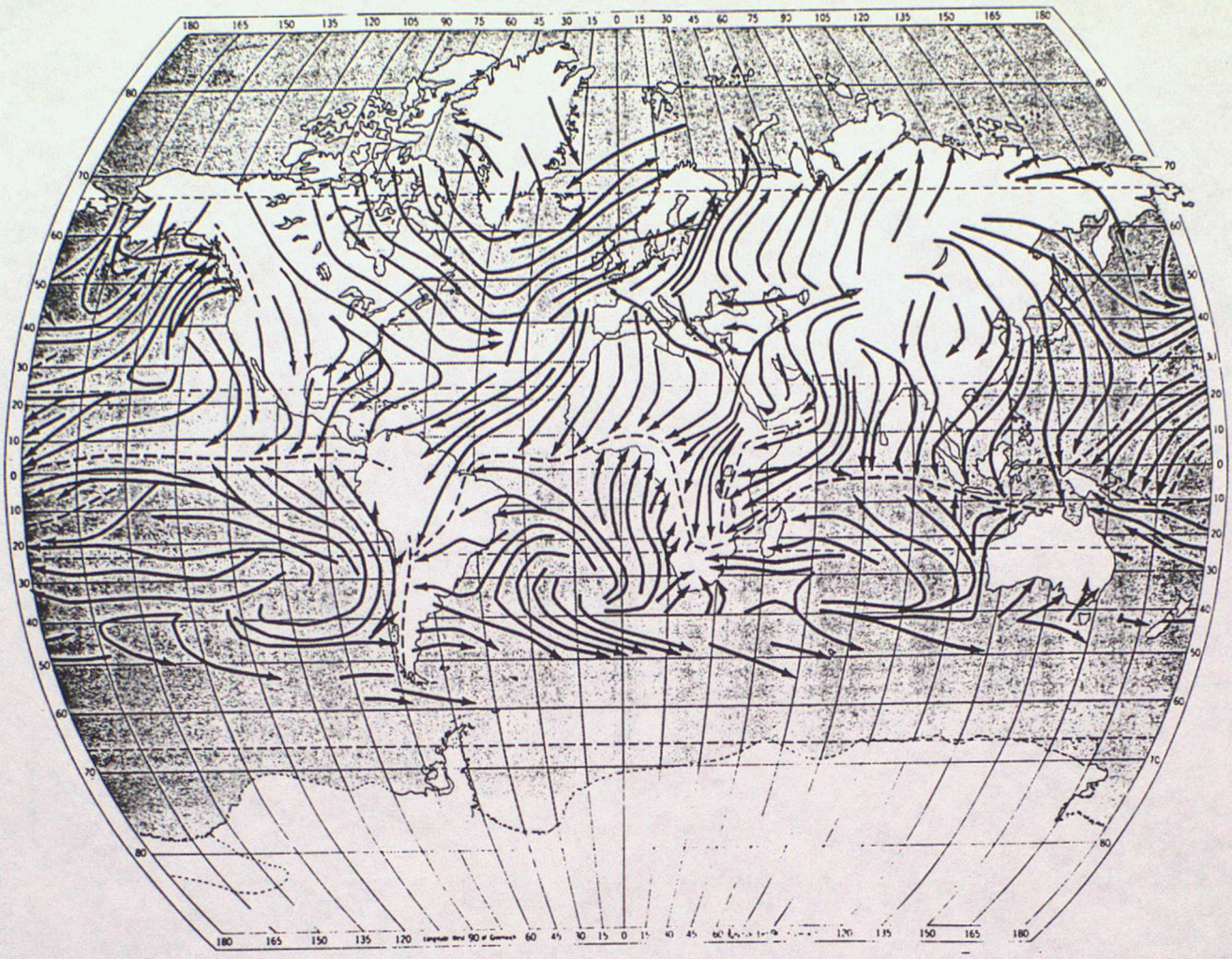

Figure 2.7A Surface winds and ITCZ January.From Critchfield(1983)

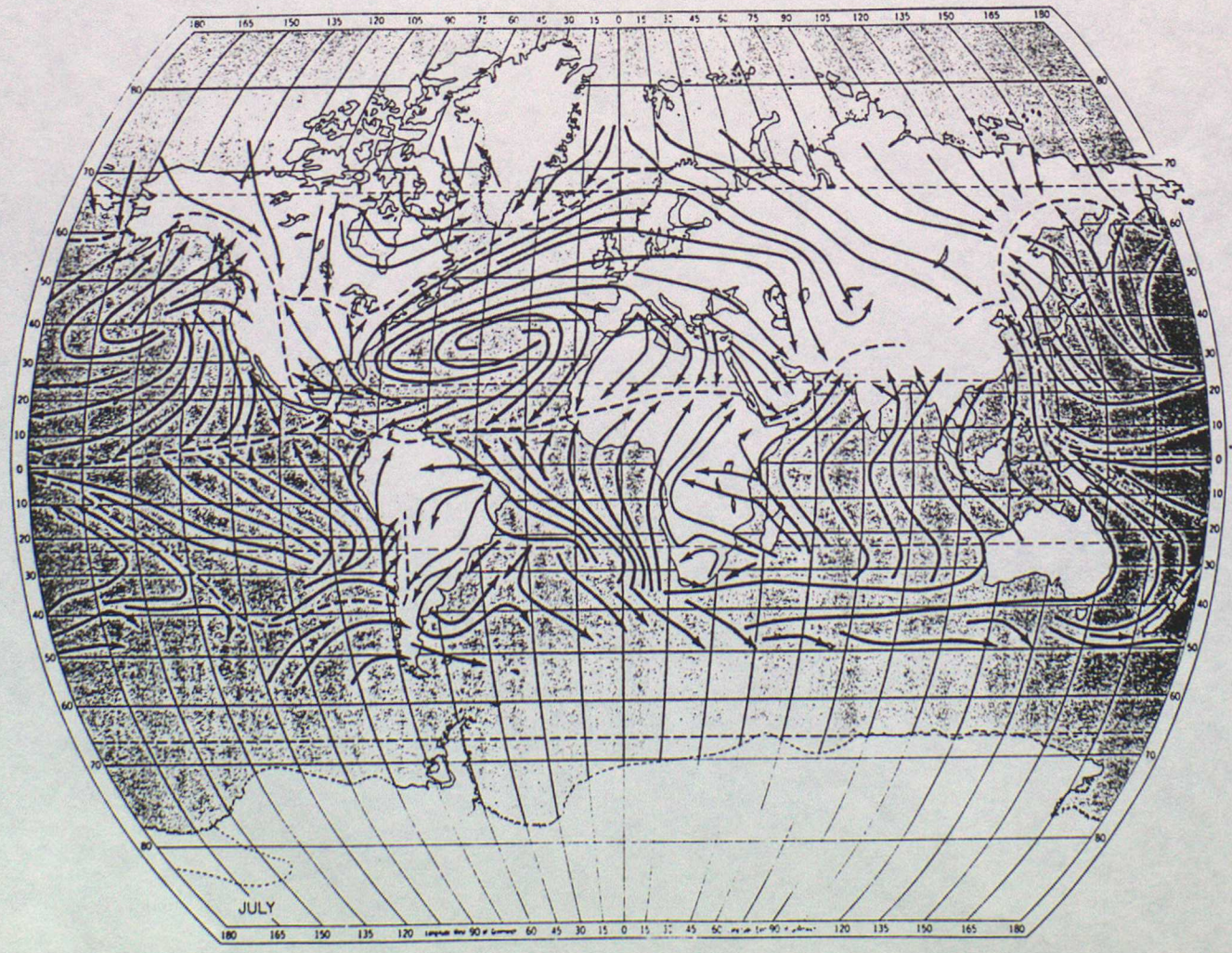

Figure 2.7B Surface winds and ITCZ July.From Critchfield(1983)

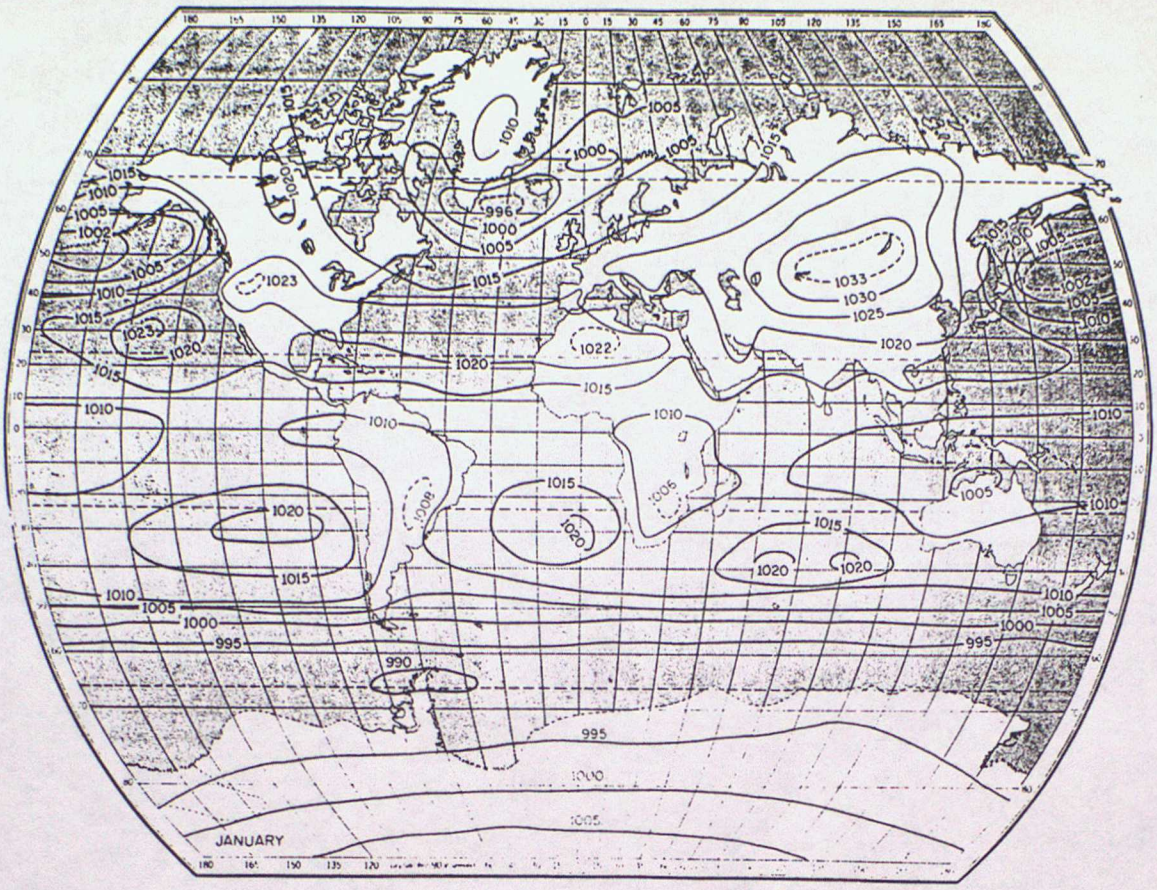

Figure 2.8A World sea-level pressure (mbs) in January. (Modified Van der Grinten projection.)
From Critchfield(1983)

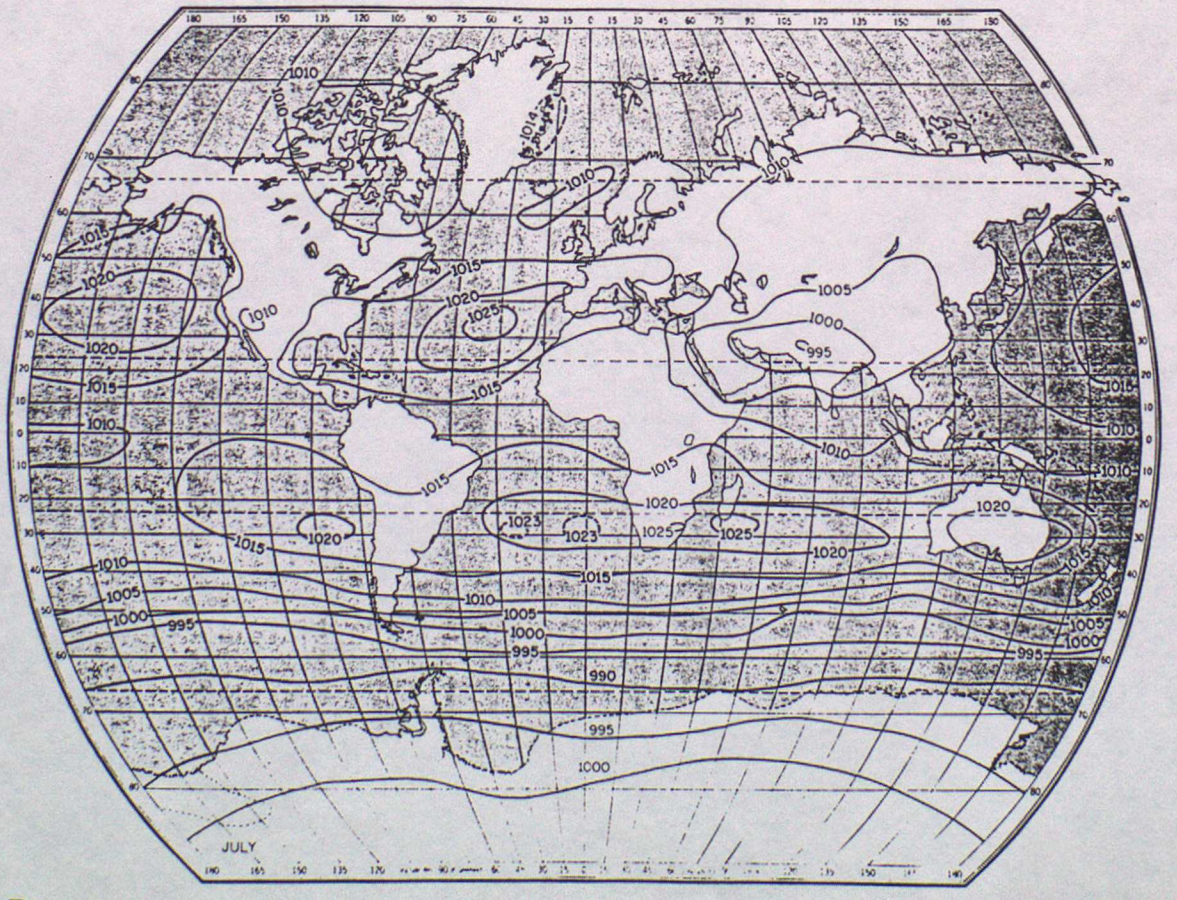

Figure 2.8B World sea-level pressure (mbs) in July. (Modified Van der Grinten projection.)
From Critchfield(1983)

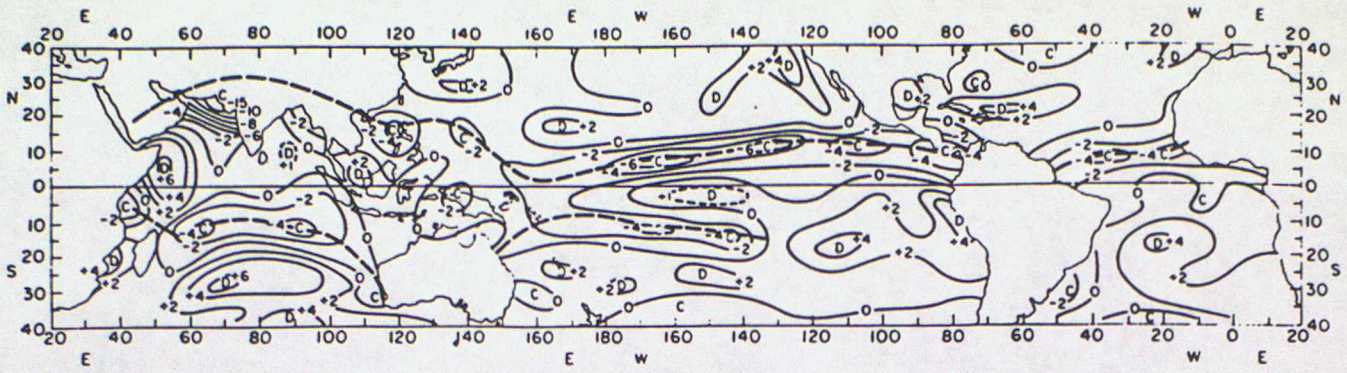

Figure 2.9 Chart of mean horizontal divergence ($10^{-6}s^{-1}$) for July at the surface over the oceans. ITCZ position dashed. After Riehl (1979)

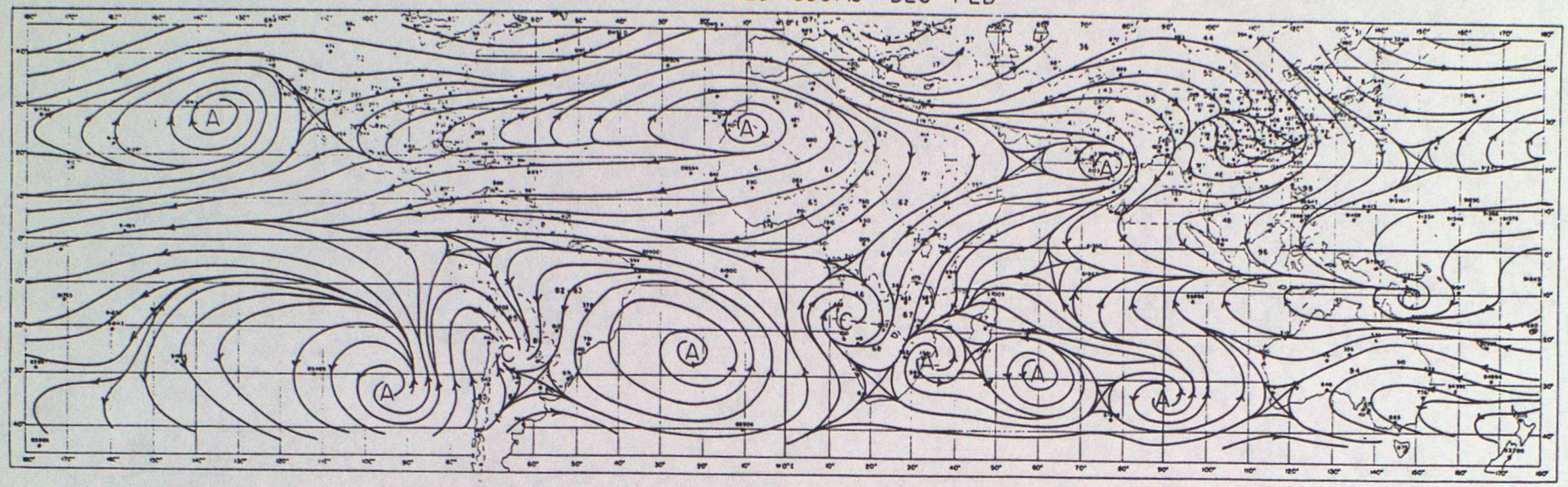

STREAMLINES 200mb – DECEMBER - FEBRUARY

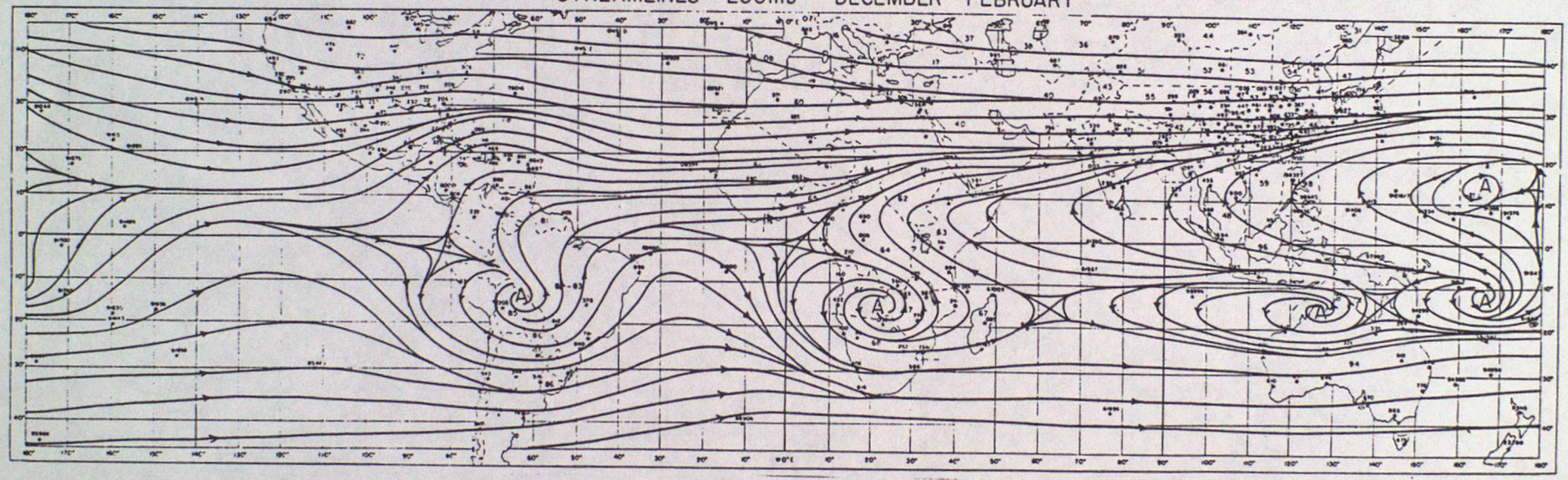

Figure 2.10. From Newell et al (1974).

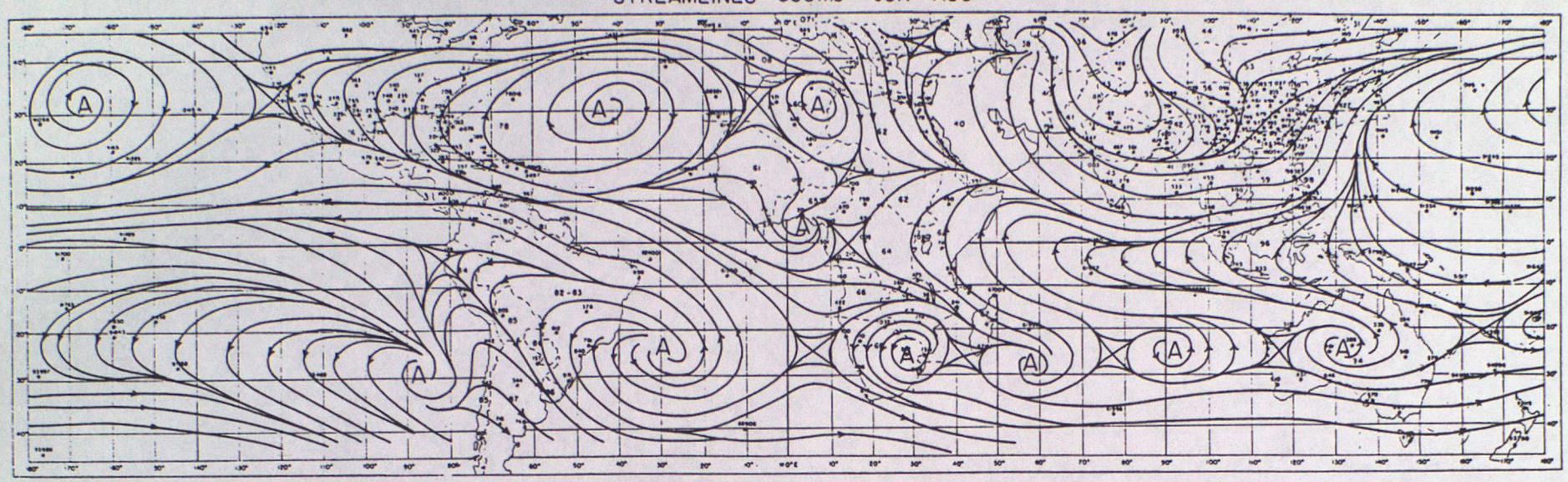

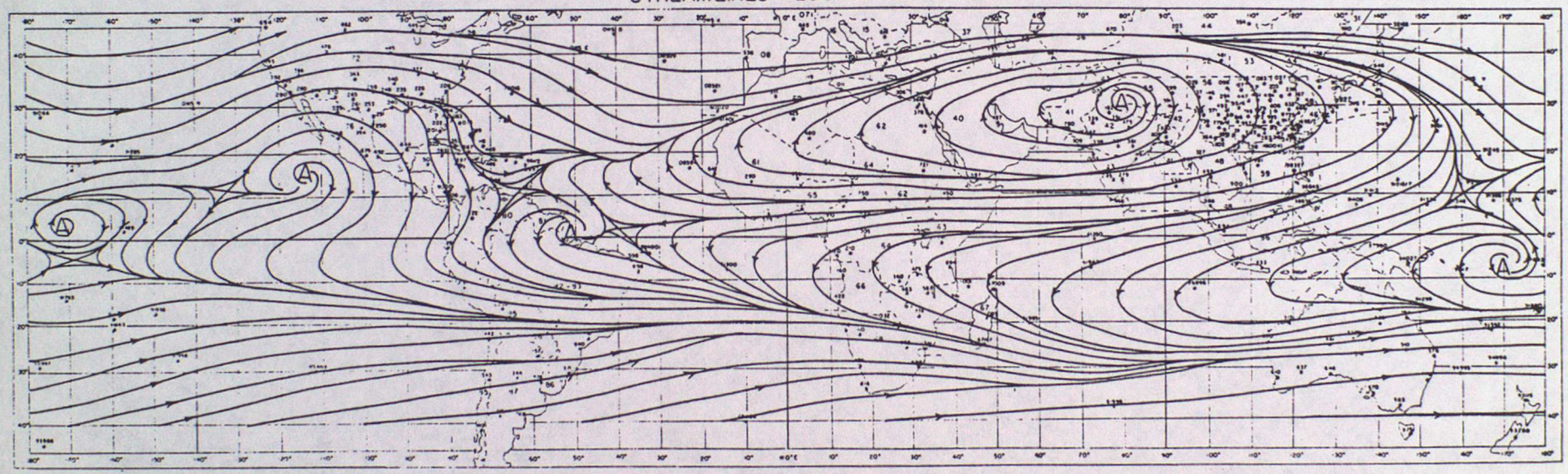

Figure 2.11. From Newell et al (1974).

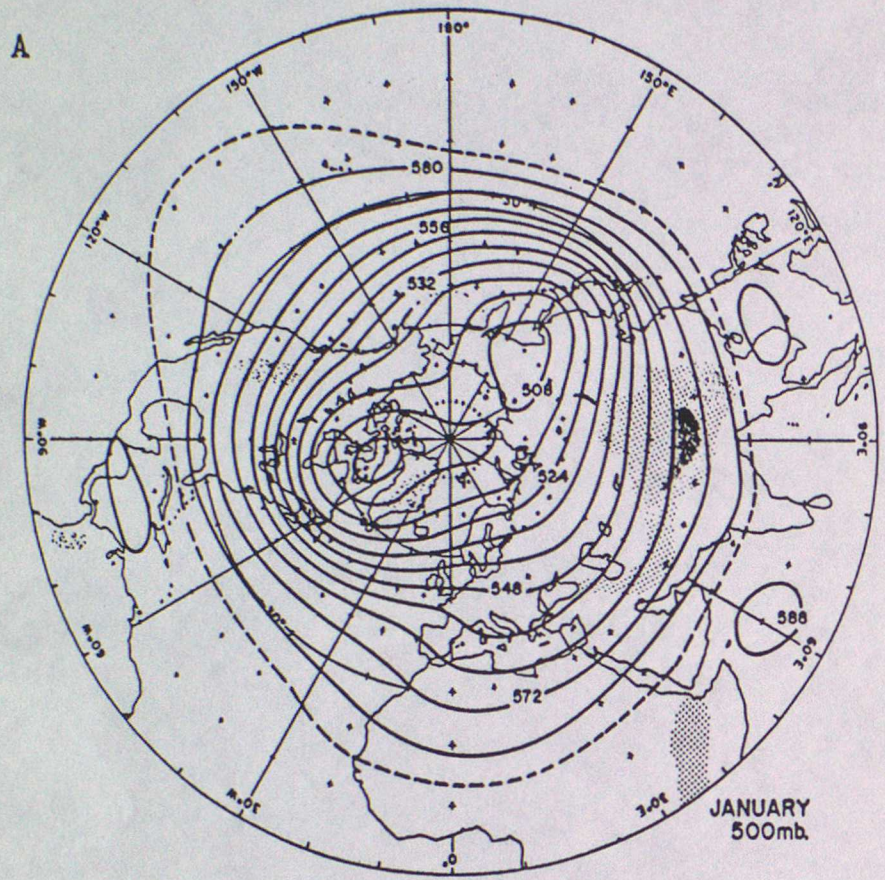

Mean 500-mb contours in January (winter), Northern Hemisphere. Redrawn at 80-m intervals from I. Jacobs (1958). Light and heavier stippling show regions where elevations are above 1.5 km and 5 km (smoothed over 5° latitude-longitude tessera), from Berkofsky and Bertoni (1955).

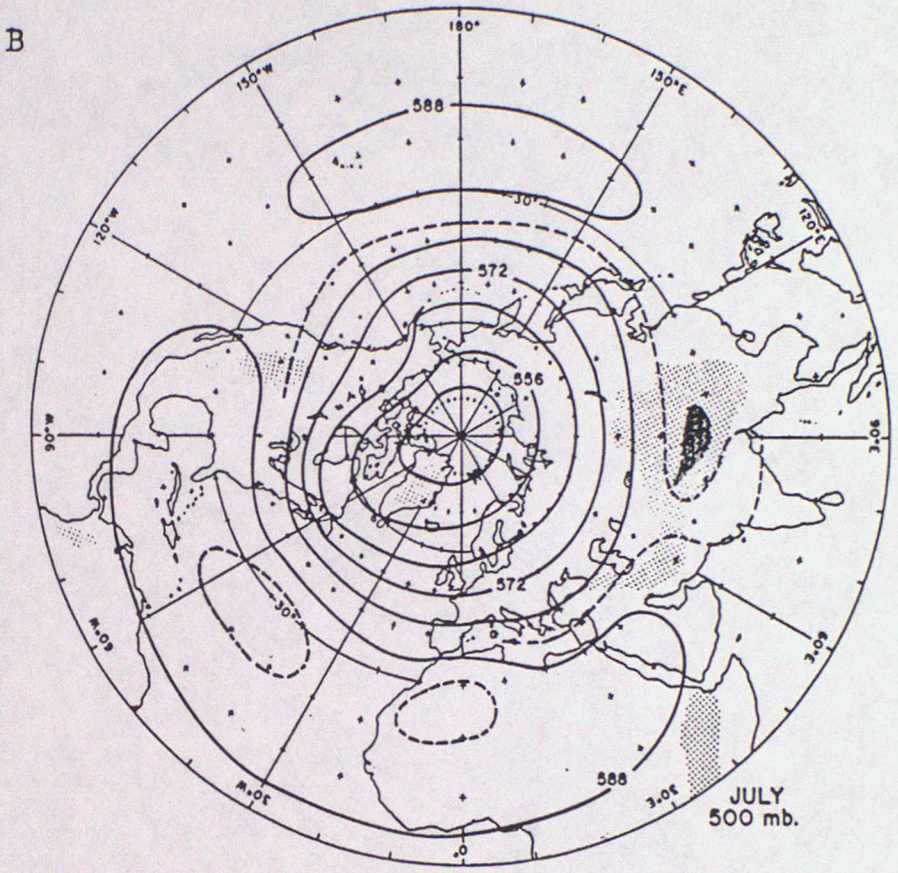

Mean 500-mb contours in July (summer), Northern Hemisphere. (Redrawn, from I. Jacobs, 1958.)

Figure 2.12

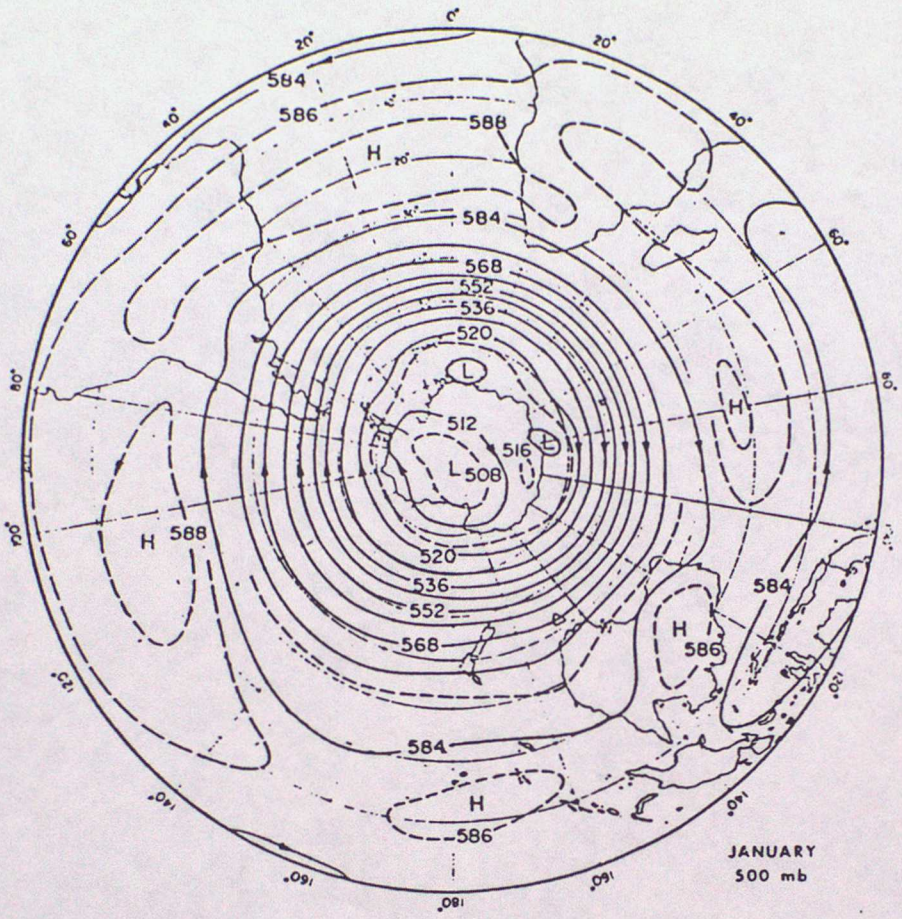

Figure 2.13 . Mean 500-mb contours (80-m interval) in January (summer), Southern Hemisphere. (After Taljaard *et al.*, (1969))

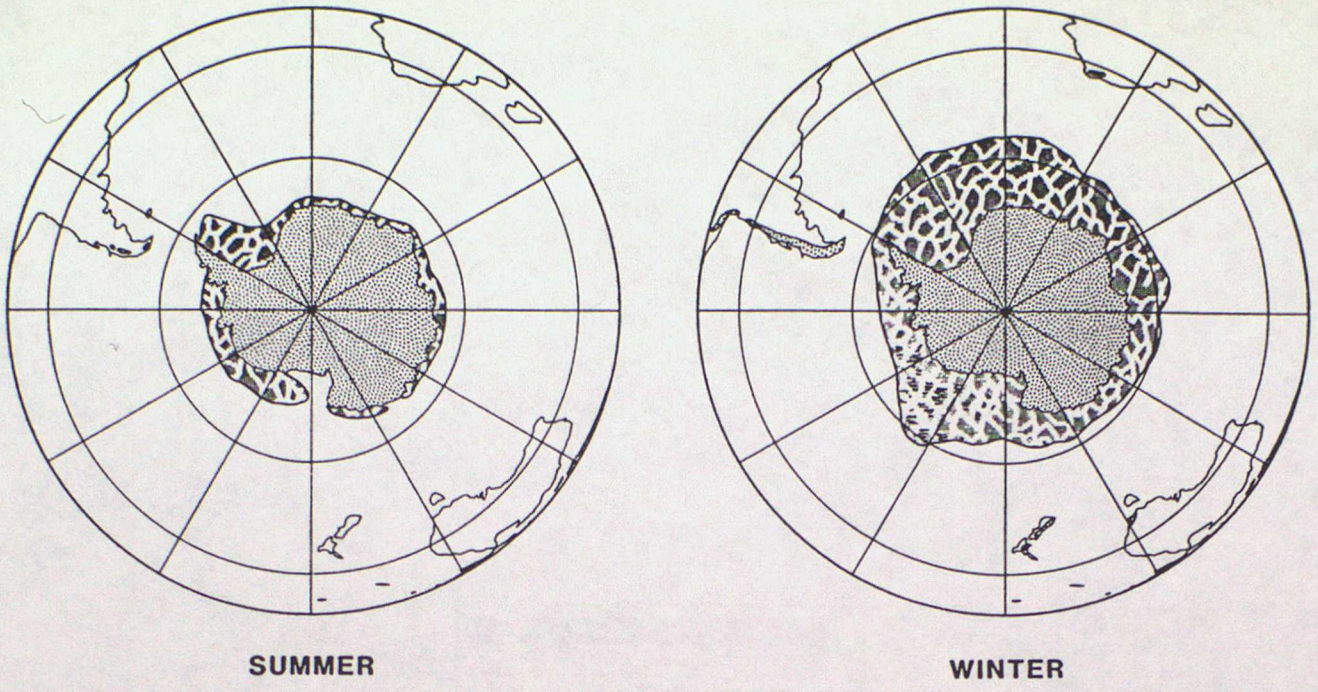

(*a*)

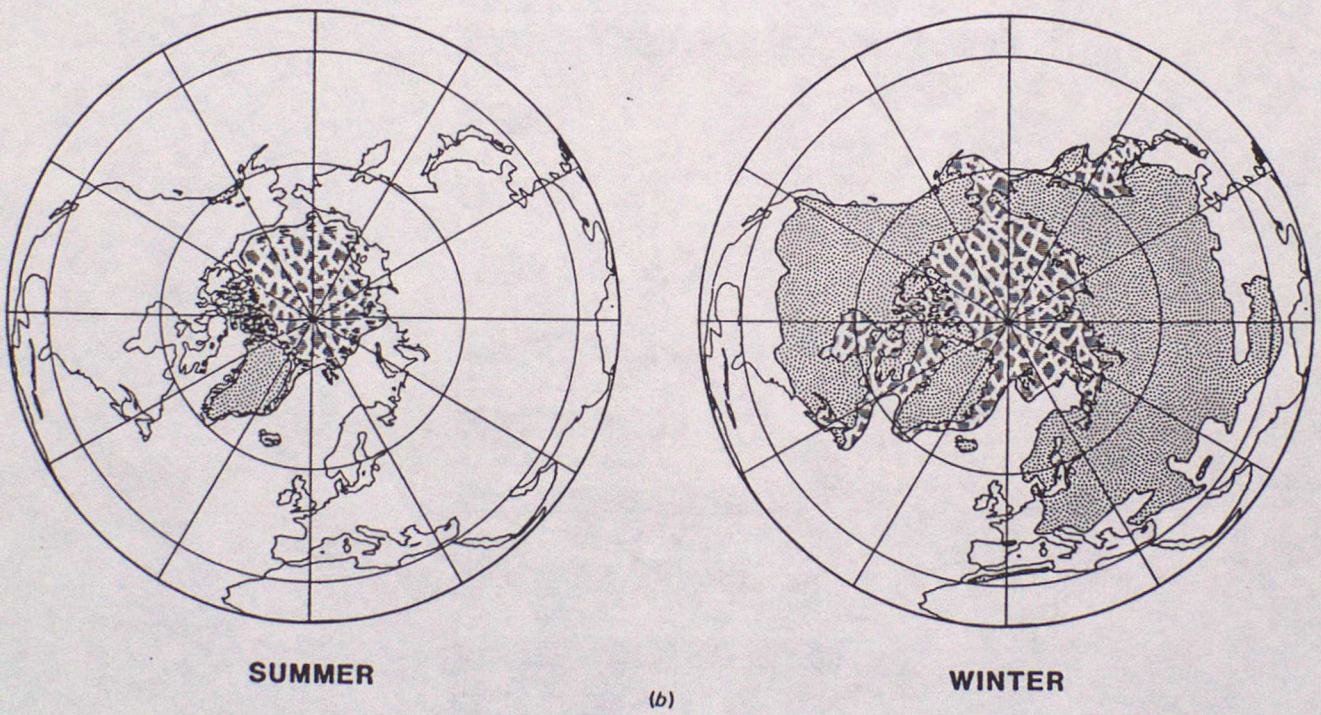

(*b*)

(*a*) Snow and ice in the southern hemisphere at their minimum and maximum extent. (*b*) Snow and ice in the northern hemisphere at their minimum and maximum extent (from Meier, 1983).

The best set of data for Antarctic sea ice was derived from passive microwave images (ESMR on NIMBUS 5, beginning in December 1972). For reasons of accuracy and unambiguous interpretation of these data, the ice limit was taken to be at concentrations of > 15%, which tends to make the total ice extent appear large. Ships reporting the encounter with ice are likely to place the 'ice margin' at a far higher concentration.

Figure 2.14A. After Untersteiner (1984).

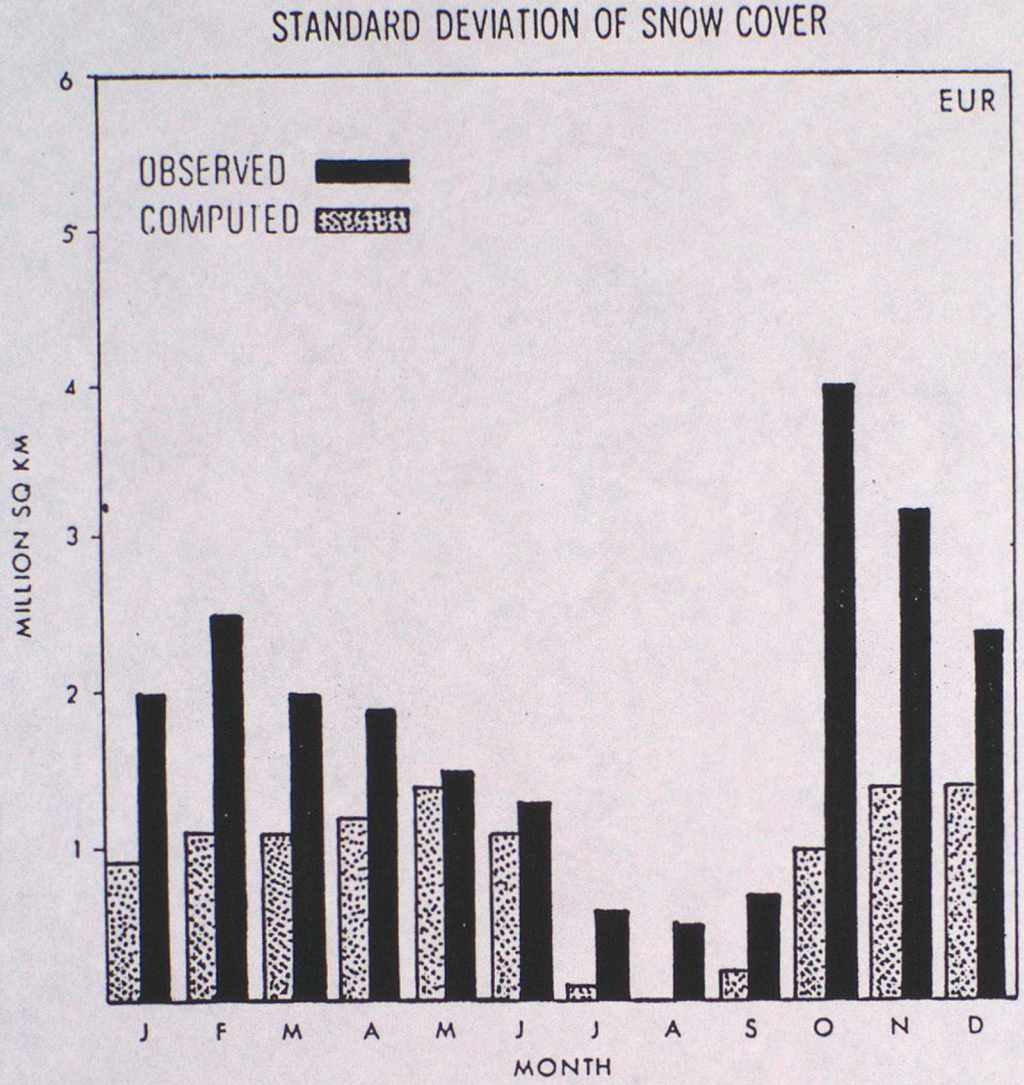

Figure 2.14B Standard deviation of monthly mean snow cover of Eurasia as observed (Matson, personal communication) and as computed by the GCM. From Hahn (1981)

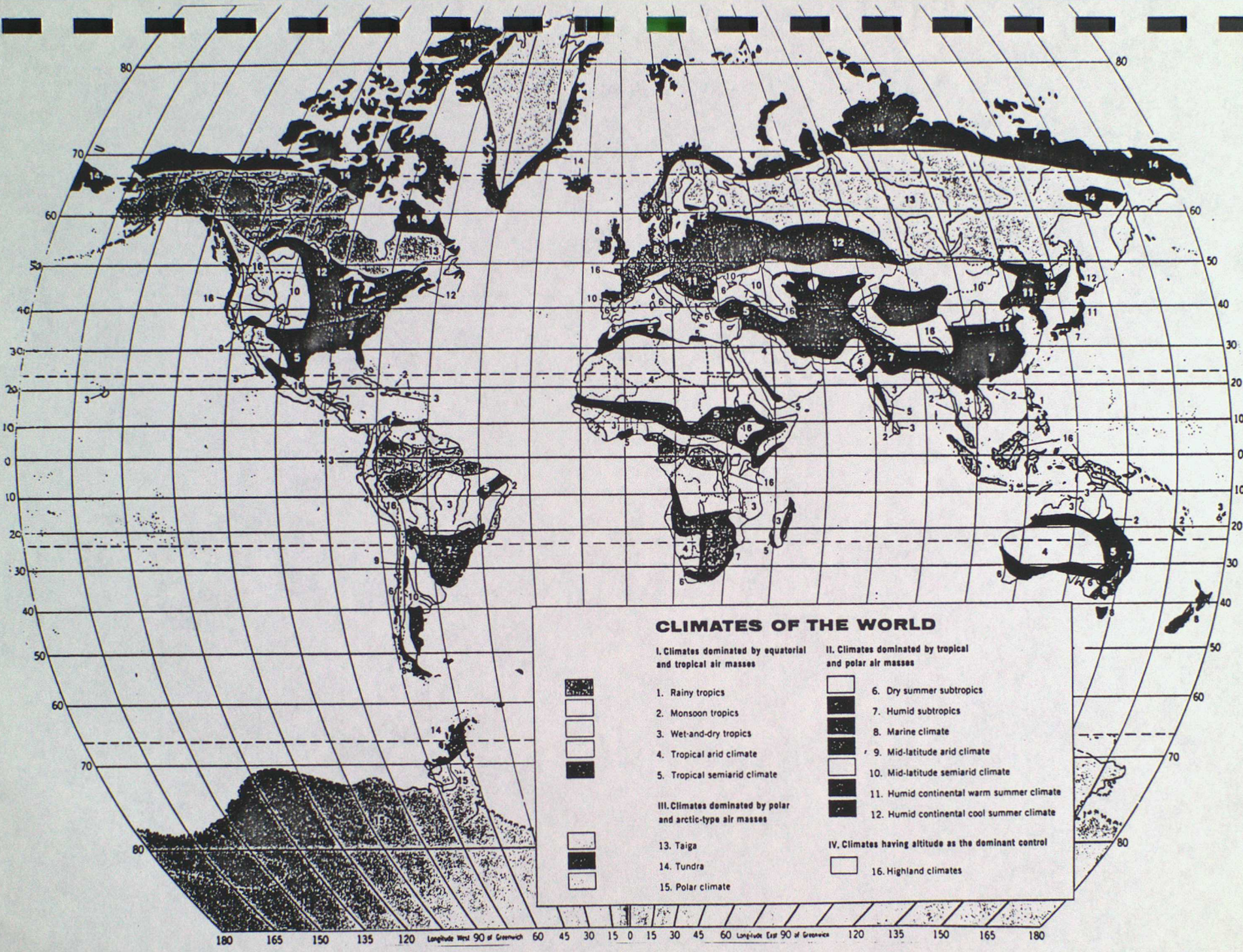

Figure 2.15. From Critchfield (1983).

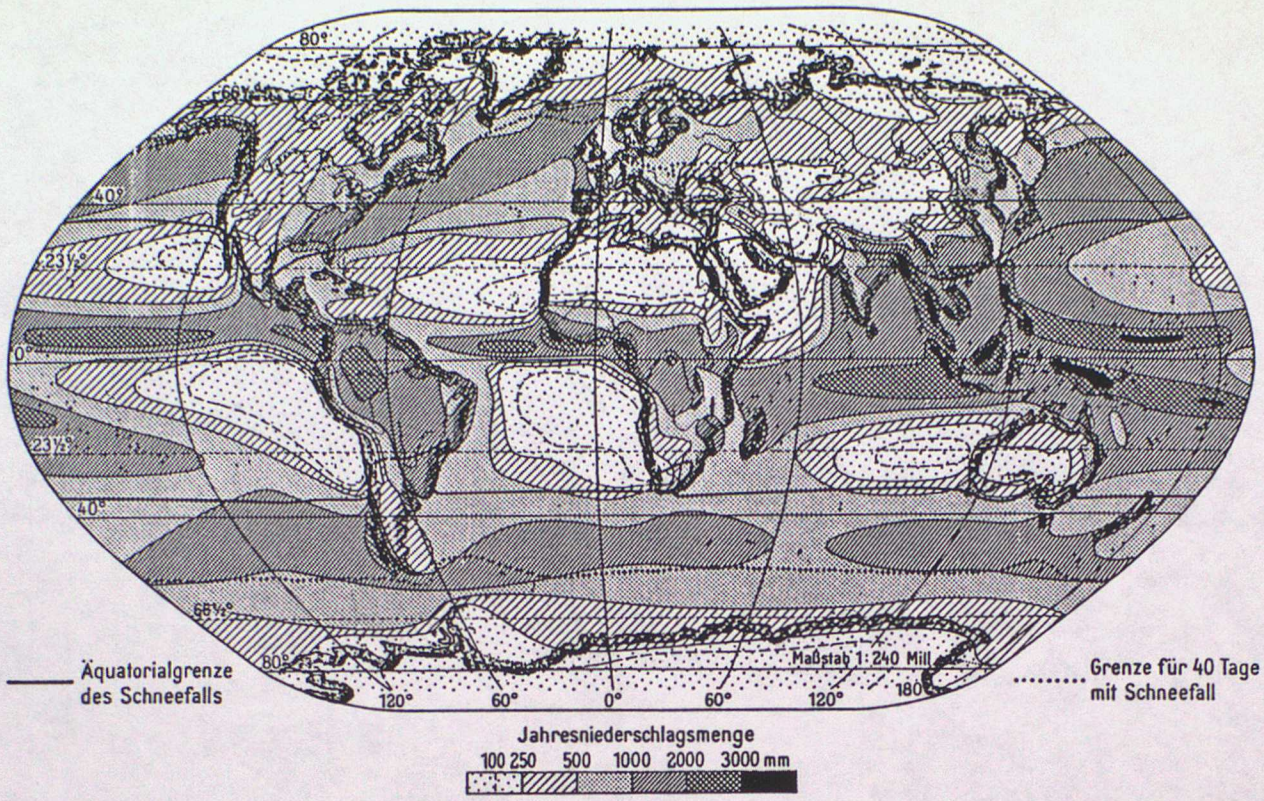

Figure 2.16. **Average annual precipitation over the earth (Jahresniederschlagsmenge) in mm. Also shown are the equatorward limits of snowfall (Äquatorialgrenze des Schneefalls) and the limits for 40 days with snowfall (Grenze für 40 Tage mit Schneefall). (*From Meinardus and Moller.*)** From Trewartha and Horn (1980).

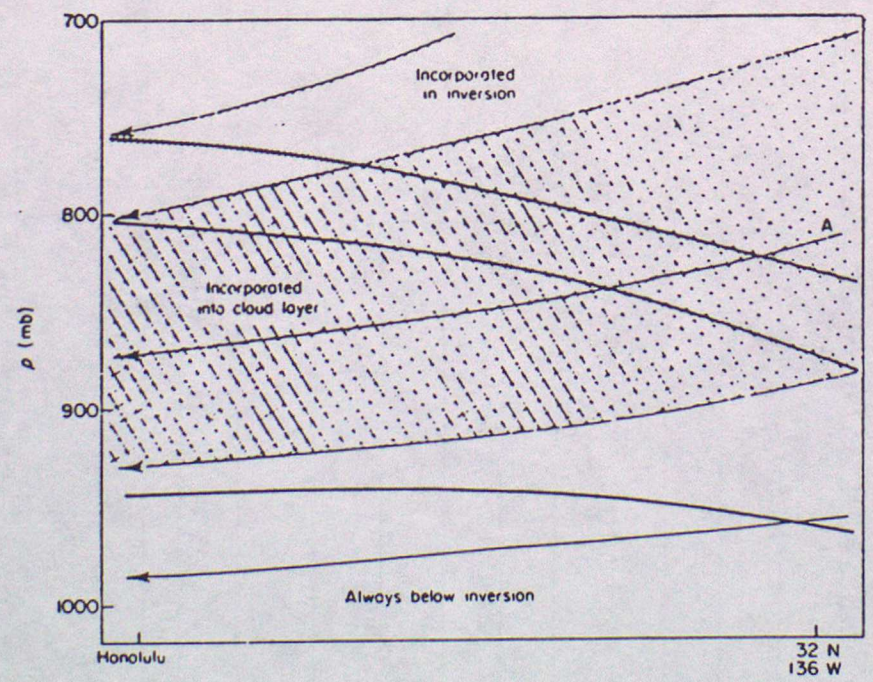

Figure 2.17. The flow of mass through the trade inversion. After Riehl (1979).

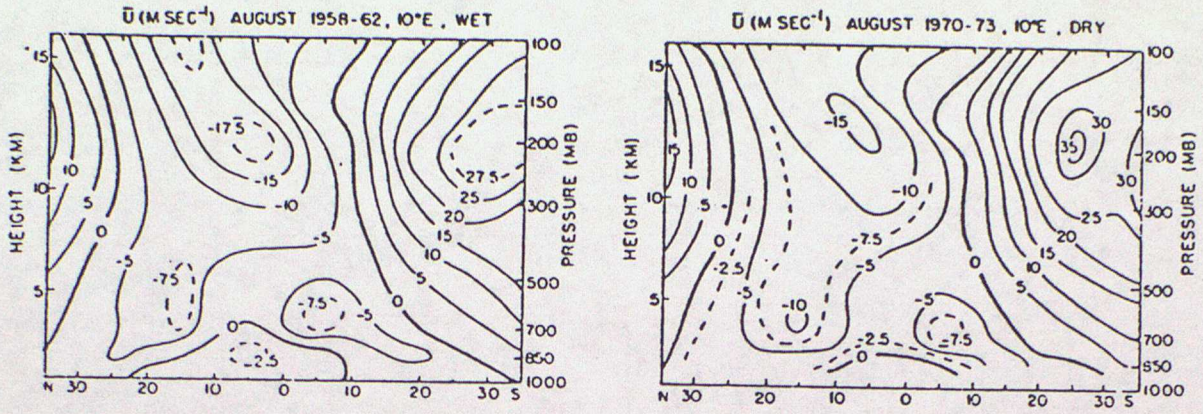

Figure 2.18A Meridional cross-sections along 10°E of mean zonal wind for August 1958–1962 and August 1970–1973. Units: $m\,s^{-1}$

After Newell and Kidson (1984)

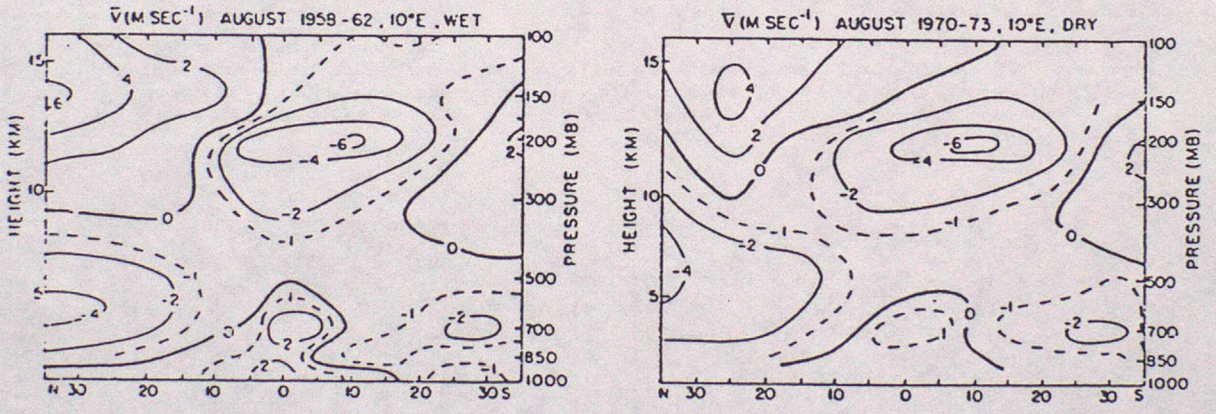

Figure 2.18B Meridional cross sections along 10°E of mean meridional wind for August 1958–1962 and August 1970–1973. Units: $m\,s^{-1}$

After Newell and Kidson (1984)

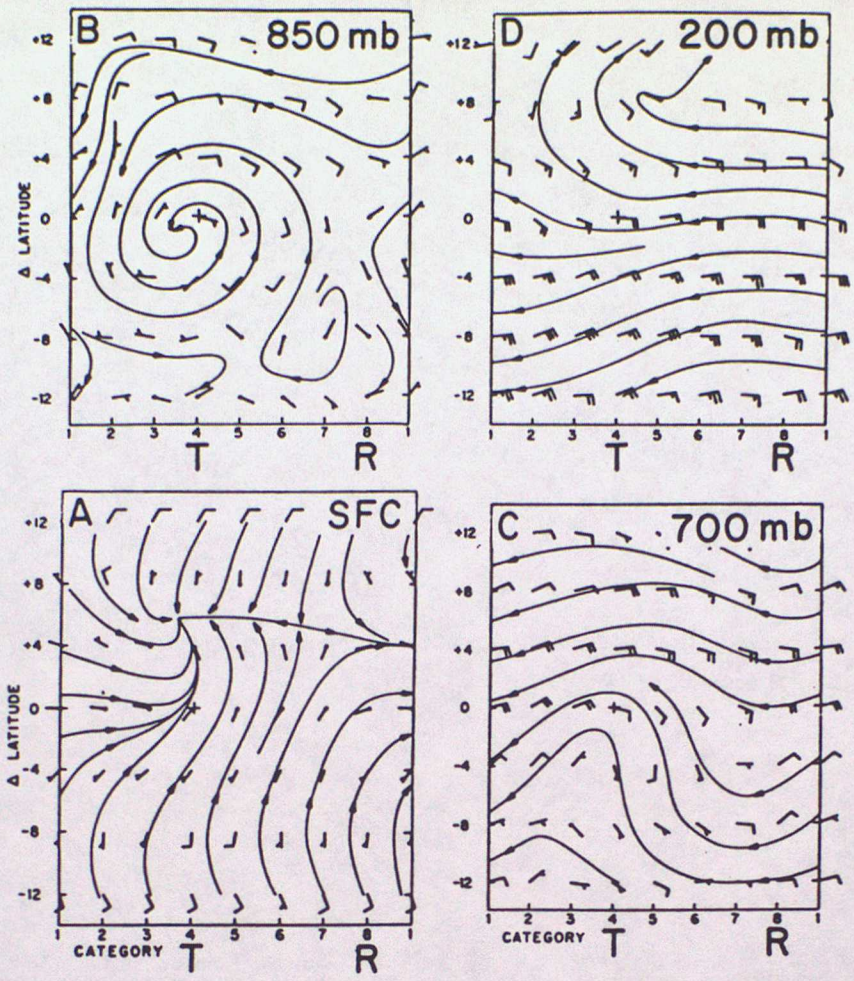

Figure 2.19.

After Hastenrath (1985)).

Streamlines and wind barbs of total flow field for composite African Wave. Category separation is approximately 3 degrees longitude, T denotes trough, R ridge, and cross disturbance center at 700 mb. Full wind barb corresponds to 5, half barb to 2.5, and no barb to 1 m s^{-1} (a) surface, (b) 850 mb, (c) 700 mb, (d) 200 mb. From Reed *et al.* (1977)

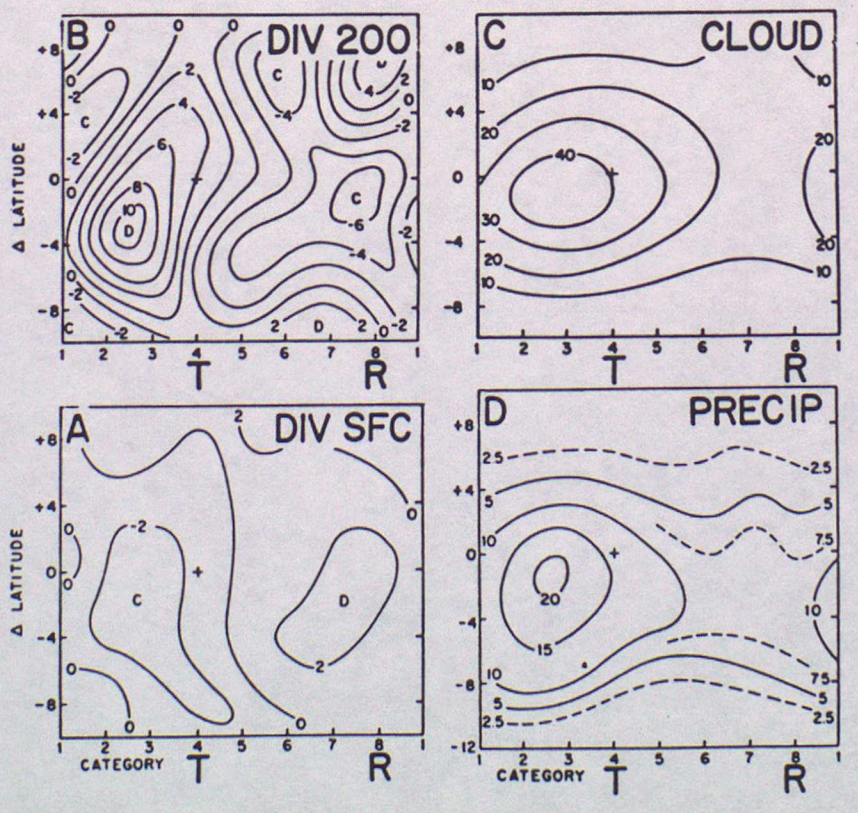

Figure 2.20.

(After Hastenrath (1985)).

Weather structure of composite African Wave. (a) Surface, divergence deviation from zonal mean in 10^{-6}; (b) same but for 200 mb level; (c) percentage of convective cloud cover; (d) average rainfall rate, in mm day^{-1}. Symbols as for Fig. 2-14. From Reed *et al.* (1977)

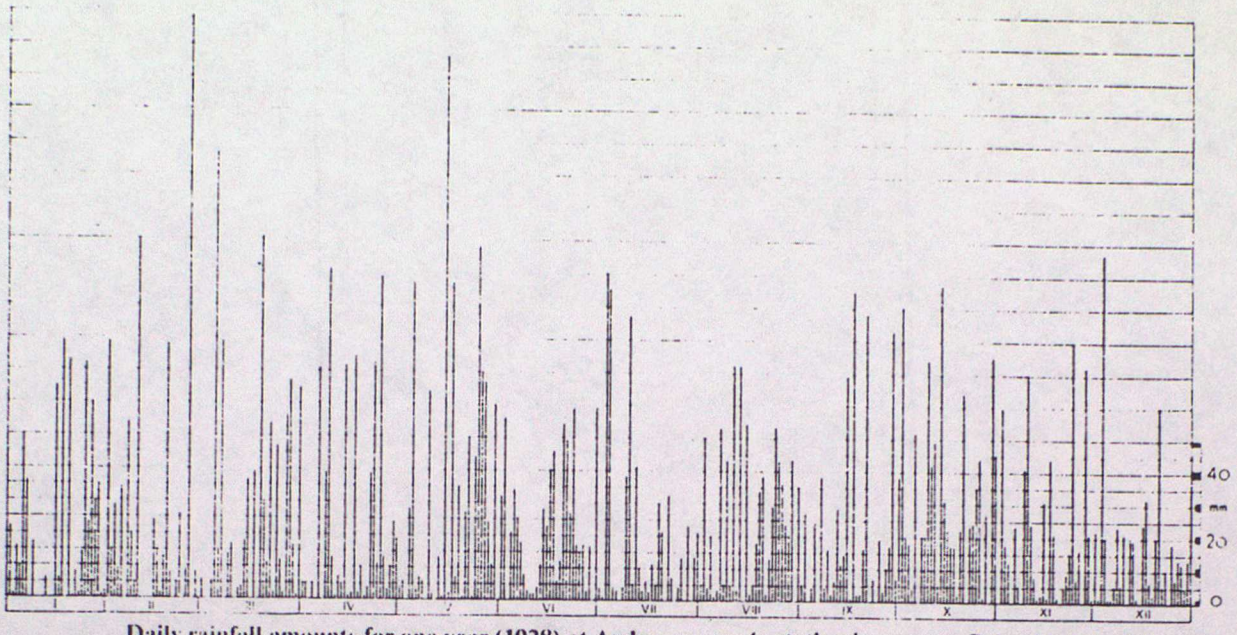

Daily rainfall amounts for one year (1928) at Andagoya, an *Ar* station in western Colombia inland from the Pacific coast. Here the average annual rainfall is exceedingly heavy (7089 mm; 282 in), and no month is dry. In 1928, there were only 48 days on which no rain fell. (*After M. Hendl,* Einführung in die physikalische Klimatologie, *Band II*)

Figure 2.21 From Trewartha and Horn (1980)

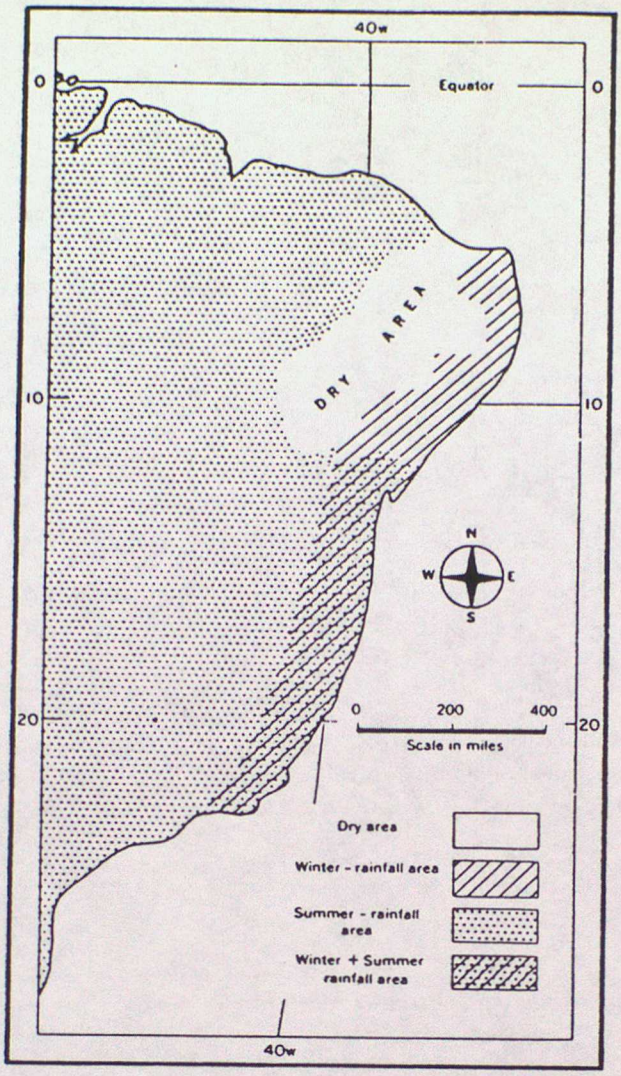

The dry area in eastern Brazil occupies an intermediate position between the winter-rainfall region to the east and south and the strong summer-rainfall region to the interior and west. It normally escapes the full effects of the disturbances which produce these contrasting seasonal rainfalls.

Figure 2.22 From Trewartha and Horn (1980)

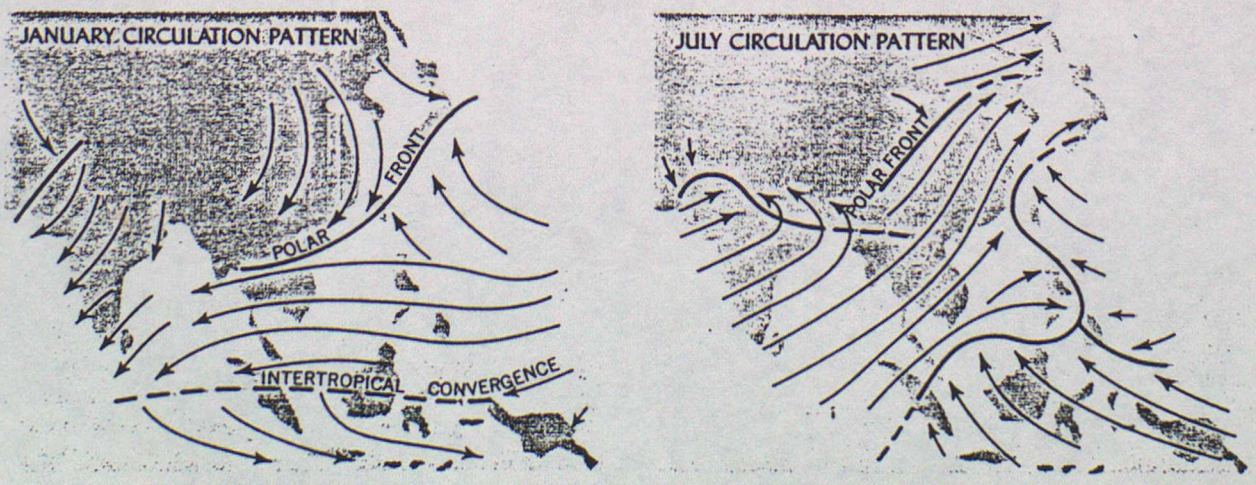

Principal elements of the low-level circulation patterns over eastern and southern Asia in the cold and the warm seasons. (*After Thompson, Watts, Flohn, and others. From Trewartha,* The Earth's Problem Climates, *University of Wisconsin Press, Madison, Wis.*)

Figure 2.23 From Trewartha and Horn (1980)

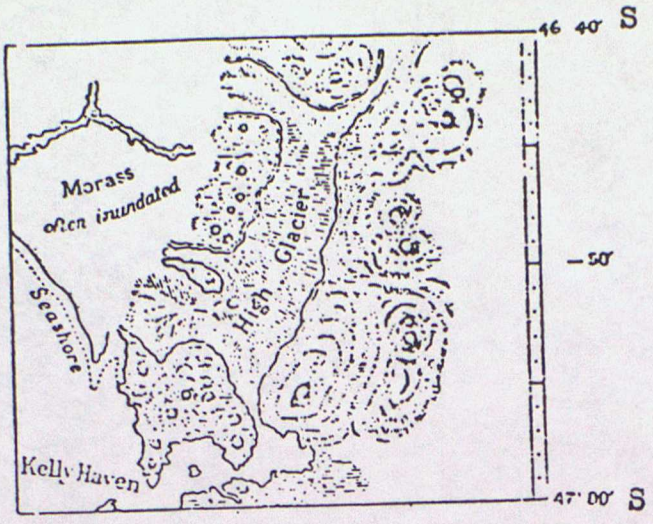

Figure 2.24 Glacier at sea level. From Darwin (1979).

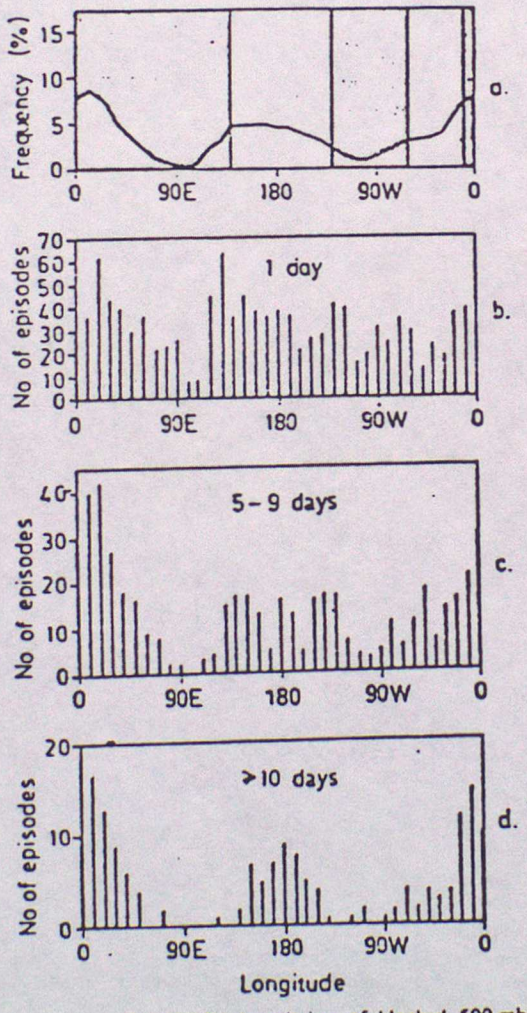

Longitudinal variation of blocked 500-mb flow averaged over the whole year. Continents are shaded. (b–d) Frequency distribution of blocking episodes as a function of longitude, 1950-1979. Duration 1 day (b), 5–9 days (c) and >10 days (d).

Figure 2.25 After Lejenas and Okland (1983)

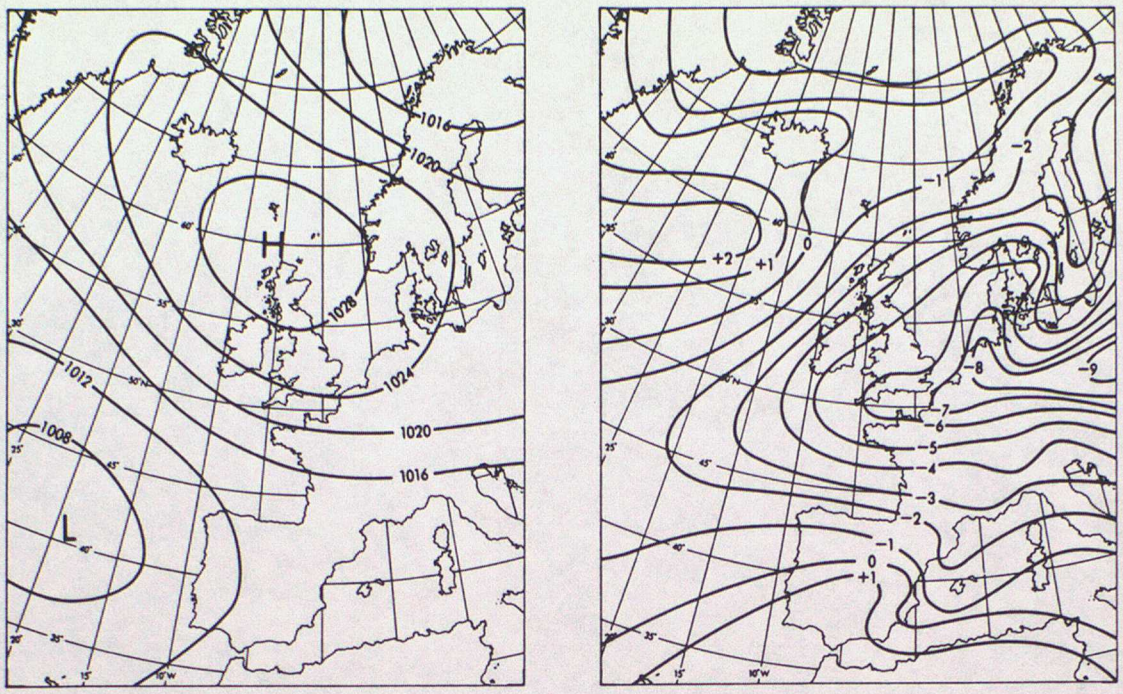

(a) Average pressure (mb) at mean sea level, January 1963.
(b) Average screen-level temperature anomaly (°C), January 1963. (Anomalies mainly from 1931–60 station averages.)

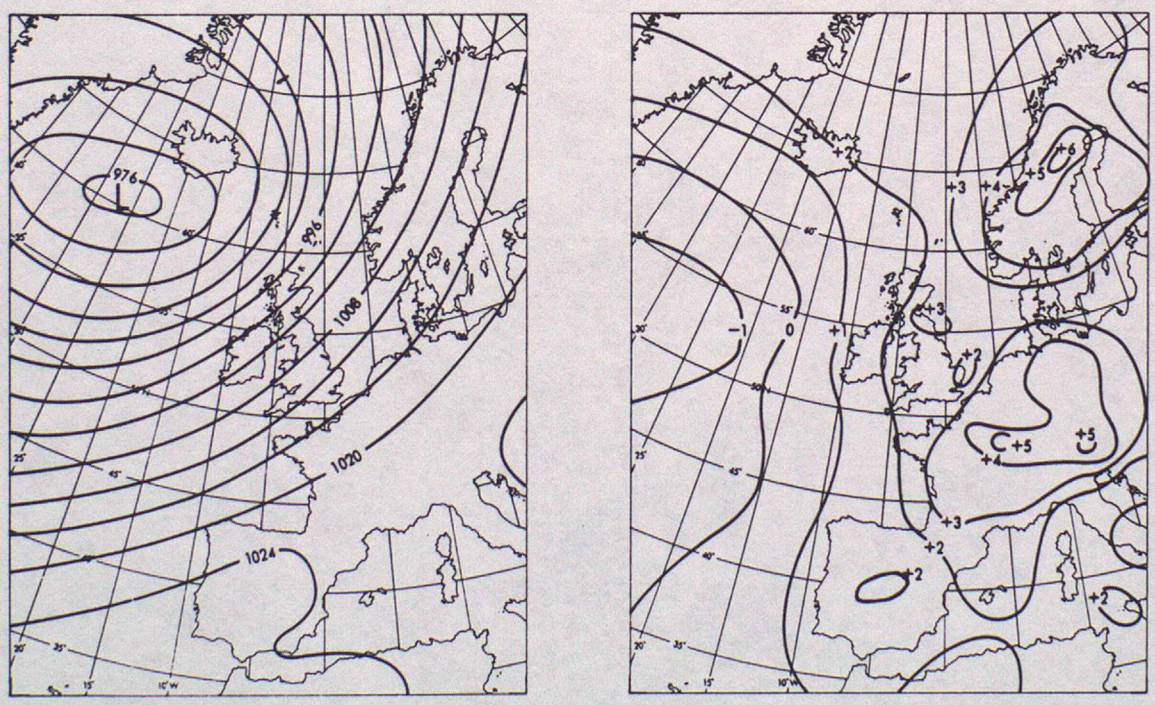

(c) Average pressure (mb) at mean sea level, January 1974.
(d) Average screen-level temperature anomaly (°C), January 1974. (Anomalies mainly from 1931–60 station averages.)

Figure 2.26. From Folland (1983).

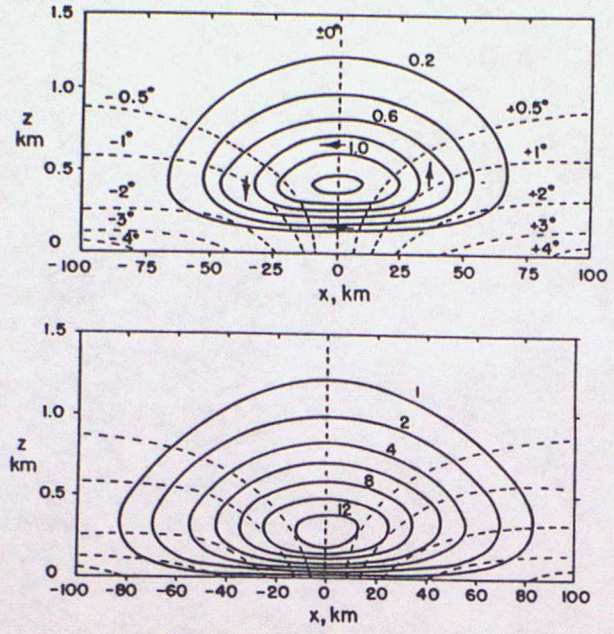

Vertical cross sections oriented perpendicular to a Southern Hemisphere low-latitude coastline (land to right of 0 km). Upper panel: Deviations of temperature °C (dashed lines) from the temperature at the coastline. A sea breeze circulation results (flow is parallel to solid lines, in sense of arrows). Lower panel: Solid lines are isotachs (lines of equal wind speed in m/s) showing a low level jet from the south (i.e., into the page). (*Courtesy of H. H. Lettau, "Explaining the World's Driest Climate," in H. H. Lettau and K. Lettau (eds.)*, Exploring the World's Driest Climate, *Institute for Environmental Studies, Rep. 101, University of Wisconsin, Madison, Wis., 1978, pp. 182-248*)

Figure 2.27 From Trewartha and Horn (1980)

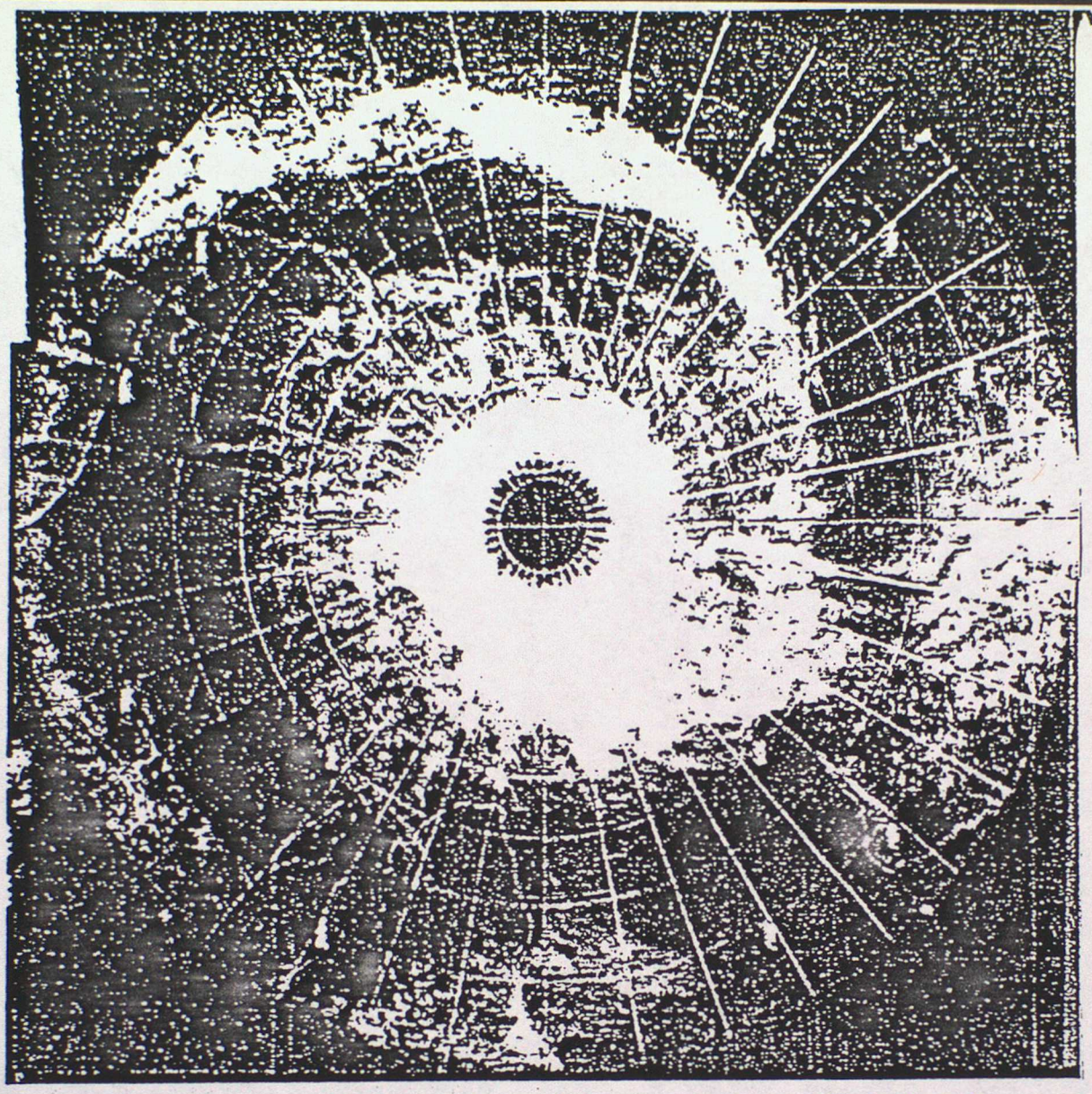

Averaged Southern Hemisphere cloud imagery (visible range) 1–15 October 1967, showing South Pacific cloud band. (After KORNFIELD and HASLER, 1969.)

Figure 2.28 From Streten and Zillman (1984)

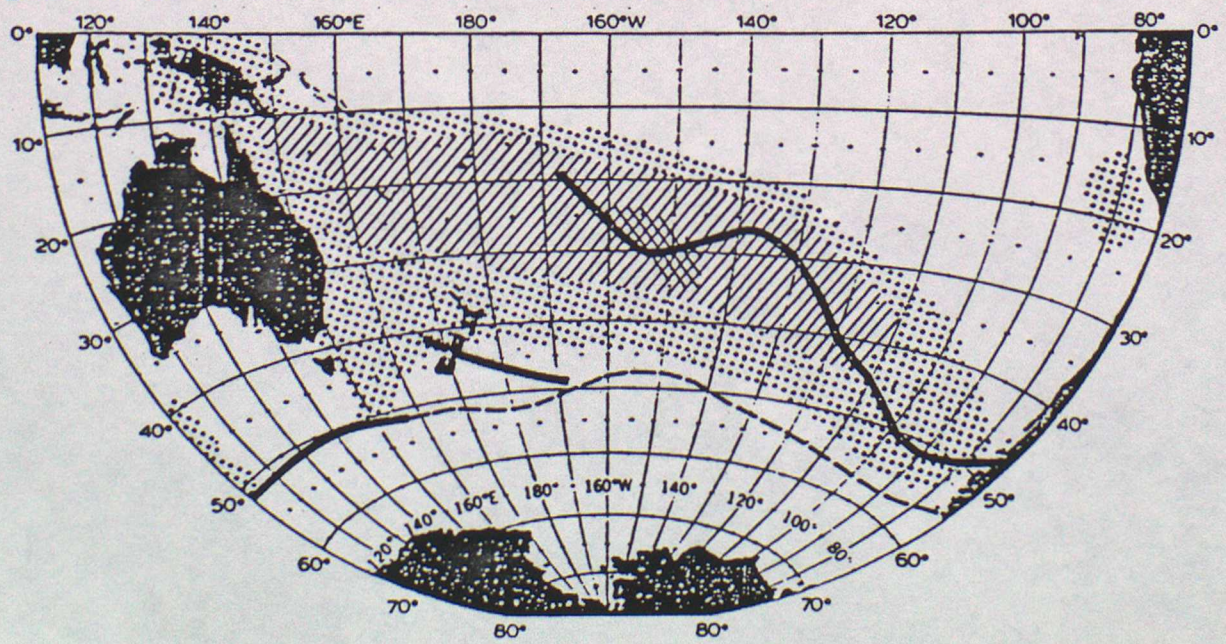

Percentage frequency of 5-day averaged mosaics having axes of major cloud bands within a 5°-lat. by 10°-long. area for spring and autumn (stippled > 10%; hatched > 20%; cross-hatched > 40%), after STRETEN (1973). Axes of zones of highest frequency of early cyclonic development for the same seasons is shown by the full line (after STRETEN and TROUP, 1973).

Figure 2.29 From Streten and Zillman (1984)

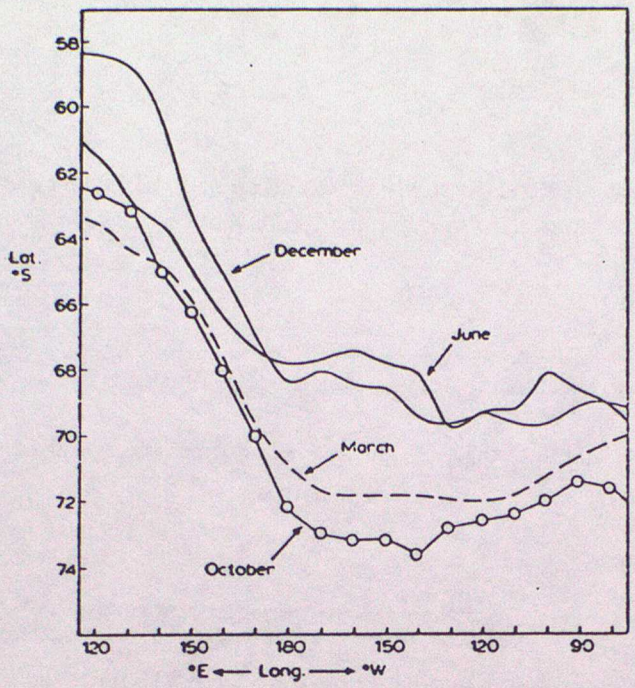

Mean latitude of the axis of the Antarctic trough in indicated months (1972–1977). (Data from STRETEN, 1980.)

Figure 2.30 From Streten and Zillman (1984)

Köppen's world-wide classification system

Climates are ranged in the following main groups:

A Tropical rain climates
B Arid climates
C (Warm) temperate rain climates
D Boreal forest and snow climates
E Cold snow climates (treeless)

A, C and D are all essentially tree climates; BS is the steppe grassland climate; BW defines the (warm) deserts (W standing for desert-waste/*Wüste*); E climates are those of the tundra and polar desert.

Subdivisions are designated as follows:

s Summer dry season
In group A climates confined to exceptional areas such as lee-sides of islands in the Trade Wind zone.
In groups C and D the wettest month of the year must have $\geqslant 3$ times the average rainfall of the driest month.

w Winter dry season
Group A climates are only designated Aw when at least one month normally has <60 mm rainfall.
In groups C and D the wettest month of the year is required to have $\geqslant 10$ times the average rainfall of the driest month.

s', w' Special cases of summer or winter dry season climates, where the chief rains come in late summer–autumn.

x Climates where the early summer is wet, late summer fine.

s'', w'' Special cases of summer or winter dry season climates, where the rainy season is split – i.e. has two peaks, with another, short dry season in between.

f Moist climates, with no marked dry season.

m Monsoon climates, with only a short dry season in the winter half-year.

On this system the chief types of climate appearing on the world map (fig.2A.1) are defined as follows:

Tropical rain climates

Mean temperature of the coldest month in all cases $> +18$°C.

Af Driest month has on average $\geqslant 60$ mm rain.

Am Driest month <60 mm but rainfall in the rainy season compensates this enough to allow forest.

Driest month R	60	40	20	0 mm
Required yearly R	1000	1500	2000	2500 mm

(Af and Am are both characteristically accompanied by tropical evergreen rain-forest.)

Aw Driest month <60 mm: annual rainfall insufficient to compensate.
(Aw produces Savanna.)

Arid climates

Defined by (i) $R < 2T + 28$ where summer is the season with most rain.
or (ii) $R < 2T + 14$ where there is no season with more liability to rainfall than another.
or (iii) $R < 2T$ where winter is the season with most rain.

In these formulae R is the average rainfall for the year in centimetres; T is the average yearly temperature (°C).

BS $R \geqslant T + 14$ for summer rain areas
$R \geqslant T + 7$ where there is no season with more liability to rain than another
$R \geqslant T$ for winter rain areas
(In BS climates the vegetation ranges from bush to grassland.)

BW $R < T + 14$ for summer rain areas
$R < T + 7$ where there is no season with more liability to rainfall than another
$R < T$ for winter rain areas
(BW produces desert.)

Temperate rain climates

Mean temperature of the coldest month between + 18°C and −3°C.

Cs Wettest (winter) month of the year has ⩾3 times the average rainfall of the driest (summer) month.
(Cs is typically accompanied by evergreen broad-leafed forest.)

Cf No marked dry season.
Sub-types:
Cfa Hot summers: warmest month > + 22°C
Cfb Warm summers: at least 4 months > + 10°C
Cfc Cool summers: only 1–3 months > + 10°C.
(Cfa and Cfb vegetation generally deciduous broad-leafed forest, but in areas with very mild winters evergreen broad-leafed forest.
Cfc vegetation needle-tree forest.)

Cw Wettest (summer) month has ⩾10 times the rainfall of the driest winter month.
(Cw, occurring mainly on mountain heights above Aw climates, produces evergreen forest vegetation.)

Boreal forest and snow climates

Mean temperature of the warmest month > + 10°C, coldest month < − 3°C.

Dw Wettest (summer) month has ⩾10 times the average precipitation of the driest (winter) month.

Df Less seasonal difference in the average downput of rain and snow.
Sub-types:
Dfa and Dwa Hot summers: warmest month > + 22°C
Dfb and Dwb Warm summers: at least 4 months > + 10°C
Dfc and Dwc Cool summers: only 1–3 months > + 10°C.
(Dfa, Dfb, Dwa, Dwb climates go with deciduous (broad-leafed) forest.
Dfc, Dwc go with needle-tree forest.)

D climates and their vegetation are only found in the northern hemisphere, where the great continents provide the requisite conditions.

Cold snow climates

Mean temperature of the warmest month < + 10°C.

ET Mean temperature of the warmest month > 0°C.
(ET vegetation is tundra, dwarf tree species and mosses.)

EF (sometimes called simply F).
Mean temperature of the warmest month < 0°C.
Brief thaws and rain can occur, but have little or no effect on the long-term condition of the surface.
(No vegetation in EF climates: polar desert.)

Further letters are sometimes used to distinguish particular climates and subdivisions of the KÖPPEN types:

- **d** coldest month < − 38°C
- **g** Ganges type climate. warmest month before the summer solstice. height of summer rainy
- **h** hot: yearly mean temperature > + 18°C
- **i** isothermal: difference between warmest and coldest months < 5°C
- **k** cold-winter climate: yearly mean temperature < + 18°C, but warmest month > + 18°C
- **l** lukewarm, even warmth: all months between +10 and +22°C
- **n** foggy
- **n′** moist, but not foggy: with mean summer temperatures over +24°C designated **n″** over +28°C **n‴**
- **t′** Cape Verde Islands type: warmest in autumn
- **t″** Sudan type: coolest month just after the summer solstice.

It may be held that the types of climate covered by group C embrace too wide a range, and that the cooler temperate climates where birch forest (or mixed birch and pine) constitutes a large element should be distinguished from those of the domain of oak forest where the average temperature of the warmest month is generally about +15°C or over.

The proportions of the Earth's surface classified as falling within KÖPPEN's various types at the present day are estimated as follows:

	Portion of land surface	*Portion of total surface*
A	20%	36%
B	26%	11%
C	15½%	27%
D	21%	7%
E	17%	19%

KÖPPEN's classification can be criticized because it makes no mention of the level of incoming radiation and allows only indirectly and crudely for differences in the rate of evaporation. But these criticisms apply equally to most other classifications.

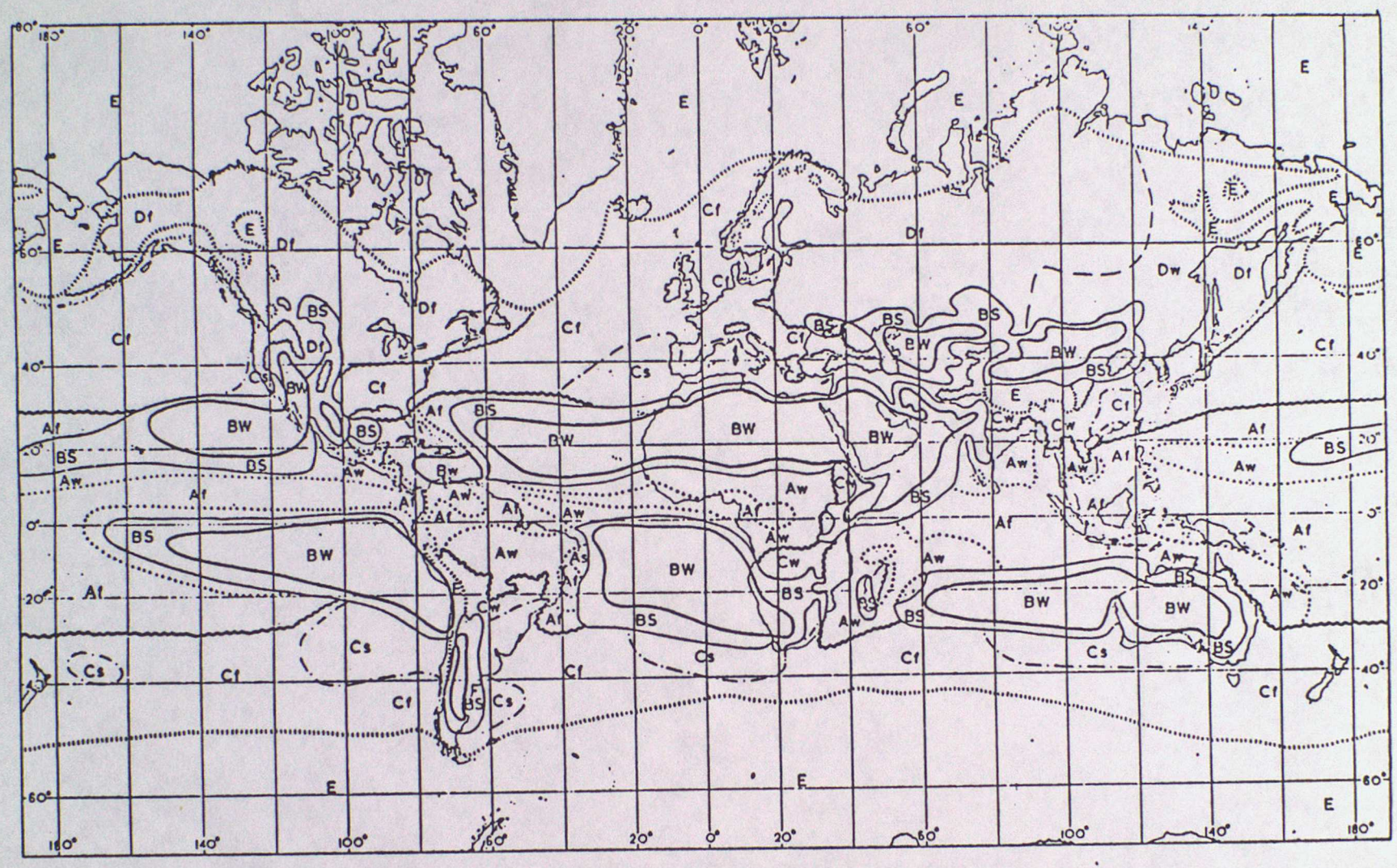

Figure 2A.1 KÖPPEN's world classification of climates.
After Lamb (1972)

CLIMATE FORCING AND FEEDBACK PROCESSES I - FORCING FROM ABOVE

C K FOLLAND AND D E PARKER

MET O 13

SUMMARY

The Earth's climate is in principle sensitive to fluctuations of incoming solar radiation and also to changes in the extent to which outgoing radiation is re-absorbed by the atmosphere. First, changes in the total flux of energy from the sun are considered, followed by changes in the distribution with latitude and season of the solar radiation received by the Earth. The latter changes are known to have occurred on time-scales of 10^4 to 10^6 years in response to changes in the Earth's orbital configuration. The effects on outgoing radiation of carbon dioxide and other trace gases, and the effects of volcanic aerosols in the stratosphere, are subjected to basic mathematical treatment.

3.1 VARIATIONS IN SOLAR RADIATION AND CLIMATIC CHANGE

3.1.1 Introduction

Earth's climate is in principle sensitive to fluctuations of solar radiation if they persist for sufficient lengths of time. The average flux of energy from the sun at the mean distance of the earth is called the solar "constant" S and is about:-

$$S = 1370 \pm 15 \ Wm^{-2}$$

The average total flux of solar radiation received by the earth is, if R is the earth's radius:-

$$E_s = \pi R^2 S$$

because the Earth's profile from space is a disk of radius R.

The area of the earth's surface is $4\pi R^2$ so the average amount of energy per unit area received by the earth-atmosphere system is

$$S/4 = 342 \pm 4 \ Wm^{-2}$$

It is easy to see that if the axis of rotation of the earth were normal to the plane intersecting the sun and all points in the earth's orbit, the incident energy per unit area would vary between a maximum (436 $Wm^{-2} = S/\pi$) at the equator and zero at the poles. However the tilt of the earth's rotation axis from this position is currently 23.44°. This results in large seasonal variations in radiation, though the simple calculation above is quite accurate close to the equator. Fig 3.1A shows the current zonally averaged radiation balance of the earth; the seasonal variations of insolation above the atmosphere are shown in Fig 3.1B. A fraction $\alpha = 0.3$ (approximately) of the radiation is reflected or scattered; this fraction is called the albedo. Figs 3.2 and 3.3 are a good guide to the surface albedo of the world with and without clouds.

The effective temperature of the earth is approximately given by

$$\sigma T_e^4 = (1-\alpha)S/4 \qquad (3.1)$$

Here we have assumed that the emissivity of the earth is one (not quite true), while T_e is approximately the mass-weighted temperature of the atmosphere, subject to some modification by dynamical processes. The sensitivity of T_e to S is shown by differentiating equation (3.1) and using

$$\Delta T_e = \frac{\partial T}{\partial S}e \ \Delta S + \frac{\partial T}{\partial \alpha}e \ \Delta\alpha \qquad (3.2)$$

If a 1% increase in S is accompanied by a 0.01 decrease in α due to the associated melting of snow and ice, or perhaps a reduction in low-level cloudiness, we obtain (using T_e = -15°C = 258°K)

$\Delta T_e \simeq$ + 1.5°C/1% increase in S

If $\Delta\alpha$ = 0 then ΔT_e is only +0.6°C/1% increase in S. So the sensitivity of the climate to S depends strongly on any associated changes in albedo. The ice/snow component of the feedback between solar radiation and climate is often called the ice-albedo feedback but its magnitude is uncertain. Nevertheless the climate system is very sensitive to long-lasting small changes in S.

3.1.2 Change of S

Does S actually change? Astronomers can say little about the fluctuations of S on short time scales but they believe it varies on geological time scales. Current theories suggest that S progressively increases as the sun gets older so that its value was perhaps 30% less 4 thousand million years ago than now. This question will be discussed in Lecture 7.

After compensation for the regular change of nearly 7% in radiation flux between January and July due to the fact that the earth currently moves in an elliptic orbit with eccentricity 0.0167, recent measurements from the solar Maximum Mission spacecraft do show small changes in S. Fig 3.4 (Hudson (1983)) shows rapid variations in S measured by an active cavity radiometer irradiance monitor (ACRIM) at a time of high solar activity, when many sunspots were sometimes visible on the solar disk. Although the mean absolute value of S shown in Fig. 3.4 (1368.2 Wm^{-2}) is in fact only accurate to about $\pm$ 0.5% ($\pm$ 7 Wm^{-2}) the relative changes in S are believed to be accurate to $\pm$ 0.1% (say $\pm$ 1 Wm^{-2}). The variations in Fig 3.4 approach four times this size and have a typical range of 0.2% over, say, a 10 day period. Reductions in S correspond to increased coverage of sunspots. Sunspots block the solar radiation at least temporarily, since the sunspot temperatures are typically about 4000°C rather than the normal

6000°C, and on daily and weekly time scales the warmer areas (faculae) sometimes surrounding sunspots apparently do not compensate. The radiation from the very small area covered by sunspots is reduced by a multiplying factor of $(4 / 6)^4$, about 0.2. These measurements were the first that indicated a real variation in the solar constant, though of course by very small amounts on short time scales. More recently, Willson and Hudson (1988) have shown that the total solar irradiance between 1980 and 1987 varied on interannual time scales in phase with the 11-year sunspot cycle (Fig 3.5), in contrast to the short-term variations in Fig 3.4 which were in antiphase with the coverage of sunspots. The short-period variations in 1980 in Fig 3.5 exceeded those after March 1984 because the sun was more active in 1980. However the short-term variability from late 1980 to March 1984 was enhanced by a fault in the satellite's stabilization, which was rectified by the space-shuttle astronauts in 1984. The 11-year sunspot cycle is also associated with in-phase fluctuation of the intensity of ultraviolet radiation (Donnelly (1983)). Because solar activity and the number of sunspots also vary on timescales of about 80 years and maybe on longer timescales ((Eddy 1983) : Fig 3.6), the findings of Willson and Hudson in Fig 3.5 may lend support to associations of widespread cooler climates with a lack of sunspots, as eg during the Maunder minimum of the 17th Century, shown in Fig 3.6, when sunspots may have been virtually absent and the "Little Ice Age" reached its climax (Lecture 8).

There is active debate about the reliability of measurements of the solar diameter in the 17th and 18th Centuries (Ribes et al (1987); Morrison et al (1988)). This debate is relevant because theories of solar dynamics relate the sun's luminosity to its diameter. Gilliland (1983) claimed to detect small changes in solar radius on a dominant time-scale of 76 years using measurements of uncertain homogeneity made by astronomers since the mid-nineteenth century. This kind of evidence has to be seriously considered until the time comes when accurate measurements of the solar constant made over many years are available.

3.1.3 Changes in the distribution of solar radiation on earth with the seasons

Changes in the seasonal distribution of radiation occur on long time scales because of fluctuations in the orbit of the earth. Assuming no intrinsic change in S, the changes in orbit are accompanied by very small annually averaged changes in S because the mean earth-sun distance changes only by small amounts. However seasonal values of radiation received at given latitudes on earth change much more. The fact that the earth's orbit has varied in a systematic way in the past was first calculated by Laplace (1798) using Newton's laws of motion and of gravity. The variations were calculated in great detail, with suggestions for their climatic consequences, by the Yugoslav mathematician Milutin Milankovitch (1941). Fig 3.7 shows the three basic types of orbital variation that occur, discussed in detail by Berger (1984):-

(a) The eccentricity of the earth's orbit changes on timescales close to 10^5 years between values of about e = 0 and e = 0.06. The current value of e is 0.0167.

(b) The angle of tilt of the earth's spin axis ('the obliquity of the ecliptic') relative to the plane passing through all points on the earth's orbit (plane of the ecliptic) varies on a timescale close to 41×10^3 years. The angle would be zero if the earth were in an 'upright' position with its spin axis normal to the ecliptic. At present the angle, q, = 23.44°. It fluctuates with variable amplitude between limits of about 22° and 24.5° and is at present decreasing on average by about 0.01°/60 years.

(c) The time of year when the earth is closest (perihelion) and furthest (aphelion) from the sun varies on timescales in the range $19\text{-}23 \times 10^3$ years. These changes are called the 'precession of the equinoxes' and are often measured by an angle, θ between the position of the earth in its orbit at the time of the Northern Hemisphere autumn solstice and the position at perihelion. At present, the earth

is at perihelion on approximately Jan 3rd so this angle is now 102°. The date of perihelion becomes later as time progresses, i.e it will be January 5th in 100 years time.

Fig 3.8 shows the computed changes in seasonal radiation at different latitudes for the last 10^6 years.Superimposed on these slow changes are much smaller, faster, changes in the geometry of the earth's orbit largely due to the orbit of Jupiter and variations in the moon's orbit which occur on timescales of decades to centuries (Fig 3.9) (Borisenkov et al (1983)).

Are these longer timescale (tens of thousands of years) radiation changes important? They are sufficient to alter the July radiation in the Northern Hemisphere through a range of at least 20% in most latitudes even though there is negligible change (0.2%) in the total mean annual radiation. (Least average radiation is received when the orbit is circular). An increase of summer radiation would warm the summer climate, balanced of course by a decrease in winter radiation which should tend to cool the winter climate and so increase the seasonal contrast. Changes in atmospheric circulation should result: eg the monsoons might tend to be more vigorous if summer radiation were more intense in the Northern Hemisphere and the ITCZ might move further north. At present summer radiation is relatively weak, though not especially so. Although the earth is furthest from the sun in July, e is fairly low. Thus the earth does not get as far away from the sun in Northern Hemisphere summer at present as it did in some previous epochs. However if radiation decreases in summer and winters are still cold enough, some areas which lose their snow in summer when summer radiation is high may retain it when summer radiation is low. Albedo will increase and amplify any cooling effect. In this way snow fields and ice sheets might grow, given other favourable circumstances.

A simple test calculation was carried out by Mason (1976) who showed that the deficiency of incident radiation in Northern Hemisphere summer between 83000 and 18000 years before present (BP) may have been just enough to balance the latent heat of fusion produced between those dates, when the Northern Hemisphere ice sheets are thought to have expanded to their maximum size. He also calculated that the excess of incident summer

radiation from 16000 BP to 6000 BP was just enough to provide the latent heat of fusion required to melt the amount of ice that is believed, from geological evidence, to have disappeared between these two dates (90% of the difference between the volume of ice-age ice and that which exists now). As Mason was at pains to point out, the calculation was over-simple because losses of radiation, and relevant feedbacks, were ignored, and thus on their own the radiation deficiencies and excesses seemed insufficient to guarantee the waxing and waning of the ice sheets. On the other hand, the variations in summer radiation were of the correct order of magnitude to make a substantial contribution, given other favourable "positive feedback" processes. So it is very important to identify these other processes. The precessional 'Milankovitch' radiation changes are not entirely negligible on millennial timescales; since the High Middle Ages (1200 AD) the flux of solar radiation incident on the atmosphere around the summer solstice at the North Pole has decreased by nearly 0.5%.

3.1.4 Energy balance models

The equilibrium sensitivity of earth's climate to changes in S can be studied in an instructive if preliminary way using simple 'energy balance' models. Appendix I, prepared by David Carson for the 1982 Advanced Lectures and attached to Lecture 10 of this series, discusses simple models and their approach to calculating the consequences of changes in S and in carbon dioxide or other greenhouse gases. The results of many of these calculations are thought-provoking even if they turn out to be somewhat misleading. Figure A10.13 of Appendix I shows that a reduction of S by a few per cent might cause the earth to become completely glaciated; a subsequent increase in S of at least 30% might be needed to melt the ice that has formed. These conclusions do indicate the potential sensitivity of climate to S in the presence of albedo feedback and the likely non-linearity of the response of the climate system.

In Lecture 7 we shall discuss the effects of the Milankovitch radiation variations in more detail and the hypothesis that they are the pace-makers of the ice-age - interglacial fluctuations that have occurred quite regularly over the last 2-3 million years.

3.2 CARBON DIOXIDE AND THE GREENHOUSE EFFECT

3.2.1 General discussion

Carbon dioxide is present in only small amounts in the atmosphere but is increasing by about 0.5% a year at present. The current concentration is about 350 parts per million by volume (ppmv). Carbon dioxide is important since it strongly absorbs long-wave radiation and re-emits it, so is radiatively very active in the climate system. The following discussion is only schematic and is oversimplified in many ways. It is adapted from Gill (1982) and applies to carbon dioxide, water vapour and other 'greenhouse' gases.

Consider a greenhouse formed by placing a horizontal thin sheet of glass above the ground (Fig 3.10). Let this glass be nearly transparent to solar radiation, absorbing only a small fraction s, but much less transparent to terrestial radiation. Suppose the glass and ground are initially cold. Let a downward flux, I, of solar radiation commence. Most of I will reach the ground; assuming the ground is a black body (ie has zero albedo), the ground will warm up to a temperature T_g and emit long-wave radiation with a flux U given by Stefan's law:-

$$U = \sigma T_g^4 \qquad (3.3)$$

Now let a fraction e of U be absorbed by the glass. The glass will warm up and emit a flux of radiation B. Equilibrium is reached when on both sides of the glass the upward and downward fluxes of radiation are equal.

Thus

$$I = (1-e)\,U + B \qquad \text{above the glass} \qquad (3.4)$$

$$(1-s)\,I = U-B \qquad \text{below the glass} \qquad (3.5)$$

It is easy to show that

$$\sigma T_g^4 = I \left[\frac{1 - s/2}{1 - e/2} \right] \qquad (3.6)$$

If s were zero and e were 1 then

$$\sigma T_g^4 = 2 I \qquad \text{from (3.6)}$$

or B = I, so the flux received by the ground would be twice the solar flux, and T_g would have increased by a factor $\Delta T_g = 2^{1/4} = 19\%$ compared with the case for e = 0. Now s is about 0.2 for present conditions and if this were true when e = 1 then $\Delta T_g = 16\%$. An increase in T_g of 19% would correspond to a surface temperature rise of about 50°C above the condition where e=0, if the albedo was zero: as the average amount of energy incident per unit area of the earth's surface is about I = 342 Wm^{-2}, and $\sigma = 5.7 \times 10^{-8}$ Wm^{-2} K^{-4}, then T_g = 278°K for e = 0 and δT_g = 53°C. In practice $T_g + \delta T_g$ would be considerably less than 331°K because e < 1 and importantly because of vertical atmospheric readjustments including the conversion of some of I to latent heat. These provide a 'radiative-convective' equilibrium in which the atmosphere above the ground takes up some of the extra heat initially absorbed at the surface.

Of course, the 'glass' is in reality distributed continuously in the vertical and water vapour is an important greenhouse gas which is very variable in concentration geographically (see Lecture 10). A point to note is that the addition of a greenhouse gas to the atmosphere does not necessarily leave the effective solar radiation received by the earth-atmosphere system unchanged if changes to the earth-atmosphere albedo also result. If we include the effect of the albedo α of the earth-atmosphere system and replace the net solar radiation received by the ground by $(1-s)(1-\alpha)I$ (ignoring αs^2) and the net downward solar radiation above the glass by $I(1-\alpha(1-s)^2)$ we obtain approximately:-

$$\sigma T_g^4 = \frac{I[1-(s+2\alpha-3\alpha s)]}{2} \Big/ \left(1 - e/2\right) \qquad (3.7)$$

Here we arbitrarily attribute the albedo (due to ground and clouds) to the whole layer below the 'glass' so T_g is not really the ground temperature. If α decreases as e increases, σT_g^4 will increase at a faster rate. This could happen if snow and ice melted or low cloudiness decreased. Under present day conditions where nominally T_g = 287°K, s=0.2 and α = 0.3, equation (3.7) gives approximately e = 0.8 for carbon dioxide, ozone, water vapour and other trace greenhouse gases together. Thus, schematically, at present $U = \sigma T_g^4 \simeq 1.1I$ which implies that the long-wave radiation B incident on the ground from the atmosphere above is about 0.6I since the absorbed solar radiation $U-B = (1-s)(1-\alpha) I \simeq 0.5I$ at the surface. Figure 3.11 summarises the current radiation balance of the earth-atmosphere system. This shows that the direct net loss of long-wave radiation from the surface contributes 0.2I to balancing U-B, the remaining 0.3I being first converted to sensible or latent heat in the lower atmosphere. The sensible heat is then lost as long-wave radiation immediately and the latent heat is lost likewise once precipitation has occurred.

Lecture 10 discusses the physical basis and evidence for the potential effects of carbon dioxide in the climate system in more detail and Lectures 7 and 8 indicate its possible role in past climatic changes.

3.3 VARIATIONS IN VOLCANIC DUST IN THE STRATOSPHERE

3.3.1 Introduction

From time to time huge volcanic eruptions of the explosive kind create world-wide veils of finely-divided dust causing optical effects such as a reddened sun or moon or halo effects around the sun like Bishop's rings. During such eruptions, carbon dioxide and water vapour are ejected into the stratosphere with, very often, compounds of sulphur such as H_2S and SO_2 in gaseous form. The quantity of carbon dioxide ejected in a typical eruption is thought to be only about 0.01 ppmv, so the addition of carbon dioxide to the atmosphere is minute compared with the current rate of annual increase (1.5 ppmv). Likewise the heat output is, in relative terms, minute. It has long been considered, however, that the dust vented from a huge volcanic eruption that reaches well into the stratosphere could affect climate. This was thought to be likely because:

(a) Estimates of surface temperature over widespread parts of the globe often showed a drop after (but also, disturbingly often, before) a huge volcanic eruption.

(b) The measured intensity of the direct solar beam was always reduced though the diffuse radiation usually increased to partially compensate.

The classic book on volcanic dust and climate is by Humphreys (1940), whose ideas are instructive and not wholly outdated. An extensive description of the development of observational studies of climatic effects in relation to volcanic dust is given by Lamb (1972). Fig 3.12, from Lamb (1972) shows examples of historical measurements of monthly average values of the strength of the direct solar beam, while Fig 3.13 shows graphs of historic regional average temperatures derived by Koppen (see p 410ff of Lamb (1972)). The timing of the largest volcanic eruptions is shown on the diagrams. Lamb has devised a "dust veil" index to measure the climatologically most important eruptions. The index is partly based on

observations of the optical effects of the dust but also on the worldwide fall in surface temperature (as far as it can be judged) following a given eruption (Lamb (1970)). This subjective index suggests that the eruptions of Tambora (1815) (Indonesia), Coseguina (1835) (Nicaragua), Krakatau (Indonesia) (1883) and Agung (Indonesia) (1963) (Fig 3.14) were among those most likely to have affected surface temperatures since the beginning of the nineteenth century, prior, that is, to the recent eruption of El Chichon (see below). On a millenial time scale, Fig 3.15, from Lamb (1972), shows an apparent association between the reconstructed extent of sea-ice near Iceland and volcanic eruptions in Iceland. Acidity measurements in cores from polar ice sheets have now been used to infer volcanic records for past centuries, and Legrand and Delmas (1987) have tentatively postulated that a hitherto unknown major eruption occurred around 1808, ie 7 years before Tambora (Fig 3.16). Hammer et al (1980) have obtained an acidity series stretching back to before 600 AD from the Greenland ice sheet.

3.3.2 Controversy concerning volcanic dust and climate

The problem of whether the apparent associations between volcanic activity and climate are real continues to be controversial. The main reasons for controversy are:-

(a) There may be sufficient variability between eruptions in the physics of the interaction between volcanic dust and solar and terrestrial long wave radiation that the sign of the effect of stratospheric volcanic dust on surface temperature may vary from eruption to eruption. The net effects depend crucially on the size distribution and chemical constitution of the dust, which may vary between eruptions.

(b) It has not yet proved possible to use an AGCM with a realistic stratosphere and including what would now be regarded as the essential physics of the radiative interactions, to attempt to simulate the

climatic effects of volcanic dust (Hofmann (1987)). In any case, the simulated response of the oceans could be crucial as volcanic 'dust' may stay in the stratosphere for several years.

It is now thought that the reason why past ground measurements have indicated long residence times for stratospheric dust, despite the appreciable scavenging that must exist through dynamical interactions between troposphere and stratosphere, is that some of the "dust" is formed after the eruption. Sulphur gases (H_2S, SO_2 etc) formed during the eruption may slowly combine with stratospheric water vapour to produce reflective, aqueous droplets of a typical diameter 1 μm or less whose terminal velocities are very low. So the quantity of sulphur gas and possibly sulphur particles ejected in an eruption is now thought to be very important. Lamb (1972) shows terminal velocities for spherical particles of several radii (Table 3.1).

Table 3.1 (from Lamb (1972))

STRATOSPHERIC RESIDENCE TIMES FOR VOLCANIC DUST

(Total times taken to fall through still air to tropopause at (a) 17 km, (b) 12 km)

Particle Diameter	Initial height (km)	(a)	(b)
2 μm	40	25 weeks	41 weeks
	30	21 weeks	37 weeks
	25	16 weeks	31 weeks
	20	7 weeks	23 weeks
1 μm	40	1.9 years	3.1 years
	30	1.6 years	2.8 years
	25	1.3 years	2.4 years
	20	0.6 years	1.7 years
0.5 μm	40	7.8 years	12.5 years
	30	6.5 years	11.3 years
	25	5.0 years	9.7 years
	20	2.2 years	6.9 years

3.3.3 El Chichon

In April 1982 a very violent, explosive eruption occurred in S Mexico from the volcano El Chichon (the "lump on the head") situated at 17°N 93°W. Fig 3.17 from Robock and Matson (1983) shows how the dust from that explosion circled the globe in about 1 month in a narrow band between 15°-25°N. Winds were easterly, and accelerating, at the 25-30 km level where much of the dust initially resided because the summer stratospheric circulation was just getting underway. At Hawaii (Central Pacific 19°N) directly under the dust cloud, direct solar radiation was reduced by up to 30% in the months following the eruption, a reduction offset, but not completely, by an increase in diffuse solar radiation (De Luisi et al (1983)). The measurements indicated that in the visible spectrum the dust produced a mean optical depth T of the order of 0.25. Optical depth is defined by

$$F = F_o\, e^{-T} \qquad (3.8)$$

F_o is the incident flux and F is that part of the flux that emerges below the dust layer without absorption or being scattered, i.e. F only measures the reduction of direct radiation. Balloon and other measurements suggested that a few months after the eruption much of the cloud was composed of droplets containing 75% sulphuric acid and 25% water with a mode radius of about 0.3 μm (MacCracken and Luther (1984) give details). There was also hydrochloric acid in the cloud (Hofmann (1987)). By July the dust cloud, now at a height of between 20-25 km, reached Italy. It became visible to the naked eye on a few evenings in August 1982 around Bracknell, with some unusual sunsets. Referring back to Table 3.1, droplets near a radius of 0.3 μm have terminal velocities so low that dynamical and other processes are likely to be important for their removal from the stratosphere, and the decay of the El Chichon stratospheric aerosol by a factor of 10 took about 2 years (Hofmann (1987)). Global surface temperatures rose soon after the eruption, because of El Nino (see Lecture 6). Parker (1985) compensated tropical tropospheric temperatures for the Southern Oscillation and found no clear evidence for

eruption-related cooling, but Angell (1988), using worldwide data, did find tropospheric and surface cooling after El Chichon and earlier eruptions when the influence of El Nino had been compensated for. Note, however, that volcanic eruptions may influence El Nino, and also the Indian Monsoon (Handler (1986)).

3.3.4 Heating of stratospheric dust layer

It is not completely obvious that a stratospheric volcanic dust cloud should become hotter than its environment. The particles may be so small that solar heating is negligible and their radiative properties could be such that infra-red radiation from below also has little effect. Newell (1981) claimed to have detected a heating of the dust cloud produced by Agung (1963) by several degrees centigrade. Theoretical work (e.g Pollack et al (1976); Vupputuri and Blanchet (1984)) has suggested that a heating of several degrees is possible for the likely sizes and chemical constituents of volcanic dust, mainly due to the absorption of infra-red radiation from below. Parker and Brownscombe (1983) cautiously concluded that the El Chichon dust cloud was heated near the equator between 30-50 mb by several degrees centigrade. Fig 3.18A (from Parker and Brownscombe (1983)) shows stratospheric temperatures at several levels in 1980-82 derived from the NOAA 6 Stratospheric Sounding Unit and Microwave Sounding Unit. Of the levels sampled, that at 50 mb shows the largest temperature increase from 1981-82. Fig 3.18B, (again from Parker and Brownscombe) shows the 30 mb temperature anomalies in August 1982 from radiosonde data. A complicating factor in this and the Agung studies is that anomalous warming was expected in both 1963 and 1982 within 15°N or S of the equator below the descending, westerly, phase of the stratospheric "quasi-biennial oscillation" (QBO) (see Lecture 6). However, an analysis by Labitzke et al (1983) of the 50 and 30 mb temperatures between 1964 and 1982 strongly suggests that the QBO contributed only a part of the 1982 warming. The location of the observed temperature anomaly maximum near the equator in Fig 3.18B, rather than at the latitude of the main dust cloud (20°N), is probably partly a result of the additional influence of the QBO.

3.3.5 A schematic, simplified, model of effects of volcanoes on surface temperature

Although literature on the modelling of the physical effects of volcanic dust on the surface temperature is in some disagreement, there is an emerging picture of the important physical processes. However the sign of the effect of volcanic dust in the surface energy balance is difficult to determine because there are two important competing physical effects and a host of smaller ones. The most important opposing effects are:-

(a) The dust layer reflects solar radiation, tending to cool the surface of the earth.

(b) The dust layer absorbs terrestrial radiation, tending to warm the surface of the earth.

Absorption of solar radiation can be significant but is now thought to be fairly small, at least in some volcanic eruptions.

Fig 3.19 shows a simple schematic model which cannot be used to make predictions. Because we shall estimate the perturbation of the surface energy balance resulting from stratospheric dust, we will not explicitly include the effects of carbon dioxide and other greenhouse gases which are assumed to be fixed. Imagine solar radiation I passing down through the dust layer; a fraction rI is reflected to space and lost while the remaining fraction tI = (1-r)I is transmitted to ground either as direct or diffuse radiation. Here we have assumed no absorption of solar radiation by the dust layer itself, which is not quite correct. The transmitted radiation, It, reaches the "ground" and a fraction αIt, is reflected upward: strictly speaking, the albedo α is not quite the same as for the "non dust" case as more of the solar radiation is diffuse and less is direct. On reaching the dust layer again, an amount of reflected radiation t(αIt) is lost and an amount r(αIt) is reflected down. So the initially reflected solar radiation is multiply -reflected between dust layer and ground with rapidly decreasing intensity. The initial loss of solar

radiation to the system, rI, is to some extent "made up" by the multiple reflections as the expected radiation loss from the ground in the absence of dust (for a non-zero value of α) is clearly reduced. However the total radiation absorbed by the ground cannot quite reach the initial amount transmitted (It) for a non-zero value of α.

Now also assume that a fraction b of the long-wave radiation U lost from the surface (partly indirectly from the troposphere itself - see Section 3.2) is absorbed by the dust layer without further reflection.

Then we find that the solar radiation absorbed by the ground I_G is:-

$$I_G = (1-\alpha)tI \ (1+r\alpha+r^2\alpha^2+\ldots)$$

or $$I_G = \frac{(1-\alpha)tI}{1-r\alpha}$$ after summation

Similarly the solar radiation lost through the dust layer to space after multiple reflection is:-

$$I' = rI+t^2\alpha I \ [1+r\alpha+\ldots]$$

or $$I' = I\left(r+\frac{t^2\alpha}{1-r\alpha}\right)$$

We can now calculate the value of I_G . The radiation balance at the ground is:-

$$-B+U = I_G \qquad (3.9)$$

where B is the longwave radiation emitted by the dust layer and U is the longwave radiation emitted by the ground.

The radiation balance above the dust layer is

$$B+(1-b)U = I-I' \qquad (3.10)$$

Adding (3.9) and (3.10) and substituting for I_G and I' we find

$$U = \left[\frac{2}{2-b}\right] I \left[\frac{1-r-\alpha+\alpha r}{1-r\alpha}\right] \qquad (3.11)$$

Now if t = 1 and r = 0, ie no dust layer exists, we found in Section 3.1.1 that $U = (1-\alpha)I$ (equation (1)). So the net change ΔU in the long-wave radiation lost (eventually) by the ground when a dust layer is interposed is:-

$$\Delta U = \frac{I(1-\alpha)}{1 - r\alpha} \{[1 + b/2](1-r)-1\} \qquad (3.12)$$

where b has been assumed to be small so that $\frac{1}{1-b/2} \simeq 1+b/2$

Now $U = \sigma T_g^4$ (approximately) as in section 3.2.1, so $\Delta U = 4\sigma T_g^3 \Delta T_g$. Table 3.2 shows calculations of equilibrium values of ΔT_g, assuming T_g = 287°C, for reasonable values of t and b. The effects of additional surface evaporation etc are neglected. MacCracken and Luther (1984), Pollack et al (1976) and Chou et al (1984) give a discussion of the detailed physics and its uncertainties and suggestions for values of t, (dust layer transmission coefficient), and b (dust layer absorption coefficient) and their effects on surface temperature.

TABLE 3.2 EQUILIBRIUM TEMPERATURE CHANGES AT THE SURFACE FROM THE SCHEMATIC MODEL, °C

1. b = 0

α	t = 0.99	t = 0.97	t = 0.95
0	-0.6	-1.9	-3.1
0.3	-0.3	-0.9	-1.6
0.6	-0.1	-0.3	-0.5
0.8	0.0	-0.1	-0.1

2. b = 0.02

α	t=0.99	t=0.97	t=0.95
0	0.0	-1.3	-2.6
0.3	0.1	-0.5	-1.1
0.6	0.2	-0.3	-0.3
0.8	0.1	+0.1	0.0

It is seen that the sign of the change in surface temperature is very sensitive to t and to b and also to α. These results agree qualitatively with existing ideas, despite the crudeness of the model. A cooling due to volcanic dust is less likely where α is high; and small changes in b, the coefficient that measures the absorption by the dust of long-wave radiation, can easily change the sign of a surface temperature response. Chou et al (1984) agree that eruptions are likely to produce varying surface temperature responses as a result of differences in particle size or chemical composition even if their dust clouds are similar in extent and optical depth. The temperature changes in Table 3.2 would be much reduced in practice because of the thermal inertia of the oceans. Fig 3.20 from Chou et al (1984) is a simple (but very uncertain) time-dependent calculation making some allowance for oceanic thermal inertia and the decay with time of the dust layer. In Lectures 8 and 9 we consider briefly whether it is likely that volcanic dust has really affected surface and tropospheric temperature in recent centuries.

REFERENCES TO LECTURE 3

ANGELL, J K (1988) Impact of El Nino on the delineation of tropospheric cooling due to volcanic eruptions. J. Geophys. Res., 93, D4, 3697-3704.

BERGER, A (1984) Accuracy and frequency stability of the Earth's orbital elements during the Quaternary. Milankovitch and Climate, Pt. I: Ed. A Berger et al, NATO ASI 126, (D. Reidel Pub. Co.), pp 3-39.

BERGER, A and PESTIAUX, P (1984) Accuracy and stability of the Quaternary terrestrial insolation. Milankovitch and Climate Pt 1. Ed: A Berger et al, NATO ASI, 126, (D. Reidel Pub. Co.), pp 83-111.

BORISENKOV, YE. P, TSVETKOV, A V and AGAPONOV, S V (1983) On some characteristics of insolation changes in the past and the future. Climatic Change, 5, 237-244.

CALDER, N (1974) The Weather Machine. BBC, London.

CHOU, M-D, PENG, L, and ARKING, A (1984) Climate Studies with a multilayer energy balance Model, Pt III: Climatic impact of stratospheric volcanic aerosols. J. Atm. Sci., 41, 759-767.

DE LUISI, J J, DUTTON, E G, COULSON, K L, DEFOOR, T E and MENDONCA, B G (1983) On some radiative features of the El Chichon volcanic stratospheric dust cloud and a cloud of unknown origin observed at Mauna Loa. J. Geophys. Res., 88, C11, 6769-6772.

DONNELLY, R F (1983) Solar UV spectral irradiance variations. In 'Weather and Climate responses to solar variations'. Ed: B M McCormac, Colorado Ass. Univ. Press, pp 43-55.

EDDY, J A (1983) A Historical review of solar variability weather and climate. In 'Weather and Climate Responses to solar variations'. Ed: B.M. McCormac, Colorado Ass. Univ. Press, pp 1-15.

GILL, A E (1982) Atmosphere-ocean dynamics. Academic Press, 664 pp.

GILLILAND, R L (1983) Climate change as a test of the influence of external perturbations. In 'Weather and Climate responses to solar variations'. Ed: B M McCormac, Colorado Ass. Univ. Press, pp 273-281.

HAMMER, C U, CLAUSEN, H B and DANSGAARD, W (1980) Greenland ice sheet evidence of post-glacial volcanism and its climatic impact. Nature, 288, 230-235.

HANDLER, P (1986) Stratospheric aerosols and the Indian Monsoon. J. Geophys. Res, 91, D13, 14475-14490.

HENDERSON-SELLERS, A and McGUFFIE, K (1987) A climate modelling primer. Chichester (Witley), 217pp

HOFMANN, D J (1987) Perturbations to the global atmosphere associated with the El Chichon volcanic eruption of 1982. Rev. Geophys., 25, 743-759

HUDSON, H S (1983) Variations of the Solar Radiation Input. In 'Weather and Climate responses to solar variations'. Ed: B M McCormac, Colorado Ass. Univ. Press, pp 31-41.

HUMPHREYS, W J (1940) Physics of the air. 3rd Edition. Reprinted by Dover (1964).

KOPPEN, W (1873) Ueber Mehrjahrige Perioden der Witterung, insbesondere uber die 11-jahrige Periode der Temperatur. Z. Met., Vienna, 8, pp 241-248, 257-267.

KOPPEN, W (1914) Lufttemperaturen, Sonnenflecke und vulkanausbruche. Met., Z. Braunschweig, 31, pp 305-328.

LABITZKE, K, NAUJOKAT, B, and McCORMICK, M P (1983) Temperature effects on the stratosphere of the April 4, 1982, eruption of El Chichon, Mexico. Geophys. Res. Letters, 10, 24-26.

LAMB, H H (1970) Volcanic dust in the atmosphere. Phil Trans, Roy Soc, A, 266 (No 1178) pp 426-533.

LAMB, H H (1972) Climate, Present, Past and Future. Vol 1, Methuen.

LAPLACE, P S (1798) Traité de Mécanique Céleste. 5 Vols. Paris (4th Ed., Paris, 1882).

LEGRAND, M and DELMAS, R J (1987) A 220-year continuous record of volcanic H_2SO_4 in the Antarctic ice sheet. Nature, 327, 671-676.

MacCRACKEN, M C and LUTHER, F M (1984) Radiative and climate effects of the El Chichon eruption. Proc of Fifth Amer. Met. Soc. Conf. Radiation, 31 October-4 November 1983, Baltimore MD.

MASON, B J (1976) Towards the understanding and prediction of climatic variations. Quart.J. Roy. Met. Soc., 102, 473-498.

MILANKOVITCH, M (1941) Canon of insolation and the ice age problem - Spec. Pub. 132, Trans. No. 1793, 1969 - Israel Program for Scientific Translations.

MORRISON, L V, STEPHENSON, F R and PARKINSON, J (1988) Diameter of the sun in AD 1715. Nature, 331, 421-423

NATIONAL ACADEMY OF SCIENCES (1975) Understanding Climatic Change. Washington DC

NATIONAL RESEARCH COUNCIL (1982) Solar Variability, Weather and Climate. Ed: J Eddy. Studies in Geophysics Ser., Geophys. Res. Board. National Academy Press.

NEWELL, R E (1981) Further studies of the atmospheric temperature change produced by the Mt Agung volcanic eruption in 1963. J. Volcanology and Geothermal Research, 11, 61-66.

NEWHALL, C G and SELF, S (1982) The volcanic explosivity index (VEI): An estimate of explosive magnitude for historical volcanism. J. Geophys. Res., 87, 1231-1238.

PARKER, D E (1985) The influence of the Southern Oscillation and volcanic eruptions on temperature in the tropical troposphere. J. Climatology, 5, 273-282.

PARKER, D E and BROWNSCOMBE, J L (1983) Stratospheric warming following the El Chichon volcanic eruption. Nature, 301, 406-408.

POLLACK, J B, TOON, O B, SAGAN, C, SUMMERS, A, BALDWIN, B, and VAN CAMP, W (1976) Volcanic Explosions and Climatic Change: A theoretical assessment. J. Geophys. Res, 81, 1071-1083.

RAMPINO, M R and SELF, S (1982) Historic eruptions of Tambora (1815), Krakatau (1883), and Agung (1963), their stratospheric aerosols, and climatic impact. Quaternary Research, 18, 127-143.

RASCHKE, E, VONDER HAAR, T H, BANDEEN, W R and PASTERNAK, M (1973) The annual radiation balance of the earth-atmosphere system during 1969-70 from Nimbus 3 measurements. J. Atm. Sci., 30, 341-364.

RIBES, E, RIBES, J C and BARTHALOT, R (1987) Evidence for a larger sun with a slower rotation during the seventeenth century. Nature, 326, 52-55.

ROBOCK, A and MATSON, M (1983) Circumglobal transport of the El Chichon volcanic dust cloud. Science, 221, 195-197.

STEPHENS, G L, CAMPBELL, G G and VONDER HAAR, T H (1981) Earth radiation budgets. J. Geophys. Res., 86, C10, 9739-9760.

VUPPUTURI, R K R and BLANCHET, J P (1984) The possible effects of El Chichon eruption on atmospheric thermal and chemical structure and surface climate. Geofis. Int., 23-3, 433-447.

WILLSON, R C (1982) Solar irradiance variations and solar activity. J. Geophys. Res., 87, A6, 4319-4326.

WILLSON, R C and HUDSON, H S (1988) Solar luminosity variations in solar cycle 21. Nature, 332, 810-812.

WINSTON, J S, GRUBER, A, GRAY, T I, VARNADORE, M S, EARNEST, C L and MANNELLO, L P (1979) Earth-atmsophere radiation budget analyses derived from NOAA satellite data June 1974 - February 1978. Vols 1 and 2, US Dept of Commerce, Washington DC.

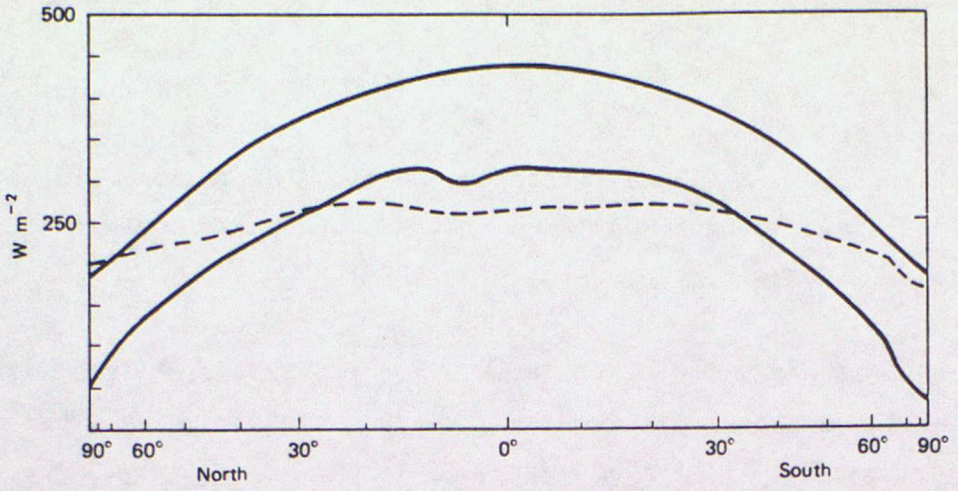

The radiation balance of the earth. The upper solid curve shows the average flux of solar energy reaching the outer atmosphere. The lower solid curve shows the average amount of solar energy absorbed; the dashed line shows the average amount of outgoing radiation. The lower curves are average values from satellite measurements between June 1974 and February 1978, and are taken from Volume 2 of Winston *et al.* (1979). Values are in watts per square meter. The horizontal scale is such that the spacing between latitudes is proportional to the area of the earth's surface between them, i.e., is linear in the sine of the latitude.

Figure 3.1A. From Gill (1982).

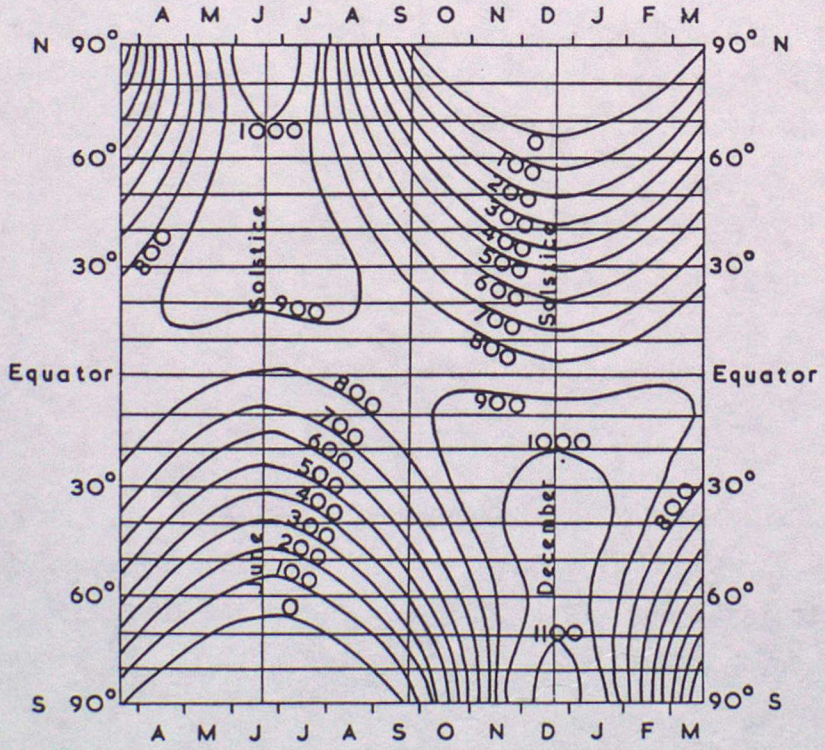

Daily totals of solar radiation available in different latitudes of the Earth in the absence of the atmosphere, in g cal/cm², around the year, at the present epoch. Divide by 2.07 to give Wm^{-2}.

Figure 3.1B. From Lamb (1972).

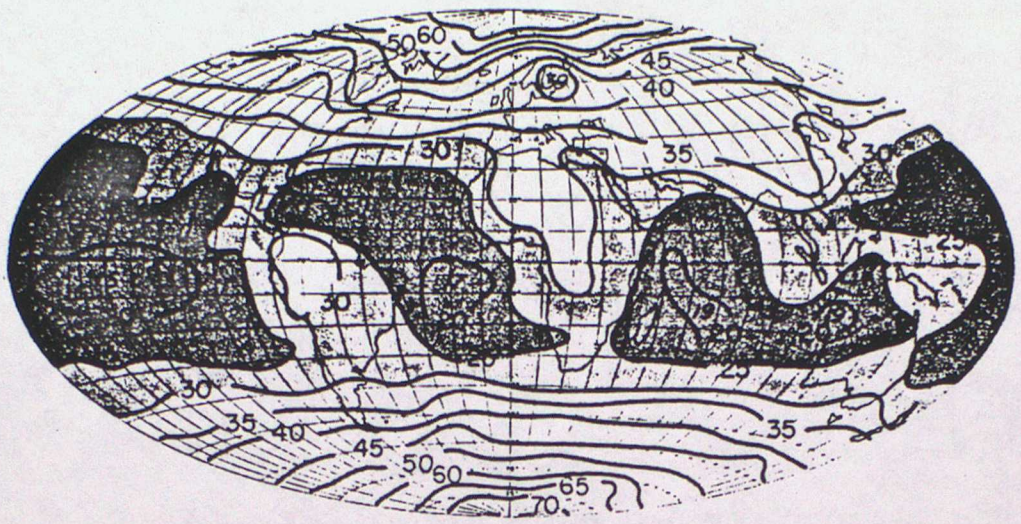

Figure 3.2. The average albedo obtained from a composite of 48 months of satellite data obtained between 1964 and 1977.
From Stephens et al (1981).

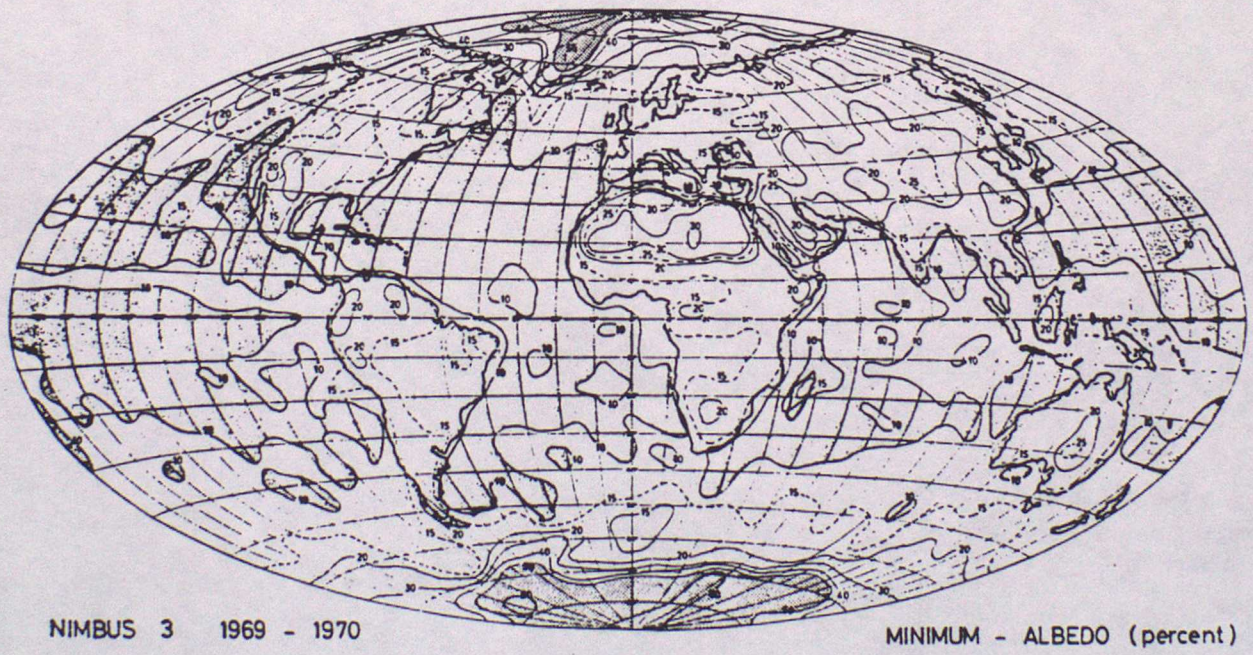

Figure 3.3. The minimum albedo of the Earth from NIMBUS 3 satellite measurements made in 1969 to 1970.
From Raschke et al (1973).

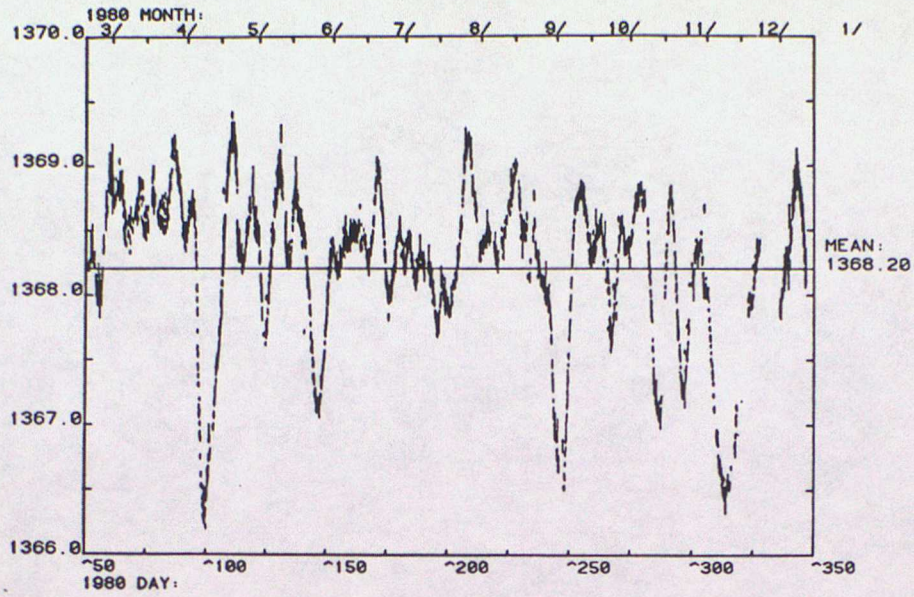

Total solar irradiance (W m^{-2}) as measured by the active cavity radiometer onboard the SMM (Willson, 1982). Each point represents the average of data for one orbit (~96 min); the observed standard deviation for each point is on the order of 15 ppm. The large dips are associated with the crossing of the solar disk by large sunspot groups.

Figure 3.4. From Hudson (1983).

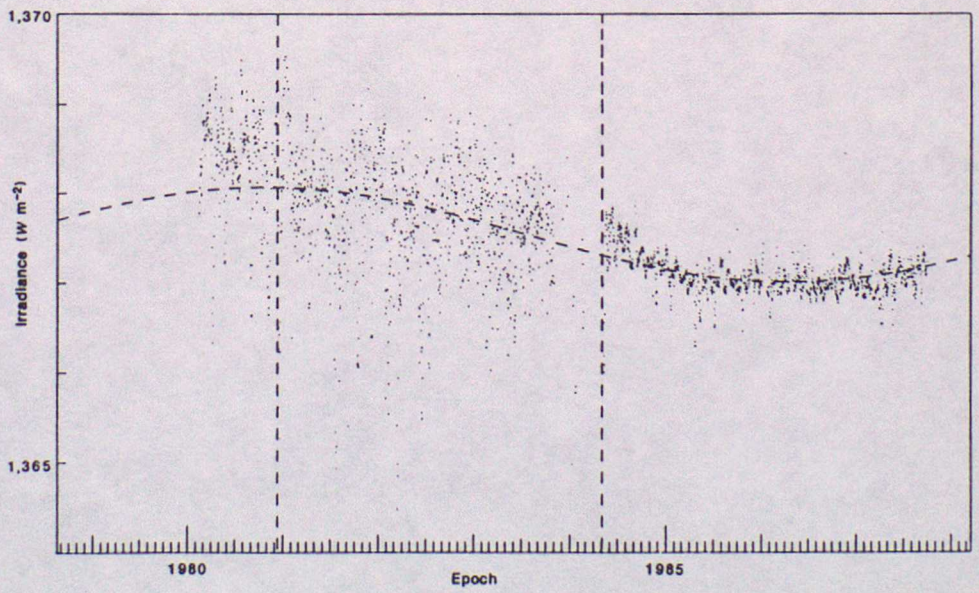

ACRIM I daily mean data from early 1980 to late 1987. The dashed vertical lines separate the two 'precision solar pointed' periods (most of 1980 and after March 1984) from the intervening 'spin-mode' period. The dashed curve is a fitted least-mean-square cosine function,

$$S = S_0(1 + 0.039 \times \cos(2\pi(t\text{-}1980.82)/10.95));$$

period 4,000 d; offset 300 d; amplitude $0.039 \pm 0.003\%$.

Figure 3.5. From Willson and Hudson (1988).

Annual mean sunspot numbers A.D. 1610 to present. Depressed period from about 1645 to 1715 is the Maunder Minimum.

Figure 3.6.

From National Research Council (1982).

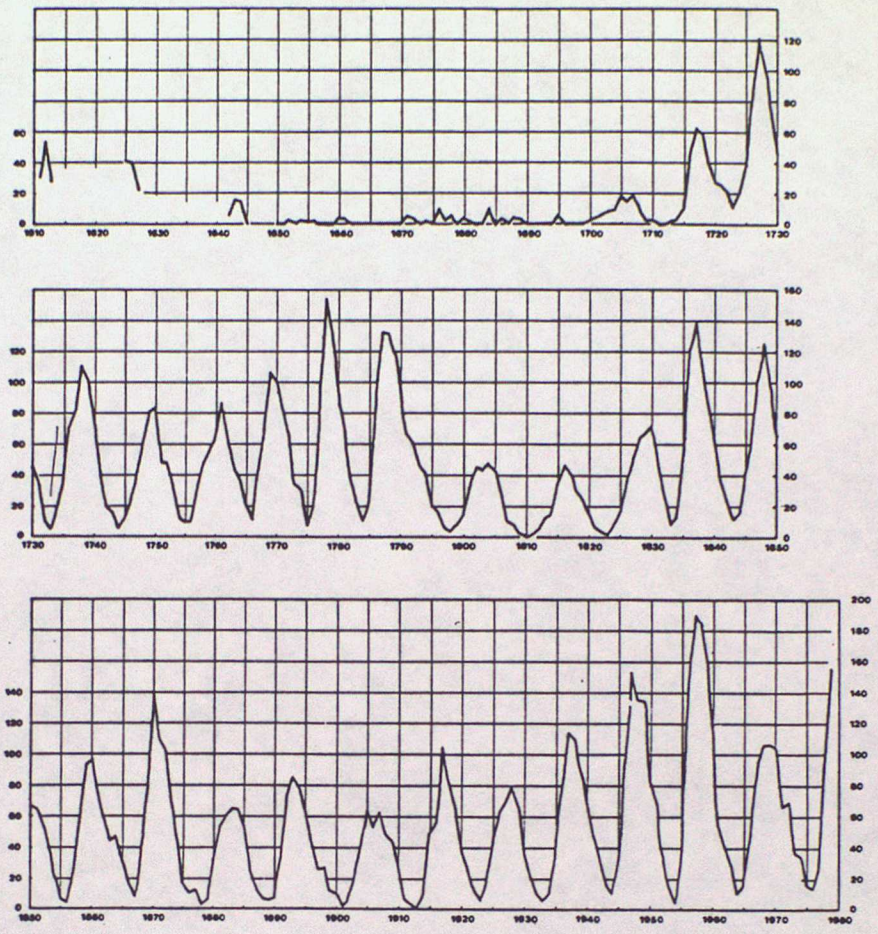

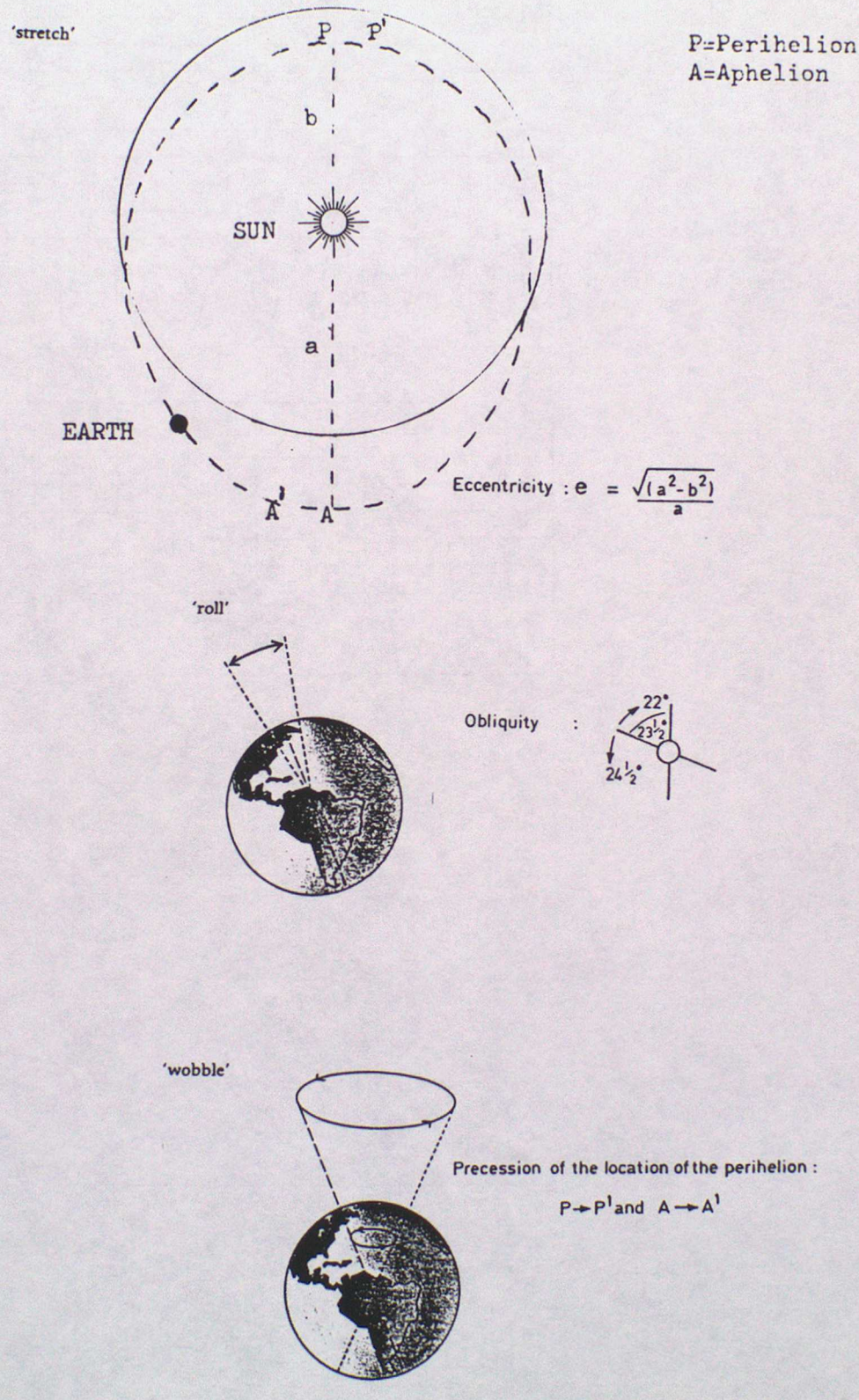

Figure 3.7. Variations in the earth's orbit.
Adapted from Calder (1974) and Henderson-Sellers and McGuffie (1987).

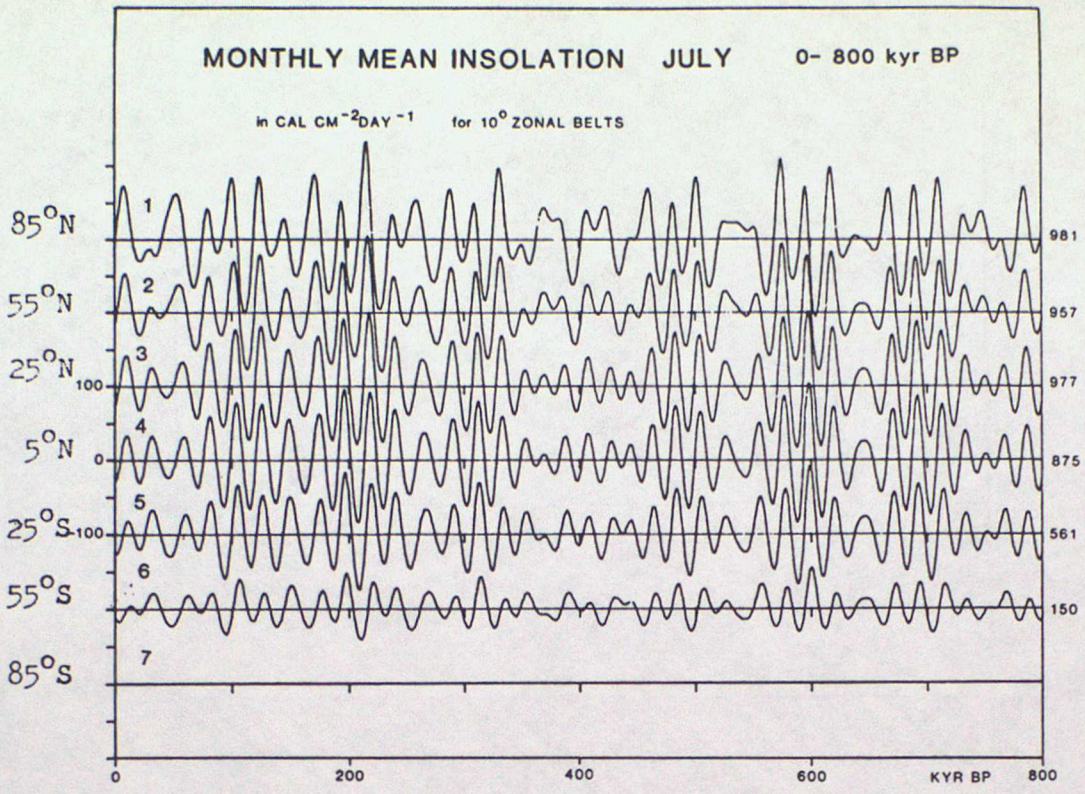

Figure 3.8. From Berger and Pestiaux (1984).

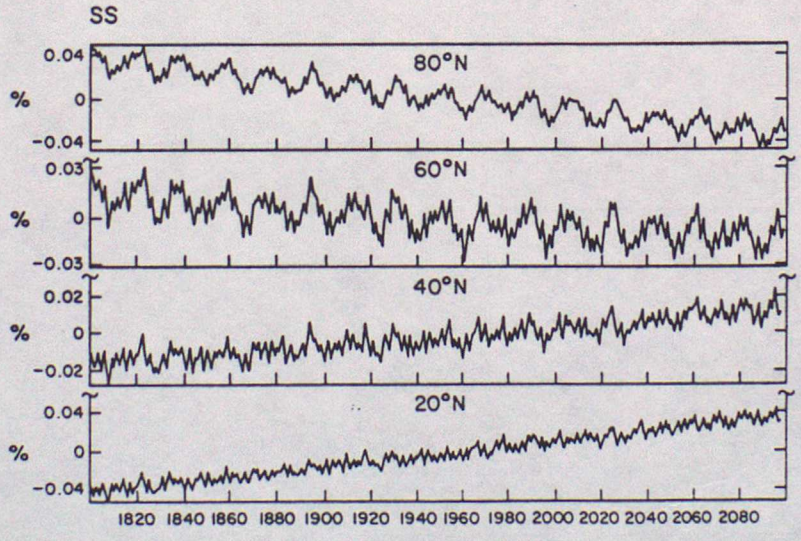

Relative insolation at summer solstice calculated for selected latitudes of the Northern Hemisphere for the period A.D. 1800–2100, as percent variation from the mean.

Figure 3.9. From Borisenkov et al (1983).

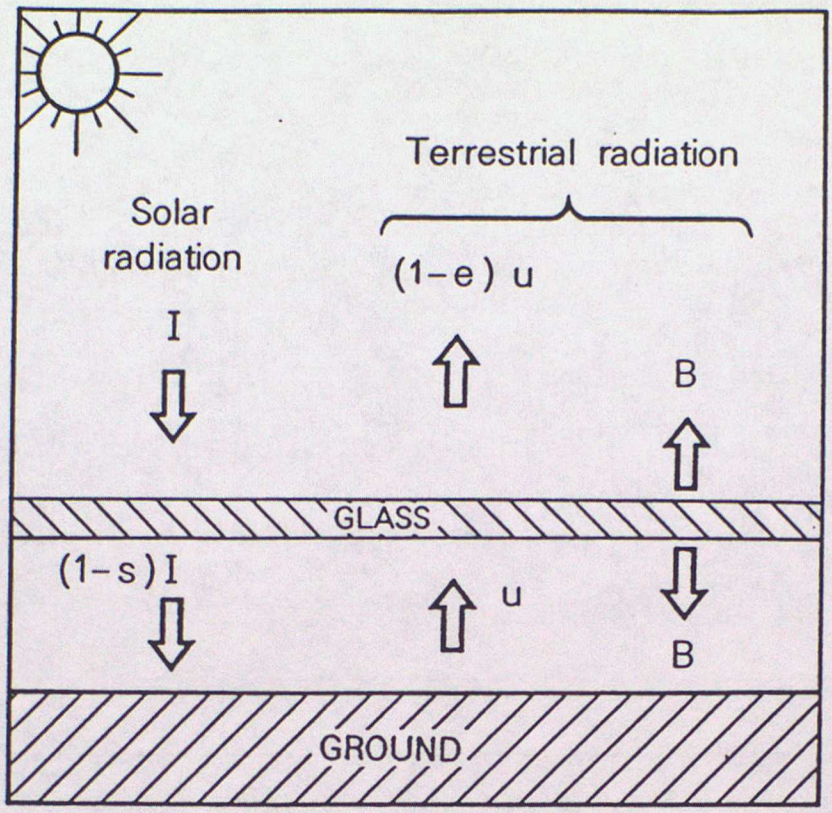

Fig. 3.10 The 'Greenhouse' effect

Adapted from Gill (1982)

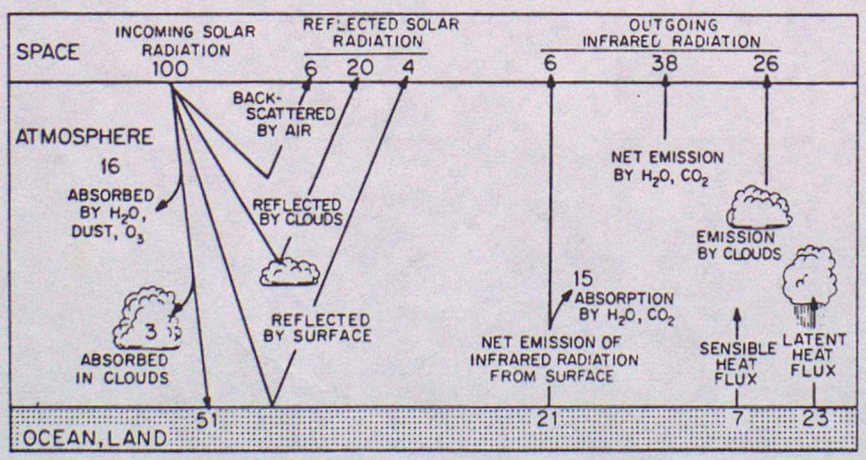

Radiation balance for the atmosphere. [Adapted from "Understanding Climatic Change," U.S. National Academy of Sciences, Washington, D.C., 1975, p. 14, and used with permission.]

Figure 3.11. From Gill (1982).

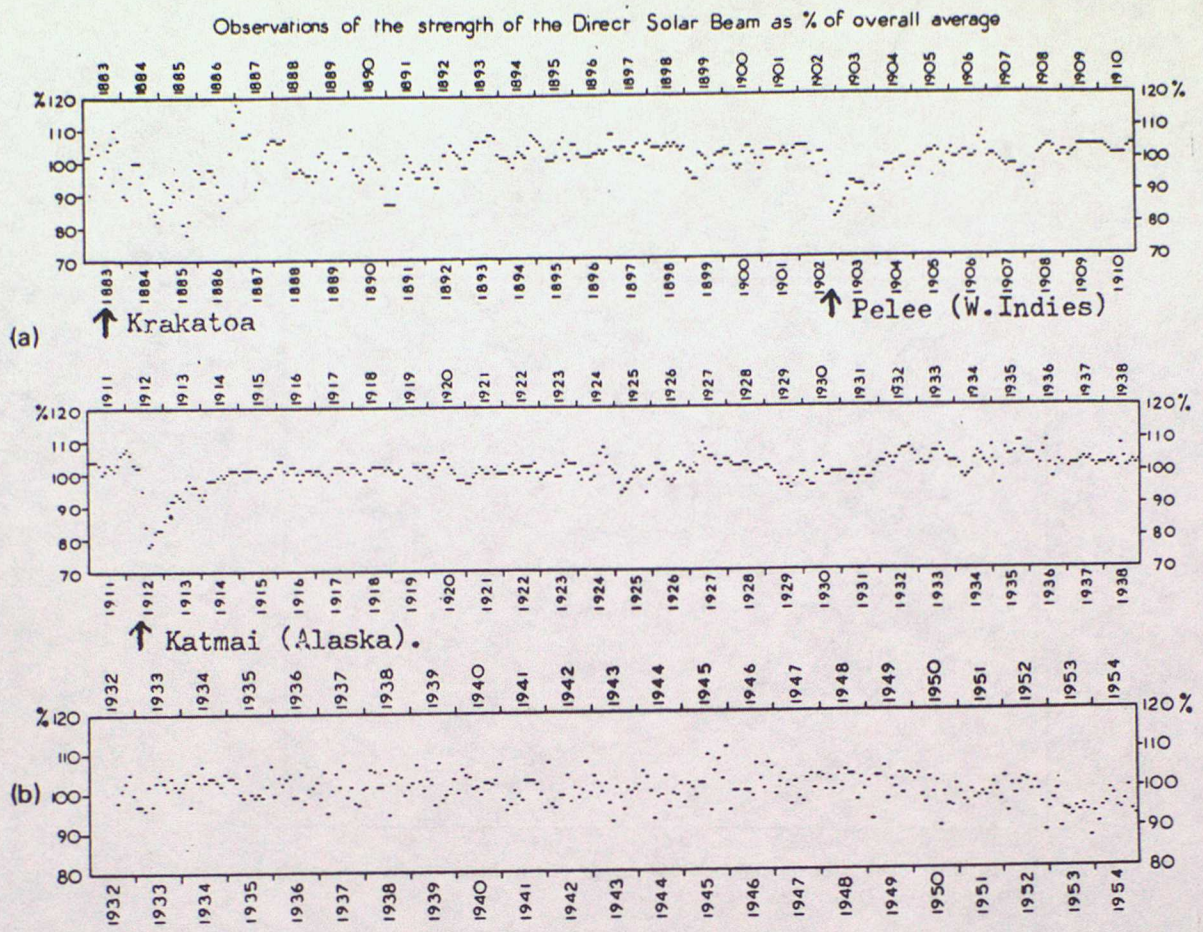

Fig. 10.16(*a*) Average monthly values of the strength of the direct solar radiation derived from observations at mountain observatories between 30° and 60°N in America, Europe, Africa and India from 1883 to 1938, as percentage of the overall mean.

(*b*) Average monthly values of the strength of the direct solar radiation derived from observations at Matsumoto (36°15′N, 137°58′E) and Shimizu (32°47′N, 132°58′E) in southern Japan from 1932 to 1954, as percentage of the overall mean.

Figure 3.12. From Lamb (1972).

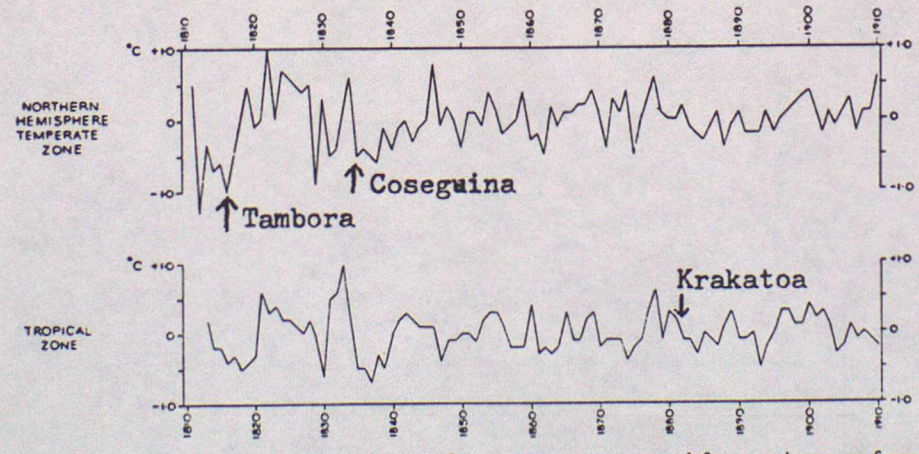

Anomalies of yearly mean surface temperature averaged for certain areas, from 1815 to 1910:

(*a*) Northern hemisphere temperate zone

(*b*) Tropical zone

Unsmoothed yearly values.

Standard deviations of the yearly values here plotted:

Northern temperate zone (land stations) 0·38°C.

Tropical zone (land stations) 0·29°C.

(*After* KÖPPEN *1873, 1914.*)

Figure 3.13. From Lamb (1972).

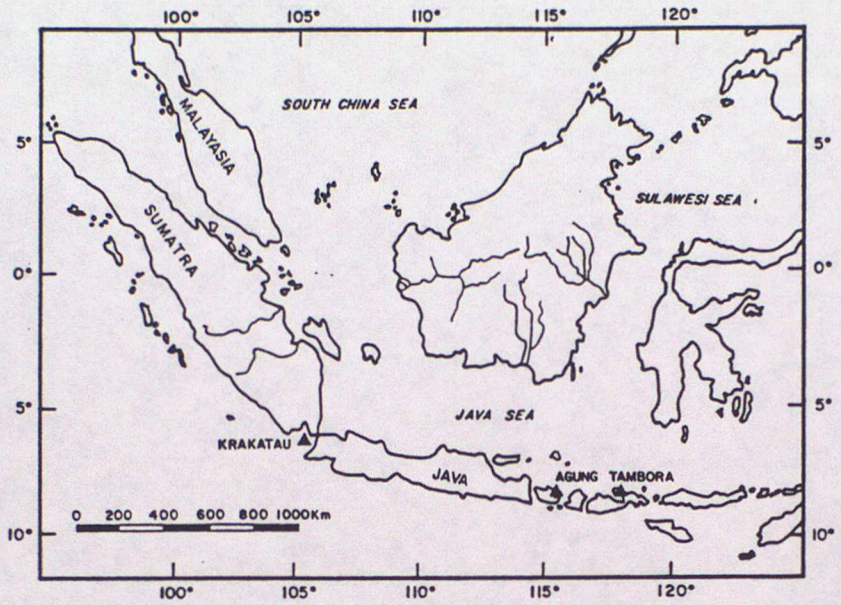

Map showing location of the three Indonesian eruptions discussed here: Tambora (1815), Krakatau (1883), and Agung (1963). (triangles).

Figure 3.14. From Rampino and Self (1982).

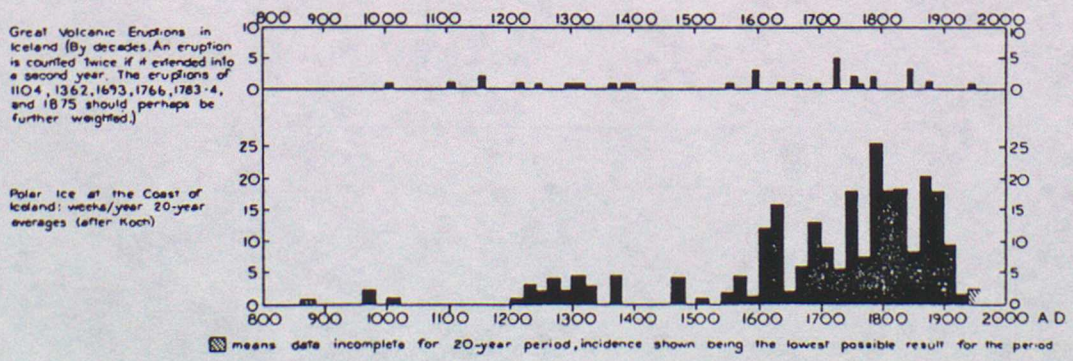

Great volcanic eruptions in Iceland and incidence of Arctic sea ice in that area since A.D. 870.

Figure 3.15 From Lamb (1972).

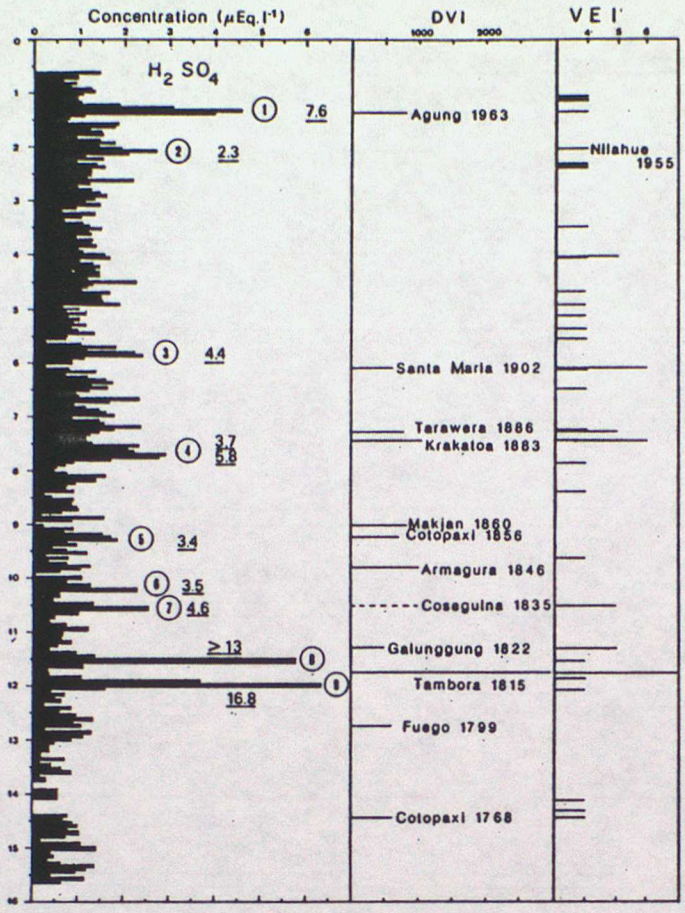

H_2SO_4 profile obtained at Dome C for the past 200 yr compared with the records of explosive volcanic eruptions south of 20° N. VEI (volcanic explosivity index) values are from ref. 6* and DVI (dust veil index) values are from ref. 5.* Major H_2SO_4 spikes, numbered 1 to 9, are of volcanic origin. The corresponding H_2SO_4 amount deposited at Dome C for each of these events is also indicated (underlined values, in kg km^{-2}).

* Ref 5 is Lamb (1970) and Ref 6 is Newhall and Self (1982).

Figure 3.16. From Legrand and Delmas (1987).

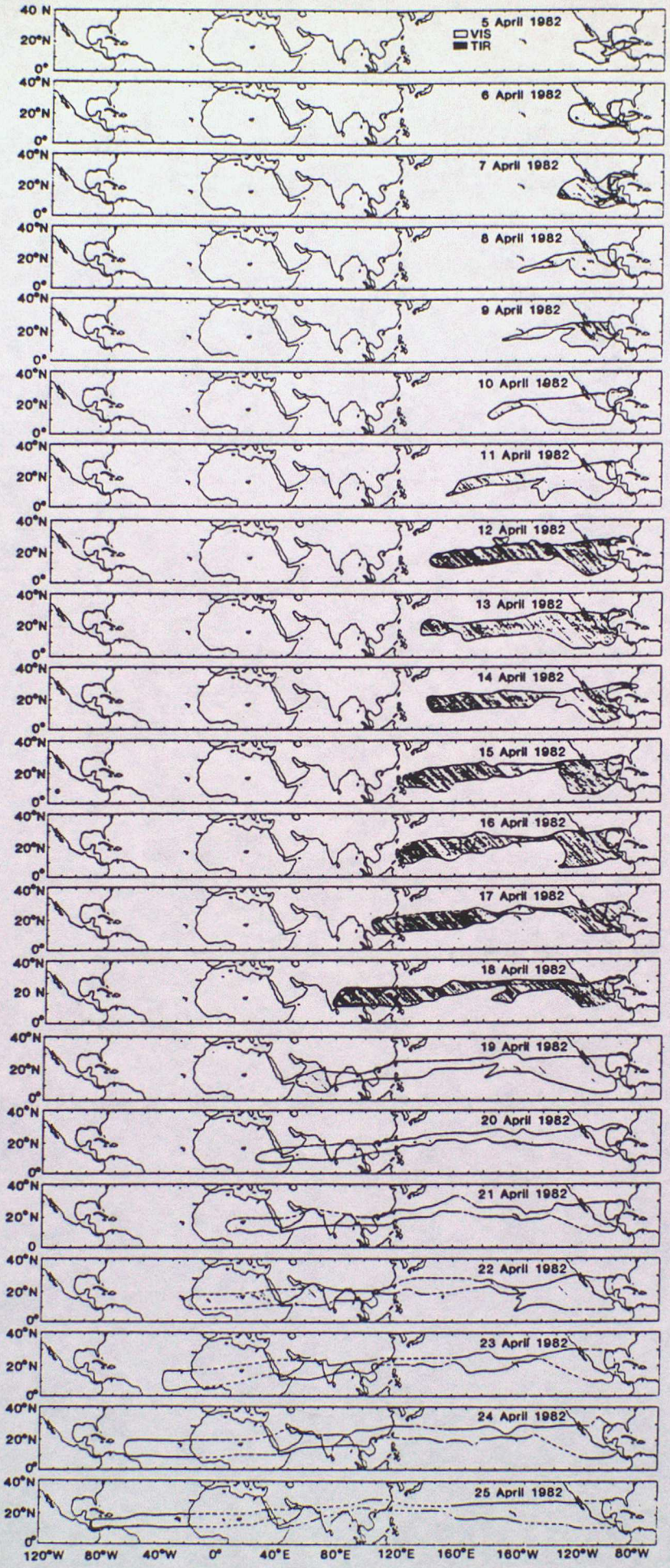

Figure 3.17. Location of the dust cloud from the El Chichon eruption as observed with visible (VIS) and thermal infrared (TIR) imagery. Portions of the cloud to the right of 180° are plotted at 0000 GMT. Portions to the left of 180° are plotted at 1500 local time. Dash-dot lines indicats difficulies in observing the exact location of the edge of the cloud. From Robock and Matson (1983).

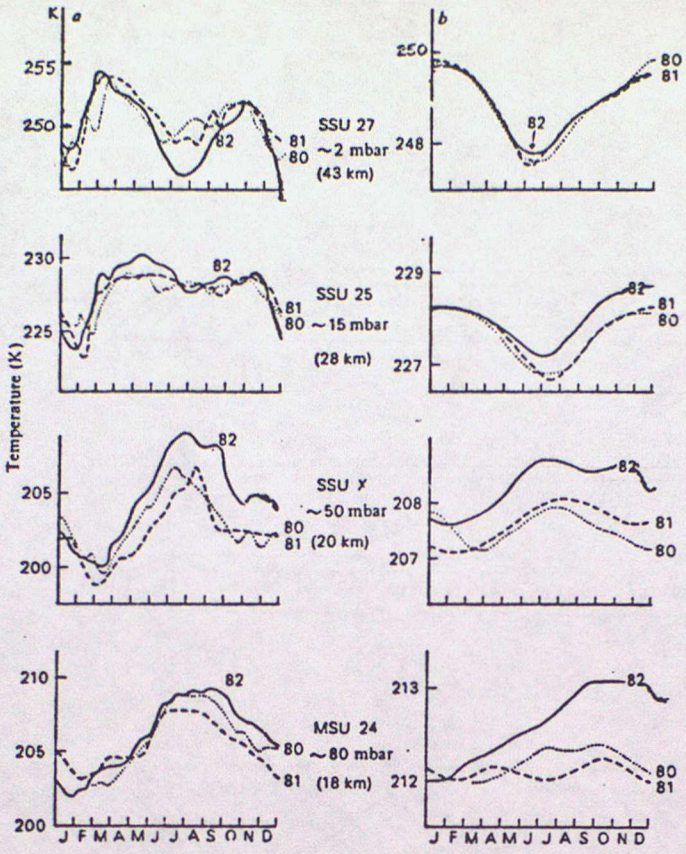

Tropical (*a*) and global mean temperatures (*b*), 1980–82. Values are based on temperatures derived from NOAA 6 Stratospheric Sounding Unit and Microwave Sounding Unit radiance channels which have vertical resolution of ~15 km.

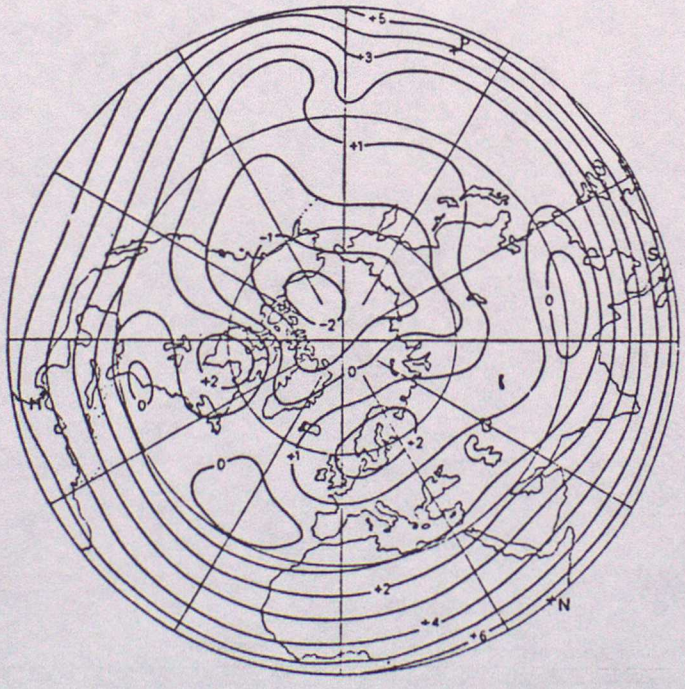

30 mbar temperature differences (K) from normal, August 1982. H, Howard Air Force Base; N, Nairobi; P, Ponape; S, Singapore.

Figure 3.18. From Parker and Brownscombe (1983).

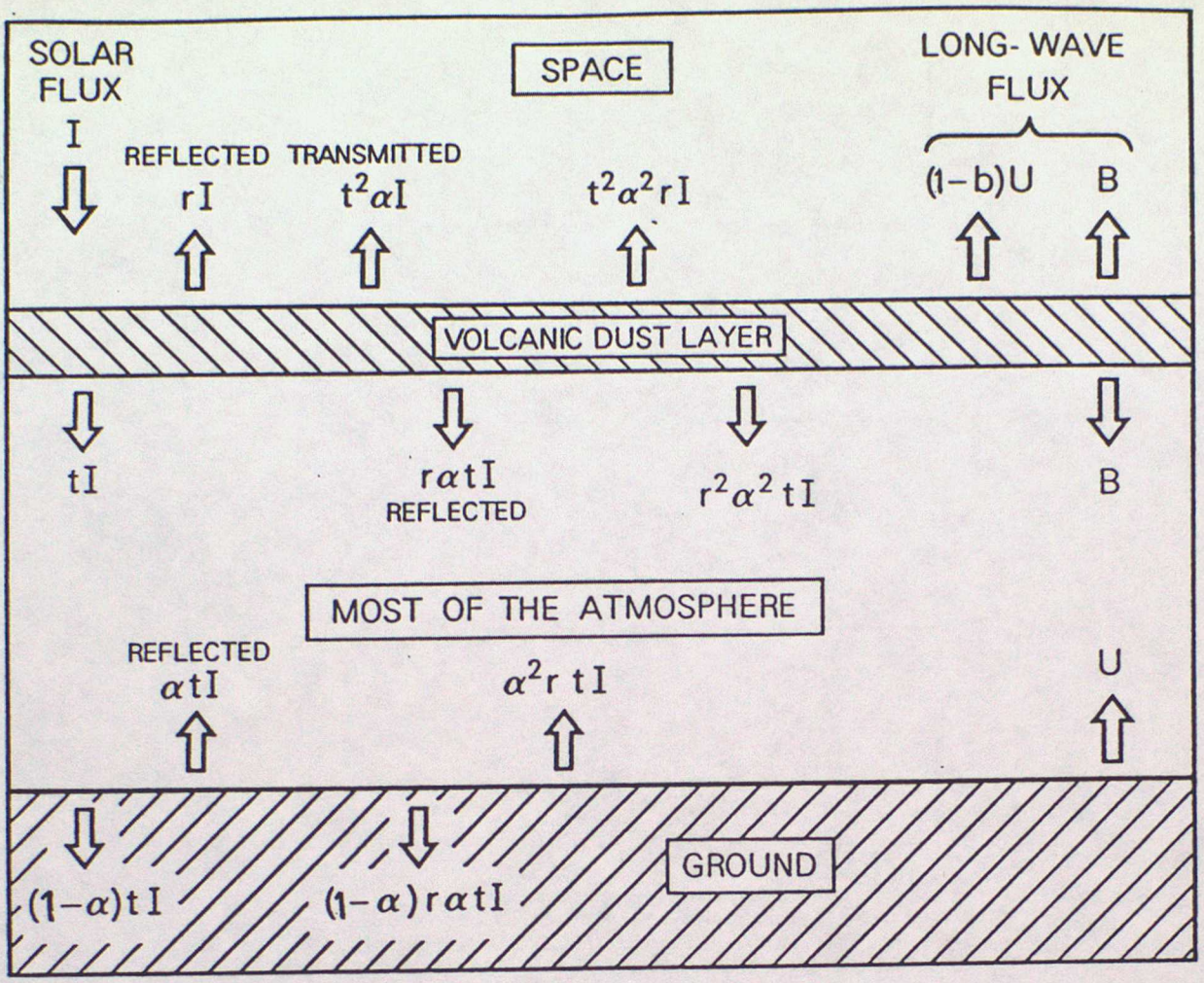

Fig. 3.19 Simple model of the effect of volcanic dust on surface radiation balance.

DO 3723

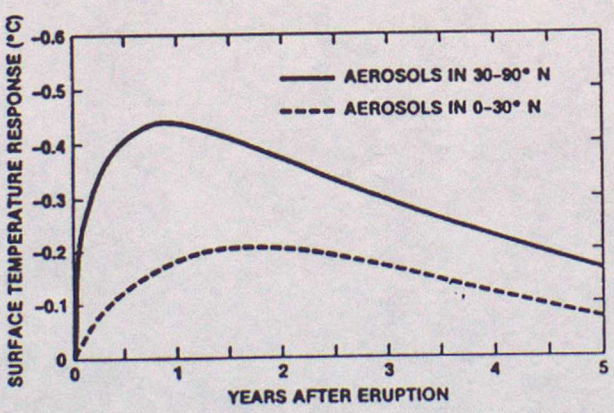

The response of the hemispherically averaged surface temperature to a uniform distribution of aerosols in the 30–90°N region (solid curve) and in the 0–30°N region (broken curve). The optical thickness of the aerosols is the same as in Fig. 7. of Chou et al(1984)

Figure 3.20 (From Chou et al (1984))

CLIMATIC FORCING AND FEEDBACK PROCESSES

II. INTERACTIONS WITH THE LAND SURFACE

C K FOLLAND and D E PARKER

MET O 13

SUMMARY

In this lecture we consider the role of persistent variations of soil moisture and land surface albedo in forcing or perpetuating anomalies of climate. The availability of soil moisture to the atmosphere depends on the vegetation cover as well as on climate, and is therefore sensitive to agricultural practices. Albedo is also a function of vegetation as well as of surface land type and snow-cover. A general introduction to the effects of variations of soil moisture and albedo on climate is followed by a selection of results from atmospheric general circulation model experiments.

4.1 INTRODUCTION

It has long been known that the albedo of the ground is affected by both the soil moisture and the vegetation cover. If the ground dries up sufficiently, it tends to increase in albedo; a further increase in albedo will result if the vegetation dies. Herein lies the potential for a feedback between the land surface and the climate, because the albedo determines the heat balance which can affect the atmospheric circulation: this in turn influences the rainfall, which has a major impact on the soil moisture and the vegetation cover.

Charney (1975) wrote an important paper which contained a simple dynamical model of drought-albedo feedback. Firstly, he noted that the Sahara, because it has a high albedo, is a net sink of radiation even in the summer (Fig 4.1). According to his simple model, and according to

observations, this overall cooling relative to surrounding areas results in subsidence in the troposphere, with large-scale convergence at the upper levels and divergence in the lower troposphere. Thus convection is suppressed and the desert conditions are perpetuated. Charney therefore, with the support of integrations of an atmospheric general circulation model (AGCM) forced with regional changes of albedo, conjectured that the Sahel drought, then about 7 years old, might have been partly caused or maintained by an extension of this subsidence as a result of an increased albedo of the ground in the Sahel. This increased albedo could have occurred initially through overgrazing by animals, or could have been a result of an initial lack of rainfall.

A possible problem with Charney's idea is that if there is initially considerable cloudiness and precipitation as a result of large-scale convergence, then although a small increase in albedo might initiate sinking motion, this would tend to reduce cloud cover. Solar heating would then increase, offsetting the effects of the reduced albedo, and perhaps preventing a further increase in sinking motion.

A more serious problem is that satellite data compiled since Charney formulated his hypothesis do not appear to show a systematic increase of albedo, at least in the western half of the Sahel, since just prior to the commencement of the drought (Fig 4.2). Norton et al (1979) (triangles in Fig 4.2) had found an increase of albedo between 1967 and 1974 in the western half of the Sahel, especially in the wet season, but Courel et al (1984) found a subsequent and stronger decrease,, which may have resulted from accumulation of plant debris in protected areas, or from recovery of grass cover.

Finally, Charney's model took no account of the direct effects of a deficiency of local soil moisture on the heat budget of the atmosphere. We will therefore now consider these effects, before giving an account of some atmospheric general circulation model experiments designed to assess the impact of variations of both soil moisture and albedo. In Lecture 5,

however, we will demonstrate that it is interhemispheric patterns of sea surface temperature change which appear to have had most impact on Sahel rainfall.

4.2 A GENERAL DISCUSSION OF THE EFFECT OF SOIL MOISTURE VARIATIONS ON PRECIPITATION

Why should we think that soil moisture variations could be important to regional precipitation? Evaporation of water from the ground surface is complex but essentially depends on three factors:-

(a) The difference in vapour pressure between the soil surface and a representative level above the soil. The vapour pressure at the soil surface is usually taken as the saturation vapour pressure of water at the temperature of the soil surface: thus evaporation is taken to depend on ground temperature.

(b) The wind speed near the ground.

(c) The availability of soil water, or "soil moisture deficit".

A simple version of Penman's climatological evaporation formula (Penman (1956)) expresses the first two factors:-

$$E_p = 0.36\ (e_s - e_a)\ (0.5 + 0.54v)$$

where e_s is the saturation vapour pressure (mb) at the prevailing surface temperature, e_a is the average average vapour pressure of the air (mb), and v is the average wind speed (m/sec) at a height of 2 m.

E_p is known as the potential evaporation and is nominally the actual evaporation over a flat, fresh-water, surface. However the actual evaporation from a ground surface, E', is often less than E_p when S, the soil water content, falls below a certain value. Thus a resistance to evaporation builds up as the surface soil layers dry out and the soil water is evaporated from deeper layers. In some AGCM's E' is parameterised as:-

$$E' = \frac{E_p S}{KS_0}$$

where S is the soil water content, ie the equivalent depth of water existing in the soil, S_0 is the maximum water content of the soil, or its "field capacity" and K is a constant; $\frac{E_p}{KS_0}$ is sometimes called ß.

This formula is a gross oversimplification for vegetated surfaces but does express the most important variations of evaporation rate. For a discussion of evaporation formulae and the water balance of the world, see the authoritative references Baumgartner and Reichel (1975), and Korzun (1978).

4.2.1 A schematic demonstration of the importance of soil moisture content to precipitation anomalies

Fig 4.3 shows an idealised picture of the exchange of energy between the ground surface and the atmosphere involving soil moisture and evaporation. Imagine there is no horizontal motion and that cloudiness is fixed. Consider the heat balance of the bottom half of the atmosphere, ie that part below the 500 mb level, and assume that this layer is directly affected by ground surface processes. The heat balance of the atmosphere can be expressed by:-

$$MC_p \frac{dT}{dt} = H + LP - LE \qquad (4.1)$$

where E is the evaporation rate, P is the precipitation rate, H is the sensible heating rate, M is the mass per unit area of the atmosphere between the surface and 500 mb, C_p is the specific heat of air and L is the latent heat of vaporisation. In AGCM's, and the real atmosphere, precipitation tends to depend on a relative humidity of almost 100% being reached at some level. Thus the rate of change of relative humidity r of an air mass moving over an evaporating land surface is a crude measure of

the time it will take for precipitation to form when convection is important. The rate of change of relative humidity will depend on the soil moisture. We can explore this as follows:-

We can write $$\frac{dr}{dt} = \frac{d}{dt}\left[\frac{Q}{Q_s}\right]$$

where

Q is the specific humidity integrated through the column of atmosphere between the surface and 500 mb, above which level moisture content is small;

Q_s is the saturation specific humidity in the same column.

Thus $$\frac{dr}{dt} = \frac{1}{Q_s}\frac{dQ}{dt} - \frac{Q}{Q_s^2}\frac{dQ_s}{dt} \qquad (4.2)$$

Now $\frac{dQ}{dt} = E - P$ by definition;

Furthermore $\frac{dQ_s}{dt} \simeq \frac{\delta Q_s}{\delta T}\frac{dT}{dt}$,

$\frac{\delta Q_s}{\delta T} \simeq cQ_s$ where c is a constant, and $Q = rQ_s$.

So $$\frac{dr}{dt} = \frac{E-P}{Q_s} - c\,r\frac{dT}{dt}$$

From equation (4.1)

$$\frac{dT}{dt} = \frac{1}{MC_p}\left[H + L(P - E)\right]$$

We can put H + LE = K, a constant, if the total net rate of heating of the ground due to fixed incident radiation remains constant even though the rate of evaporation may vary due to a reduction in soil moisture. It is easily found that

$$\frac{dr}{dt} = (E - P) \left[\frac{1}{Q_s} + \frac{2cLr}{MC_p} \right] - \frac{cr}{MCp} (K-LP)$$

$$\frac{dr}{dt} = (E - P) \left[\frac{1}{Q_s} + \frac{2cLr}{MC_p} \right] - \frac{crK}{MC_p} \text{ if P is small (LP<<K).}$$

The total net heating rate in reasonably sunny conditions in June in S England is approximately the equivalent of 5 mm of evaporation each day, ie K/L is about 0.5 g day $^{-1}$ cm^{-2}. Now c $\simeq$ 0.07°K^{-1} from tables or the Clausius-Clapeyron equation; L = 2500 Jg^{-1}; MC_p = 500 J cm^{-2} °K^{-1} for a 500 mb depth of atmosphere; Q_s is typically about 3 gm cm^{-2} for the lowest 500 mb. Thus,

if $r = \frac{Q}{Q_s} = 0.75$ then $\frac{dr}{dt} \simeq 0.86 (E-P) - 0.135$ day^{-1}.

If E = 3 mm/day ie 0.3 gm cm^{-2} day^{-1} and P = 0, then $\frac{dr}{dt} \simeq 0.12$ day^{-1}

ie relative humidity increases by 12% per day. If E were 1 mm per day in drought conditions, ie where evaporation is much below the "potential rate", then, still assuming that K remains the same and that P = 0:-

$\frac{dr}{dt} \simeq -5\%$ day^{-1}.

In reality, K might be reduced as a result of increased albedo, but even a change as large as 25%, which is not supported by Fig 4.2 for the Sahel, would still yield $\frac{dr}{dt} = -1.5\%$ per day if E were 1 mm per day. So the likelihood of precipitation is much increased by a wet ground surface and decreased by a dry one. In fact most of the evaporation into a mass of air occurs by day, and thus E reaches twice the values indicated above for part

of the day; consequently an air mass need only remain over a soil moisture anomaly for about 12 hours for its relative humidity to be affected by the amount calculated. With typical advecting winds of 10 ms^{-1}, the horizontal scale of the soil moisture anomaly need only be about 400-500 km to appreciably affect the humidity of an air-mass moving over it.

4.3 EXAMPLES OF THE SENSITIVITY OF CLIMATE TO ALBEDO (α) AND S AS SHOWN BY AGCM EXPERIMENTS

Mintz (1984) provides a very good summary of 11 AGCM experiments. Some of these are among the examples below, which are chosen to elucidate the problems.

4.3.1 Experiments with α fixed and different anomaly and control S

(From Shukla and Mintz (1982))

This experiment used the global AGCM of the NASA Goddard Space Flight Center's Laboratory for Atmospheric Sciences (GLAS).

(a) Control - land-surface evaporation was everywhere set at the potential rate E_p i.e. β was always 1 where $E = \beta E_p$. So the soil was wet everywhere. Albedo varied according to a standard climatology. Initial conditions were for 15 June of a specific year.

(b) Anomaly - no evaporation was allowed anywhere, i.e. the soil was completely dry. Otherwise initial conditions were identical.

The results shown are averages for the following "July". Fig 4.4 shows the precipitation fields for both anomaly and control, Fig 4.5 shows the ground surface temperatures and Fig 4.6 the MSL pressure fields.

Precipitation was greatly reduced over the continents in the anomaly experiment, except over northern South America and in part of Southern Asia. Sahel rainfall, which is a product of the intertropical convergence

zone (ITCZ), was reduced in this experiment. Furthermore, in the anomaly experiment, there was some reduction of overall precipitation over the oceans.

The most dramatic effect of stopping evaporation over land was to greatly increase the surface temperature of the ground in the summer half of the world and in the tropics. Part of this increase in temperature resulted from decreased cloudiness as is shown by the increase of R_s, the solar heating rate, in Fig 4.7. The ground also warmed because there was less evaporative cooling (Fig 4.7). Not surprisingly, long-wave radiation losses from the ground were larger and the sensible heating of the air by the ground increased. Above-normal surface air temperatures have been observed in the Sahel and surrounding regions during the drought (Fig 4.8). These warmings, though of up to 3°C, are not as large as the ground temperature increases simulated by Shukla and Mintz, because the changes in evaporation in their experiment were unrealistically large and because ground temperature is even more sensitive to surface heat exchanges than is air temperature.

Fig 4.6 shows that, on the whole, pressure fell over the continents and rose over the oceans in Shukla and Mintz's anomaly experiment, giving a strong global monsoon circulation component to the anomalous atmospheric response. No estimates of statistical significance were given but a qualitative response of the kind shown is physically reasonable and was shown in other similar AGCM experiments e.g, those designed to simulate changes in the latitudinal distribution of solar radiation (Lecture 8).

4.3.2 Different values of α but fixed values of S

(Charney et al (1977))

Here we look at a restricted but interesting aspect of Charney et al's results; the Sahel drought is a theme of these lectures, so we will look at the energy balance over the Sahel when α is changed.

(a) Control - where the continents are ice and snow free they were given an albedo of 0.14 though where true deserts are observed, the albedo was set to 0.35 (Fig 4.9).

(b) Anomaly - conditions were the same except that the albedo was increased from 0.14 to 0.35 in the "Sahel", in Rajputana (India) and also in the Western Great Plains (USA), all adjacent to true deserts (see Fig 4.9). Table 4.1 shows detailed results for the energy balance of the Sahel which are instructive, given Charney's original paper of 1975. The main points are:

(i) The evaporation rate, βE_p, was fixed at 0.51 E_p in both experiments.

(ii) The rate of solar heating of the ground, R_s, increased slightly as α increased; this paradoxical result arose because the model cloudiness, N, decreased greatly from 0.7 to 0.46, more than was necessary to offset the effects of an increased value of α.

(iii) Evaporation E decreased in the anomaly experiment, though only by 1 mm/day.

(iv) Sensible heating H of the atmosphere by the ground increased in the anomaly experiment.

(v) In the anomaly experiment net outgoing long-wave radiation R_L increased because the skies were clearer and the air was less humid.

(vi) Net radiation, R_N, became less positive in the anomaly experiment.

(vii) Surface temperature T_A fell in the anomaly experiments but only very slightly.

(viii) The convergence of water vapour in the anomaly experiment decreased very strongly, by the equivalent of 2.5 mm of precipitation per day.

(ix) Precipitation was considerably reduced in the anomaly experiment, by 3.4 mm per day, mostly because of the decreased moisture convergence rather than because of the decreased evaporation.

So the dynamical effect of decreased convergence from more distant locations was dominant when α was increased. But surface temperatures hardly altered, even though the availability of soil moisture was fixed, as effectively assumed in Charney's original model. Such results clearly depend on the model used but show the fascinating complexity of the problem. They do not prove however that an increase in albedo is necessarily the chief (local) cause of the Sahel drought as the next section will suggest.

4.3.3 Fixed α, but different time-dependent soil moisture variations

(Owen et al (1988))

The AGCM integrations of Owen et al (1988) were designed to assess the impact of observed worldwide sea surface temperature anomalies, and the additional impact of soil moisture feedback, on rainfall in the Sahel. The experiments were carried out with the Meteorological Office 11-layer GCM (Slingo (1985)) which has a resolution of 2.5° latitude by 3.75° longitude. A control integration with climatological sea surface temperatures and interactive soil moisture was used to determine the model's climatology of soil moisture as well as its atmospheric climatology. Then eight anomaly integrations were carried out, using observed worldwide sea surface temperatures for 1950, 1958, 1983 and 1984 respectively, firstly with interactive soil moisture, and secondly with the soil moisture constrained to equal the model's climatological values. Each integration covered approximately the period April to October inclusive. The first two months were intended to allow the model to adjust to the imposed sea surface

temperatures from the identical starting atmospheric conditions, which were those of 26 March 1984. The results for June to October are summarised in Fig 4.10, where (I) and (C) denote interactive and climatological soil moisture respectively. Fig 4.10A includes the observed rainfalls in the Sahel. It is clear that the encouraging ability of the model to simulate the very different rainfalls observed in each of the four years derived largely from the differences in sea surface temperatures (see also Lecture 5). However, soil moisture feedback did have an impact on the results. This is clearly seen in 1950 when the simulated soil moisture was very plentiful (Fig 4.10B) and in 1983 when the simulated soil was very dry, though the inclusion of interactive soil moisture did not systematically either improve or degrade the simulated rainfalls (Fig 4.10A). Owen et al found that the use of interactive as opposed to climatological soil moisture had little effect on the AGCM's atmospheric circulation, despite a substantial impact on surface and lower-tropospheric temperatures over and around the Sahel (Fig 4.11), such that hotter conditions occurred in the dry years, in agreement with observations (Fig 4.8), when interactive soil moisture was used (Fig 4.11A), but not with climatological soil moisture (Fig 4.11B).

4.3.4 Simulation of deforestation

(Dickinson and Henderson-Sellers (1988))

We give a brief description of this simulation of the deforestation of the Amazon basin in order to draw attention to a few of the complexities involved. Dickinson and Henderson-Sellers's AGCM anomaly simulation included the following changes to the surface over much of South America between 10°N and 15°S, representing the replacement of broad-leaved evergreen forest by scrub-grassland:

Vegetation cover:	reduced by 10% of land area
Roughness length of vegetation:	reduced from 2 m to 5 cm
Vegetation albedo at wavelengths	

< 0.7 μm:	increased from 0.04 to 0.08
≥ 0.7 μm:	increased from 0.20 to 0.30

Dry soil albedo at wavelengths

< 0.7 μm:	increased by 0.04
≥ 0.7 μm:	increased by 0.08

Saturated soil albedo at wavelengths:

< 0.7 μm:	increased by 0.02
≥ 0.7 μm:	increased by 0.04
Soil depth:	reduced from 1.5 m to 1 m
Runoff:	formulation modified so that runoff decreased less rapidly with drying of the surface layer.

Dickinson and Henderson-Sellers' AGCM control and anomaly integrations of 13 months were too short for statistically significant changes in local rainfall, or non-local climatic effects, to be confirmed. Over the deforested area, however, surface air temperatures were systematically higher in the anomaly run by an average of nearly 2°C, and soil surface temperatures were raised by an average of over 3°C. Total evaporation decreased by an average of about 0.5 mm per day. Total soil moisture decreased by up to 20 cm but this change was a result of the specified reduced depth of soil: the soil actually became a little more saturated. Interception of precipitation by the vegetation canopy was decreased by an average of about 0.4 mm per day: intercepted precipitation is re-evaporated in the model. Dickinson and Henderson-Sellers interpreted their AGCM results in terms of the effects on a land-surface model, with prescribed

atmospheric conditions, of the various changes to the surface layer accompanying deforestation, and concluded that the reduction in the vegetation roughness length had the largest overall effect on the thermodynamics of the surface.

4.4 CONCLUSION

The results presented in this section suggest that correct treatments of soil moisture and albedo will contribute limited increases of predictability on monthly, seasonal and interannual time-scales. In forested areas other features such as vegetation-induced roughness are also likely to be important, but their non-local effects have yet to be demonstrated. By contrast, we show in the next lecture that interactions between the atmosphere and the sea surface have major implications on a worldwide scale.

We are grateful to Dr P Rowntree for the basis of Section 4.2.1.

TABLE 4.1 COMPONENTS OF THE ENERGY AND WATER BUDGETS, IN EXPERIMENT OF CHARNEY ET AL (1977)

Region	Case No	(1) β	(2) (1-A)	(3) R_S	(4) R_L	(5) R_N	(6) LE	(7) H	(8) N	(9) T_A	(10) E	(11) (-V.qv)	(12) P
Sahel	2a (Control)	0.51	0.86	169	58	111	107	4	0.70	26.0	3.7	3.7	7.4
(16°-20°N 17.5°W-37.5°E	3a (Anomaly)	0.51	0.65	177	84	93	81	12	0.46	25.7	2.8	1.2	4.0

KEY

β: ratio of actual to potential evaporation rates

α: albedo

R_S: rate of solar heating of the ground (Wm^{-2})

R_L: net longwave radiation from the ground (Wm^{-2})

R_N: rate of net radiative heating of the ground = $R_S - R_L$ (Wm^{-2})

LE: rate of latent heat transfer from the ground to the atmosphere (Wm^{-2})

H: rate of sensible heat transfer from the ground to the atmosphere (Wm^{-2})

N: cloudiness fraction

T_A: surface temperature (°C)

E: evaporation rate (mm/day)

-V.qv: convergence of water vapour (mm/day)

P: precipitation (mm/day)

REFERENCES TO LECTURE 4

BAUMGARTNER A and REICHEL E (1975) The World Water Balance: Mean annual global, continental and maritime precipitation, evaporation and run-off. Elsevier.

CHARNEY, J G (1975) Dynamics of deserts and drought in the Sahel. Q J Roy Met Soc, 101, 193-202.

CHARNEY J, QUIRK W J, CHOW S-H AND KORNFIELD J (1977) A comparative study of the effects of albedo change and drought in semi-arid regions. J Atmos Sci, 34, 1366-1385.

COUREL, M F, KANDEL, R S and RASOOL, S I (1984) Surface albedo and the Sahel drought. Nature, 307, 528-531.

DICKINSON, R E and HENDERSON-SELLERS, A (1988) Modelling tropical deforestation: a study of GCM land-surface parametrizations. Q.J.R Meteorol. Soc., 114, 439-462.

KORZUN V I (Ed) (1978) World Water balance and water resources of Earth. Studies and Reports in Hydrology, Vol 25, Unesco Press, Paris.

MINTZ Y (1984) The sensitivity of numerically simulated climates to land-surface boundary conditions. The Global Climate, pp 79-105. Ed: J T Houghton, Cambridge University Press.

NORTON, C C, MOSHER, F R and HINTON, B (1979) An investigation of surface albedo variations during the recent Sahel drought. J. Appl. Met., 18, 1252-1262.

OWEN, J A, FOLLAND, C K and BOTTOMLEY, M (1988) Numerical simulation of seasonal Sahel rainfall in four past years using observed sea surface temperatures. Long Range Forecasting and Climate Research Memo No 15, Meteorological Office, Bracknell.

PENMAN H L (1956) Estimating Evaporation. Trans Amer Geophys Union, 37(1), 43-46.

SHUKLA J AND MINTZ Y (1982) Influence of land-surface evapotranspiration on the earth's climate. Science, 215, 1498-1501. Also presented at the Joint Scientific Committee Study Conference on Land Surface Processes in Atmospheric General Circulation Models, Greenbelt, USA, 5-10 January 1981 (this is reference on diagrams).

SLINGO, A (1985) Handbook of the Meteorological Office 11-layer atmospheric general circulation model. Dynamical climatology Tech Note No 29, Meteorological Office, Bracknell.

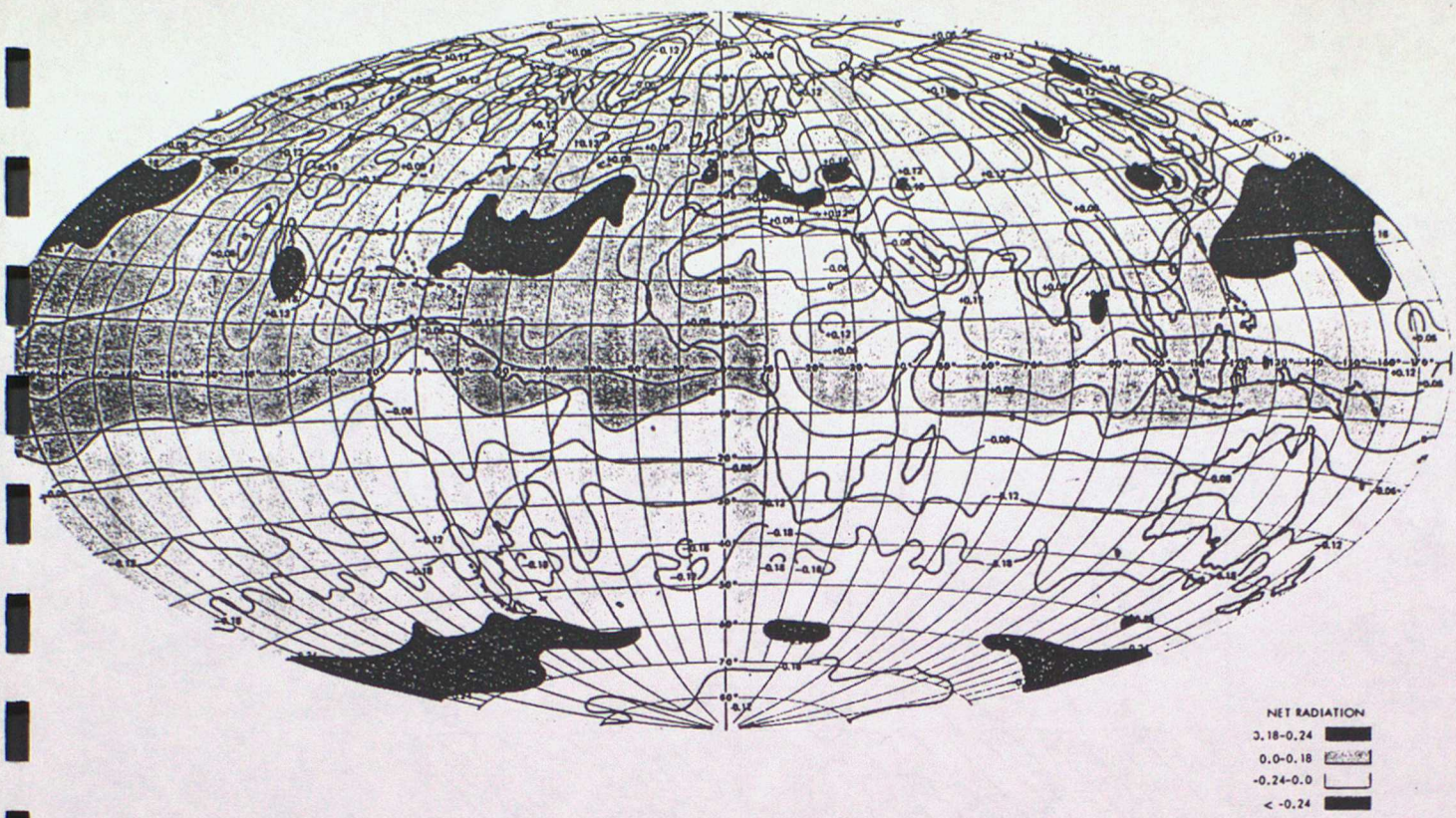

Net radiation at the top of the atmosphere (cal/cm²/min) measured from Nimbus III, 1–15 July 1969.
Multiply by 697 to give Wm^{-2}.

Figure 4.1. From Charney (1975).

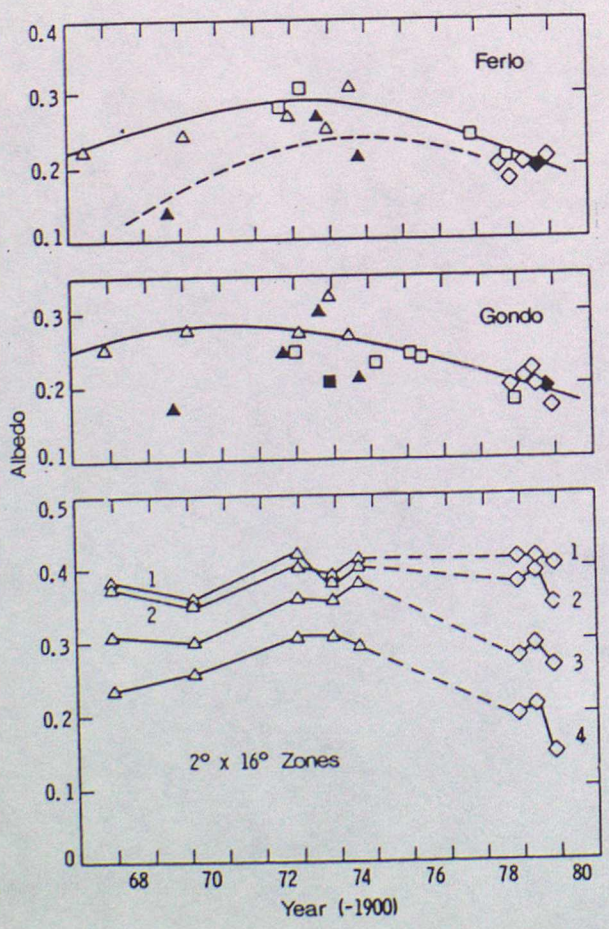

Figure 4.2.

Albedo history of the western Sahara and Sahel between 1967 and 1979. Triangles, estimates based on the 2° maps of Norton et al (1979); squares, Landsat data for Ferlo (15-17N, $13\frac{1}{2}$-$15\frac{1}{2}$W) and Gondo ($13\frac{1}{2}$-15N, $2\frac{1}{2}$-$4\frac{1}{2}$W); lozenges, Meteosat-1 data. The filled symbols correspond to observations in the rainy season. Curves 1-4 are integrated albedo values for the strips 22-20N, 20-18N, 18-16N, 16-14N extending from 16W to the Greenwich meridian.

After Courel et al (1984).

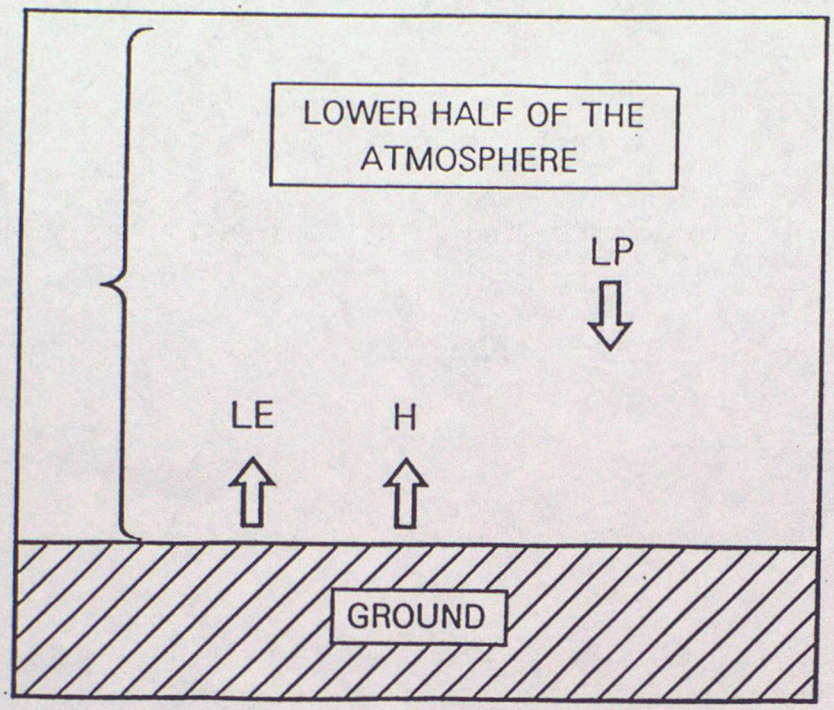

Figure 4.3. Schematic of exchanges of latent and sensible heat at the surface.

Precipitation (mm/day) in wet-soil case (top) and dry-soil case (bottom), in experiment of Shukla & Mintz (1981). (Precipitation greater than 2 mm/day is shaded.)

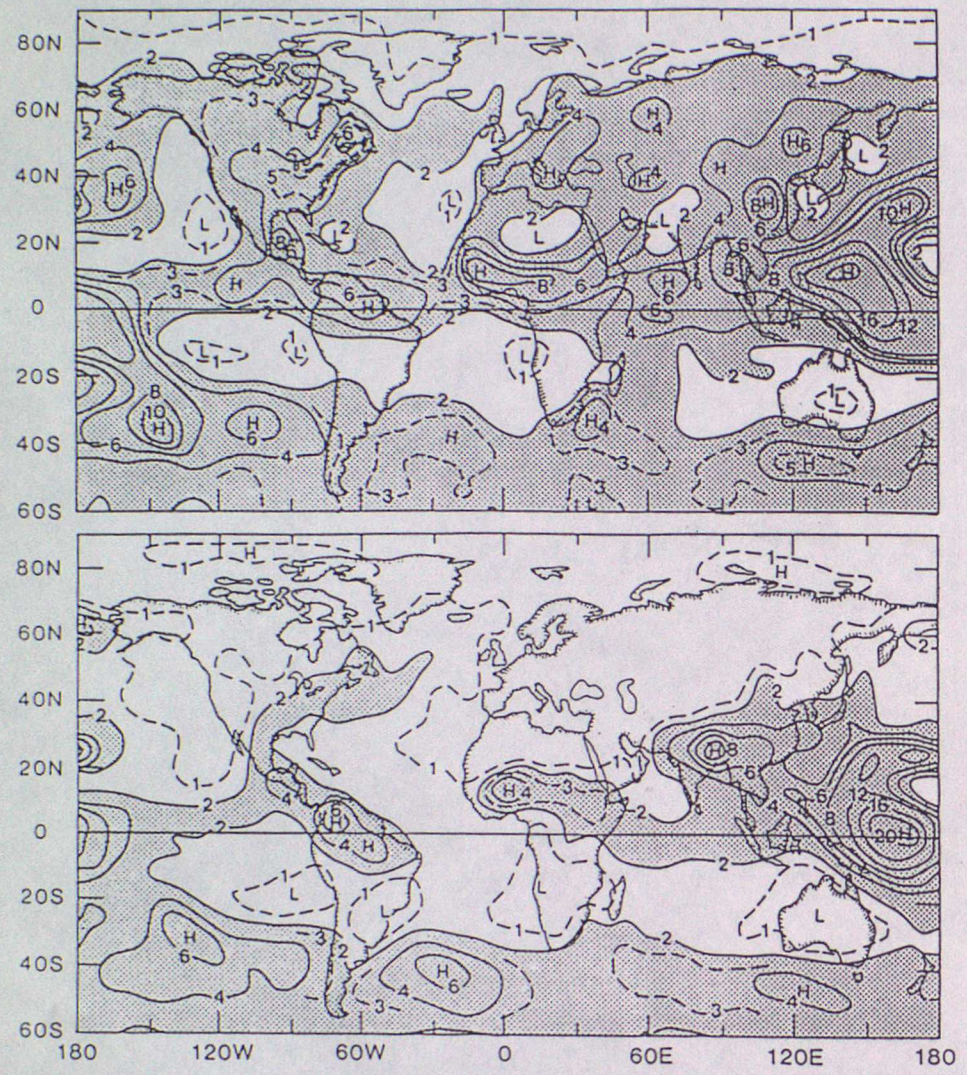

Figure 4.4.

Ground surface temperature (°C) in wet-soil case (top) and dry-soil case (bottom), in experiment of Shukla & Mintz (1981).

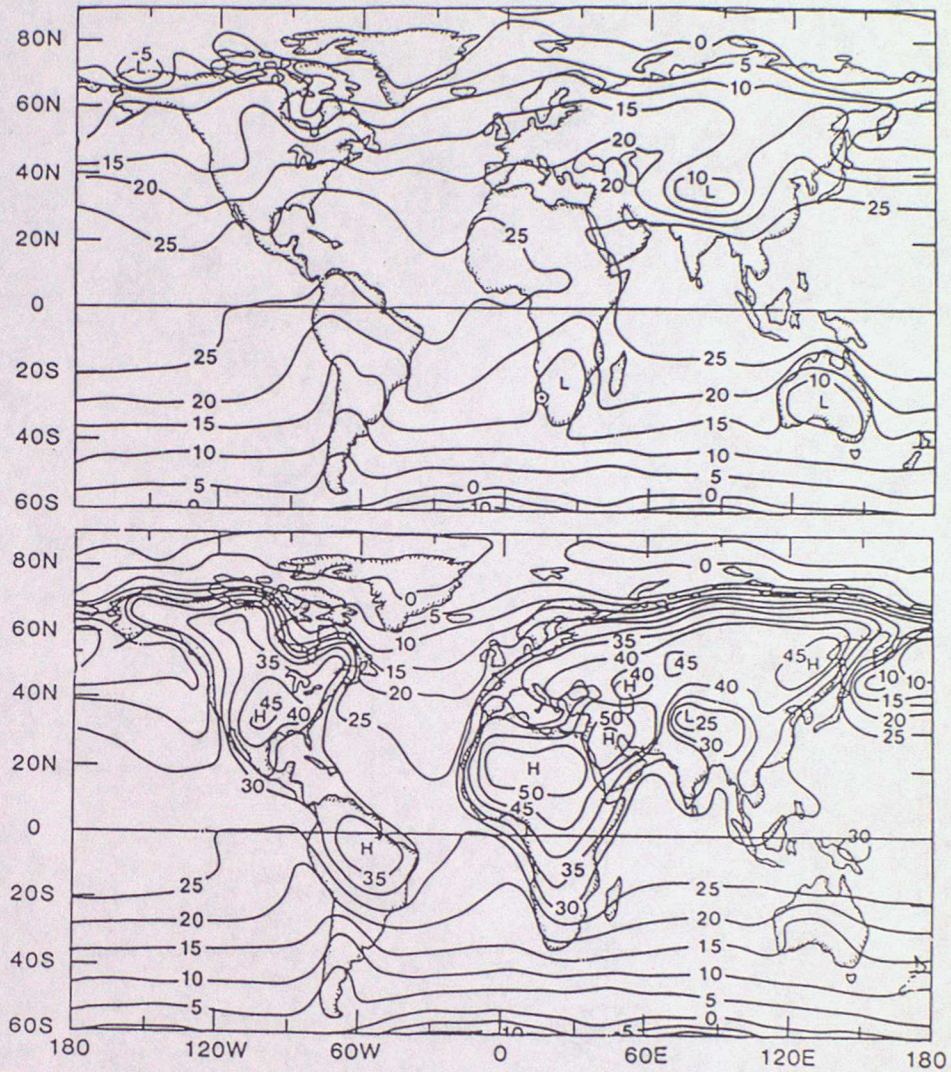

Figure 4.5.

Surface pressure reduced to sea level (mb minus 1000) in wet-soil case (top) and dry-soil case (center), in experiment of Shukla & Mintz (1981). Bottom map show the difference between the two surface pressures (mb).

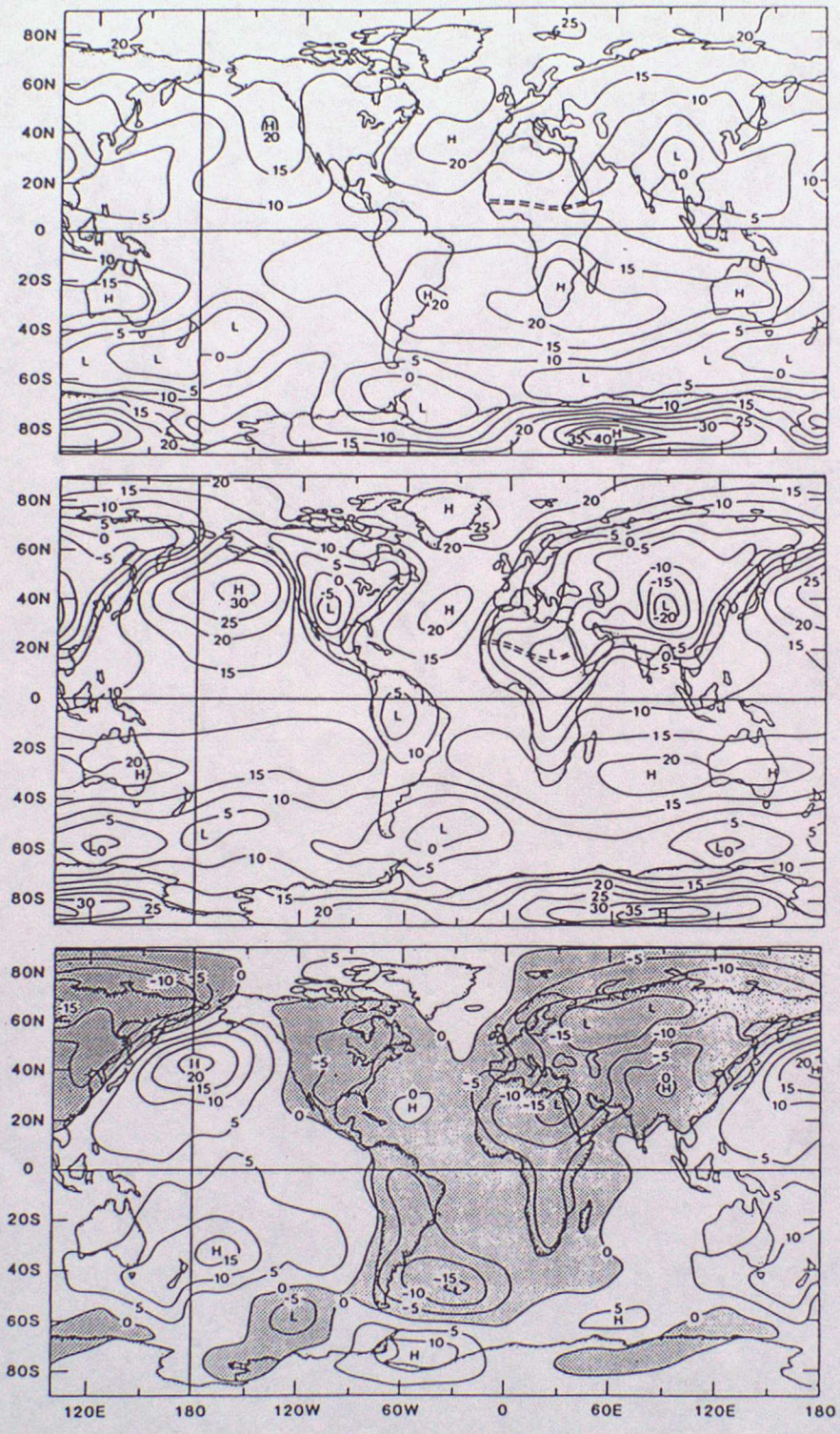

Figure 4.6.

Surface energy transfers (watt/m²) averaged for the continents between 20°S and 60°N, in experiment of Shukla and Mintz (1981).

R_S solar raditional heating of the ground.

R_L long wave radiational cooling of the ground (difference between radiation emitted by ground and radiation absorbed by ground).

$R_N = (R_S - R_L)$ net (all-wavelength) radiational heating of the ground.

LE latent heat transfer from ground to atmosphere (evaporative cooling of the ground).

H conductive-convective heat transfer from ground to atmosphere.

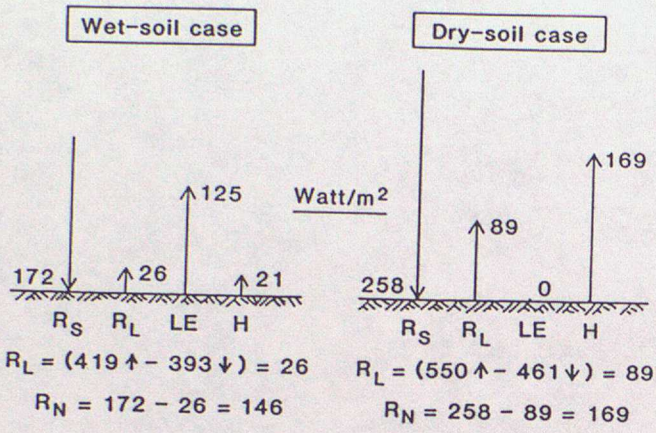

Figure 4.7.

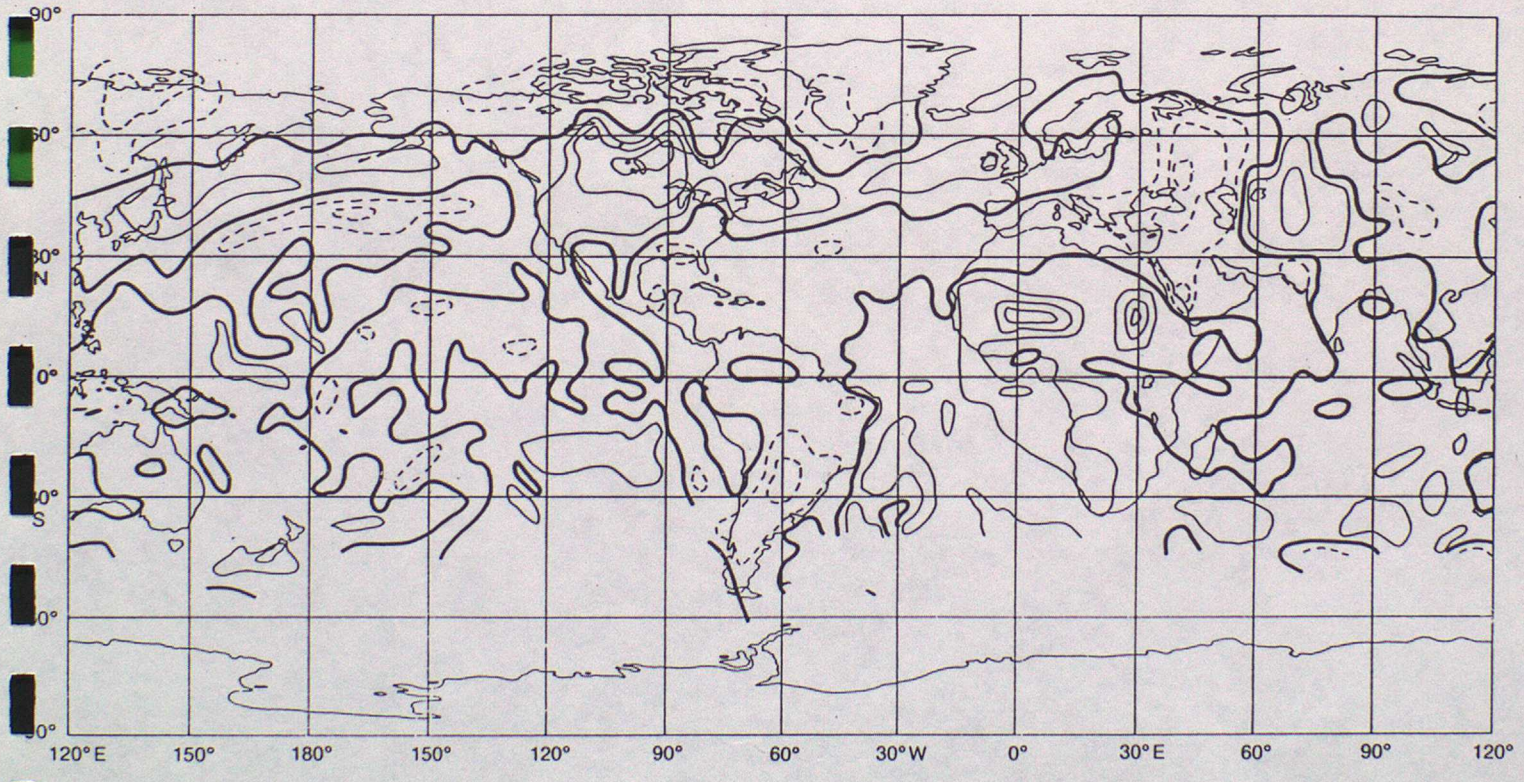

Figure 4.8. Sea surface temperature and land air temperature (w.r.t.1951-80), August 1984. Contours every 1°C (Light solid, positive; heavy solid, zero; dashed, negative). Values over land from P.D.Jones (Univ. East Anglia).

Bottom panel: the assigned albedos in experiments of Charney *et al.* (1977). Unshaded land areas have an albedo of 0.14 in all cases, and dot-shaded areas have an albedo of 0.35 in all cases. In the cross-ruled areas the albedo was changed from 0.14 (in cases 2a and 2b) to 0.35 (in cases 3a and 3b). Top panel: precipitation (mm/day) in case 3b.

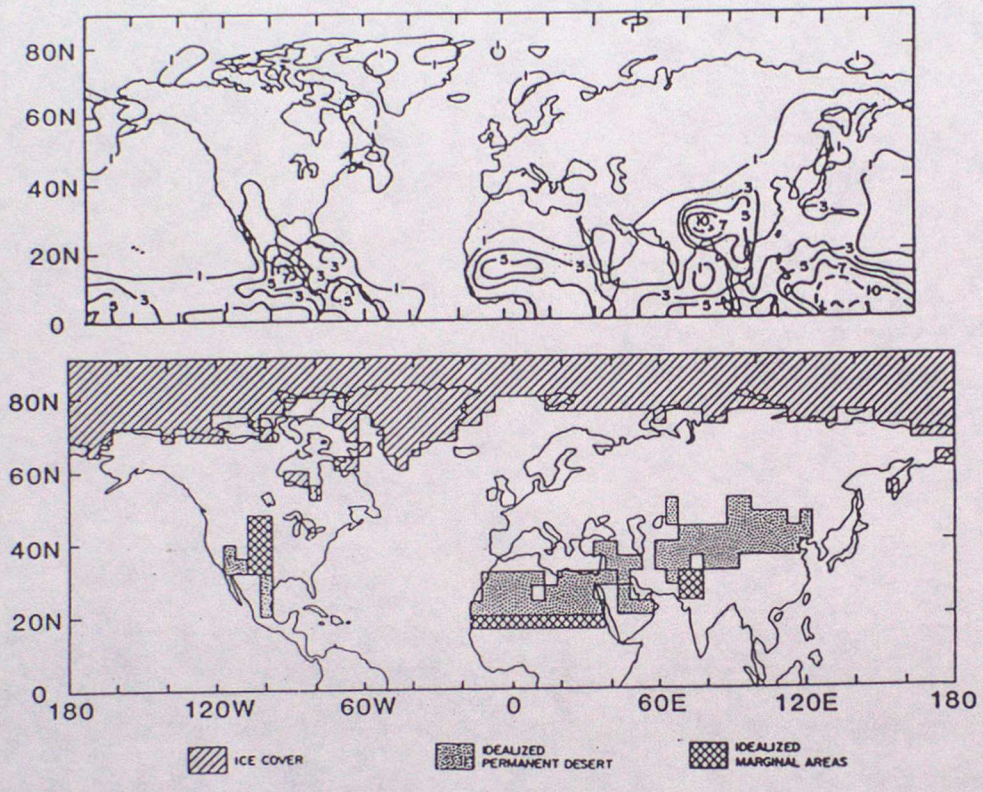

Figure 4.9.

From Mintz (1984).

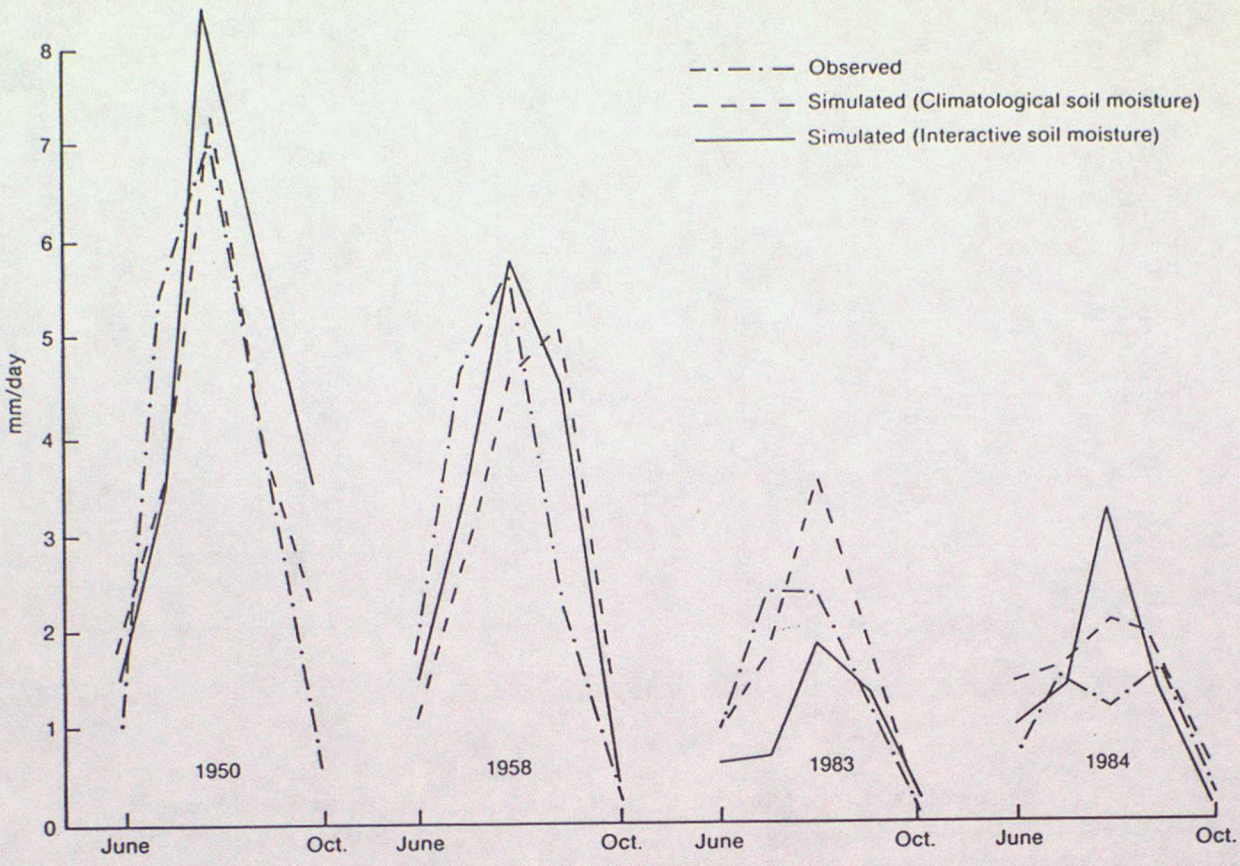

A. Time series of simulated rainfall for the whole Sahel for experiments 1950(I), 1958(I), 1983(I), 1984(I), 1950(C), 1958(C), 1983(C) and 1984(C), together with the corresponding observed rainfall.

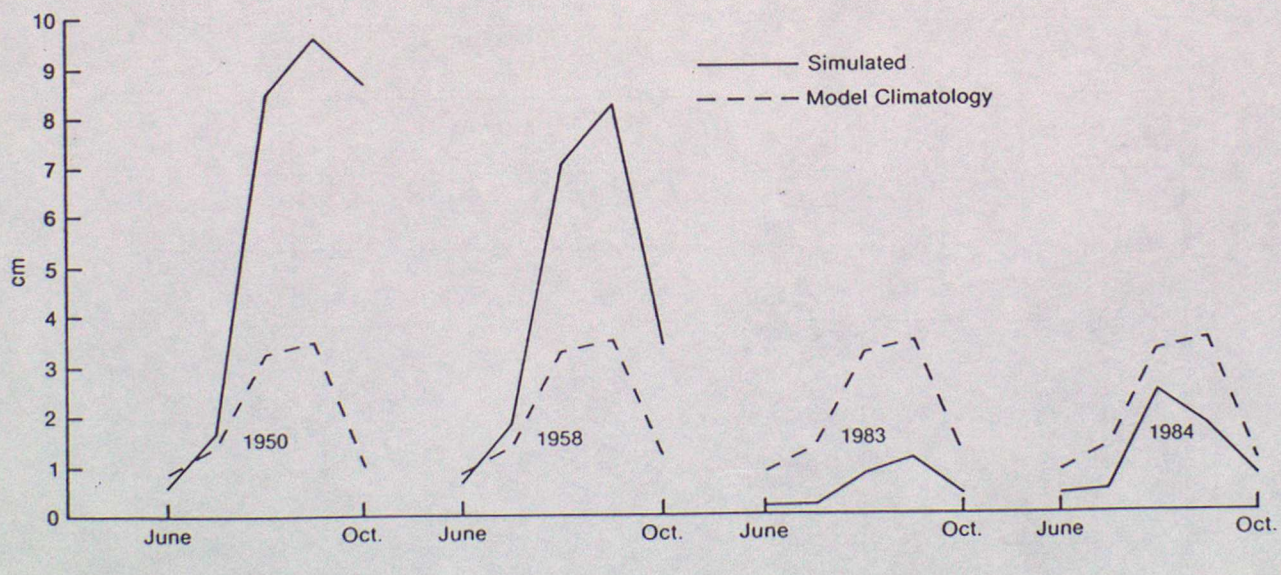

B. Time series of simulated soil moisture for the whole Sahel for experiments 1950(I), 1958(I), 1983(I) and 1984(I).

Figure 4.10. From Owen et al (1988).

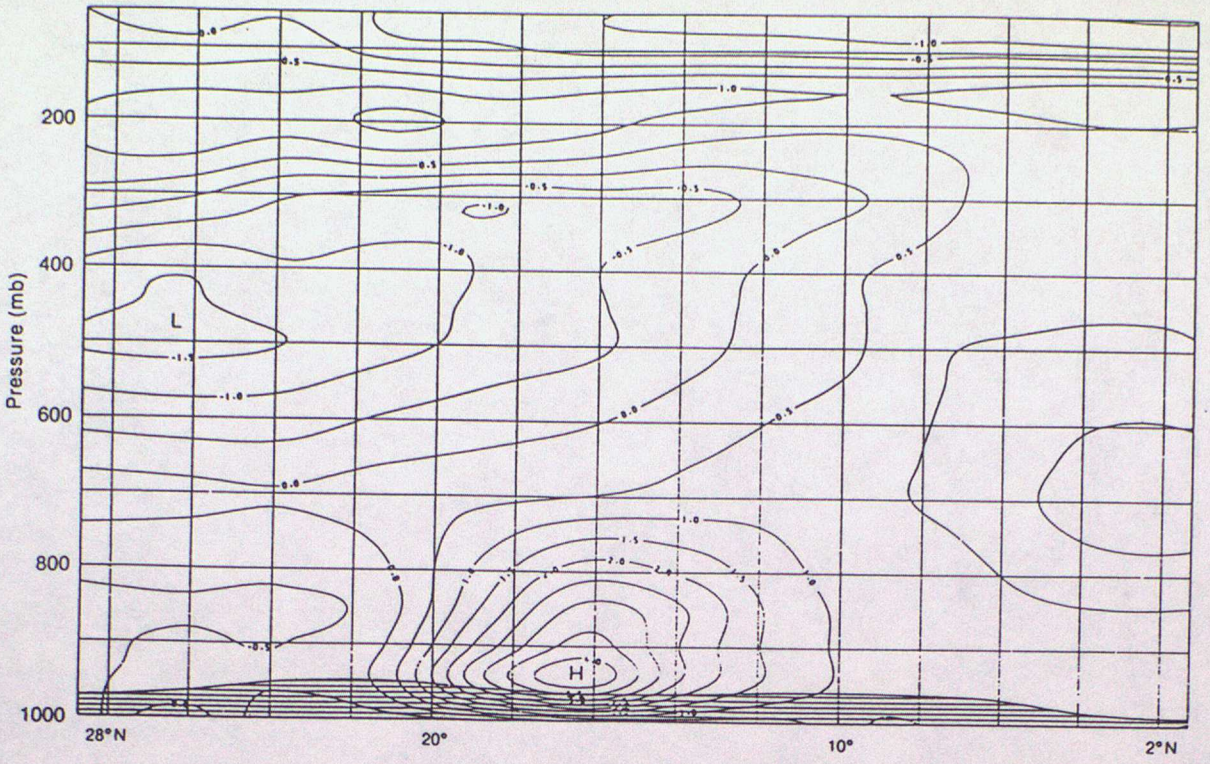

A. Cross-section (average over longitudes 10°W to 30°E) of the temperature difference between experiments 1984(I) and 1950(I) for July to September. Contour interval is 0.5 °C.

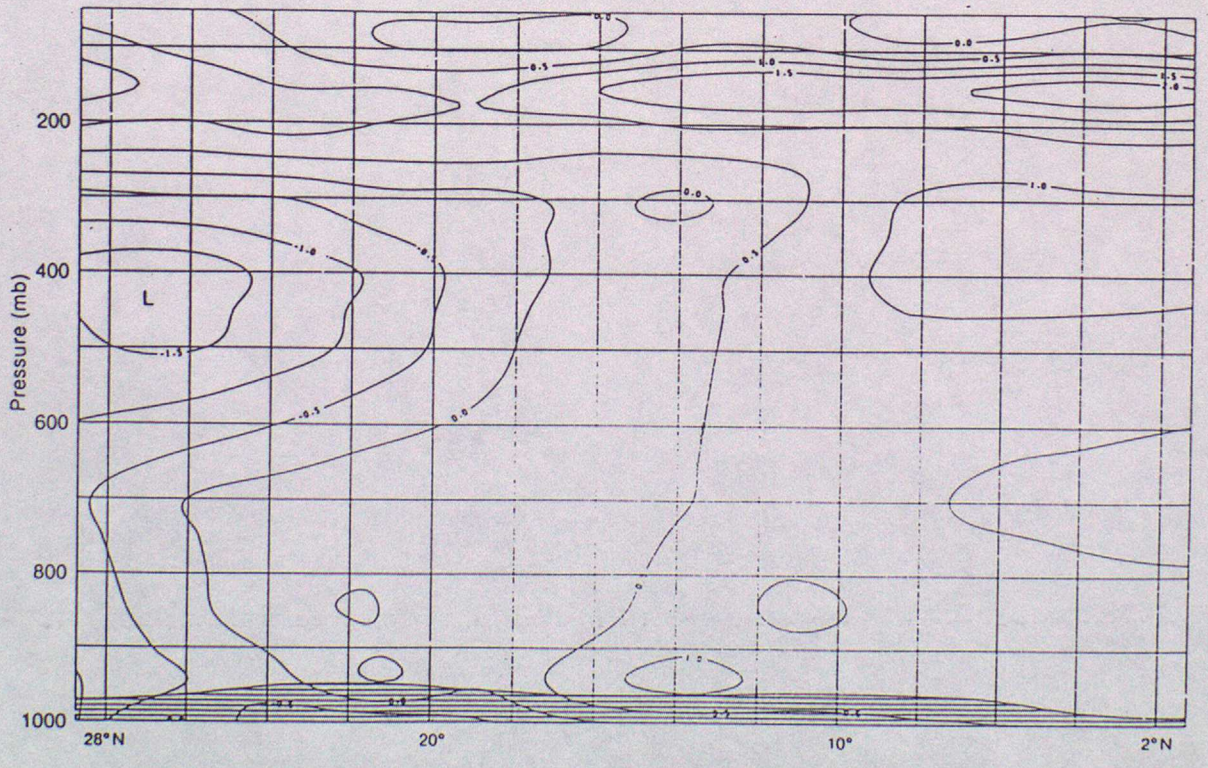

B. As A but for experiments 1984 (C) and 1950 (C).

Figure 4.11. From Owen et al (1988).

OCEAN-ATMOSPHERE INTERACTION

D E PARKER AND C K FOLLAND

MET O 13

SUMMARY

It is well-known that differences in temperature between land and sea play an important role in shaping the observed seasonal variations in atmospheric circulation. We demonstrate from theoretical, empirical and numerical-modelling results that variations in sea surface temperature on several time-scales additional to the climatologically averaged seasonal variations are an important influence on climatic variability. Examples are given both for the midlatitudes and for the tropics. Recent research into the causes and predictability of the droughts in sub-Saharan Africa indicates that modulation of the tropical atmospheric circulation by worldwide sea surface temperature anomalies has a greater influence on sub-Saharan rainfall than do regional anomalies of soil moisture. Furthermore, these atmospheric circulation changes may reinforce the decadal and longer time-scale variations in sea surface temperature, by modulating surface ocean currents.

5.1 INTRODUCTION

In many parts of the world, sea surface temperature (SST) varies substantially through the seasons, but the greater seasonal cycle of air temperature over land (Fig 5.1) results in seasonally varying differences in temperature between land and sea, which play an important role in shaping the observed seasonal variations in atmospheric circulation.

At first sight, however, it is not self-evident that variations in SST that occur in addition to the mean seasonal variations are an important influence on climatic variability. In this lecture, therefore, we

demonstrate the importance of regional and global-scale nonseasonal variations or "anomalies" of SST in relation to climatic variations on seasonal, interannual and decadal time-scales. We leave century time-scale variations to Lecture 9, and geological time-scale variations to Lectures 7 and 8. Also we leave discussion of the El Nino-Southern Oscillation to Lecture 6, and, after discussions of general principles and of the effects of extratropical and tropical SST anomalies on climatic variability, we concentrate on recently-discovered links between worldwide SST anomalies and rainfall in sub-Saharan Africa.

5.2 SST ANOMALIES

5.2.1 The importance of SST anomalies

The following discussion is based on considerations raised by Sawyer (1965). Suppose that an SST anomaly is suddenly "switched on". Before the atmosphere has begun to readjust there will be anomalous heat transfer ΔQ into the ocean consisting of anomalous sensible and latent heating ΔH and ΔE such that

$$\Delta Q = \Delta H + \Delta E$$

$$= 2.4U\Delta (T_a - T_s) + 3.7U\Delta (e_a - e_s) \ Wm^{-2} \qquad (5.1)$$

where $\Delta (T_a - T_s)$ is the change in the difference between the air temperature T_a and the sea surface temperature T_s; $\Delta (e_a - e_s)$ is the change in the difference between the vapour pressure e_a of the air (mb) and the saturation vapour pressure e_s at temperature T_s; U is the wind speed in ms^{-1}; and the constants are empirically determined. Suppose that it is midlatitude winter with $U = 10\ ms^{-1}$ and $T_s = 15°C$. Then if T_s is raised by 1°C, which is a typical magnitude for an SST anomaly (Section 5.2.2), but U, T_a and e_a are held constant, ΔQ is about $-65\ Wm^{-2}$ representing anomalous heat transfer of this magnitude into the atmosphere. This quantity is over 25% of the annual mean absorption of solar energy by the Earth at midlatitudes, which is about $200\ Wm^{-2}$ (Gill (1982)). In practice this calculation exaggerates ΔQ because e_a and T_a are held fixed, but it

suggests that, if equilibrium is to be restored, significant changes of atmospheric circulation are needed, especially if the SST anomaly is in regions of strong winds and of high T_s so that $\frac{de_s}{dT_s}$ is large from the Clausius-Clapeyron equation. In summer, when typical wind speeds are about half their winter values, the anomalous heat transfer for a given magnitude of SST anomaly would be rather more than half its winter value because $\frac{de_s}{dT_s}$ would be greater. In the warmest parts of the oceanic tropics with T_s = 29.5°C and U = 5 ms^{-1}, ΔQ would be about -55 Wm^{-2} if an SST anomaly of 1°C were suddenly generated. This anomalous transfer is comparable with the average net heat transfer (including radiation) at the ocean surface in tropical regions (Fig 5.2), and is nearly 20% of the annual mean abosrption of solar energy by the Earth in the tropics (300 Wm^{-2}, Gill (1982)).

An order-of-magnitude estimate of the impact of a regional SST anomaly on the dynamics of the overlying atmosphere may be made by considering the effects of a regional increase ΔT_a of air temperature throughout the troposphere, taken as the 1000 mb to 200 mb layer, with no change in temperature outside the region. If there is no immediate dynamically-induced response from the surrounding atmosphere other than to accept an outflow at higher levels of excess warm air from the heated region, the density of the heated layer will fall by approximately $\frac{\Delta T_a}{T_a}$ and the surface pressure by 0.8 $\frac{\Delta T_a}{T_a} P_s$, where P_s is the initial surface pressure and the factor 0.8 arises because the top 20% of the atmosphere is assumed not to be heated. If P_s = 1000 mb, T_a = 270°K and ΔT_a = 1°C, then the surface pressure will fall by about 3 mb. In practice, an SST anomaly ΔT_s is likely to result in an air temperature anomaly $\Delta T_a \simeq \Delta T_s$ in the lower troposphere but $\Delta T_a > \Delta T_s$ in the upper troposphere because of enhanced release of latent heat, especially in the tropics.

A change of surface pressure of 3 mb is an order of magnitude smaller than the typical changes associated with midlatitude synoptic systems: thus, a typical SST anomaly of order 1°C appears to be insufficient to play a leading role in the development of an individual system. However, monthly averages of surface pressure in midlatitudes have standard deviations of the order of 5 mb in winter (Parker (1982)) and 3 mb in summer, so persistent SST anomalies on the same space scale (several thousand km) as typical anomalies of surface pressure may be important influences on monthly and especially seasonal mean conditions in midlatitudes. In the tropics, the largest surface pressure anomalies on seasonal time-scales are associated with the El Nino-Southern Oscillation (ENSO), in which SST anomalies of several degrees C covering much of the eastern and central tropical Pacific are a key feature (Lecture 6). The influence of other observed tropical SST anomalies on a variety of space and time scales is also expected to be significant in view of the above computations, since these anomalies are often of order 1°C, and since pressure changes of a few millibars entail substantial changes in flow regimes at low latitudes.

5.2.2 The characteristics of SST anomalies

Figs 5.3A and B show the interannual standard deviations of January and July SST as given by Bottomley et al (1988) for the period 1951-80. Areas of high interannual variability include the tropical central and eastern Pacific, the central North Pacific, and the Kuroshio and Gulf Stream regions. Figs 5.3 C and D show one-month lag correlations of SST anomalies between January and February and July and August, respectively. Persistence is greatest in the extratropical North Atlantic, and, except from January to April (Bottomley et al (1988)) in the eastern tropical Pacific. The midlatitude North Pacific also sometimes exhibits persistent SST anomalies, as do parts of the tropical central Pacific, and the tropical Atlantic. Figs 5.3 A to D suggest that the magnitude, spatial scale and persistence of typical SST anomalies in many parts of the world are sufficient to have the significant effects on the atmosphere suggested by the considerations of Sawyer and of Section 5.2.1 above.

Figs 5.4 A, B, C characterise major global patterns of SST anomalies (SSTA) by showing the first three covariance eigenvectors of variation of worldwide fields of SSTA. The eigenvectors were computed from a matrix of seasonal SSTA on a worldwide 10° latitude x longitude grid for the period 1901 to 1980. Missing data in the matrix had first been replaced by interpolated values derived by a combination of polynomial interpolation in time and linear interpolation spacewise. Data for before 1942 had been adjusted to compensate for the use of uninsulated buckets (Bottomley et al (1988)). The first eigenvector (Fig 5.4A) is of the same sign almost everywhere, accounts for 10.9% of the total variance, and represents worldwide long-term trends of SST (Lecture 9). The second eigenvector (Fig 5.4B) represents the signature of El Nino (Lecture 6) and accounts for 7.7% of the total variance. The third eigenvector (Fig 5.4C), which accounts for 3.9% of the total variance, represents a basically interhemispheric contrast of SSTA, but with the northern Indian Ocean and a few other parts of the northern tropics in phase with the Southern Hemisphere, and with weak SSTA in the S Pacific. This eigenvector has been shown to be strongly related to sub-Saharan rainfall (Section 5.4 below).

Corresponding eigenvectors were also computed using SSTA for particular seasons only (eg northern winter = December to February), again for 1901-80. For all 4 seasons, the first two eigenvectors were very similar to Figs 5.4A and B, demonstrating the computational stability of the eigenvectors and their independence of the annual cycle. For northern spring and autumn the third eigenvector was similar to Fig 5.4C, but for northern summer the features of Fig 5.4C were split between the fourth and fifth eigenvectors, and for northern winter between the third and fourth eigenvectors (Folland and Colman (1988)). The pattern in Fig 5.4C is clearly a natural mode of variability in each individual season.

5.3 GENERAL EVIDENCE FOR THE EFFECTS OF SST ANOMALIES

5.3.1 Effects of extratropical SST anomalies on atmospheric circulation

Smagorinsky (1953) carried out the first physically realistic analysis, using a baroclinic model, of the perturbations to an extratropical zonally symmetric wind flow caused by imposed large-scale diabatic heating that varied with longitude. Fig 5.5 is representative of his results. Smagorinsky defined a sinusoidal heating function such that the maximum diabatic heating, Q_{max}, was 209 Wm^{-2} relative to the minimum heating, Q_{min}. The wavelength of the heating function was 160°, and for the results shown in Fig 5.5 the maximum heating is placed at 40° relative longitude and the minimum heating at -40°. Smagorinsky designed the wavelength of this heating variation to correspond roughly with the variation in surface heating in winter due to the distribution of land and sea in the N American sector. He showed (which can be deduced from Fig 5.5) that the Iceland low at the surface should be placed about 20-30° longitude east of the 500 mb Canadian trough in the winter. In Fig 5.5, D is the meridional wavelength of the heating, and h is the height of maximum heating, which includes the effects of latent heat release: for our purpose D = 35° is quite appropriate (Fig 5.5 (A), (B)). This value corresponds to an appreciable positive (or negative) heating anomaly that occupies at least 10° of latitude. Fig 5.5A suggests that the maximum PMSL response would be of magnitude 2 mb/25 Wm^{-2} of forcing and the maximum 500 mb height response would be about 1 dm/25 Wm^{-2}: Fig 5.5B, for which the height of maximum heating is greater and possibly more realistic, suggests a somewhat smaller response.

We can attempt to apply these ideas to work carried out by Ratcliffe and Murray (1970) (RM), who showed from observations an association between Northern Hemisphere mean sea level pressure (PMSL) anomalies and SST anomalies (SSTA) in the previous month in the "Ratcliffe region" south east of Newfoundland. Fig 5.6 shows the SSTA patterns, in a generalised way, and Fig 5.7 (A), (B) the response of the PMSL to warm and cool anomalies; their wavelike pattern is reminiscent of Smagorinsky's results.

Concentrating on the February PMSL response, the magnitude of the PMSL anomalies is roughly the same for both cool and warm SSTA, but the patterns are not the inverse of each other, suggesting non-linearity in the response of PMSL to SSTA, and that Smagorinsky's model is not wholely appropriate for the shapes and sizes of the areas of SST anomalies in Fig 5.6. In February, U is approximately 11 m sec^{-1} south east of Newfoundland and T_s is approximately 10°C, so a mean maximum SSTA of 1.5°C might give a maximum heating anomaly of nearly 90 Wm^{-2}. Fig 5.5B suggests a PMSL response of about 5 mb downstream of this SSTA value. This response is quite similar to RM's values. In summer the general shape of the PMSL anomaly pattern is similar but anomalies are rather less than half those observed in February. This seems reasonable as on average U will be about half the value observed in February, but is a little less than might have been expected from Section 5.2.1 in view of the greater value of $\frac{de_s}{dT_s}$ in summer.

RM's results have been tested in winter by Palmer and Sun (1985) (PS) using the Meteorological Office 5-level AGCM supported by an observational analysis employing better SST data than were available to RM. The modelling study used warm and cold SSTA whose maximum magnitude just exceeded 3°C, ie double that used by RM; these anomalies are still realistic and correspond to the maximum observed anomalies. The model was initialised from real November atmospheric data and used winter radiation. Four pairs of anomaly (warm SSTA) and control (cold SSTA) runs were made. December climatological mean SST was used away from the anomaly. The differences in model 1000 mb height and 500 mb height between warm and cold cases are shown in Figs 5.8 A and B; in each diagram the difference is averaged over the four pairs of integrations for model days 21-50. The patterns are reminiscent of those of RM but the high and low centres, which are statistically significant, are further apart. The maximum response of about 1.5 mb/°C is weaker than RMs results, possibly because the area of $|SSTA| > 2°C$ was only about 8° latitude x15° longitude. Other details of the model response are given in the paper including the anomalous tracks of depressions. PS believe that the anomalous advection of low-level warm, humid air into the SST anomaly area from the south is an important component of the atmospheric response, which also tends to maintain the SST

anomaly. This provides an important difference between the Smagorinsky model and the probable atmospheric response over the "Ratcliffe" area. However, PS found, by using halved SSTA, that their model's response was approximately linear.

The observational study consisted of a calculation of PMSL and 500 mb height differences between winter months (Nov-Feb) having a warm SSTA (> 0.8°C) and those having a cool SSTA (< -0.8°C) in the region 40°-50°N, 40°-60°W. The epoch 1951-80 was studied first and gave similar results to those of the AGCM though with a slightly shorter wavelength between high and low centres at both levels, when monthly mean SSTA, PMSL and 500 mb height were calculated for the same month. The analysis was repeated for 1901-30 and gave similar results. Fig 5.9 is an example of the results for 1951-80. However, when PMSL was allowed to lag one month behind SSTA the relationships did not hold up well nor did they agree well with those of RM: weak low pressure anomalies were indicated stretching across the Atlantic when data for months following warm SSTA were subtracted from those following cold SSTA. PS pointed out that RM's results for December to January were not statistically significant, and that SSTA southeast of Newfoundland are not persistent at that season. On the other hand, PS found that the relationships were strong (and of the same form as for zero lag) when SSTA was allowed to lag one month behing PMSL, and they therefore suggested that the SSTA develop in response to anomalous atmospheric forcing.

Rowntree (1984) has summarised a number of AGCM experiments carried out in the Atlantic and Pacific on mid-latitude SSTA; Fig 5.10 shows his summary diagramatically; the overall conclusions are surprisingly consistent and broadly in harmony with the ideas of Smagorinsky, though in reality, as hinted above, the relative importance of different physical effects in the atmosphere may vary considerably.

5.3.2 Effects of tropical SST anomalies on atmospheric circulation

Because the Coriolis parameter is small near the equator, the nature of atmospheric forcing by tropical SSTA differs from that by extratropical SSTA. Anomalous tropical heating gives rise to mainly colocated anomalous vertical atmospheric motion, and thus the most direct results of forcing by positive tropical SSTA are local falls of pressure in the lower troposphere and the creation of anomalous anticyclonic vorticity in the upper troposphere. An SSTA centred on or very near the equator forces a pair of low-level low pressure anomalies, one on each side of the equator near the maximum SSTA, with upper-level anticyclonic anomalies overlying them (eg Palmer and Mansfield (1986 a, b)). Simmons (1982) used a relatively simple baroclinic model to show that the anomalous atmospheric vorticity forcing may give rise to a Rossby wave-like response in the extratropics in association with the stimulation of barotropic instability in the upper flow. The atmospheric response in the northern winter was largest in his model when the vorticity forcing in the tropics was placed in specific longitudes and the prescribed climatological mean upper flow included the mean troughs and ridges. The longitudinally varying response did not occur for a prescribed zonally averaged mean flow. Simmons suggested that the effects of tropical vorticity forcing propagate into mid latitudes more easily when the forcing is overlain by upper westerly winds. Upper-tropospheric anticyclonic vorticity responses may be amplified when they coincide with a climatological upper ridge as in the north-east Pacific in winter. Fig 5.11 shows a few of Simmons' results at 500 mb, using a prescribed mean flow defined by a January mean 500 mb height climatology, and with vorticity forcing at 135°E in different tropical latitudes:SST forcing was not explicitly used. Fig 5.11 shows that the strongest extratropical response that Simmons found was for forcing centred at 15°N, 135°E. Note that the 500 mb height response is quite large near the UK in the model.

Palmer and Mansfield (1986b) used the Meteorological Office 11-layer AGCM to explore the impact of tropical W Pacific SSTA on the atmospheric circulation in northern winter. They found that an anomaly

with a maximum of 1.5°C centred on the equator in the tropical W Pacific (see Fig 5.12 A) produced a strong wave-like response in the upper troposphere (Fig 5.12B). The response was statistically significant and was qualitatively similar to that of Simmons. Palmer (1985) argued that the atmospheric response to tropical vorticity forcing may be non-linear; vorticity forcing from positive SSTA mainly results from the increased release of latent heat which would be expected to increase non-linearly with increasing SSTA. Similarly it might be expected that a negative SSTA of given magnitude would produce a smaller vorticity forcing and atmospheric response than a positive SSTA of the same magnitude. Palmer, however, found in his model with negative SSTA a similar magnitude of atmospheric response, though of opposite sign, and gave a straightforward dynamical explanation: the relative vorticity tends to cancel (amplify) the planetary vorticity when the SSTA is positive (negative). However it remains to be seen to what extent such results depend on the AGCM used. Also, extratropical responses to some tropical SSTA may be more barotropically stable than those to other tropical SSTA, and, as a result, less variable and more statistically significant (Palmer (1988)). A contributory reason for the very strong atmospheric response to SSTA over the tropical W Pacific is that a given SSTA produces a larger anomaly of latent heating there than elsewhere because the saturation vapour pressure of ocean water changes faster as temperature changes in the very warm W Pacific water. Typical tropical W Pacific SST's exceed 29°C; occasionally SST exceeds 31°C near the location of the maximum tropical W Pacific SST anomaly used by Palmer and Mansfield (1986).

Fig 5.13 (from Simmons (1982)) shows the response of a steady state linear model to an isolated positive heating anomaly centred on the equator. To the west of the heating maximum, the low level winds tend to be westerly and the upper level winds easterly, a similar situation to that in the real atmosphere west of the diabatic heating maximum in the SE Asian monsoon/W Pacific region in northern summer (see Lecture 2). To the east of the heating maximum, the model winds are reversed: ie the upper winds are westerly and the lower winds easterly. Sinking motion should occur over the well-defined SST minimum near the equatorial S American coast and connect the mean upper westerly to the mean lower easterly flows that exist

to the east of the W Pacific SST maximum. The closed circulation that results is like the Walker circulation discussed in Lecture 2: the mechanism underlying Fig 5.13 probably explains an appreciable part of the Pacific Walker circulation and, perhaps, similar circulations near the equator in other longitudes.

Rowntree (1976) carried out experiments using the Meteorological Office 5-level AGCM which indicated that north of a positive SST anomaly placed in the tropical NE Atlantic in winter a surface low was formed, with an upper-tropospheric high almost over the SST anomaly. North of the low, in fact well into upper middle latitudes, a high anomaly was found. Fig 5.14 shows the model response for selected experiments by comparison with control integrations. The SST anomaly was based on that observed at the beginning of the very cold European winter of 1962-3 but it remains unclear to what extent Rowntree's results "explain" that winter. The differences between Figs 5.14B and C arise because of small changes in model formulation and indicate the sensitivity of the results to such small changes. This is clearly not enough to change the nature of the response in a fundamental way but Figs 5.14B and C show that caution is needed in interpreting the results of model integrations. Statistical significance of model-generated fields needs to be assessed, by Monte Carlo sampling, which may be computationally expensive, or by other techniques described by Livezey and Chen (1983).

Hastenrath (1984) carried out observational studies of tropical Atlantic SSTA and atmospheric circulation anomalies in relation to precipitation in the drought-prone Brazilian Nordeste. Positive SSTA in the tropical South Atlantic and negative SSTA in the tropical North Atlantic were associated with enhanced rainfall in the Nordeste. At the same time, the intertropical convergence zone was displaced southwards and therefore affected the Nordeste to a greater extent. Inverse anomalies were associated with drought in the Nordeste. Hastenrath et al (1984) extended this work by making skilful hindcasts of Nordeste rainfall on the basis of indices of SSTA and atmospheric circulation in the tropical Atlantic region in months prior to the Nordeste's March to May rainy season. Subsequently Ward et al (1988) developed a method of predicting

Nordeste rainfall using only the coefficients of regional eigenvectors of SSTA. One of their eigenvectors corresponded to Hastenrath's North versus South Atlantic SSTA contrast, and another represented El Nino. Skilful predictions were issued for 1987 and 1988.

Tropical SSTA have also been used in the prediction of the Indian Monsoon. In a statistical study, Hastenrath (1987) found that SSTA in the Arabian Sea had predictive value for Indian Monsoon rainfall, and Kershaw (1988) used an atmospheric general circulation model to simulate the effect of a positive SSTA in the eastern Arabian Sea on the onset of the 1979 Indian Monsoon. The SSTA (Fig 5.15A) was appropriate to early June 1979. Beginning with real atmospheric conditions for 11 June 1979, the control integration with climatological SST maintained low-latitude westerlies in the lower troposphere through to 19 June (Fig 5.15B) whereas the anomaly integration produced a lower-tropospheric vortex slightly northwest of the SSTA (Fig 5.15C) and was in generally better agreement with observation (Fig 5.15D), though the strong flow covered too large an area, the centre of the vortex was too far southeast, and the orientation of the strong flow was westerly instead of southwesterly. At 200 mb the anomaly experiment was slightly superior in that it predicted a stronger easterly jet than did the control. The anomaly experiment predicted more precipitation over and to the northwest of the SSTA, with differences exceeding 40 mm per day. Kershaw used diagnostic information from the integrations, as well as a linear model, to elucidate the feedbacks taking place in the model (Fig 5.15E). However the SSTA was held fixed in the model, so the representation of ocean-atmosphere interaction was not complete. In reality, the SSTA would probably have diminished as a result of the increased windiness and cloud cover. This may explain the excessive area of strong flow (ie excessive total kinetic energy) in the lower troposphere in the anomaly experiment (Fig 5.15C: compare with Fig 5.15D).

5.4 SST ANOMALIES AND RAINFALL IN SUB-SAHARAN AFRICA

5.4.1 Introduction

The drought in sub-Saharan Africa has now persisted, with only partial intermissions, for 20 years (Fig 5.16). Folland et al (1986) observed that the decline in Sahel rainfall between the 1950's and the 1970's was accompanied by a warming of the ocean surface in the Southern Hemisphere and northern Indian Ocean (SHNI) and a cooling of the ocean surface in the rest of the Northern Hemisphere (RNH). Since the late 1970's the oceans of both hemispheres have warmed slightly and the difference (SHNI minus RNH) has changed little. Fig 5.17, from Parker and Folland (1988), shows that SSTA differences between 1951-1960 (Sahel wet) and 1971-87 (Sahel dry) exceeded 1°C in some areas. For 1901-84, the correlation between annual Sahel rainfall and the approximately simultaneous (July to September) values of (SHNI minus RNH) was - 0.62 (Folland et al (1984)). Folland et al constructed a difference field between the average July to September SSTA for the very dry years 1972-3, 1982-4 and that for the very wet years 1950, 1952-4, 1958 (Fig 5.18). They then computed the covariance C_i between each year's global field of July to September SSTA field and Fig 5.18, after subtracting the global average SSTA from each field. The correlation between C_i and annual Sahel rainfall was -0.72 for 1901-84. Furthermore, it was -0.85 for 1946-84 and -0.43 for 1901-39. These results suggested that, despite enhancement of the correlations by data-dependence and reduction of significance by lag autocorrelation, the relationship was very strong for the period after 1946 when the prominent fluctuations in Sahel rainfall were interdecadal (Fig 5.16), and still significant for the period 1901-39 which was dominated by interannual variability (Fig 5.16). A parallel exercise using a field corresponding to Fig 5.18 but based on years before 1940 also yielded statistically significant results. The field was similar to Figure 5.18 but with weaker SSTA in the Southern Hemisphere and no major positive SSTA in the East Tropical Pacific. Folland et al (1986) confirmed their findings by applying the SSTA field in Fig 5.18 to the anomaly integration of an atmospheric general circulation model run in perpetual July mode. The

anomaly integration produced a substantially drier Sahel than the control run with climatological SST. The mechanism for reduction of the rainfall in the model appeared to be mainly a reduction in moisture flux covergence, as a result of changes of atmospheric circulation. There was also reduced upper-tropospheric divergence over the Sahel. The modelling experiments were extended by Palmer (1986) who applied the Atlantic, Pacific and Indian Ocean portions of Fig 5.18 separately in a series of anomaly integrations. Over the western Sahel, the Atlantic and Pacific SSTA had a comparable effect in reducing the model's rainfall: over the eastern Sahel, the Indian Ocean had the dominant role.

5.4.2 Confirming the relationships

The pattern in Fig 5.18 has the disadvantage of being based on a small sample of years, and therefore in subsequent studies eigenvector patterns based on the entire 1901-80 data set, rather than composites, have been used to elucidate relationships between SSTA and Sahel rainfall. Comparison of Fig 5.18 with Fig 5.17 suggests that the warm East Tropical Pacific is not a major part of the true Sahel drought signature in SSTA, and that its occurrence in Fig 5.18 is a fortuitous result of the coincidence between the 1982-3 El Nino and very dry conditions in the Sahel. This conclusion is supported by the correlations of only about -0.2 between Sahel rainfall and the simultaneous coefficient of the second worldwide SSTA covariance eigenvector (Fig 5.4B) found by Parker et al (1988). On the other hand, the correlations with the simultaneous coefficient of the third eigenvector (Fig 5.4C) were -0.58, -0.50 and -0.71 for 1901-87, 1901-45, and 1946-85, and both interdecadal and interannual fluctuations contributed to this relationship (Fig 5.19). Note the similarity between the third eigenvector and the recent interdecadal changes in SST shown in Fig 5.17: note also that (SHNI minus RNH) is an approximate measure of the coefficient of the third eigenvector. A smaller part of the SSTA-Sahel rainfall relationship is, however, described by the sixth worldwide eigenvector of SSTA, which mainly represents a contrast between North and South Atlantic SSTA, especially in the Benguela current region, but with the Indian Ocean in phase with the South Atlantic and much of the Pacific Ocean in phase with the North Atlantic (Fig 5.20). The

simultaneous correlation with Sahel rainfall was 0.44 for 1901-86, but the relationship of Sahel rainfall with the sixth eigenvector appears only to have applied during periods when variations have been predominantly interdecadal: see the correlations marked on Fig 5.21, which show that a warm South Atlantic and cold North Atlantic in association with the sixth eigenvector were associated with Sahel drought from 1940 onwards and for a short period at the beginning of the century, but not in the intervening interval. This observation is in accord with the results of Lough (1986), who found that significant relationships established for 1948-72 between Sahel rainfall and a tropical Atlantic SSTA pattern quite similar to the sixth eigenvector did not apply in 1911-39.

A major implication of these results is that Sahel rainfall is related to intrinsic modes of worldwide variability of SSTA. This conclusion could not be drawn from the composite presented in Fig 5.18 or from the pattern of interdecadal trends shown in Fig 5.17 because these were not constructed independently of the known changes in Sahel rainfall.

5.4.3 Prediction by statistical methods

A further extension of this work has been to demonstrate that relationships very similar to those described above hold between Sahel rainfall and SSTA observed several months in advance, and that there is therfore potential for statistical prediction of the Sahel rainfall. Two methods of prediction are described by Parker et al (1988). The first produces a forecast by creating global fields of regression slopes of SSTA on subsequent Sahel rainfall: an index of the similarity between each year's SSTA field and the regression slope field is then regressed linearly against Sahel rainfall to provide a prediction equation. The second method uses multivariate linear discriminant prediction, a technique also used to make experimental monthly long-range forecasts for the United Kingdom (Folland and Woodcock (1986)). The predictors are selected from the coefficients of the eigenvectors of global SSTA measured several months in advance of the Sahel rainfall season, and, as expected, the coefficients of the third and sixth eigenvectors have been found to dominate the predictors. If SSTA as early as February and March are used, the second

eigenvector (El Nino) also has a beneficial impact on predictive skill, but if later SSTA are used this effect disappears, in accord with the low simultaneous correlations with the second eigenvector reported above. The reason for this decline in influence is likely to be that heat from the mature phase of El Nino has been transmitted into the SSTA fields in the Atlantic and Indian Oceans (Pan and Oort (1983); Wolter (1987)), thus incorporating the aftermath of El Nino into the coefficients of the third and sixth eigenvectors. The quantities predicted by the multivariate linear discriminant method are the probabilities that the Sahel rainfall will be in each of five climatologically equi-probable ranges or "quints". Despite the change in the statistical characteristics of the Sahel rainfall series, both methods showed significant though not consistent skill when used to hindcast years outside the "training periods" used to develop the relationships: see Table 5.1 which is an abridged version of the results of Parker et al (1988). Forecasts issued for 1986 and 1987 correctly indicated very dry years (Fig 5.16), and a prediction of very dry conditions (88% probability of the driest quint) has been issued for 1988.

5.4.4 Advances in the numerical modelling studies

Confidence in the validity of the statistical studies described above has been increased by the results of a series of experiments with an atmospheric general circulation model with an annual cycle (Owen et al (1988)). These experiments used observed fields of SSTA for the wet Sahel years 1950 and 1958 and the dry Sahel years 1983 and 1984, and covered approximately the period April to October inclusive. The first two months were intended to allow the model to adjust to the imposed SSTA from the identical starting conditions, which were those of 26 March 1984. The impact of the SSTA in the model was to give regionally-averaged Sahel rainfall in general accord with observation (Fig 5.22) whether interactive (I) or climatological (C) soil moisture was used (cf Lecture 4). Fig 5.23A is a map of the difference between the simulated rainfall for 1984 and that for 1950, with interactive soil moisture in each case: Fig 5.23B presents the observed differences, which are very similar except that the Guinea coastal region shows a relatively wetter 1984 than was simulated. The rainfall changes in the model were accompanied by a weakened low-level

monsoon flow into the western Sahel (Fig 5.24A) and by weakened upper-tropospheric easterlies over Africa, the Atlantic and the Indian Ocean (Fig 5.24B). The African Easterly Jet centred near 10-15N at 700 mb was strengthened in the model, possibly because of increased heating in the relatively rainless Sahel to the north. The changes in the model when 1983 and 1958 were compared were only slightly weaker, and the results are in accord with the observational study of Newell and Kidson (1984) in which the atmospheric circulation over the Sahel and surrounding areas in dry and wet Sahel years was compared.

A further set of experiments carried out by Owen et al (1988) involved hindcasting Sahel rainfall for the same years by using observed SSTA only up to mid July, then keeping SSTA fixed to simulate a forecasting operation where future SSTA is unspecified. The results were little different from the experiments which used observed SSTA throughout the integrations. Subsequently, an integration using SSTA for April 1988 has produced Sahel rainfall as low as that simulated for 1983 (Fig 5.22).

Finally, experiments were conducted with the SSTA limited to prescribed parts of the globe. When 1984 data were used, extratropical SSTA alone gave results wetter than model climatology, ie their effect was opposite to that observed. However, for 1950 the extratropical SSTA were found to have a more favourable influence than tropical Atlantic SSTA on the skill of the model in simulating Sahel rainfall. This somewhat surprising result is still being assessed.

5.4.5 Atmospheric forcing of the ocean

A noteworthy feature of Fig 5.24A is that, in the model, the wind changes at low levels over the western equatorial Atlantic, when SSTA appropriate to Sahel drought are imposed, are such as to tend to weaken the northward wind-driven surface currents in the ocean off northeastern Brazil. This result has been characteristic of many of the numerical model simulations of Sahel drought conditions (eg Folland et al (1986)), and is in accord with observed differences between the 1950's and the 1970's (Fig 5.25; also Newell and Hsiung (1987)). The significance of these findings is

that most of the oceanic heat flux from the Southern to the Northern Hemisphere takes place in the Atlantic (Charnock (1987); Hsiung (1985)). Thus it is feasible that the wind changes reduce this heat flux and therefore maintain the interhemispheric SSTA contrast (Fig 5.17) which drives them. Alternatively, or additionally, there could have been a weakening of the Indian Ocean heat source which supplies the South Atlantic; or the oceanic circulation of the Atlantic could have been weakened by atmospheric circulation changes over the extratropical North Atlantic (Newell and Hsiung (1987)). Confirmation of these hypotheses will require experiments with models of the ocean, suitably forced by observed atmospheric conditions or, ultimately, interacting with atmospheric general circulation models.

TABLE 5.1 SKILL OF TECHNIQUES FOR PREDICTING SAHEL RAINFALL FROM APRIL AND MAY SST ANOMALIES

Training period	Hindcast period	Persistence of Sahel rainfall in period (autocorrelation with one year's lag)	Regression technique: correlation between forecast and observed values	Discriminant technique: correlation between forecast category and observed category*
1901-45	1946-86	0.69	0.57	0.71
1946-86	1901-45	0.11	0.30	0.34

* Categories are measured on a scale of 1 (very dry) to 5 (very wet)

REFERENCES TO LECTURE 5

BOTTOMLEY, M, FOLLAND, C K, HSIUNG, J, NEWELL, R E and PARKER, D E (1988). Global Ocean Surface Temperature Atlas. Meteorological Office and Massachusetts Institute of Technology. In Press.

CHARNOCK, H (1987) Ocean currents and meridional transfers. Quart J Roy Met, Soc, 113, 3-18.

FOLLAND, C K (1983) Regional-scale interannual variability of climate - a north west European perspective. Met Mag, 112, 163-183.

FOLLAND, C K and COLMAN, A (1988) An interim analysis of the leading covariance eigenvectors of worldwide sea surface temperature anomalies for 1901-80. Long-Range Forecasting and Climate Research LRFC 20, Meteorological Office, Bracknell.

FOLLAND, C K, PALMER, T N and PARKER, D E (1986) Sahel rainfall and worldwide sea temperatures, 1901-85. Nature, 320, 602-607.

FOLLAND, C K and WOODCOCK, A (1986) Experimental monthly long-range forecasts for the United Kingdom. Part I. Description of the forecasting system. Met. Mag., 115, 301-318.

GILL, A E (1982) Atmosphere-ocean dynamics. Academic Press. 664 pp

HASTENRATH, S (1984) Interannual variability and annual cycle: Mechanisms of circulation and climate in the tropical Atlantic sector. Mon Weath Rev, 112, 1097-1107.

HASTENRATH, S (1987) On the prediction of India monsoon rainfall anomalies. J. Clim. Appl. Met. 26, 847-857.

HASTENRATH, S, WU, M-C and CHU, P-S (1984) Towards the monitoring and prediction of north-east Brazil droughts. Quart. J. Roy. Met. Soc, 110, 411-425.

HSIUNG, J (1985) Estimates of global oceanic meridional heat transport. J. Phys. Oceanog., 15, 1405-1413.

KERSHAW, R (1988) The effect of a sea surface temperature anomaly on a prediction of the onset of the south-west monsoon over India. Quart. J. Roy. Met. Soc., 114, 325-345

LAMB, H H (1972) Climate Present, Past and Future, Vol 1. Methuen

LIVEZEY, R E and CHEN, W Y (1983) Statistical field significance and its determination by Monte Carlo techniques. Mon. Weath. Rev 111, 46-59.

LOUGH, J M (1986) Tropical Atlantic sea surface temperatures and rainfall variations in Subsaharan Africa. Mon. Weath. Rev, 114, 561-570.

MONIN, A S (1975) The role of the oceans in climatic models. ICSU/WMO, GARP Publ Ser No 16, Geneva, pp 201-205.

NEWELL, R E and HSIUNG J (1987) Factors controlling free air and ocean temperature of the last 30 years and extrapolation to the past. In "Abrupt Climatic change - Evidence and Implications" (Eds. W H Berger and L D Labeyrie), NATO ASI series C: Mathematical and Physical Sciences, Vol 216, pp 67-87. D Reidel.

NEWELL, R E and KIDSON, J W (1984) African mean wind changes between Sahelian wet and dry periods. J. Climatology, 4, 27-33.

NICHOLSON, S E (1985) Sub-Saharan rainfall 1981-84. J. Clim. Appl. Met, 24, 1388-1391.

OWEN, J A, FOLLAND C K and BOTTOMLEY, M (1988) Numerical simulation of seasonal Sahel rainfall in four past years using observed sea surface temperature. Long-Range Forecasting and Climate Research LRFC 15, Meteorological Office, Bracknell.

PALMER, T N (1985) Response of the UK Meteorological Office general circulation model to sea surface temperature anomalies in the Tropical Pacific Ocean. Coupled Ocean-Atmosphere Models, pp 83-106. Ed: J Nihoul, Elsevier.

PALMER, T N (1986) Influence of the Atlantic, Pacific and Indian Oceans on Sahel rainfall. Nature, 322, 251-253.

PALMER, T N (1988) Medium and extended range predictability and stability of the Pacific North American mode. Quart. J. Roy. Met. Soc., 114, 691-713

PALMER, T N and MANSFIELD, D A (1986a) A study of wintertime circulation anomalies during past El Nino events using a high resolution general circulation model. I. Influence of model climatology. Quart. J. Roy. Met. Soc., 112, 613-638.

PALMER, T N and MANSFIELD, D A (1986b) A study of wintertime circulation anomalies during past El Nino events using a high resolution general circulation model. II. Variability of the seasonal mean response. Quart. J. Roy. Met. Soc., 112, 639-660.

PALMER, T N and SUN-Z (1985) A modelling and observational study of the relationship between sea surface temperature in the North West Atlantic and the atmospheric general circulation. Quart. J. Roy. Met. Soc., 111, 947-975.

PAN, Y H and OORT, A H (1983) Global climate variations connected with sea surface temperature anomalies in the eastern equatorial Pacific Ocean for the 1958-73 period. Mon. Weath. Rev., 111, 1244-1258.

PARKER, D E (1982) Large-scale interannual variability of climate. Met. Mag., 111, 193-208.

PARKER, D E and FOLLAND, C K (1988) The nature of climatic variability. Met. Mag., 117, 201-210.

PARKER, D E, FOLLAND, C K and WARD, M N (1988) Sea surface temperature anomaly patterns and the prediction of seasonal rainfall in the Sahel region of Africa. In "Recent Climatic Change - A Regional Approach", Ed. S. Gregory, Belhaven Press, pp 166-178.

RATCLIFFE, R A S and MURRAY, R (1970) New lag associations between North Atlantic sea temperature and European pressure applied to long-range weather forecasting. Quart. J. Roy. Met. Soc., 96, 226-246.

ROWNTREE, P R (1976) Response to the atmosphere to a tropical Atlantic ocean temperature anomaly. Quart. J. Roy. Met. Soc., 102, 607-626.

ROWNTREE, P R (1984) A survey of ocean surface temperature anomaly experiments for the Northern Hemisphere winter. Met O 20 Technical Note II/220.

SAWYER, J S (1965) Notes on the possible physical causes of long-term weather anomalies. WMO Tech Note, No 66, pp 227-48, Geneva.

SIMMONS, A J (1982) The forcing of stationary wave motion by tropical diabatic heating. Quart. J. Roy. Met. Soc., 108, 503-534.

SMAGORINSKY, J (1953) The dynamical influence of large-scale heat sources and sinks on the quasi-stationary mean motions of the atmosphere. Quart. J. Roy. Met. Soc., 79, 342-366.

WARD, M N, BROOKS, S and FOLLAND, C K (1988) Predictability of seasonal rainfall in the Nordeste region of Brazil. In "Recent climatic change - a regional approach", Ed S Gregory, Belhaven Press, pp 237-251.

WOLTER, K (1987) The Southern Oscillation in surface circulation and climate over the tropical Atlantic, eastern Pacific and Indian Ocean as captured by cluster analysis. J. Clim. Appl. Met., 26, 540-558.

WOODRUFF, S D, SLUTZ, R J, JENNE, R L and STEURER, P M (1987) A Comprehensive Ocean-Atmosphere Data Set. Bull. Amer. Met. Soc., 68, 1239-1250.

The world map of annual range of surface temperature.
(After Monin 1975.)

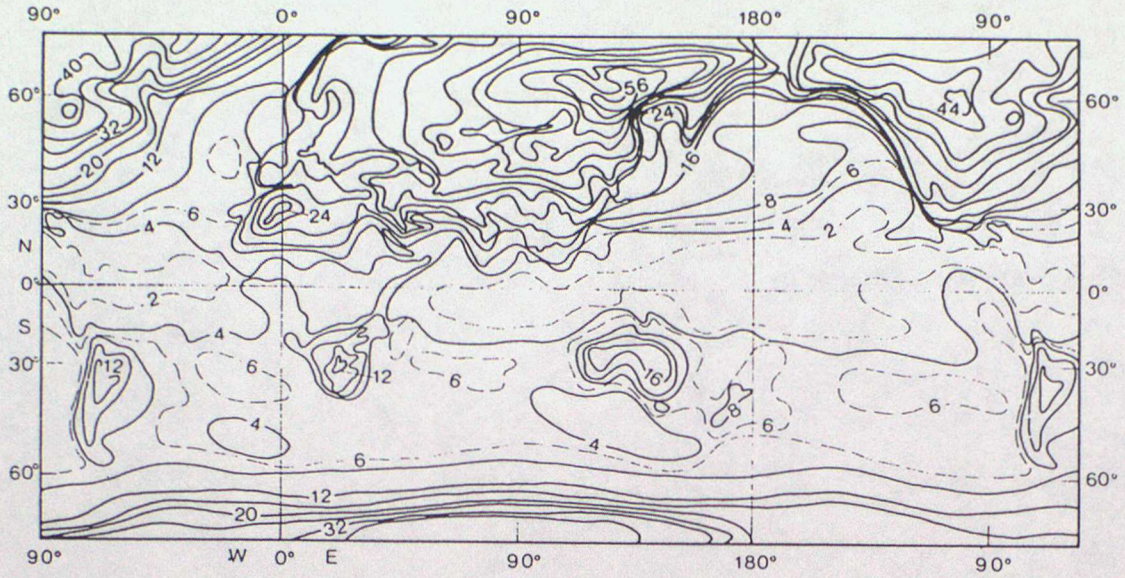

Figure 5.1.

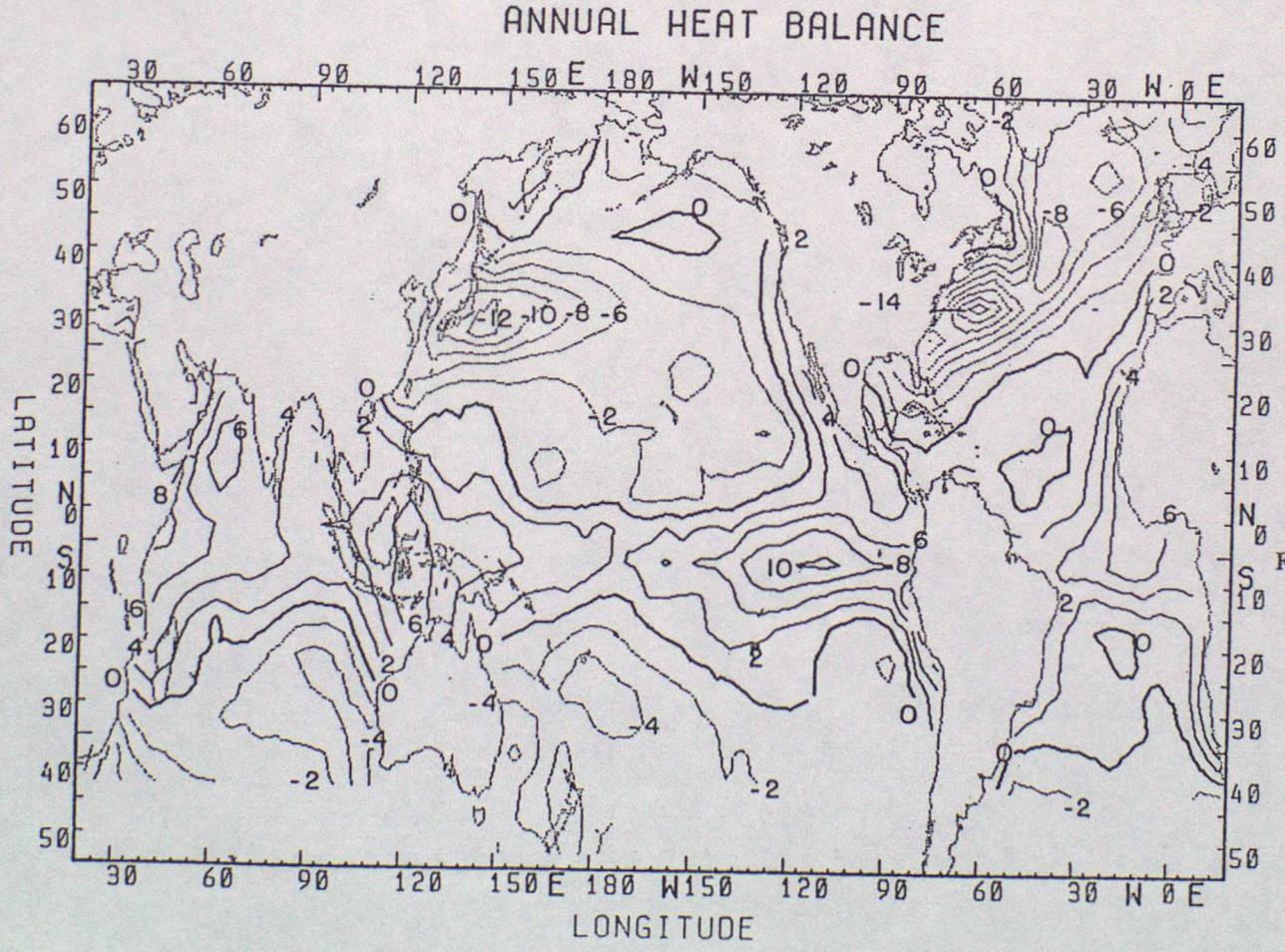

The annual mean net energy balance at the surface. The units are in W m^{-2} when multiplied by 10.

Figure 5.2
From Hsiung (1

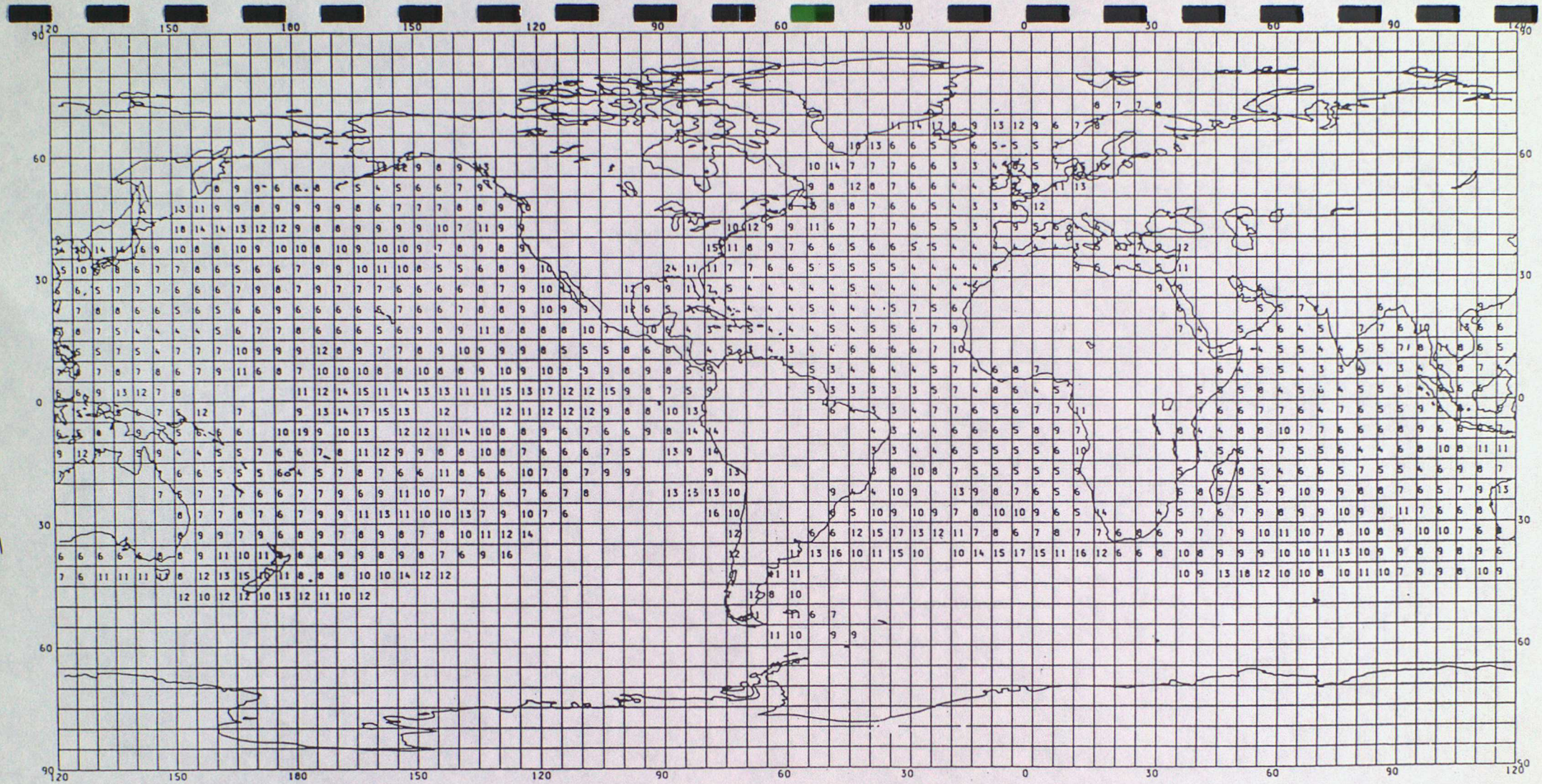

Figure 5.3A Standard deviation of monthly SST, January. After Bottomley et al (1988). Values in tenths °C.

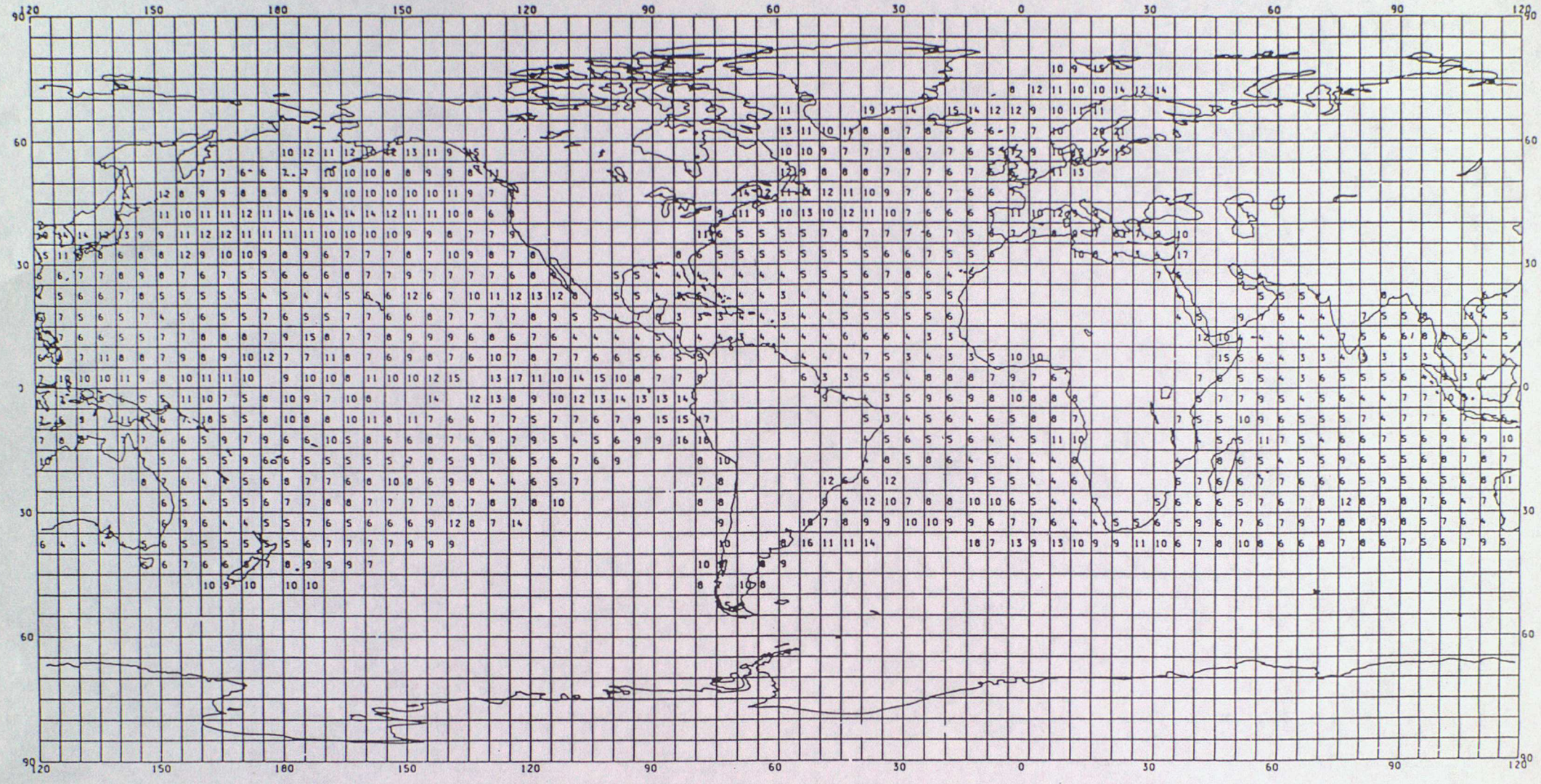

Figure 5.3B Standard deviation of monthly SST, July.
After Bottomley et al (1988). Values in tenths °C.

ONE MONTH LAG CORRELATIONS OF SST ANOMALY FOR FEBRUARY - JANUARY

CORRELATIONS ARE *100

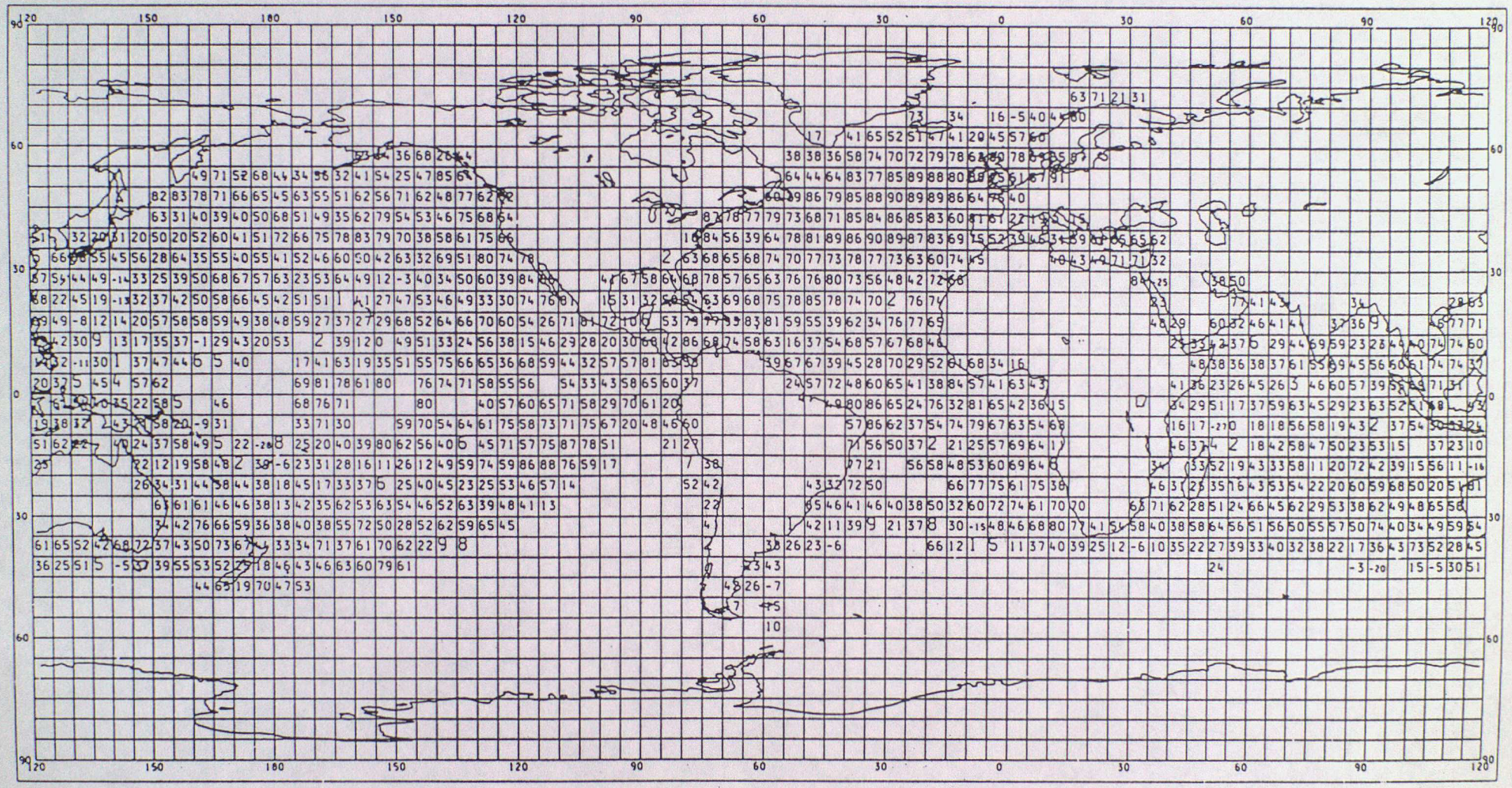

Figure 5.3C After Bottomley et al (1988).

ONE MONTH LAG CORRELATIONS OF SST ANOMALY FOR AUGUST - JULY

CORRELATIONS ARE ×100

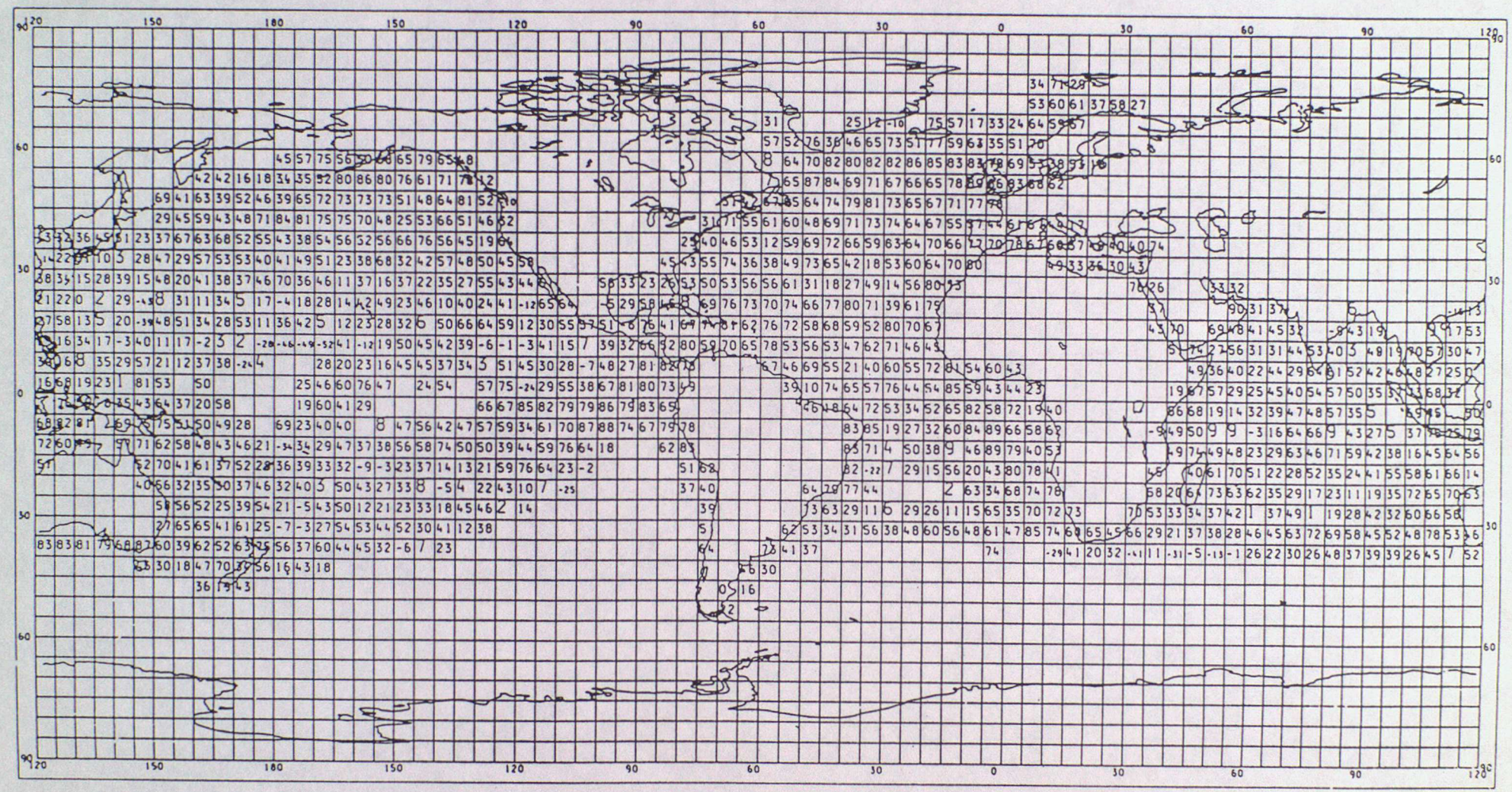

Figure 5.3D After Bottomley et al (1988)

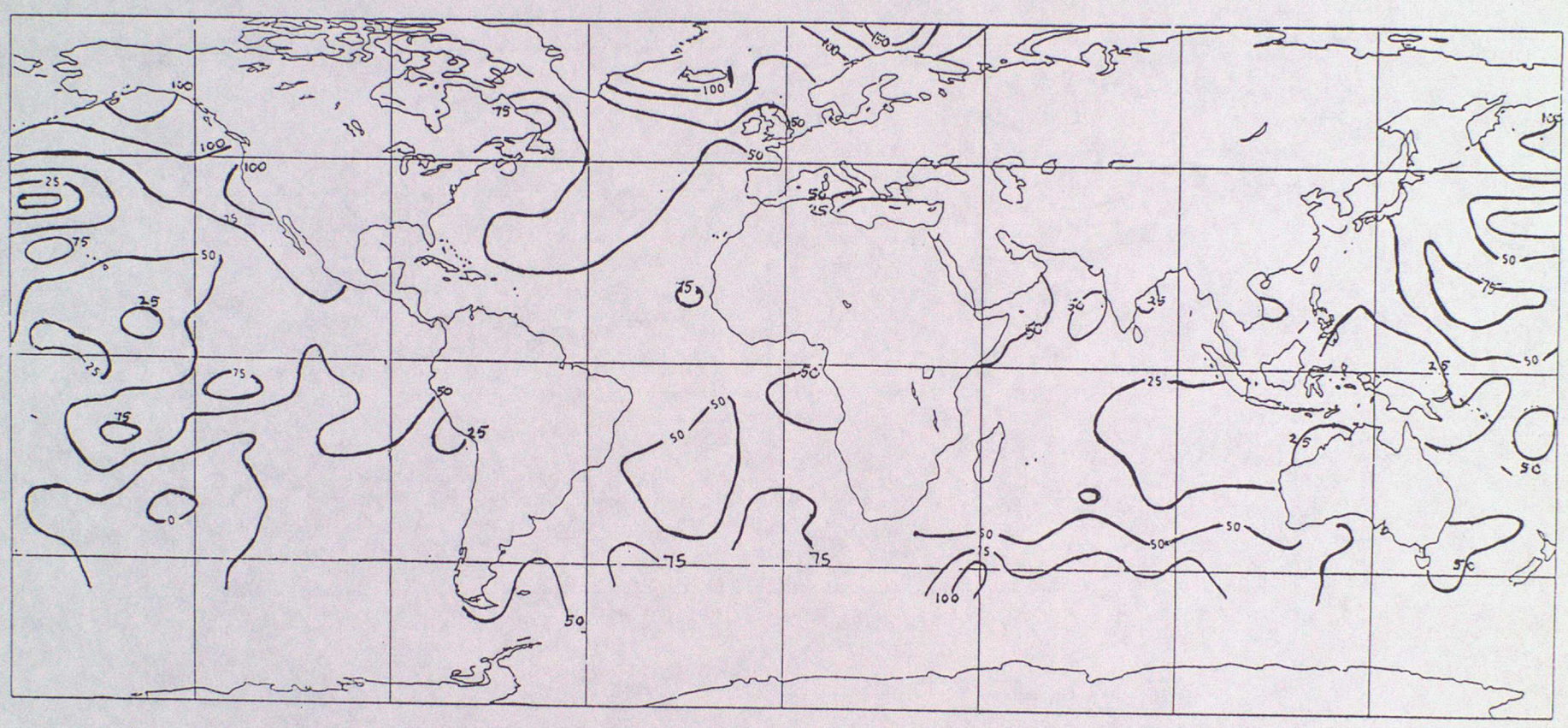

Figure 5.4A. The first all-seasons covariance eigenvector of global SSTA, 1901-80. The pattern is scaled so that the sum of squares of 10^{o} latitude x longitude values equals 10^{6}.

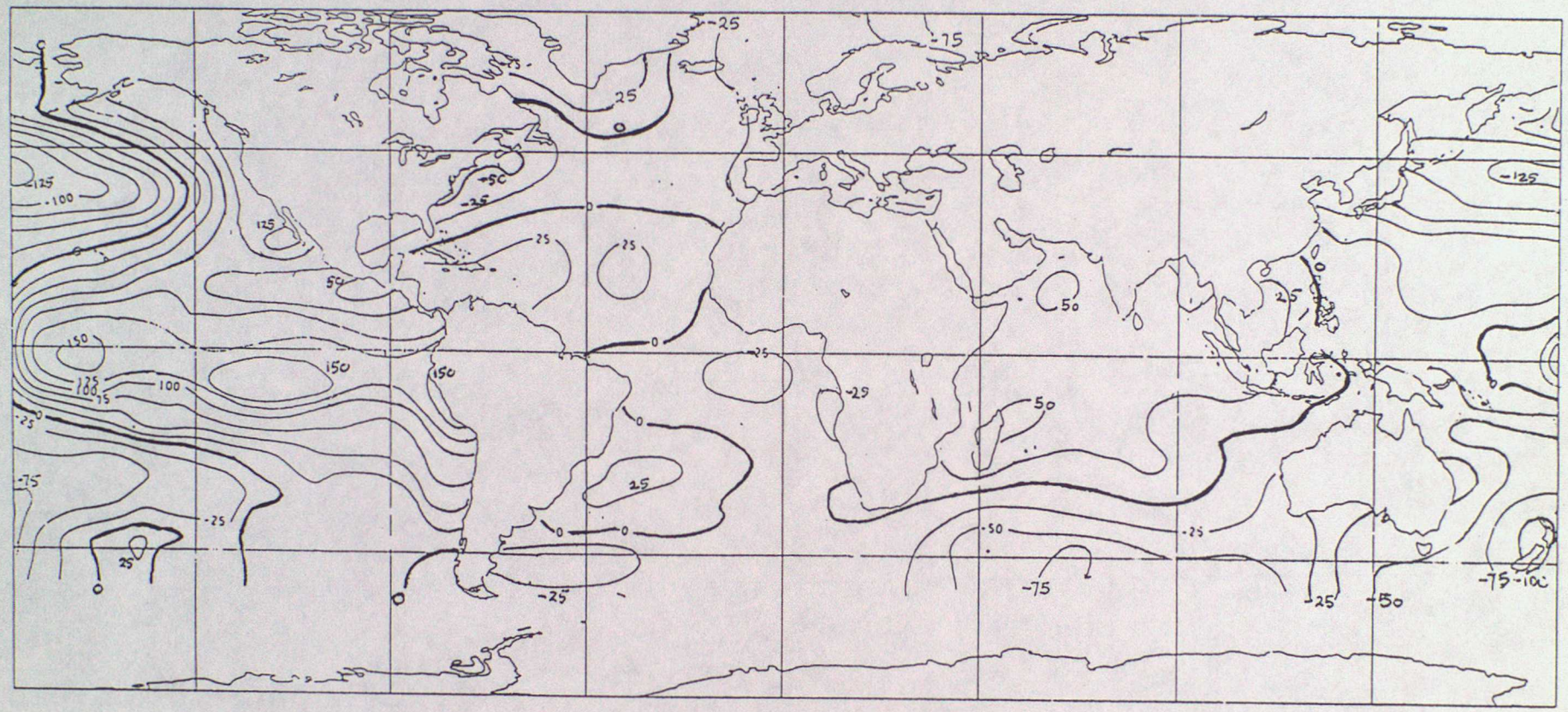

Figure 5.4B. The second all-seasons covariance eigenvector of global SSTA, 1901-80. Scaling as in Fig. 5.4A.

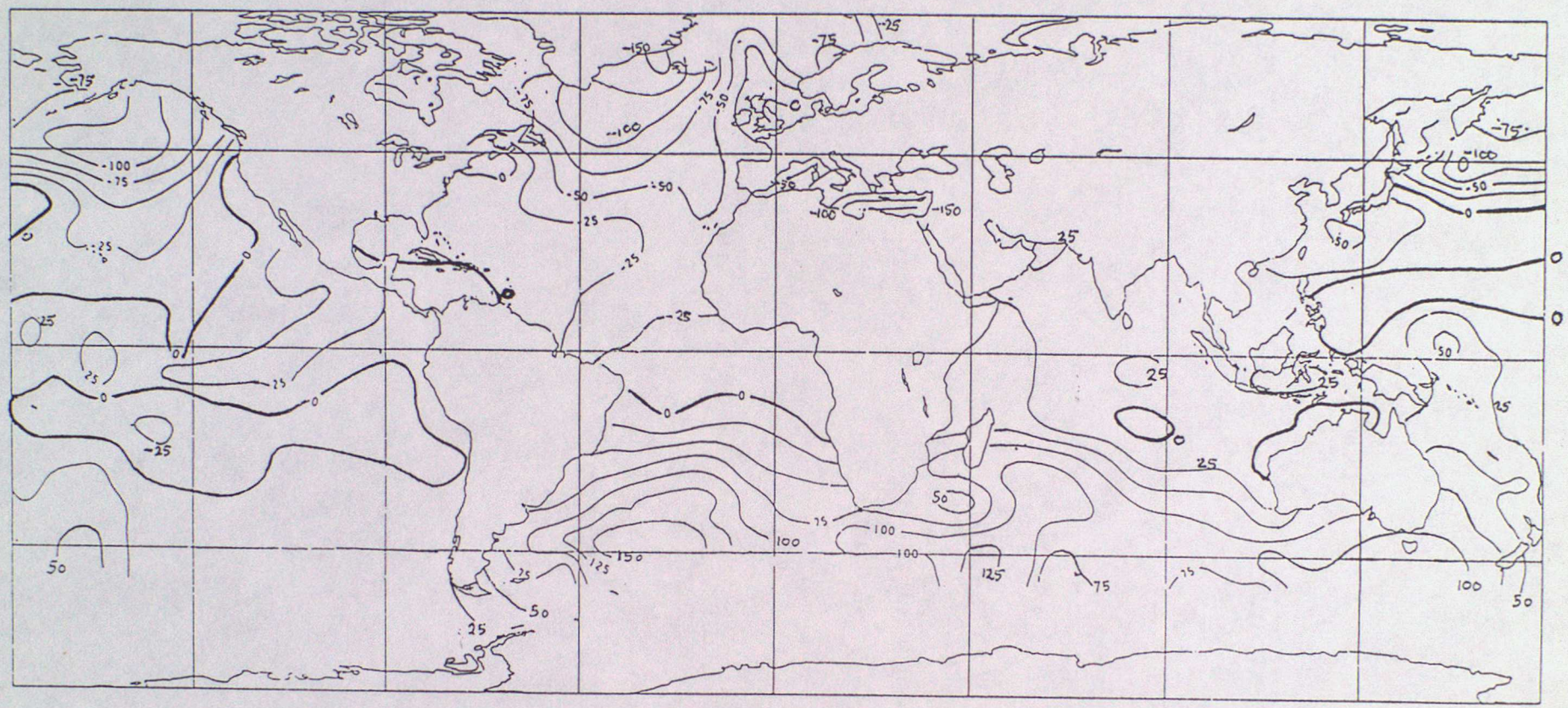

Figure 5.4C. The third all-seasons covariance eigenvector of global SSTA, 1901-80. Scaling as in Fig. 5.4A.

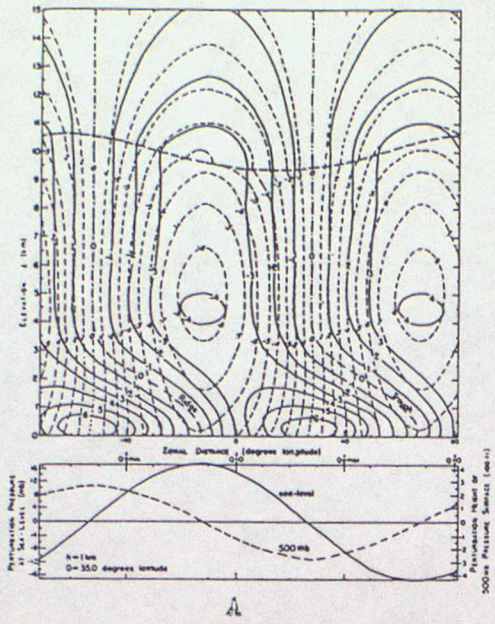

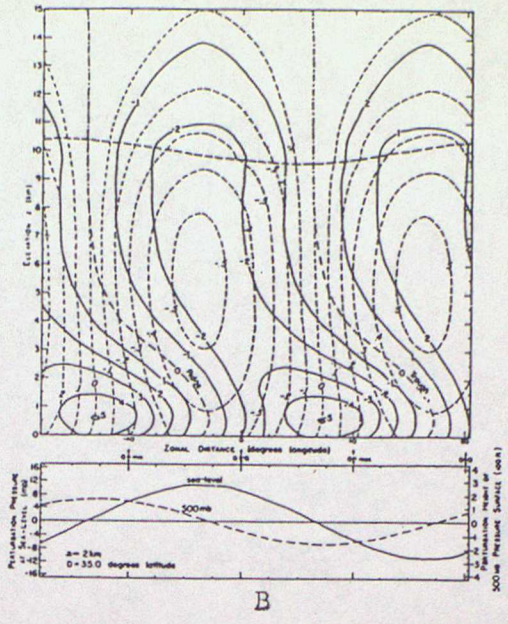

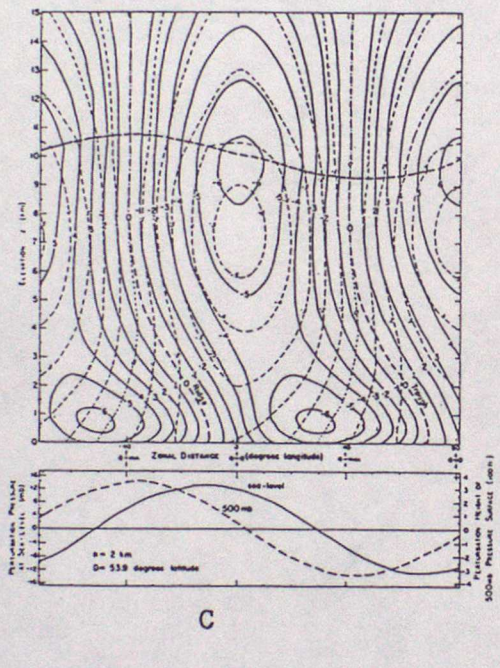

Figure 5.5.

General baroclinic model with surface friction, at latitude of maximum heating and cooling. Stable stratosphere taken into account. Upper part : zonal section of perturbation meridional velocity v (solid lines) in m sec^{-1} and perturbation vertical velocity w (dashed lines) in cm sec^{-1}. Lower part : zonal profile of perturbation pressure at sea level (solid lines) and perturbation height of 500-mb pressure surface (dashed lines).

From Smagorinsky (1953)

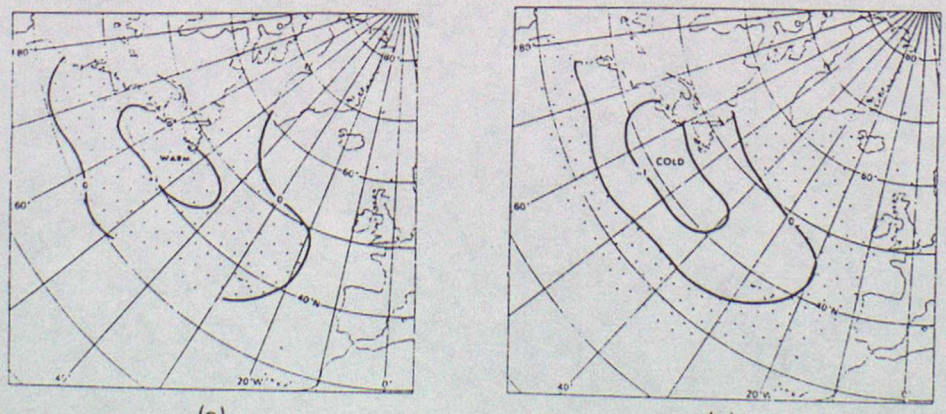

Generalized sea surface temperature anomaly distributions (°C):
(*a*) Type here designated as 'warm sea' cases.
(*b*) Type here designated as 'cold sea' cases.

Figure 5.6. From Lamb (1972).

Figure 5.7A.
From Lamb (1972).

Pressure anomalies (mb) averaged for the following months:

(*a*) Octobers, given 'warm sea' (fig. 5.6(*a*)) in September.

(*b*) Februarys, given 'warm sea' in January.

(*c*) Mays, given 'warm sea' in April.

(*d*) Julys, given 'warm sea' in June.

Shaded areas are statistically significant at the 95% level according to a t-test.

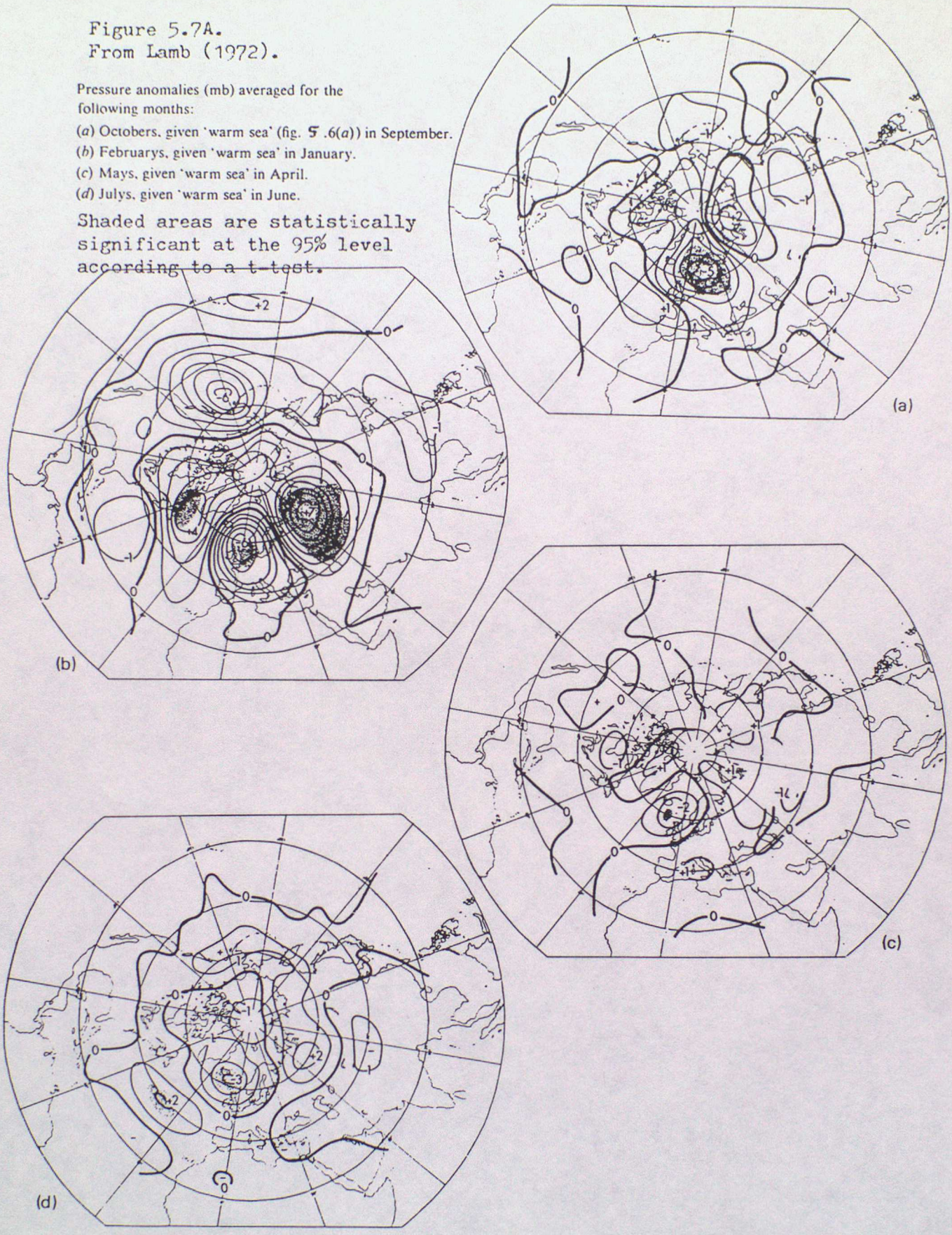

Figure 5.7B.
From Lamb (1972).

Pressure anomalies (mb) averaged for the following months:

(*a*) Octobers, given 'cold sea' (fig. 5.6(*b*)) in September.
(*b*) Februarys, given 'cold sea' in January.
(*c*) Mays, given 'cold sea' in April.
(*d*) Julys, given 'cold sea' in June.

Shading as in Fig 5.7A.

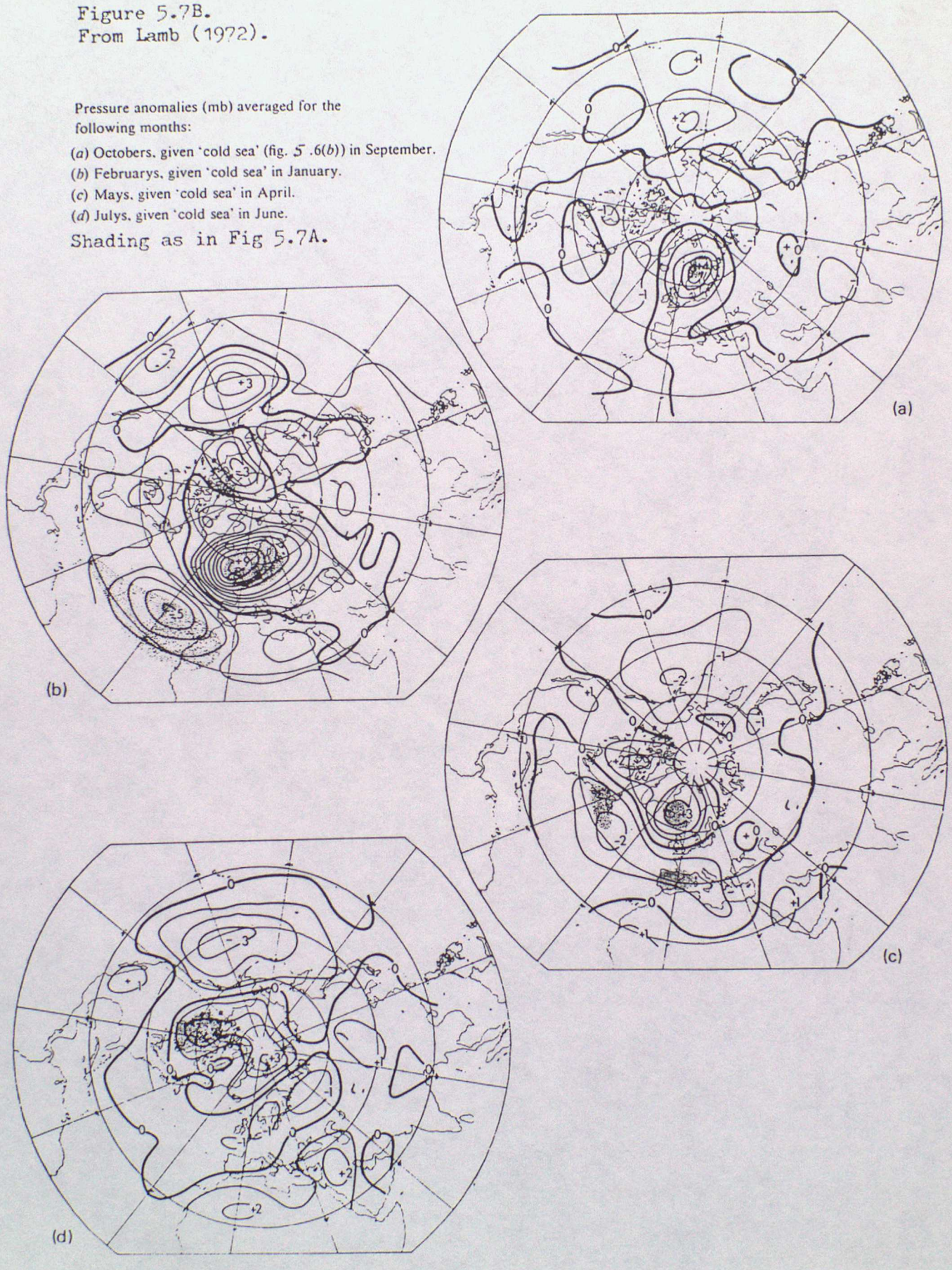

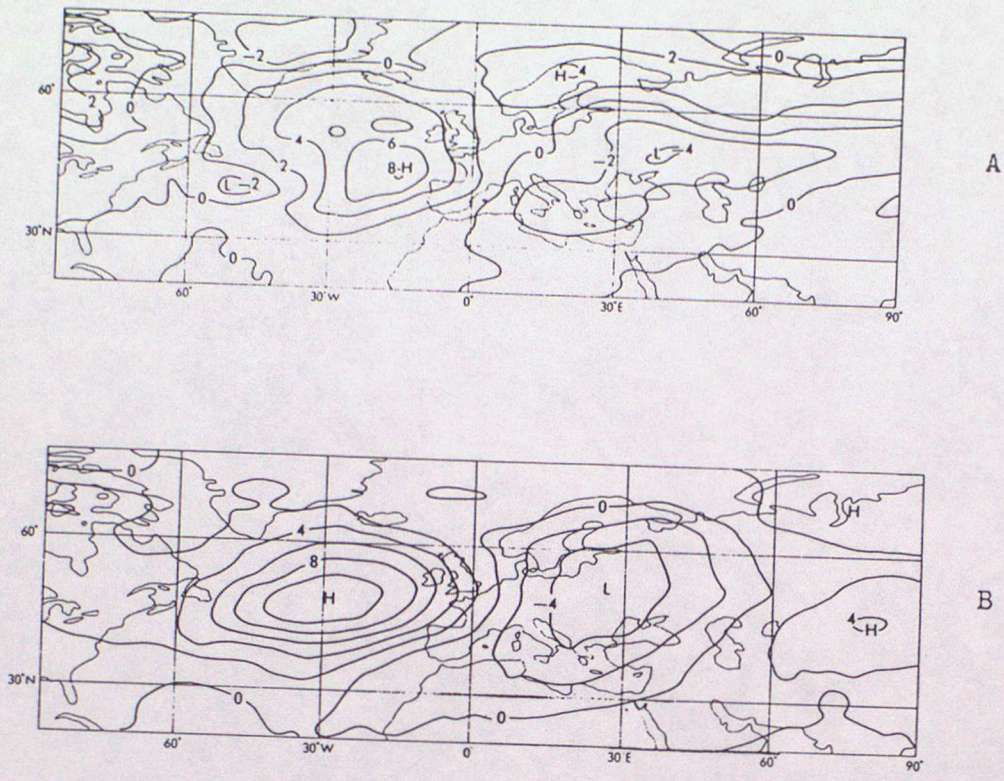

Figure 5.8. Geopotential height difference (dam) for warm minus cold "Ratcliffe region" , averaged over four pairs of integrations. Winter.
A. 1000mb. B. 500mb.

After Palmer and Sun (1985).

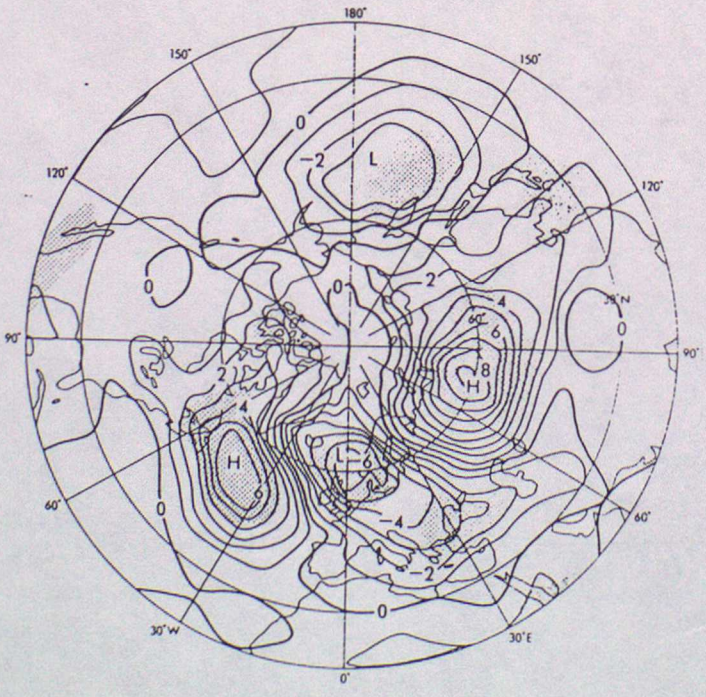

Figure 5.9 Observed synchronous MSL pressure difference (mb) for warm minus cold "Ratcliffe region" averaged over November to February 1951-80. Shading as in Fig 5.7.
After Palmer and Sun (1985).

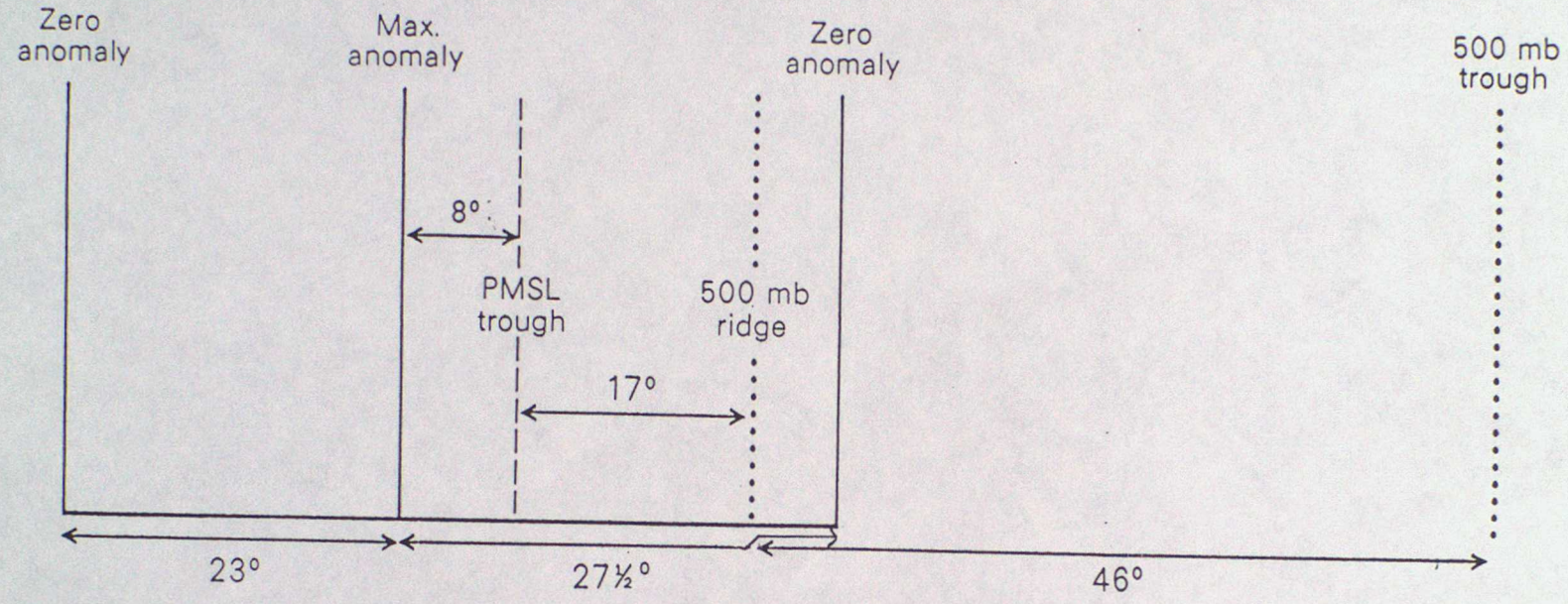

Summarised effects of warm mid-latitude SST anomalies on PMSL and 500 mb height (from Rowntree 1984)

Figure 5.10.

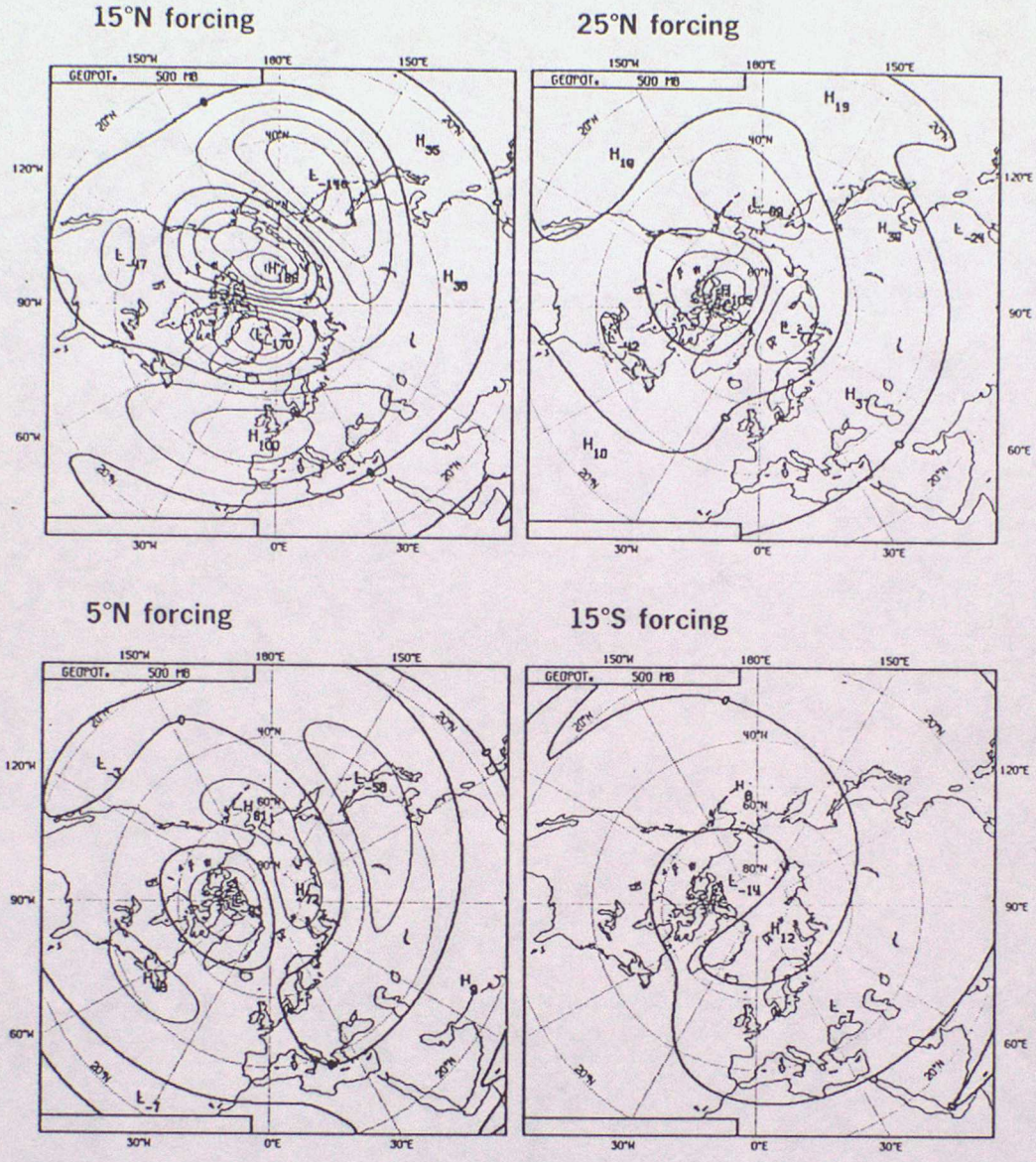

500 mb height perturbations for heatings centred at 135 °E and various latitudes.

January.

Figure 5.11. From Simmons (1982)

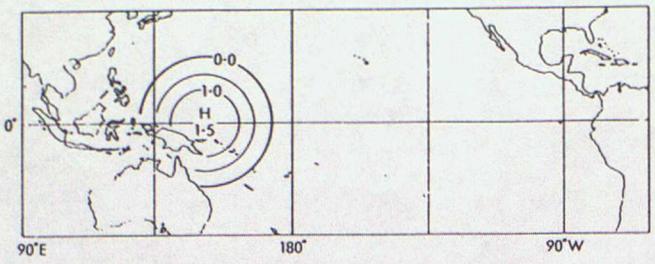

Figure 5.12A. West Pacific SST anomaly (°C) used by Palmer and Mansfield (1986b)

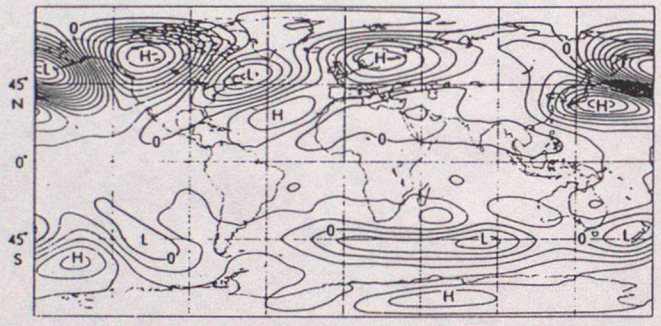

Figure 5.12B. 250mb geopotential height anomaly produced by the model of Palmer and Mansfield (1986b) in response to the SST anomaly shown in Fig. 5.12A
This was a 540-day "perpetual January" experiment.

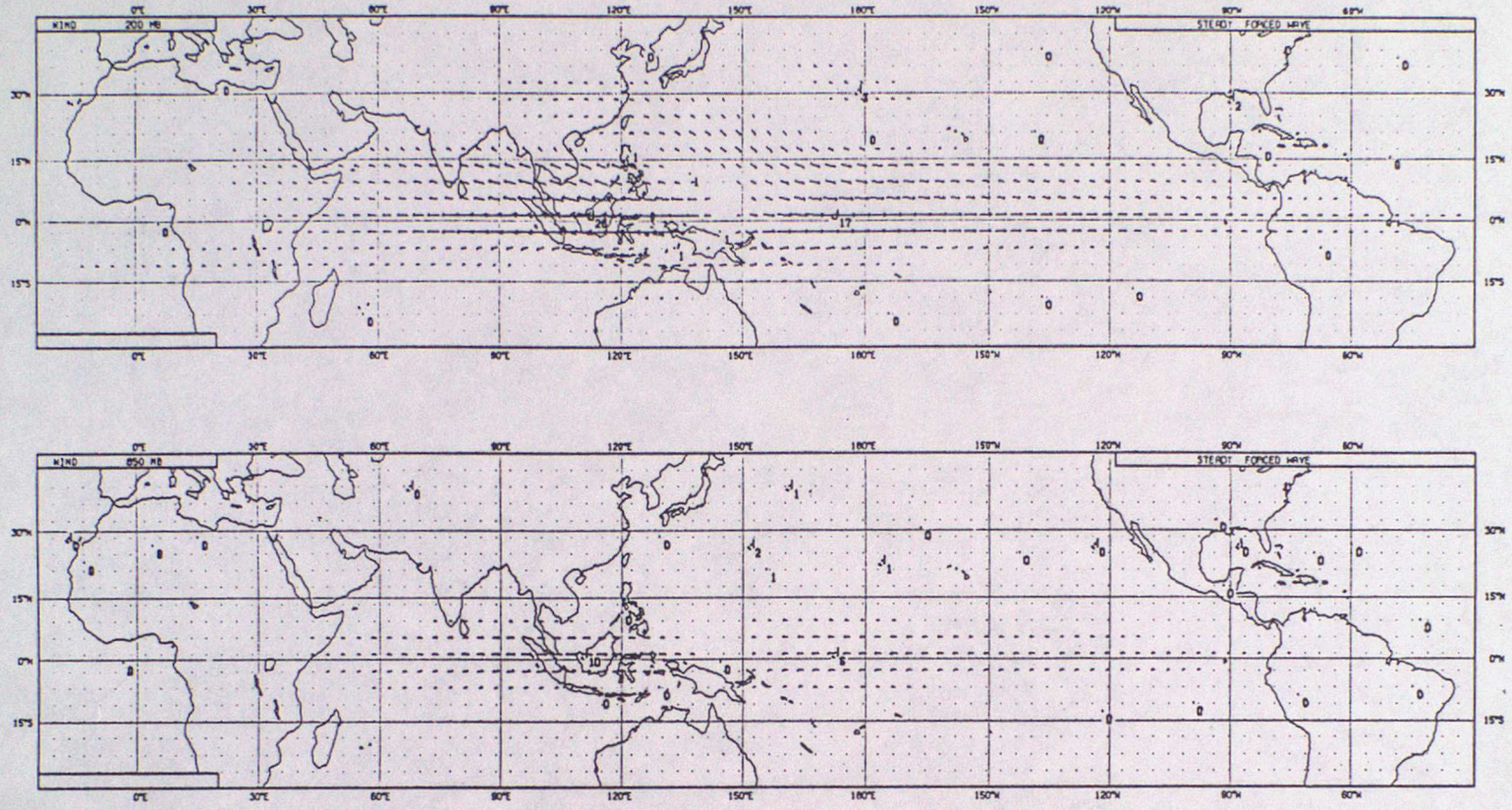

Perturbation winds at 200 mb and 850 mb for a heating centred on the equator at 135 °E. Velocity maxima (in $m\,s^{-1}$) are marked.

Figure 5.13. From Simmons (1982).

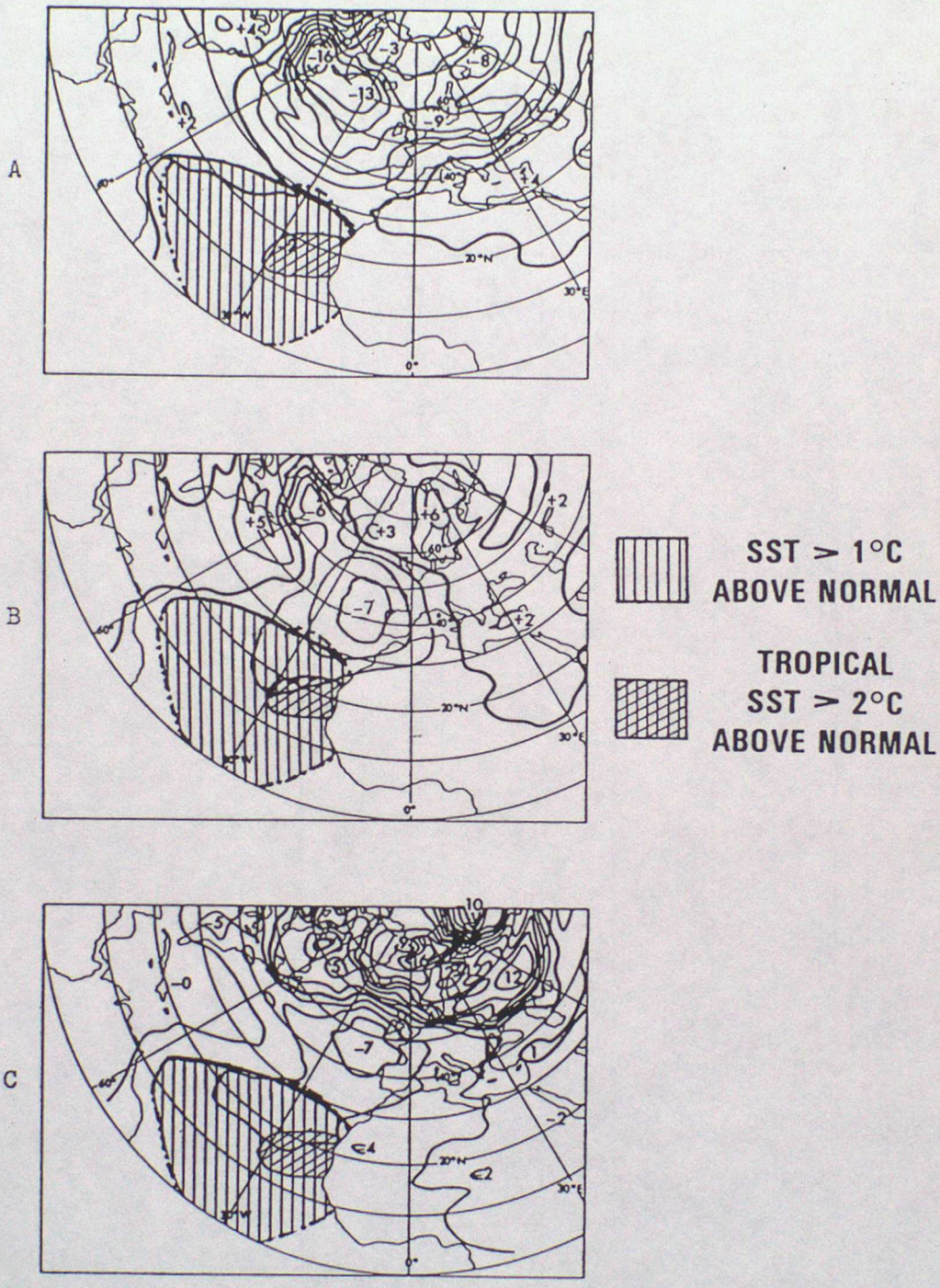

Difference in mean surface pressure (mb) averaged over days 41–80 of model integrations between surface pressure obtained with tropical Atlantic warming and the control experiment without the warming. (A) experiment 1 using isothermal initial data, (B) experiment 2 using initial real data, and (C) experiment 3 also using initial real data. Both (B) and (C) use initial data for 29 December 1965. SST averages taken from US Naval Oceanographic Office data.

Figure 5.14. Taken from Rowntree (1976) by Folland (1983).

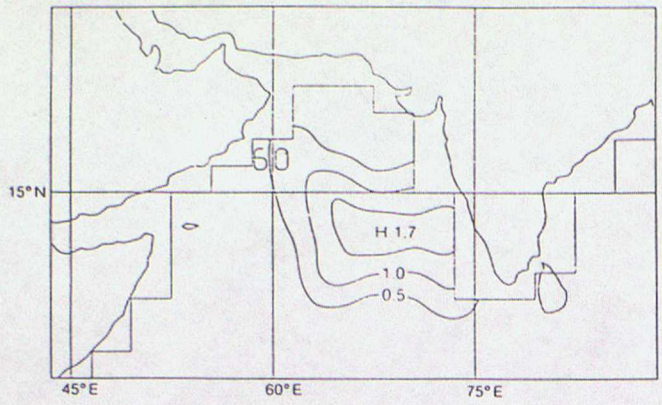

Figure 5.15A SST anomaly used by Kershaw (1988)

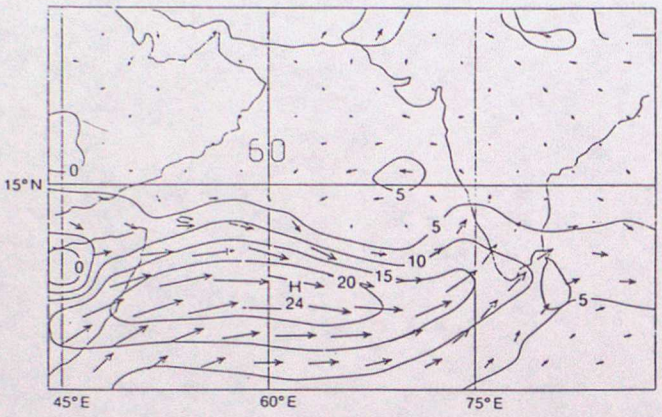

Figure 5.15B 850mb wind vectors and isotachs (m/sec) predicted for 12GMT 19 June 1979 in the control integration of Kershaw (1988)

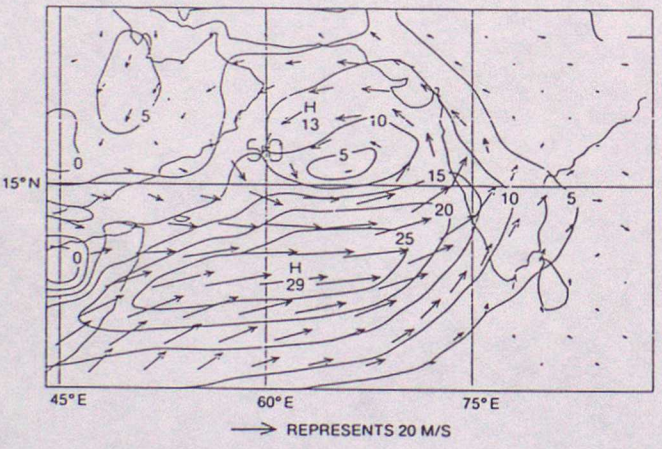

Figure 5.15C As fig 5.15B but for the anomaly integration

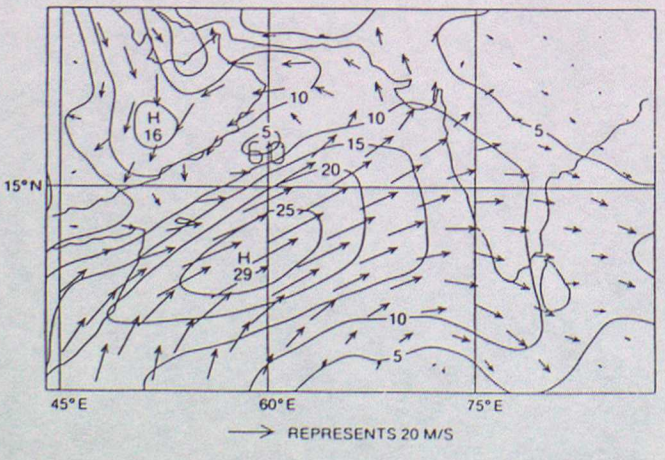

Figure 5.15D Observed 850mb wind vectors and isotachs (m/sec) for 12GMT 19 June 1979

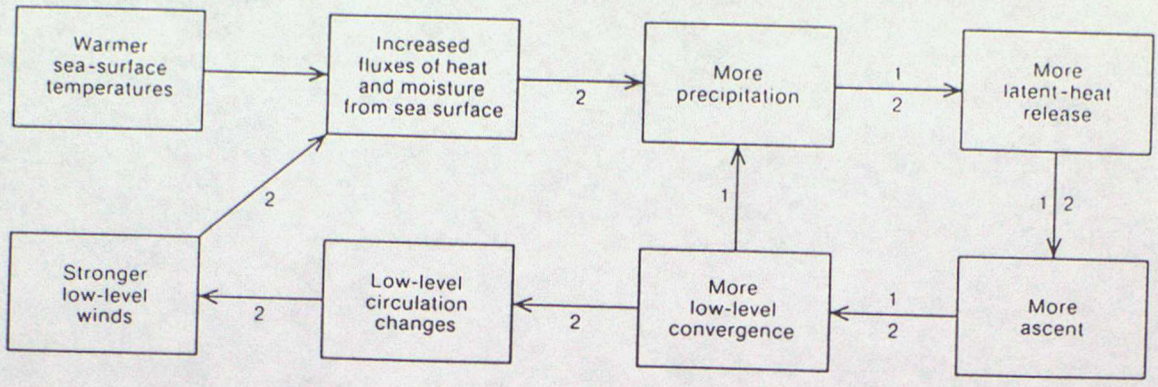

Figure 5.15 E Two feedback loops relating an Arabian sea SST anomaly to atmospheric changes associated with the Indian Monsoon onset. After Kershaw (1988)

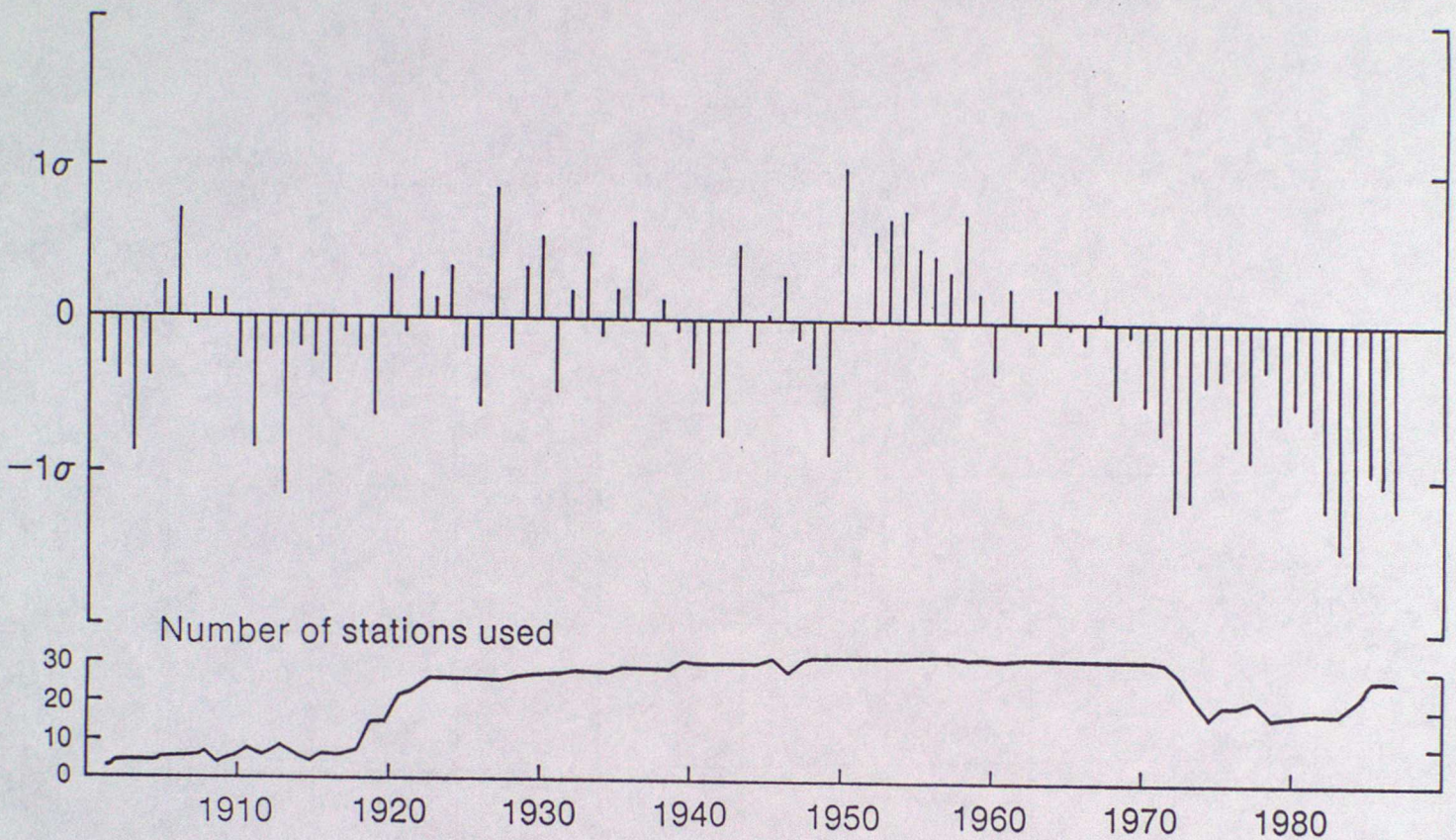

Figure 5.16. Standardised annual rainfall anomalies for the Sahel, 1901-87. Values to 1984 after Nicholson (1985): 1985-87 estimated from CLIMAT reports.

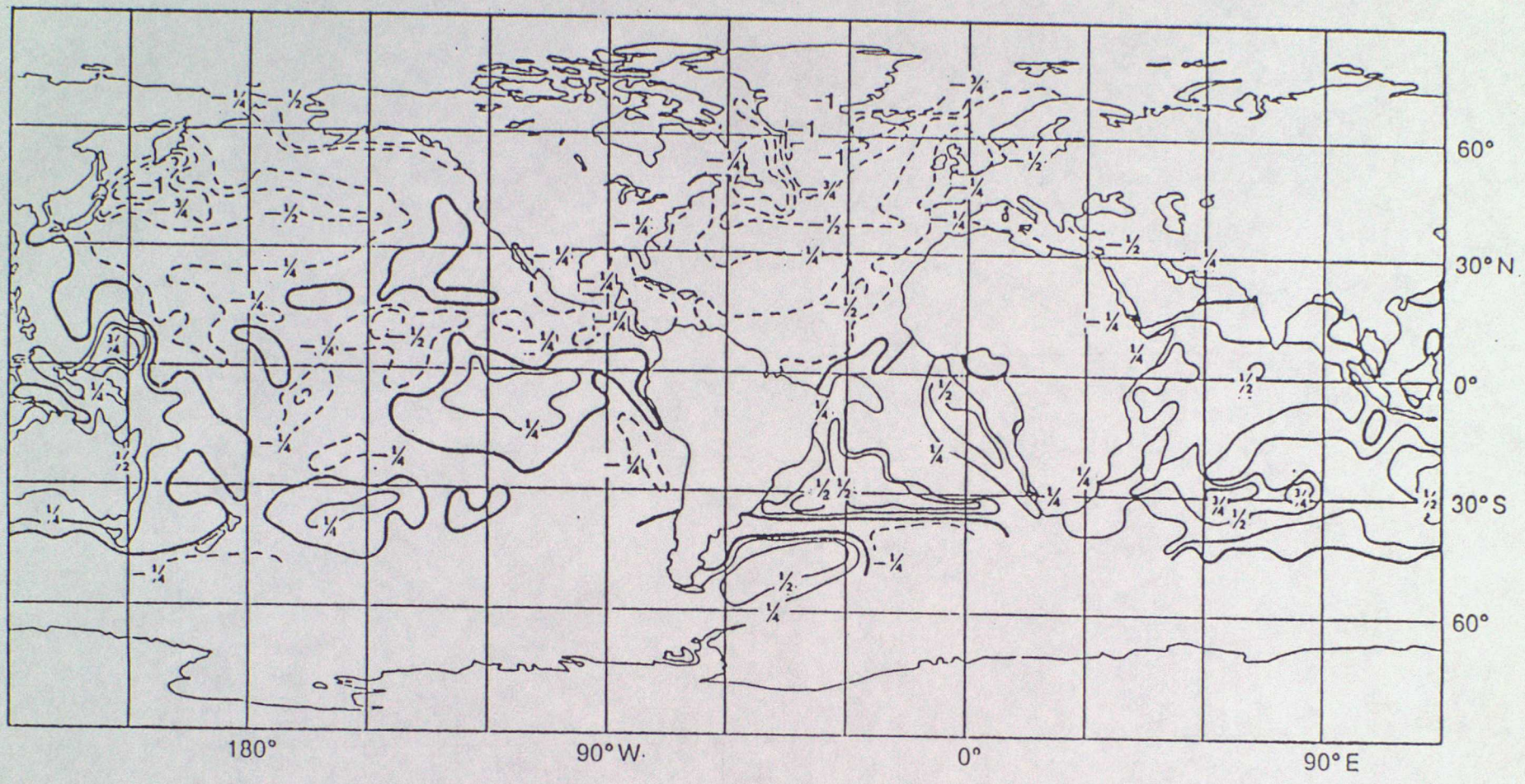

Mean sea surface temperature difference (°C) for 1971–1987 relative to 1951–60.

Figure 5.17. From Parker and Folland (1988).

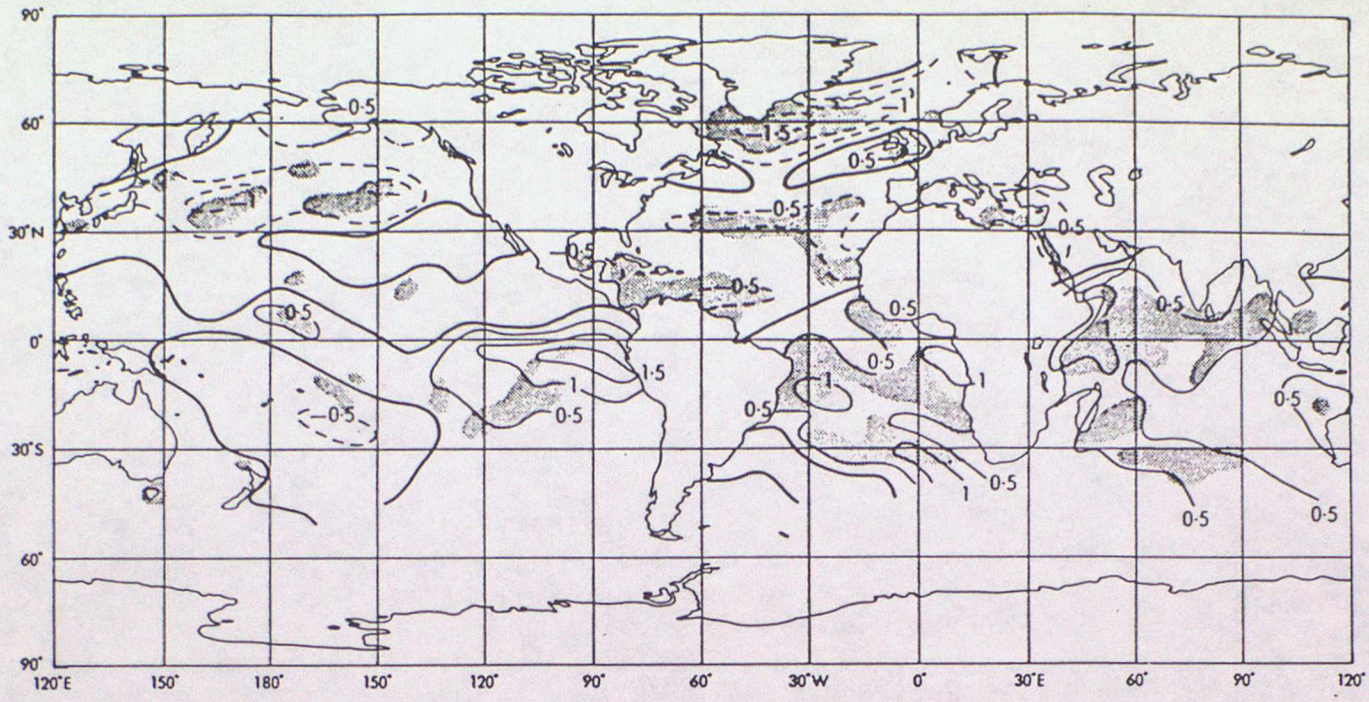

a, SST, July to September: average of (1972–73, 1982–84) (Sahel dry) minus average of (1950, 1952–54, 1958) (Sahel wet). Contours every 0.5 °C. Shaded areas are different from zero at the 90% level of significance according to a *t*-test.

Figure 5.18. From Folland et al (1986).

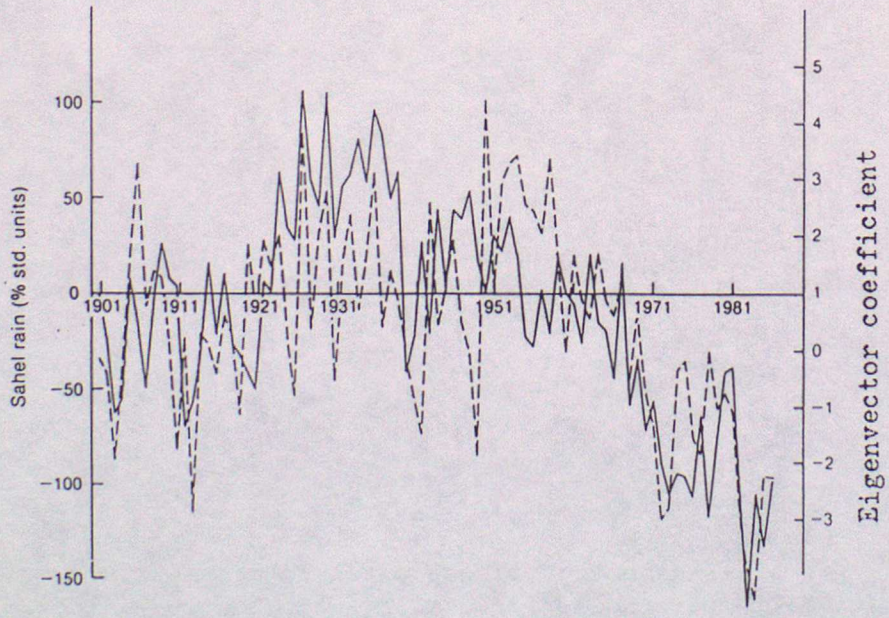

Coefficient of the third all-seasons covariance eigenvector of global SSTA in July to September (solid line) along with Sahel rainfall (dashed line) 1901-86.

Figure 5.19. From Parker et al (1988).

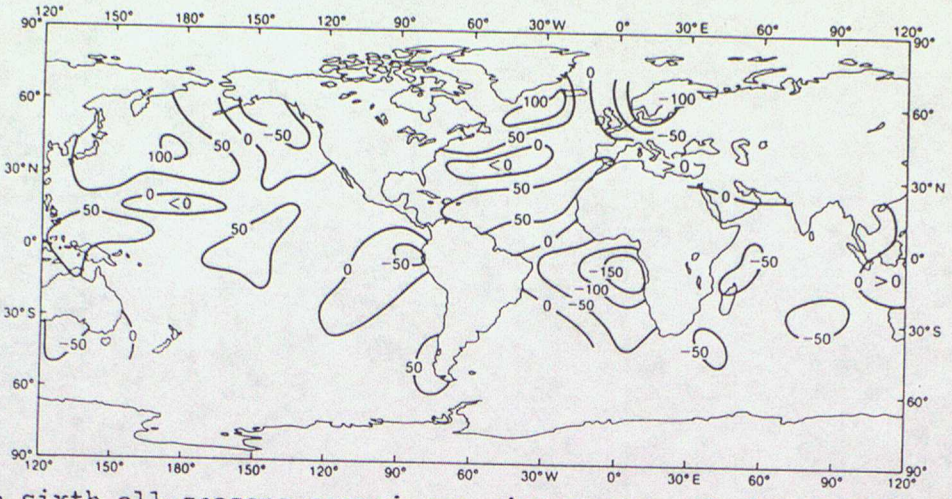

The sixth all-seasons covariance eigenvector of global SSTA, 1901-80. The pattern is scaled so that the sum of squares of 10° latitude x longitude values equals 10^6.

Figure 5.20. From Parker et al (1988).

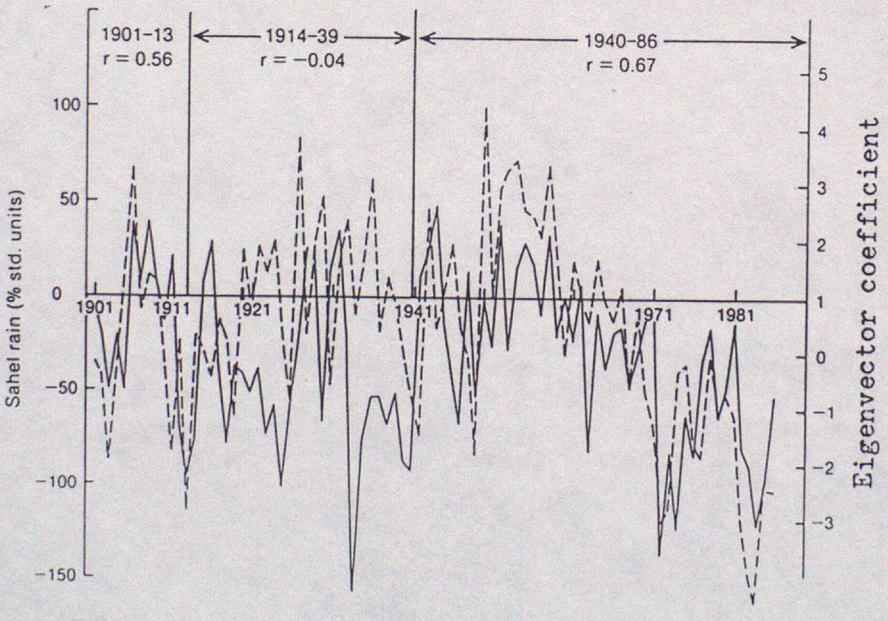

Coefficient of the sixth all-seasons covariance eigenvector of global SSTA in July to September (solid line) along with Sahel rainfall (dashed line) 1901-86.

Figure 5.21. From Parker et al (1988).

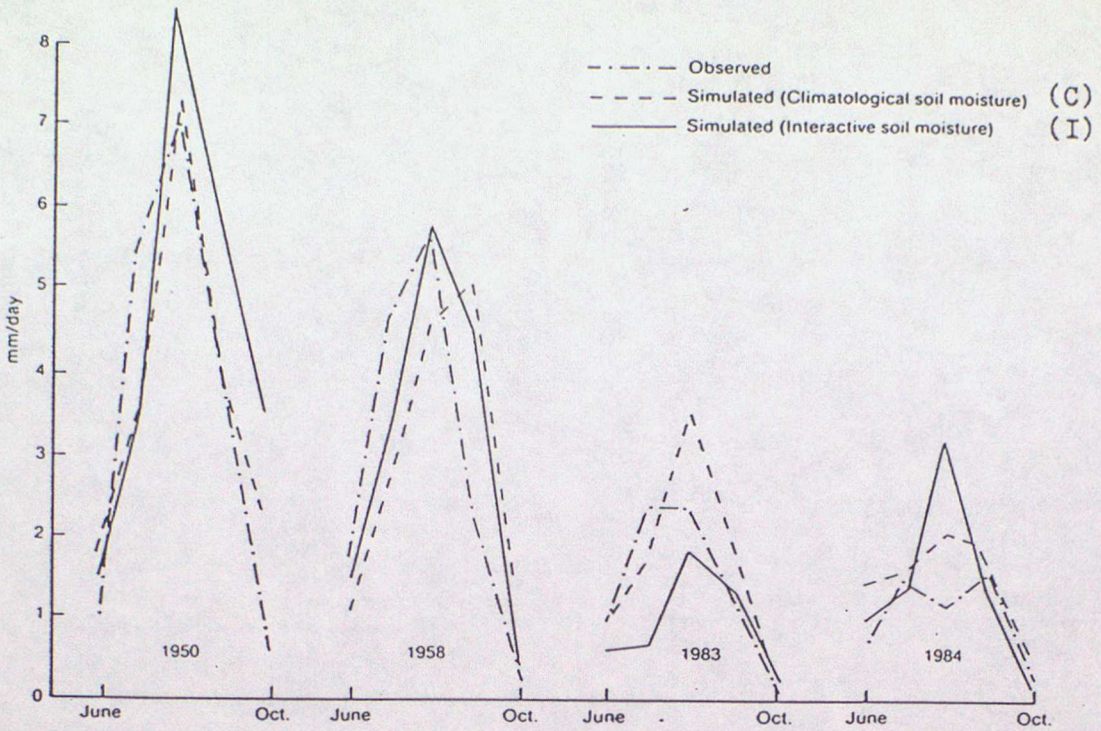

Time series of simulated rainfall for the whole Sahel for experiments 1950(I), 1958(I), 1983(I), 1984(I), 1950(C), 1958(C), 1983(C) and 1984(C), together with the corresponding observed rainfall.

Figure 5.22. From Owen et al (1988).

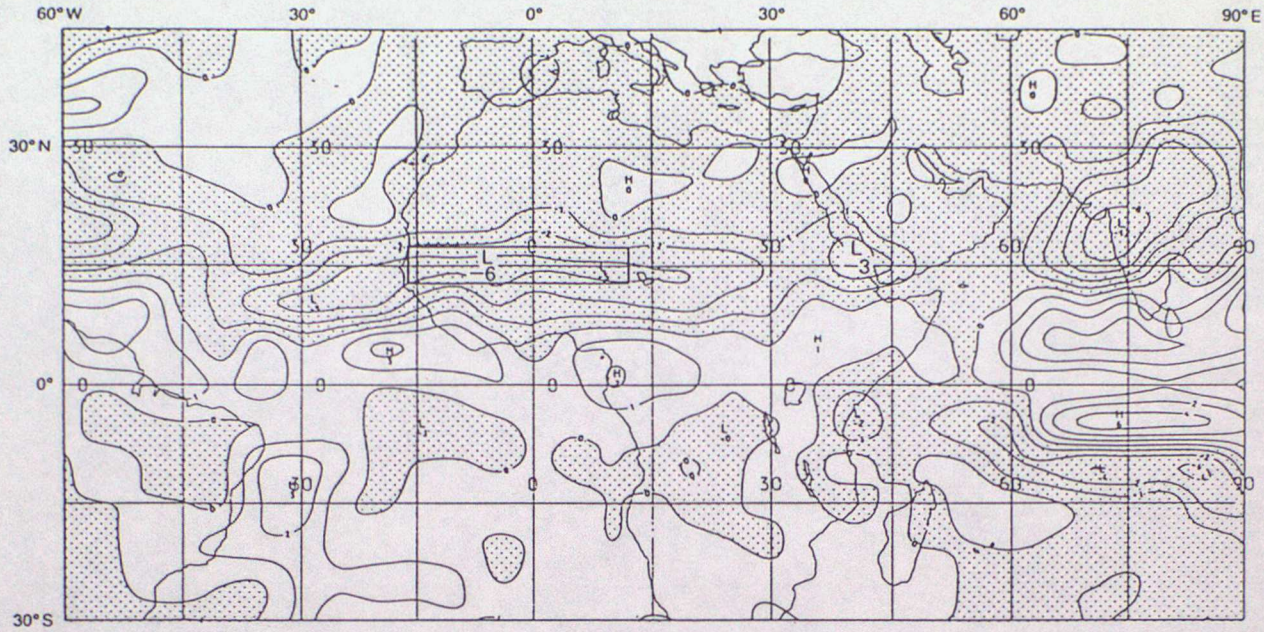

A

Modelled rainfall, difference between experiments 1984(I) and 1950(I) for July to September. Contours are at 0, ±1, 2, 4, 8, and 16 mm day^{-1}, with negative areas stippled.

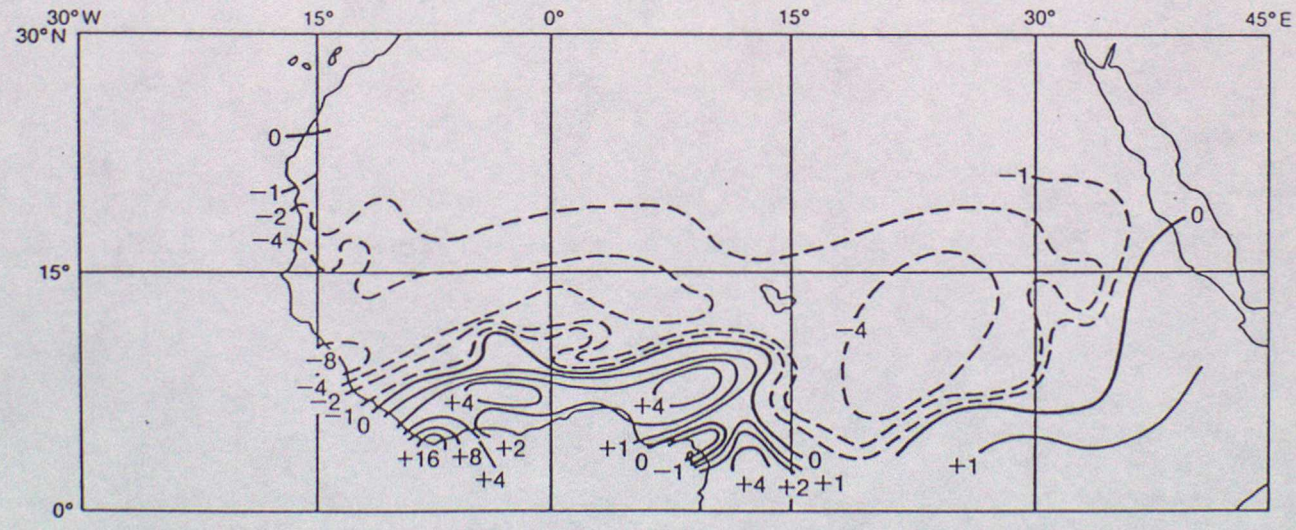

B

Observed rainfall, difference between 1984 and 1950 for July to September. Contours as in A.

Figure 5.23. From Owen et al (1988).

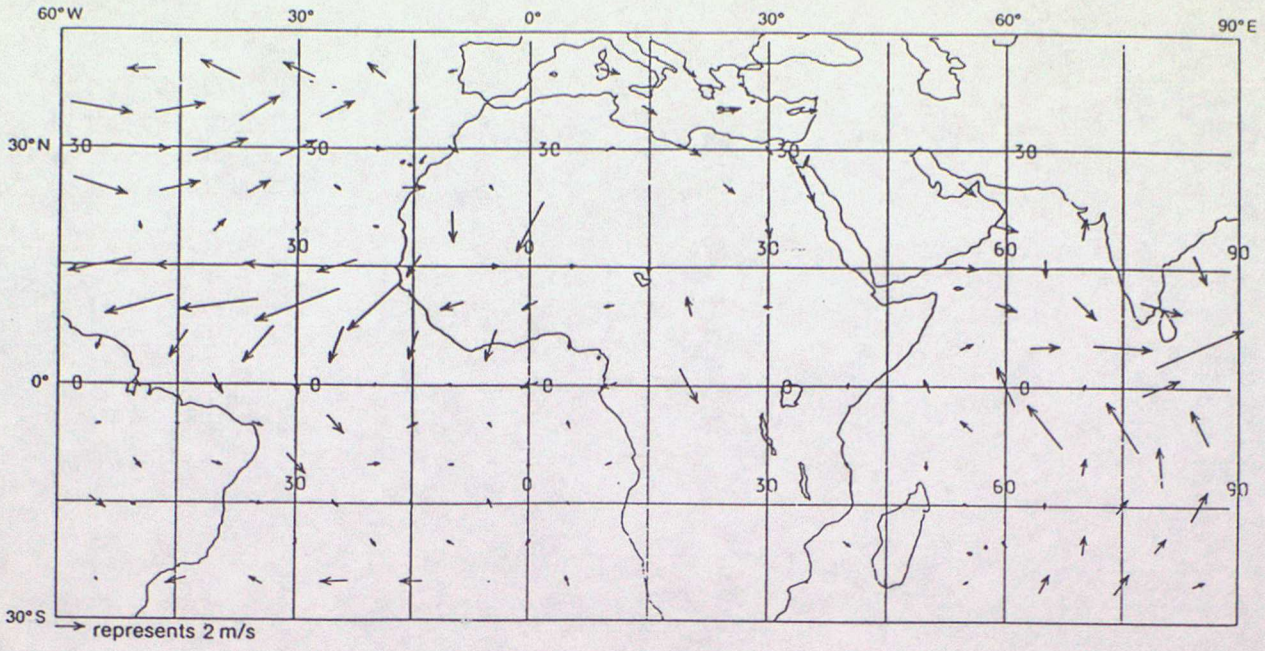

A. 950 mb vector wind difference between experiments 1984(I) and 1950(I). July to September.

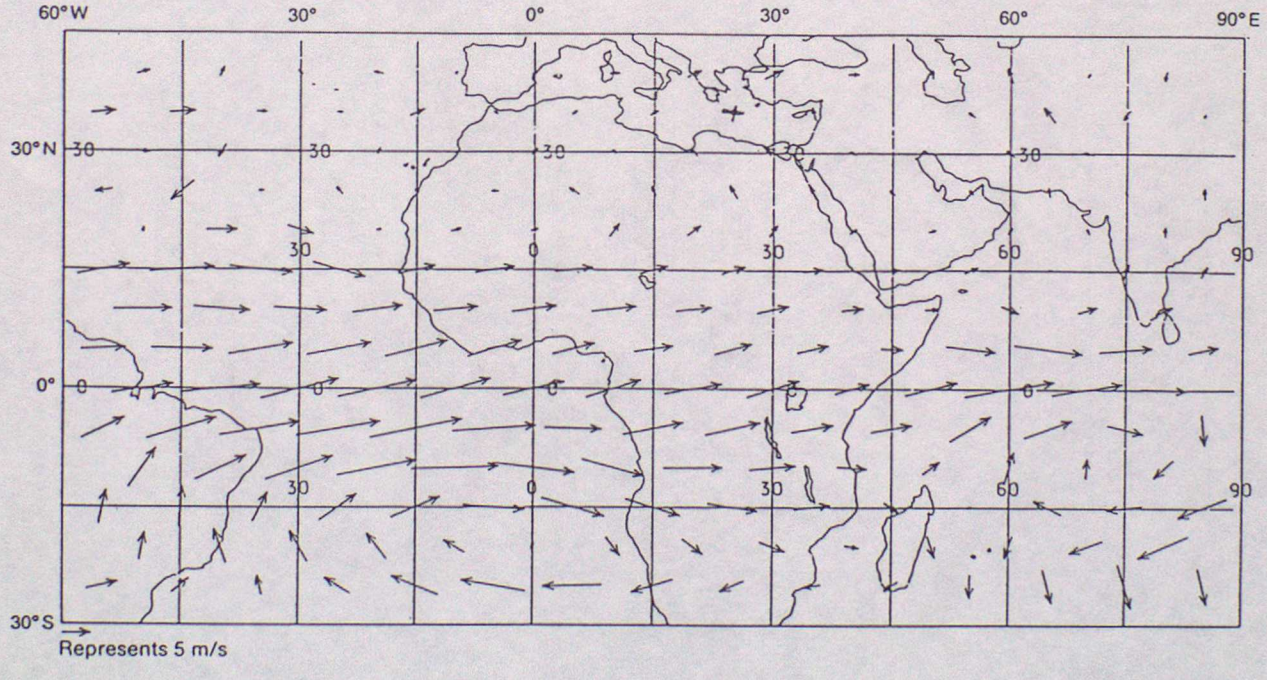

B. 250 mb vector wind difference between experiments 1984 (I) and 1950 (I). July to September. Note the change of wind scale from A.

Figure 5.24. From Owen et al (1988).

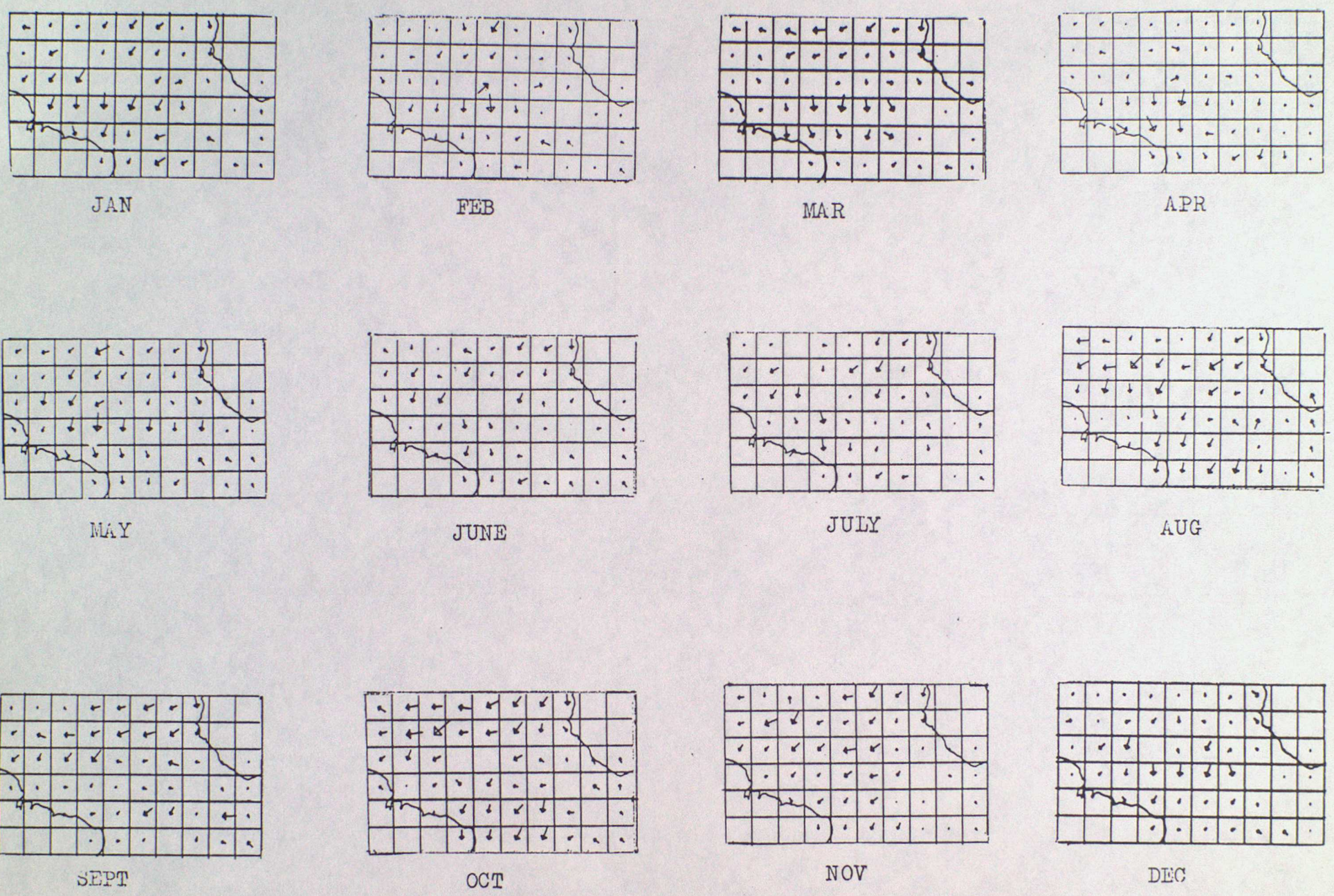

Figure 5.25 Surface winds, 1968-79 relative to 1950-59.
From the Comprehensive Ocean-Atmosphere Data Set (COADS).
(Woodruff et al (1987))